

ANALYSIS OF METABOLIC DISORDERS OF DAIRY COWS  
EMPLOYING MULTIDIMENSIONAL AND MULTINUCLEAR  
NMR SPECTROSCOPY



DISSERTATION ZUR ERLANGUNG DES DOKTORGRADES  
DER NATURWISSENSCHAFTEN (DR. RER. NAT.)  
DER FAKULTÄT FÜR BIOLOGIE UND VORKLINISCHE MEDIZIN  
DER UNIVERSITÄT REGENSBURG

vorgelegt von

Matthias S. Klein  
aus  
Bad Reichenhall

im Jahr 2011

Das Promotionsgesuch wurde eingereicht am: 30.11.2011

Die Arbeit wurde angeleitet von: Prof. Dr. Wolfram Gronwald

Unterschrift:

*Meinem Vater*

# Danksagung

Ich möchte mich bedanken bei

Prof. Dr. Wolfram Gronwald für das interessante und wichtige Thema der Doktorarbeit

Prof. Dr. Peter J. Oefner für die Möglichkeit, die Doktorarbeit an seinem Institut durchzuführen

allen Mitgliedern der Arbeitsgruppe Gronwald: Florian Fink, Jochen Hochrein, Ann-Kathrin Immervoll, Steffi Kohl, Carrie Louis, Sebastian Miemczyk und Helena Zacharias für die vielen Tipps, Hilfe und die nette Büronachbarschaft

allen Mitgliedern der zweiten Metabolomik-Arbeitsgruppe des Instituts: Martin Almstetter, Katja Dettmer-Wilde, Stephan Fagerer, Hanne Kaspar, Nadine Nürnberger, Axel Stevens, Steffi Stöckl, Magda Waldhier, Chris Wachsmuth und Wentao Zhu für die gute Zusammenarbeit unter „Metabolomikern“

zusätzlich Hanne Kaspar, Nadine Nürnberger und Magda Waldhier für die Unterstützung bei den Laborarbeiten

Fritz Kastner für die technische Hilfe am Spektrometer

allen anderen Mitgliedern des Instituts: Nadine Aßmann, Sabine Botzler, Karin Eberhart, Corinna Feuchtinger, Jörg und Yvonne Reinders, Sophie Schirmer und Anja Thomas, der Arbeitsgruppe von Prof. Dr. Rainer Spang: Benedict Anchang, Inka Appel, Stefan Bentink, Peter Butzhammer, Tully Ernst, Julia Engelmann, Daniela Herold, Christian Hundsrucker, Philipp Knollmüller, Christian Kohler, Claudio Lottaz, Matthias Maneck, Katharina Meyer, Mohammad Sadeh und Marian Thieme und den Mitgliedern des KFB für die angenehme Arbeitsatmosphäre

den Mitgliedern des Lehrstuhls Kalbitzer für die interessanten fachlichen Gespräche und für das nette Rahmenprogramm auf den gemeinsamen Tagungen

meinen Eltern für die Unterstützung während der Doktorarbeit

und meiner Freundin Margit für die unermüdliche Unterstützung, für ihr Lächeln und für ihre strahlenden Augen unterm Sternenhimmel!

Danke!

# Table of Contents

Abbreviations.....	i
Glossary .....	iii
Abstract.....	v
Zusammenfassung .....	vi
1 Introduction .....	1
1.1 Background .....	1
1.2 Motivation and Specific Aims .....	2
2 Method Development.....	4
2.1 Basics of Nuclear Magnetic Resonance .....	4
2.2 Alternative Methods .....	13
2.3 Data Analysis.....	15
2.4 Quantitative Measurements.....	21
2.5 Measurement of Urine Specimens .....	24
2.6 QUANTIFY: A Tool for Accurate Quantification .....	31
2.7 Urine Test Samples.....	35
2.8 Measurement of Bovine Milk .....	44
2.9 Measurement of Tissue Extracts.....	50
2.10 Measurement of Blood Serum and Blood Plasma .....	53
2.11 Data Preprocessing for Machine Learning Algorithms .....	57
3 Biomedical Application .....	59
3.1 Autosomal Dominant Polycystic Kidney Disease .....	59
3.2 Metabolic Differences Between Dairy Cow Breeds .....	61
3.3 Metabolic Predictors for Dairy Cow Health Status .....	67
3.4 Nonalcoholic Fatty Liver Disease and Steatohepatitis.....	79
3.5 Analysis of Early Liver Disease Progression.....	89
4 Summary .....	90
5 References.....	93
6 About the Author .....	104
6.1 Curriculum Vitae.....	105
6.2 Publications .....	106
6.3 Poster Presentations.....	107
6.4 Conference Talks .....	107
Appendix.....	108
Appendix I: Tables .....	108
Appendix II: Attached Files.....	133
Appendix III: Manual for QUANTIFY 1.0.....	134

## Abbreviations

1D	One-dimensional
<sup>1</sup> H	Hydrogen-1 (proton)
2D	Two-dimensional
<sup>13</sup> C	Carbon-13
<sup>31</sup> P	Phosphorus-31
ADPKD	Autosomal dominant polycystic kidney disease
Acetyl-CoA	Acetyl coenzyme A
ANOVA	Analysis of variance
ATP	Adenosine triphosphate
BHBA	Beta-hydroxybutyric acid
°C	Degrees Celsius
Ca	Calcium
ck	Choline kinase
CPMG	Carr, Purcell, Meiboom, Gill
DIM	Days in milk
EB	Energy balance
EDTA	Ethylenediaminetetraacetic acid
FDA	Food and Drug Administration
FDR	False discovery rate
FID	Free induction decay
FPR	Fat-to-protein ratio
g	Gravitational acceleration
GC	Gas chromatography
GC-MS	Gas chromatography-mass spectrometry
GPC	Glycerophosphocholine
HF	Holstein-Friesian
HFD	High-fat diet
HMBC	Heteronuclear multiple bond correlation
HSQC	Heteronuclear single quantum coherence
Hz	Hertz
IC	Independent component
ICA	Independent component analysis
kDa	Kilodalton
kg	Kilogram
LC	Liquid chromatography
LC-MS/MS	Liquid chromatography-tandem mass spectrometry
LLOQ	Lower limit of quantification
lpl	Lysophospholipase
Mg	Magnesium
mg	Milligram
MHz	Megahertz
MJ	Megajoule
mL	Milliliter
mmol/L	Millimole per liter
mol/L	Mole per liter

m/Q	Mass-to-charge ratio
MUFA	Monounsaturated fatty acid
MS	Mass spectrometry
μL	Microliter
μmol/L	Micromole per liter
n	Number
NAC	N-acetyl-carbohydrates
NAFLD	Non-alcoholic fatty liver disease
NASH	Non-alcoholic steatohepatitis
NEL	Net energy content for lactation
NIST	National Institute of Standards and Technology
NMR	Nuclear magnetic resonance
NOE	Nuclear Overhauser effect
NOESY	Nuclear Overhauser enhancement spectroscopy
nte	Neuropathy target esterase
OMS	Octamethylcyclotetrasiloxane
p	Probability value
PC	Phosphocholine
PCA	Principal component analysis
pH	Power of hydrogen
pla/b/c/d	Phospholipase A/B/C/D
ppm	Parts per million
PtC	Phosphatidylcholine
PUFA	Polyunsaturated fatty acid
PUI	Polyunsaturation Index
R	Correlation coefficient
RF	Radio frequency
RSD	Relative standard deviation
SCC	Somatic cell count
SD	Standard deviation
SI	Saturation index
SIM	Selected ion monitoring
S/N	Signal-to-noise ratio
SRM	Standard reference material
SVM	Support vector machine
TE	Technical error
TEG	Triethylene glycol
TMA	Trimethylamine
TMAO	Trimethylamine-N-oxide
TMR	Total mixed ration
TMS	Tetramethylsilane
TSP	3-Trimethylsilyl-2,2,3,3-tetradeuteropropionate
wt%	Weight percent

## Glossary

### **BALB/c**

A mouse strain commonly used in laboratory disease models. The name is derived from the name of its original breeder and reads *Bagg's albino*.

### **Biomarker**

A molecule whose concentration in a biological sample can provide information about the physiological status of the organism.

### **C57/BL6**

A mouse strain commonly used for laboratory disease models. The name is derived from the ancestor of the mouse strain, female mouse number 57. The name is usually read as *black six*.

### **Chemical Shift**

The resonance frequency of a nucleus in a nuclear magnetic resonance (NMR) spectrum. Chemical shifts are measured relative to a reference resonance signal from a standard molecule. They are calculated as the frequency difference between the nucleus of interest and the reference nucleus divided by the operating frequency of the spectrometer for a given nucleus, measured in Hertz [Hz]. As the resulting value is rather small, it is usually given in parts per million [ppm].

### **Energy Balance**

The difference between energy from food uptake and energy needed for milk production and basal metabolism in lactating individuals. If the energy balance is negative, the individual uses more energy than it can take up with its nutrition. This status is somewhat comparable to starvation.

### **Heteronuclear**

Involving atomic nuclei of different chemical elements, for example hydrogen-1 ( $^1\text{H}$ ) and carbon-13 ( $^{13}\text{C}$ ) nuclei.

### **Lock**

Calibration of the NMR spectrometer frequency by matching it to a given reference, for example the signal of deuterium oxide contained in the sample.

### **Metabolic Fingerprinting**

The discriminatory analysis of samples based on comprehensive measurements. Instead of using concentration levels of predefined compounds, whole spectra are used. Usually, a metabolite identification step is performed after a fingerprinting analysis to identify the discriminatory spectrum features. The exact definition of this term and the delimitation to targeted profiling are subject to discussion (Nielsen & Jewett 2007; Lindon & Nicholson 2008).

## **Metabolite**

A small molecule that is part of metabolic pathways, for example amino acids and other organic acids.

## **Metabolome**

The entirety of all metabolites associated to an organism (Nielsen & Jewett 2007).

## **Metabolomics**

The comprehensive study of metabolites in an organism in order to gain insight into metabolic status or disease progression (Lindon & Nicholson 2008).

## **Probe Head**

A device containing a sample tube, coils for sending and receiving radio frequency (RF) signals, shim coils and gradient coils. The NMR probe head is mounted at the place of the strongest magnetic field in the magnet.

## **Shim**

The magnetic field homogeneity of an NMR spectrometer at the place of the sample. The homogeneity can be raised by using coils incorporated in the probe head (*shimming*). Inhomogeneous magnetic fields cause bad line shapes in NMR spectra.

## **Targeted Profiling**

The discriminatory analysis of concentration levels of selected compounds in a sample. A prerequisite for this method is the beforehand choice of the analyzed compounds, in contrast to metabolic fingerprinting approaches. The exact definition of this term and the delimitation to metabolic fingerprinting are subject to discussion (Nielsen & Jewett 2007; Lindon & Nicholson 2008).

## **Tuning and Matching**

The sending and receiving coil of an NMR spectrometer work as resonant circuits. The act of changing the circuit's resonance frequency to the resonance frequency of the observed sample is called tuning. Tuning is necessary to get the maximum signal intensity from the receiver coil. Matching means adjusting the impedance of the circuit to the impedance of the respective transmission line. This is necessary to get a maximum energy transmission from the sending coil to the sample. As tuning and matching affect each other, both have to be performed iteratively.

## Abstract

In this thesis, metabolism profiles of different diseases were measured in body fluids and tissues using high-resolution one-dimensional (1D) and two-dimensional (2D) proton ( $^1\text{H}$ ) and carbon-13 ( $^{13}\text{C}$ ) nuclear magnetic resonance (NMR) spectroscopy at natural  $^{13}\text{C}$  abundance. Protocols for measuring and quantifying low-molecular weight organic molecules in urine, milk, plasma, serum and tissue extracts were established and validated by comparison with established analytical techniques such as gas chromatography-mass spectrometry (GC-MS), liquid chromatography-tandem mass spectrometry (LC-MS/MS) and routine methods from clinical chemistry. It was shown that NMR allowed the quantification of small molecules in complex biofluids. A software named QUANTIFY was developed to enable accurate and reliable quantification from NMR spectra by using spectral integrals and additional information on the respective molecules. For 2D spectra and a recording time of 55 minutes, the lower limits of quantification (LLOQ's) were between 78 and 350 micromole per liter [ $\mu\text{mol/L}$ ]. For 1D spectra and a recording time of 15 minutes, LLOQ's as low as 3  $\mu\text{mol/L}$  were observed, although 1D quantification is not applicable to all metabolites due to signal overlap.

Among others, urine specimens obtained from patients with autosomal dominant polycystic kidney disease (ADPKD), and urine and liver samples from mice with non-alcoholic fatty liver disease (NAFLD) and non-alcoholic steatohepatitis (NASH) were investigated. Additionally, milk and plasma specimens from dairy cows suffering from production diseases such as ketosis were analyzed. The focus of the latter analyses lay on metabolic traits connected to lipid synthesis and breakdown. The analyses were performed both in a targeted manner, with selected molecules quantified and compared between diseased and healthy individuals, and in fingerprinting approaches, where whole spectra were used to identify unknown biomarkers for different diseases.

Results show that NMR spectra of biofluids or tissue extracts may be used for the diagnosis of disorders such as NASH and ADPKD, and the prognosis of ketosis in dairy cows. Urinary compounds that distinguish NASH from NAFLD were found to be, among others, citric acid, creatinine, leucine, phenylalanine, phosphocreatine, taurine and trimethylamine-N-oxide (TMAO). For ADPKD, the most striking result was a raised urinary methanol level in the ADPKD patient group. In dairy cows, a high ratio of milk glycerophosphocholine (GPC) to phosphocholine (PC) was found to be associated with a low incidence of ketosis. A hypothesis about the biochemical backgrounds of these compounds in disease progression was created and validated by additional NMR measurements of blood plasma.

## Zusammenfassung

In dieser Doktorarbeit wurden eindimensionale (1D) und zweidimensionale (2D) Protonen- ( $^1\text{H}$ ) und Kohlenstoff-13 ( $^{13}\text{C}$ )-Kernspinresonanz (NMR) verwendet, um Stoffwechselprofile verschiedener Krankheiten in Körperflüssigkeiten und Geweben zu erstellen. Es wurden Protokolle für die Messung und die Quantifizierung von kleinen organischen Molekülen in Urin, Milch, Plasma, Serum und Gewebeextrakten entwickelt. Die Resultate wurden durch Vergleiche mit etablierten Analysemethoden wie Gaschromatographie-Massenspektrometrie (GC-MS), Flüssigkeitschromatographie-Tandemmassenspektrometrie (LC-MS/MS) und Routinemethoden der klinischen Chemie validiert. Es wurde gezeigt, dass NMR die Quantifizierung kleiner Moleküle in komplexen Mischungen wie Urin, Plasma, Serum, Milch und Gewebeextrakten ermöglicht. Für diesen Zweck wurde eine Software namens QUANTIFY entwickelt, die mit Hilfe spektraler Intensitäten und zusätzlicher Informationen über das betreffende Molekül eine genaue und zuverlässige Quantifizierung ermöglicht. Für 2D-Spektren mit einer Aufnahmezeit von 55 Minuten wurden untere Quantifizierungsgrenzen (LLOQ's) zwischen 78 und 350 Mikromol pro Liter [ $\mu\text{mol/L}$ ] beobachtet. Für 1D-Spektren mit Aufnahmezeiten von 15 Minuten wurden LLOQ's bis zu 3  $\mu\text{mol/L}$  beobachtet, wobei allerdings wegen Signalüberlagerungen eine Quantifizierung aus 1D-Spektren nicht für alle Metaboliten möglich ist.

Diese neu entwickelten Methoden wurden auf verschiedene Krankheiten angewendet, untersucht wurden unter anderem Urin von Patienten mit autosomal-dominanter polyzystischer Nierenerkrankung (ADPKD) sowie Urin und Leberproben von Mäusen mit nichtalkoholischer Fettlebererkrankung (NAFLD) und nichtalkoholischer Steatohepatitis (NASH). Zusätzlich wurden Milch und Plasma von Milchkühen mit Produktionskrankheiten wie Ketose analysiert. Schwerpunkt dieser Untersuchungen waren Stoffwechselprodukte aus der Synthese und dem Abbau von Lipiden. Durchgeführt wurden sowohl gezielte Untersuchungen, bei denen die Konzentrationen von ausgewählten Stoffen bestimmt wurden, um Unterschiede zwischen gesunden und kranken Individuen zu finden, als auch „Fingerprinting“-Untersuchungen, bei denen komplette Spektren genutzt wurden um bisher unbekannte Biomarker für verschiedene Krankheiten zu identifizieren.

Die Ergebnisse zeigen dass mit NMR-Spektren von Körperflüssigkeiten und Gewebeextrakten die Diagnose von Krankheiten wie NASH und NAFLD sowie die Vorhersage von Ketose in Milchkühen möglich sind. Für NASH und NAFLD wurden im Urin differenzierende Biomarker gefunden, unter anderem Zitronensäure, Creatinin, Leucin, Phenylalanin, Phosphocreatin, Taurin und Trimethylamin-N-Oxid (TMAO). Bei der Untersuchung von ADPKD war ein unerwartetes Resultat ein erhöhter Methanolspiegel im Urin von ADPKD-Patienten. In Milchkühen war ein hohes Verhältnis der Konzentrationen von Glycerophosphocholin (GPC) zu Phosphocholin (PC) mit einem geringen Ketoserisiko verbunden. Es wurde eine Hypothese zu den biochemischen Mechanismen dieser beiden Stoffe bei der Krankheitsentstehung aufgestellt und durch zusätzliche NMR-Messungen von Plasma bestätigt.

---

# 1 Introduction

## 1.1 Background

Nuclear magnetic resonance (NMR) spectroscopy has become a widely used tool for chemical and biological analyses during the last decades. Originally and mainly used for protein structure determination, it is now increasingly applied to metabolomics. Metabolomics aims at providing a comprehensive overview of all small organic molecules (*metabolites*) of a biologic sample to gain insight into the metabolic status of an organism. This quite new field is part of the so-called *-omics* research family that includes genomics and proteomics (Pearson 2007). Starting from gene variations and gene expression, gene transcription leads to protein synthesis, with the proteins in turn affecting metabolite levels. The combination of these different fields shall give an almost complete insight into the various processes of an organism.

In the following paragraph, some important metabolic processes of an organism will be briefly described according to (Alberts et al. 2001). The energy metabolism includes the metabolic pathways leading to the formation of the energy-carrying molecule adenosine triphosphate (ATP). Most of the ATP is created within the mitochondria, with acetyl coenzyme A (acetyl-CoA) as a starting point for the citric acid cycle. Acetyl-CoA may be derived either from carbohydrates via glycolysis, from fatty acids via beta-oxidation or from amino acids from protein breakdown. Acetyl-CoA, on the other hand, is also the starting product for fatty acids synthesis in the cytosol. Amino acids are synthesized in the cytosol by amination of  $\alpha$ -keto acids stemming from glycolysis or the citric acid cycle, for example by glutamic acid. Nucleotide synthesis is a quite complex process taking

place in the cytosol with partial mitochondrial involvement. Here, amino acids, sugars and organic acids are involved.

Techniques used for metabolomic analyses include many varieties of chromatography and mass spectrometry (MS) methods. Generally, these “classical” metabolomics methods have a high sensitivity, which means their lower limits of quantification (LLOQ’s) are lower than those of NMR. For gas chromatography-quadrupole mass spectrometry (GC-MS) in selected ion monitoring (SIM) mode, LLOQ’s have been found in the range of 0.3 - 30 micromole per liter ( $\mu\text{mol/L}$ ) for free amino acids (Kaspar et al. 2008). On the other hand, derivatization and column selection narrow the nature of compounds amenable to analysis. Unknown or unexpected biomarkers may therefore be missed. Here, NMR can provide a more comprehensive picture as only little sample pretreatment is required and the whole range of organic molecules is accessible within one measurement (Lindon et al. 2006; Lindon & Nicholson 2008; Wishart 2008). Additionally, it has been shown that when analyzing the same sample set using MS and NMR, only little overlap between the metabolites identified with both methods occurs (Wishart et al. 2008). Hence, NMR is an important tool as it will show other aspects of a sample than other techniques (Blow 2008). An additional advantage of NMR is that the sample is not destroyed during the measurement, and thus can be further analyzed using other methods after the NMR measurement.

The simple sample preparation for NMR measurements, in combination with automated measuring and data processing routines, paves the way for high-throughput analyses, where hundreds or even thousands of samples can be analyzed, giving a broad base for statistical analyses.

## 1.2 Motivation and Specific Aims

Several questions are posed in this thesis. These are described in the following in terms of specific aims.

The first specific aim is to elucidate whether reliable quantification can be performed using NMR spectra of complex biofluids. Quantification in one-dimensional (1D) spectra is hampered by the large number of signals present in a typical spectrum, leading to overlapped signals. Intensity values from two-dimensional (2D) spectra have the drawback that different signals show different intensities even when equal concentrations are observed. This aim shall be pursued using a test set of urine and milk samples that shall be measured in parallel by established methods to allow for a comparison.

The second specific aim is to identify whether the metabolic status of an individual gives rise to a distinct change in its body fluid composition, and if this change is within the scope of the used measurement techniques. This could be used for diagnostic purposes. This question shall be first elucidated using mice as a model organism for non-alcoholic steatohepatitis (NASH), and later on extended by using urine specimens obtained from human autosomal dominant polycystic kidney disease (ADPKD) patients.

The third specific aim is whether biofluid samples allow the prediction of diseases in dairy cattle. To answer this question, time series of samples and complete medical records in the follow-up after sample collection are needed. For this reason, time series of milk, plasma and urine specimens were collected for more than 300 dairy cows.

This thesis has in parts already been published (Gronwald et al. 2008; Gronwald et al. 2011; Klein 2007; Klein et al. 2010; Klein et al. 2011a; Klein et al. 2011b; Kohl et al. 2011) and was funded by the Bavarian Genome Network BayGene of the Bavarian State Ministry of Sciences, Research and the Arts (Munich, Germany), the Fugato-plus MeGA-M program of the German Federal Ministry of Education and Research (Berlin, Germany) and the intramural ReForM program of the Regensburg School of Medicine (Regensburg, Germany). All persons named in the thesis are with the Institute of Functional Genomics of the University of Regensburg (Regensburg, Germany) unless stated otherwise.

---

## 2 Method Development

### 2.1 Basics of Nuclear Magnetic Resonance

Nuclear magnetic resonance (NMR) is a spectroscopic method able to give a comprehensive overview of the most abundant organic compounds in a sample employing one measurement (Nicholson & Lindon 2008). It is based on the magnetic moment caused by the spin of atomic nuclei. A spin is a concept from quantum mechanics that can be described using similar equations as an angular momentum. For a better understanding, one might think of the atomic nucleus as a sphere that is rotating around an axis that goes through its center of gravity. This rotation is called spin. Far from all atomic nuclei possess a spin, atoms with nuclear spins include hydrogen-1 ( $^1\text{H}$ ), deuterium, carbon-13 ( $^{13}\text{C}$ ), nitrogen-14, nitrogen-15 and phosphorus-31 ( $^{31}\text{P}$ ), amongst others.

A rotating electrically charged particle creates a magnetic field along its rotation axis, and the particle gets a magnetic dipole moment  $\mu$ . In an outer magnetic field  $B_0$ , the particle then has the energy

$$E = -\vec{\mu} \cdot \vec{B}_0$$

To reach their lowest energy, all particles should align along the outer field, comparable to a compass needle that aligns with the earth's magnetic field.

When coming to particles on atomic scales, one observes a different picture. In an outer magnetic field, measuring the spin orientation along the magnetic field lines will show that all particles are aligned either parallel or anti-parallel along the magnetic field, as seen in Figure 1 (Klein 2007).

The reason for this behavior is called energy quantization. This idea from quantum mechanics assumes that not all energy states are possible, rather that only a few defined energy states are allowed.

All elementary particles have a property called spin ( $s$ ) that can take the values  $0, \frac{1}{2}, 1, \frac{3}{2}, 2, \frac{5}{2}$  and so on. Depending on its spin, a particle can have different spin quantum numbers  $s_z$ . Possible values for  $s_z$  are  $-s, -s+1, \dots, s-1, s$ . A particle with spin  $s = \frac{1}{2}$ , such as a proton, can therefore be only in one of two states: Either  $s_z = -\frac{1}{2}$  or  $s_z = \frac{1}{2}$ . This property can be visualized as a clockwise or an anti-clockwise rotation, as shown in Figure 1 (Klein 2007). The two possible states of a spin explain the alignment pattern observed in an outer magnetic field. The two states are usually called *spin down* and *spin up*.

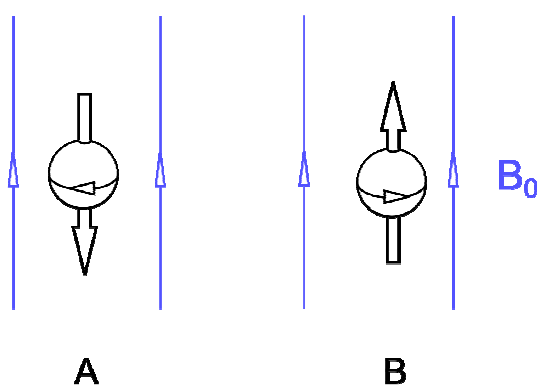


**Figure 1.** Atomic nuclei with spin  $\frac{1}{2}$  in an outer magnetic field  $B_0$  (blue lines).

A: Clockwise rotation is called *spin down*; B: Anti-clockwise rotation is called *spin up*.

Shown is the projection to the axis of the outer magnetic field. Adapted from (Klein 2007).

Without an outer magnetic field, the two spin states have the same energy, this is called degeneration. As the states have the same energy, none of them will be preferred, so the two states will be observed equally often. When placed in a magnetic field, the two spin orientations will have different energies, as seen in Figure 2 (Klein 2007).

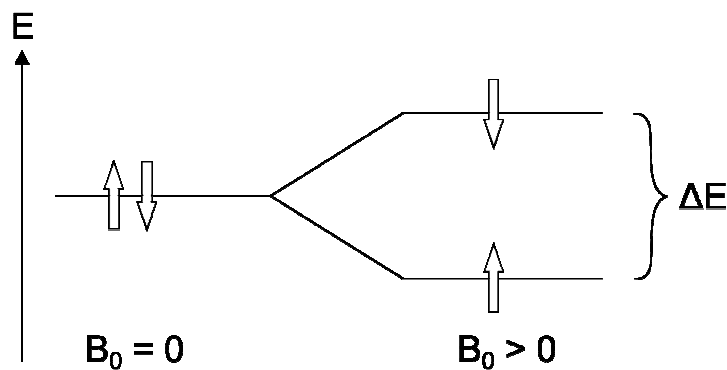


**Figure 2.** An energy difference occurs between the two spin states when placed in an outer magnetic field  $B_0$ . Abbreviation: E: Energy,  $\Delta E$ : Energy difference.

Adapted from (Klein 2007).

In this case, the state with lower energy is preferred, and under ideal conditions all particles will be in the lower energy state. In reality, both states are populated due to thermodynamic effects as described by the Boltzmann equation:

$$\frac{n_h}{n_l} = e^{-\frac{\Delta E}{k_B T}}$$

where  $n_h$  is the number of particles in the higher state,  $n_l$  is the number of particles in the lower state,  $\Delta E$  is the energy difference,  $T$  is the temperature and  $k_B$  is the Boltzmann constant. The energy provided by thermal motion may be sufficient to raise particles into their higher state, depending on the temperature and the energy difference. For atomic nuclei, the energy difference between the different states is very low compared to the thermal energy. Therefore the occupation number of the two states is almost identical under equilibrium conditions. Depending on the magnitude of the outer magnetic field  $B_0$ , temperature and energy difference, the number of particles in the two states differ only by a ratio of approximately  $10^{-5}$  for protons at room temperature. Therefore, NMR experiments always have a problem of relatively low sensitivity compared to other spectroscopic methods, as only this small fraction of all nuclei can be detected. The excess of protons in the lower spin state results in a bulk magnetic field in the sample parallel to the outer magnetic field. The bulk magnetic field is called magnetization.

To raise a particle into the other spin state, one has to transfer the matching amount of energy; this can be done using electromagnetic waves (Purcell et al. 1946). This effect is called absorption and is shown in Figure 3A (Klein 2007).

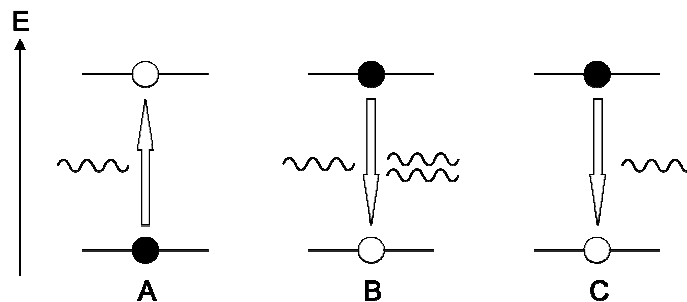


**Figure 3.** Possible state transitions in a two-state spin system.

A: Absorption; B: Induced emission; C: Spontaneous emission. Abbreviation: E: Energy  
Adapted from (Klein 2007).

The energy difference between the states of a proton can be described as

$$\Delta E = \mu_N g B_0$$

where  $\Delta E$  is the energy difference,  $\mu_N$  is the nuclear magneton,  $g$  is the Landé factor of the proton and  $B_0$  is the magnitude of the outer magnetic field.

The matching frequency of the electromagnetic wave and the energy difference are connected in the equation

$$\Delta E = hf$$

where  $\Delta E$  is the energy difference,  $f$  is the frequency of the electromagnetic wave and  $h$  is the Planck constant.

### Pulse Fourier Transformation NMR

To measure the spectra, NMR instruments use the so-called pulse Fourier transformation technique. A short, high-power radio frequency (RF) pulse containing many frequencies is applied. The magnetic field of the RF pulse is called the  $B_1$  field. The  $B_1$  field causes the spins to rotate by a certain angle (Figure 4B). For maximal effect a rotation by  $90^\circ$  is preferable. After the RF pulse, the bulk magnetization is no longer aligned with the outer magnetic field  $B_0$  and the magnetization vector starts a precession movement around the magnetic field direction (Figure 4C).

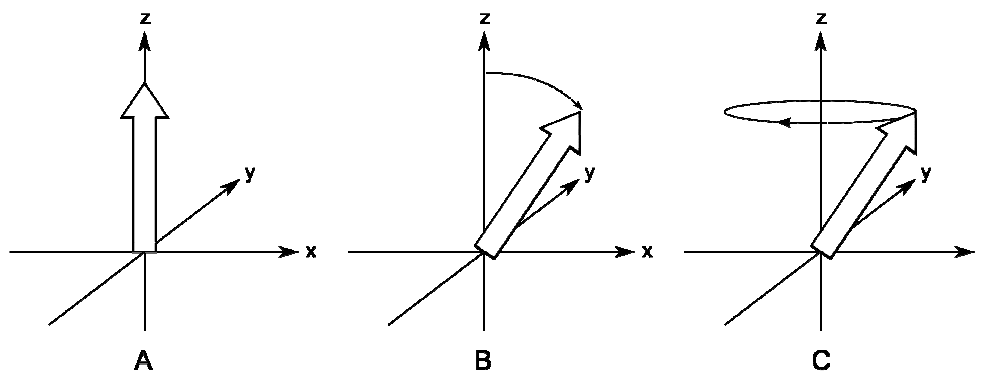


**Figure 4.** Scheme of a pulsed NMR experiment.

A: Bulk magnetization of all spins in the sample in thermal equilibrium is parallel to the outer magnetic field  $B_0$  along the z-axis.

B: An on-resonance RF pulse rotates the magnetization vector around the y-axis.

C: The magnetization vector precesses around the outer magnetic field vector  $B_0$  along the z-axis.

The magnetization precession movement induces a voltage in the receiver coil of the spectrometer (Bloch 1946). This time-dependent signal called free induction decay (FID) is recorded and turned into a frequency-dependent spectrum by a Fourier transformation.

Simultaneously with the precession movement, the spins want to return into the equilibrium state described by the Boltzmann equation above, and start moving toward the z-axis. This process is called relaxation and is usually catalyzed by interactions with other electromagnetic fields in the surrounding. Different mechanisms may lead to relaxation. One mechanism is called  $T_1$  relaxation and is caused by interactions between the spin and the surrounding lattice.  $T_1$  relaxation causes the magnetization vector to grow in the z-axis. The second important relaxation process is called  $T_2$  relaxation and is caused by interactions between neighboring spins.  $T_2$  relaxation causes the magnetization

vector to diminish in the x-y-plane. In the end, the vector is completely aligned along the z-axis. As only a precession around the z-axis can induce measurable voltages in the receiving coil, this effect reduces the NMR signal drastically. Usually the  $T_2$  relaxation is faster than the  $T_1$  relaxation. A third relaxation mechanism is relaxation due to magnetic field inhomogeneities ( $T_2^*$  relaxation).

During the return to the equilibrium magnetization, radiation may be emitted in two different ways. The first way is spontaneous emission (Figure 3C). This is a stochastic process and can be described with a half-life period. Spontaneous emission, however, is an unlikely process concerning the energy differences present in NMR. The far more common way of emitting radiation is induced emission (Figure 3B). This is triggered by the irradiation with waves matching the energy difference. The fluctuating magnetic field of the matrix, e.g. caused by water molecules, is a common source for induced emission. When a radio signal is applied to a sample, spins will get raised into the upper energy state by absorption. As the number of spins in the upper state rises, more and more induced emission will occur, moving the spins to the lower energy state. Using long irradiation times, at some point equilibrium between absorption and induced emission is reached, this is called saturation. In saturation, no signal from the spins can be measured.

Please note that although the explanations for NMR effects given above are widely adopted and seem reasonable at first sight, they fail to explain all effects observed in NMR experiments. Instead of thinking of absorption and emission of real photons, NMR effects have been shown to be consistent with effects of zero energy *virtual photons* in the near field of the sample (Hoult & Ginsberg 2001). This concept goes too far into quantum electro dynamics to be presented in the scope of this thesis, though.

### Chemical Shift

The energy difference between two spin states is proportional to the magnetic field at the nucleus. Therefore, local changes of the outer field cause shifts in the resonance frequency of the nucleus. These local magnetic field aberrations can be caused by nearby electrons and are thus specific for the molecule in which the nucleus is located. This effect is shown in Figure 5 for a one-dimensional (1D) spectrum. The resulting resonance frequency of a nucleus is called *chemical shift*.

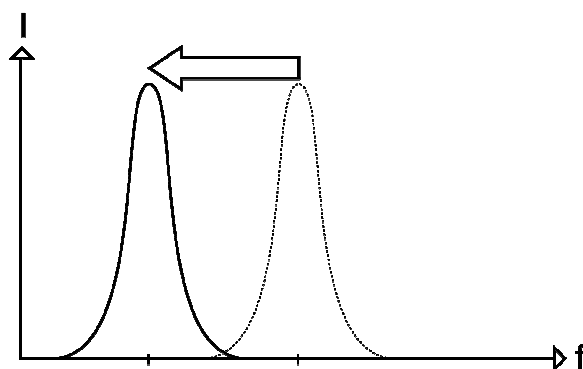


**Figure 5.** Shifting of the signal due to local magnetic field distortions.

Abbreviations: f: Frequency; I: Intensity

## Coupling

When a nucleus with a spin is located near another nucleus carrying a spin, it may interact or *couple* with this spin. One important way of coupling is the indirect dipole-dipole coupling, also called *J-coupling*. J-coupling is mediated by the electron bonds connecting the two nuclei.

Consider two spins, spin A and spin B, who are neighbors in a molecule. When measuring the resonance frequency of spin A, spin B can be either in state *spin up* or in state *spin down*. Spin B has a small magnetic field due to its electric charge. This small field adds to the (stronger) outer magnetic field. Depending on the direction of spin B, the magnetic field at the location of spin A is either strengthened or weakened. The resonance frequency of spin A is proportional to the strength of the outer magnetic field. Therefore spin A may either have an increased or a decreased resonance frequency, depending on the direction of spin B. In a real sample, the considered molecule will be present many times, in each of which spin B will have either direction, on average at almost the same rate. Therefore, both the increased and the decreased resonance frequency of spin A will show up in the NMR spectrum. This results in a splitting of the signal of spin A into two signals, each having a lower intensity than the original signal (Figure 6). The same considerations are true for spin B, so the signal of spin B will be split in the same manner.

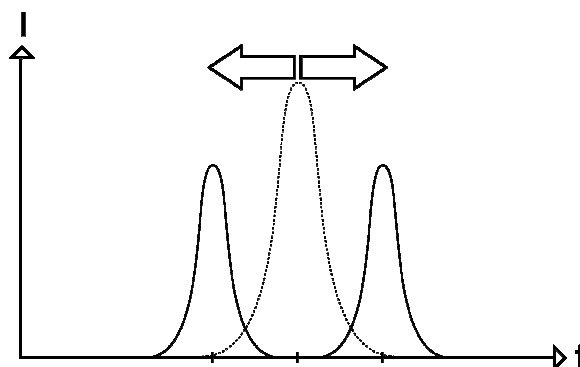


**Figure 6.** Splitting of a signal due to coupling to spins in the nuclear surrounding of the particle.  
Abbreviations: f: Frequency; I: Intensity

J-coupling is scalar, which means it is not dependent on the spatial orientation of the two neighboring spins. The coupling constant  $J$  is the distance between the two signals measured in Hertz (Hz).

The second important coupling mechanism is dipolar coupling that couples two spins directly without mediating electrons. Dipolar coupling depends on the orientation of the vector connecting the two nuclei. In freely moving molecules, the dipolar coupling is averaged out as every orientation has the same likelihood. Dipolar coupling is not visible in the NMR spectrum in this case, but still acts as a relaxation mechanism. In case where the movement or rotation of the molecules is restricted, the dipolar coupling may be visible in the spectrum.

Signal splitting due to coupling may occur simultaneously and repeatedly for each nucleus. Coupling mechanisms may lead to different coupling patterns. A signal that is

not coupled will show a single, sharp line called *singlet*, a signal showing a two-peak pattern is called a *doublet*, a signal with three peaks is called a *triplet* and so on. Signals with a large number of peaks are called *multiplets*.

Most organic molecules will have several protons, each of which will undergo shifting and coupling. This creates a characteristic NMR spectrum for each molecule. This fact renders NMR a valuable tool for analytic purposes and for molecular structure determination. Please note that NMR signals of an acid and its salt usually cannot be distinguished.

### Multidimensional Experiments

The use of RF pulses allows the combination of several pulses in one experiment. Usually, a program of several pulses is repeated several times with different increments of the delay time between two of the pulses. This yields a matrix of data points in the time domain. These are transformed to the frequency domain by a double Fourier transformation (one for each dimension axis).

Magnetization can be transferred from one nucleus to a neighboring nucleus. This can be used for measuring nuclei with a low sensitivity indirectly by measuring the magnetization transferred to a more sensitive nucleus. An example for this sensitivity gain is the indirect measurement of  $^{13}\text{C}$  spectra using more sensitive  $^1\text{H}$  spectra. Magnetization transfer also allows the elucidation of molecule structure, as the intramolecular distance between different nuclei can be estimated. Two-dimensional (2D) NMR spectra are usually displayed in a map-like style, where lines mark areas of equal intensity. As in a geographic map, narrow lines indicate steep signal increases, whereas large distances between the lines indicate only low intensity changes. In the following paragraphs, some standard multidimensional experiments are briefly explained.

#### NOESY

The nuclear Overhauser enhancement spectroscopy (NOESY) experiment, which is measured mostly in a multidimensional fashion, is based on the nuclear Overhauser effect (NOE). It is caused by dipolar couplings. These are interactions between neighboring spins that are mediated through space, and not through electron bonds. The NOE describes the fact that spins are raised into the upper energy state through cross-relaxation when a neighboring spin is saturated (Overhauser 1953). This may be utilized to enhance the sensitivity of the measurement of one proton by saturating the neighboring proton. Another application of NOESY makes use of the through-space nature of the NOE to gain information about the spatial conformation of a molecule (Berger & Braun 1998). In addition, the first increment of a 2D NOESY sequence is often used for the measurement of 1D spectra, because it offers enhanced suppression of unwanted resonances such as the strong water signal (Nicholson et al. 1995).

#### CPMG

The Carr-Purcell-Meiboom-Gill (CPMG) experiment is used to measure 1D spectra without disturbing signals from macromolecules such as proteins. The experiment is named after its developers. CPMG experiments utilize the fact that large molecules have faster spin relaxation than small molecules due to the higher number of neighboring spins

enabling spin-spin interactions. To reduce the contribution of macromolecules to the recorded FID, the start of the recording is delayed by a filtering period. After the filtering period, the RF signals from macromolecules have decayed, while signals from small molecules are still present at noteworthy intensities, leaving a spectrum of small molecules. The length of the filtering period is defined by the number of waiting loops.

### **HSQC**

In a heteronuclear single quantum coherence (HSQC) experiment, magnetization is transferred from the excited nucleus to a neighboring nucleus of another chemical element that is connected by an electron bond. This nucleus is called the indirect nucleus. After a waiting period, the magnetization is transferred back to the original (direct) nucleus. Variations in the time before the retransfer are used to create a second dimension axis. In these spectra, the frequency of the directly excited nucleus is connected to the frequency of the indirect nucleus by a cross peak (Berger & Braun 1998).

### **HMBC**

The heteronuclear multiple bond correlation (HMBC) experiment is quite similar to the HSQC experiment, apart from the magnetization being transferred to the indirect nucleus over more than one electron bond. In a HMBC spectrum, the frequency of the direct nucleus is connected to the frequency of the indirect nuclei that have a distance of two or more electron bonds (Berger & Braun 1998). This fact can be used as complementary information for molecule structure elucidation.

## The Used Spectrometer

The instrument used in this thesis is an Avance III spectrometer (Bruker BioSpin, Rheinstetten, Germany) and is shown in Figure 7. The spectrometer has an operating frequency for protons of 600 megahertz (MHz), corresponding to a magnetic field strength of 14.1 Tesla.



**Figure 7.** The 600 MHz Avance III cryo probe spectrometer with a cooled automatic sample changer was used for all NMR measurements in this thesis.

The magnetic field is created by a superconducting magnet cooled by liquid helium, the helium Dewar in itself is cooled by liquid nitrogen to reduce helium evaporation loss. The magnet is surrounded by a magnet of inverse polarization to reduce (*shield*) the magnetic field outside of the instrument. The probe head is a so-called triple-resonance head and contains emitter/receiver coils for the frequencies of three different nuclei:  $^1\text{H}$ ,  $^{13}\text{C}$  and  $^{31}\text{P}$ . These coils are cryogenic, this means they are superconducting and are cooled by a flow of cooled helium gas. The use of superconducting coils can lower electronic noise tremendously and enables faster measurements at the same signal-to-noise (S/N) ratio. Additionally, the probe head has a coil for the deuterium resonance frequency for frequency calibration (so-called locking) purposes. A coil to produce magnet field gradients along the z-axis is implemented. It can be used for de-phasing and, thus, reducing the disturbing solvent signal. The probe head has a bore for 5-millimeter diameter glass tubes that are held at 298 Kelvin (25 degrees Celsius ( $^{\circ}\text{C}$ )) by a flow of heated compressed air. The spectrometer is equipped with a sample changer for around 500 sample tubes to enable automated measurements of large sample quantities. The samples are cooled to 4  $^{\circ}\text{C}$  as long as they are in the sample changer to minimize sample degradation.

## 2.2 Alternative Methods

To confirm the results obtained by NMR, selected samples were measured by other common metabolomics techniques for comparison reasons. These techniques are briefly described in the following paragraphs.

### Mass Spectrometry

Mass spectrometry (MS) uses the fact that charged particles change their velocity and/or direction when they are placed in an electric field. The magnitude of this effect depends on the charge and the mass of particle and can thus be used to calculate the mass-to-charge ratio ( $m/Q$ ) of this particle. Technically, the particles are vaporized and ionized and then led into an electric field. Many organic molecules have identical  $m/Q$  values, though. Therefore, in metabolomics, MS spectrometers are usually coupled to some sort of separation apparatus like liquid chromatography (LC) or gas chromatography (GC) to reduce the number of simultaneously analyzed substances (Grob & Barry 2004).

### Tandem Mass Spectrometry

In tandem mass spectrometry, two mass spectrometry measurements are combined in one experiment. This can be done using two separate yet coupled mass spectrometers or using one mass spectrometer to perform two measurements that are separated in time. Usually, the first MS run separates the molecules based on their  $m/Q$  ratios, then the molecules are fragmented by chemical or physical means, and then the fragments are separated in the second MS run. As fragmentation follows specific chemical rules, the fragments can give more detailed information about the molecule they originate from (Grob & Barry 2004). Also tandem mass spectrometry may be combined with additional separation methods.

### Liquid Chromatography

LC is a commonly used separation method. It is based on the fact that different molecules will travel through a substrate at different speeds, depending on adhesion effects of the substrate. The analyzed liquid is therefore led through a column that has an inner coating or a packing with the desired adhesion properties. At the end of the column, the different molecules of the mixture will elute at different time points, this can be used for identification of the molecules (Cammann 2000). A tandem mass spectrometry system may be coupled to the end of the column to further analyze the eluting molecules. This is called liquid chromatography-tandem mass spectrometry (LC-MS/MS).

### Gas Chromatography

GC is a separation method that has much in common with LC. It does not operate with molecules in the liquid or aqueous phase though, but needs to evaporate the molecules to the gas phase. This is done by heating the sample using a predefined temperature program, commonly including periods of rising temperature and periods of constant temperature. The evaporated molecules are transported through a column with an adhesive inner coating by a carrier gas, usually helium. Commonly used column lengths are around 15 meters, with diameters of 0.25 millimeters (Kaspar et al. 2008). As not all molecules can be evaporated, a derivatization step is performed before the analysis. In this step the molecules are adapted in a way to enable evaporation (Grob & Barry 2004). To allow further separation, for example of enantiomers, two columns with different

properties can be coupled (Waldhier et al. 2011). GC may also be used in connection with MS analyses of the eluting fractions, this technique is called gas chromatography-mass spectrometry (GC-MS). GC-MS allows hundreds of metabolites to be identified and quantified in a single run (Almstetter et al. 2009).

## 2.3 Data Analysis

### Technical Errors

To assess the measurement precision, NMR experiments were performed in duplicate and the technical errors (TE's) were calculated according to the following equation:

$$TE = \sqrt{\frac{\sum_{i=1}^n (x_{i,1} - x_{i,2})^2}{2n}}$$

where n is the number of samples that were measured in duplicate, and  $x_{i,1}$  and  $x_{i,2}$  are the first and second measurement of a specific sample, respectively.

### Bland-Altman Plots

A Bland-Altman plot (Bland & Altman 1986) is a graphical model, also known as Tukey mean difference plot that is used to analyze the agreement between two experimental methods. The difference  $y_n$  between the value  $x_0$  obtained by method #1 and the value  $y_0$  obtained by method #2

$$y_n = x_0 - y_0$$

is plotted for each sample against the average  $x_n$  of the two methods

$$x_n = \frac{x_0 + y_0}{2}$$

to allow a visual inspection of the differences between the methods.

### P-Values, T-Tests and ANOVA

To assess whether two or more groups of individuals differ in their properties, different analysis methods may be used. If concentration values are known for the compounds of interest in a targeted profiling approach, or bin integral values are known in a fingerprinting approach, one of the most common approaches is calculating p-values. A p-value is a probability value that measures how likely it is that the observed groups have the same properties on average. The hypothesis that the groups have the same properties is called the null hypothesis. Groups stemming from the same overall distribution will have slightly different properties due to statistical fluctuations, and due to the limited number of observed group members. A p-value may take all values between zero and one. Low p-values indicate that it is unlikely that the groups share the same medium properties. This means that the null hypothesis may be rejected.

To decide whether a calculated p-value indicates differences between the observed groups, significance levels may be defined. This can be based on arbitrarily chosen levels, such as the commonly used levels  $p \leq 0.05$  (so-called *significant* differences) and  $p \leq 0.001$  (so-called *highly significant* differences).

P-values may be calculated by different approaches having different prerequisites concerning the kind of distributions observed (Gaussian or non-Gaussian), means, standard deviations, number of observed groups, and so on. The choice of the approach depends on the observed problem.

The most common way to compare two groups is Student's t-test. This test compares means and standard deviations of the groups. The test has as prerequisites that only two groups may be compared and that the observed variable is normally distributed. The test was calculated as a two-sided test, which means that it was tested both whether group one has a higher or a lower mean than group two. Unequal standard deviations for the two groups were assumed.

In case more than two groups shall be compared, an analysis of variance (ANOVA) test may be used. ANOVA tests whether all groups share the same mean and variance, or whether one or more groups differ from the others. Anyway, ANOVA does not tell which group or groups differ from the rest. Thus, a significant ANOVA result has to be further analyzed to identify the group or groups differing from the other groups. This might be done by pairwise comparing all groups using Student's t-tests. In this thesis, single factor or one-way ANOVA was used. In this test, the groups may be described by a single factor or variable, for example one individual may either be in group #1, #2 or #3, resulting in the value of the variable being one, two or three. In this setting, an individual can never be in group #1 *and* group #3 at the same time. An example for this case would be an individual suffering from two distinct diseases at the same time.

### **False Discovery Rate**

Low p-values do not guarantee actual differences between groups, as they can also result from random fluctuations. This is a cause of error especially when p-values are calculated for many different variables of the same data set. This is called the problem of multiple testing. Although these "false" significances cannot be avoided, it is possible to estimate the number of "true" and "false" significant results. One way to do this is the false discovery rate (FDR) according to (Benjamini & Hochberg 1995).

This method is based on the distribution of p-values calculated from one data set. In case of randomly chosen groups, p-values should be equally spread over the whole range from zero to one. In case real differences exist between the groups, more p-values will be observed in the low range than in the mid and high range. This is used to estimate the number of erroneously classified significant differences within a selected range of p-values. For example, when using all p-values below 0.05, this may correspond to an FDR of 13 %, depending on the data set, indicating that 13 % of the variables with p-values below 0.05 are not significantly different in fact. Another possibility is to set the FDR to a desired value, for example 5 %, and to calculate the p-value below which this FDR is fulfilled.

### **Odds Ratios**

Odds ratios can be used to investigate whether two groups of individuals differ in their rates of developing certain diseases (Cornfield 1951). The odds ratio takes values between 0 and infinity. Values larger than one indicate that the first group has a higher disease risk, values smaller than one indicate a lower disease risk for the first group and a value of one indicates equal disease risks. The odds ratio was calculated as

$$\text{Odds ratio} = \frac{n_1 \cdot n_4}{n_2 \cdot n_3}$$

where  $n_1$  is the number of diseased individuals in the first group,  $n_2$  is the number of diseased individuals in the second group,  $n_3$  is the number of healthy individuals in the first group and  $n_4$  is the number of healthy individuals in the second group.

### Normal Distributions

To test whether a distribution is a normal (Gaussian) distribution, the Lilliefors-Kolmogorov-Smirnov-test may be used (Lilliefors 1967). This test has as a result the p-value for the null hypothesis that the underlying distribution is Gaussian. Gaussian distributions were fitted to distributions of real data using the mathematical software Origin (OriginLab, Northampton, MA, USA).

### Correlation Coefficients

To gain information which metabolites are connected with each other in their synthesis or degradation, correlation analyses can give important information. A compound is said to be correlated with another compound, if their concentrations both show high respective low concentrations in the same samples. A common measure of correlations is the correlation coefficient (R). A correlation coefficient is a value in the range between -1 and 1, with values close to -1 or 1 indicating a high correlation.

The most common correlation coefficient is Pearson's R (Köhler et al. 2002). It compares the covariance of the measured values of a variable. Although commonly used, it is prone to outliers as it uses the measured values directly. It is only able to detect linear correlations. The squared Pearson correlation coefficient  $R^2$  is often used to describe the proportionality of a set of paired variables.

A more robust measure is Spearman's R, named after its developer Charles Spearman (Spearman 1904). It is calculated as Pearson's R with the exception that it uses the ranks instead of the absolute values. This makes it robust against outliers and enables to detect not only linear correlations, but also other monotonous dependencies, such as exponential correlations.

Pearson and Spearman correlation coefficients were calculated using Excel 2007 (Microsoft, Redmond, WA, USA). For each correlation coefficient, a matching p-value can be calculated based on the number of samples used. For large sample numbers, even small correlation coefficients may be significant, whereas in low sample numbers even very large correlation coefficients may not be a sign for a significant correlation.

### Partial Correlation Coefficients

To check that high correlations are really due to direct correlations, and not due to a third variable that is correlated to both variables, partial correlation coefficients were calculated in an approach similar to that suggested by (de la Fuente et al. 2004). Partial correlation coefficients were calculated using the statistical programming language R and the function *pcor.test* available at <http://www.yilab.gatech.edu/pcor.html>.

For all pairs of significantly correlated variables, common variables showing significant correlations to both variables were searched. For each of these a first-order partial correlation coefficient and the corresponding p-value were calculated. If the p-value of a first-order partial correlation was above the significance level, this pair of variables was removed from the list of significantly correlated pairs. For all pairs of variables that were still marked as significant after all first-order-calculations, second-order calculations were performed for all possible pairs of common significant variables. If the p-value of a second-order partial correlation was above the significance threshold, this pair of variables was removed from the list of significantly correlated pairs. By using this approach, many high correlation coefficients were marked as non-significant. It shall be noted that this approach is rather conservative and will exclude many “true” correlations in order to reduce the number of false positive correlations. The R code for the calculation of partial correlations can be found in Appendix II.

### **Metabolic Networks**

Correlations between metabolites are created when two metabolites are closely neighboring in the underlying metabolic network. Partial correlation coefficients are a first step into the deduction of the structure of the underlying metabolic networks, although to gain a real insight into the network, measurements of the undisturbed status are not sufficient, but an interventional step is necessary, for example the administration of labeled substances, to be able to analyze the induced change propagating through the metabolic network (Fan et al. 2009).

### **Hierarchical Clustering and Heatmaps**

Hierarchical clustering is a method to divide samples into clusters in which the samples have similar properties. The clusters are created in a pairwise manner and then each of them is subdivided into a new pair of clusters and so on, until the “lowest” clusters contain one sample each. Hierarchical clustering is a so-called unsupervised algorithm. An unsupervised algorithm has no knowledge about the underlying groups, e.g. whether a sample comes from the healthy or the diseased group. If an unsupervised algorithm identifies the underlying groups within the sample set, this is an indication that strong differences exist between the groups.

Heatmaps are a visualization method for complex data and may be integrally combined with hierarchical clustering methods. Heatmaps show the observed data in a matrix style, with samples as rows and features or metabolites as columns. The intensities or concentrations are represented by a color-code to enable a quick manual inspection. Usually the color coding uses a three-color scheme, with colors for low, medium and high values. This allows for a good visualization of binary distributions.

Heatmaps with hierarchical clustering were generated using the R-package *compdiagTools*. All bin intensities were centered and scaled to unit variance for a better visualization in the heatmap. All R code used for this thesis is attached in Appendix II.

### **Principal Component Analysis**

Principal component analysis (PCA) is another commonly used unsupervised algorithm (Pearson 1901). A PCA defines new axes in the subspace spanned by the measured

variables (metabolite concentrations). The axes are chosen in a way that the first axis lies along the maximal variance observed in the data. The next axis is added orthogonally to the first axis in a way to lie along the highest remaining variance (Abdi & Williams 2010). This process is usually repeated until a convergence criterion is reached, e.g. until 95 % of the variance present in the data are explained by the new axes. As the amount of variance gets lower and lower for each added axis, usually the first few axes are sufficient to explain the structures underlying the data set. The result of a PCA is a set of vectors that define the axes of the calculated principal components. Each vector contains a set of weight factors called loadings. For each spectral bin an individual loading is obtained, which is a measure of the contribution of a specific bin to a given principal component. Plotting the new found axes, group separations may be observed between the groups present in the data set. In this case, identifying the compounds having high loadings will reveal the chemical basis of differences between the observed groups.

Since many compounds have several distinct peaks in an NMR spectrum, they will show up in more than one bin. In turn, a single NMR peak can contain signals from several compounds, which may impede the unambiguous identification of discriminatory compounds.

### **Independent Component Analysis**

Independent component analysis (ICA) is a method similar to PCA. As in PCA, new axes are defined for the subspace spanned by the measured variables. These axes are chosen in way that the variance of the new-defined axes is maximized. Additionally, the independence of the axes is optimized to gain components that are independent of each other. The data have to fulfill some prerequisites, one of these is that the data has to be non-normally distributed. However, the actual distribution does not have to be known. The new axes do not need to be orthogonal to each other as in PCA (Hyvärinen & Oja 2000). Analyses of ICA results are similar to the analysis of PCA results explained above.

It has been shown (Scholz et al. 2004) that ICA often gives more meaningful results than PCA in biological data sets. Anyway, ICA has some drawbacks such as the lack of determining the variance explained by single independent components (IC's), as it is possible in PCA (Hyvärinen & Oja 2000). ICA was performed using the *JADE* (Joint Approximate Diagonalization of Eigen-matrices) algorithm (Cardoso & Souloumiac 1993) available at <http://cran.r-project.org/>.

### **Support Vector Machines**

A support vector machine (SVM) is a so-called supervised algorithm. Supervised algorithms use knowledge about the group membership of the analyzed samples to identify significant differences between groups. As these algorithms always will find group differences, even between randomly chosen groups, cross-validation of the results with an independent set of samples is highly recommended.

An SVM defines a plane that separates the given groups in the multidimensional space spanned by the values of the observed bins, with each bin equaling one dimension. This separating plane is optimized in a manner that it lies in the middle between the nearest points of each group, i.e. that the distances to the nearest point of each group are equal.

The plane's parameters are calculated on a training set of samples. Afterward, unclassified samples can be classified according to their location left or right of the plane. To assess the accuracy of the classification, the original data set is divided into a training set and the remaining samples are used as test samples. The test samples are classified and the amount of correctly and incorrectly classified test samples is saved. This method may be repeated with different combinations of training and test samples, thus allowing the calculation of a mean accuracy.

## 2.4 Quantitative Measurements

As a first step in the analysis of biofluids, protocols for sample preparation and measurements had to be established. Milk is quite complex in its composition, being an emulsion of aqueous and lipophilic parts and containing microscopic structures such as lipid droplets and casein micelles (Töpel 2004). As a more straight-forward way of getting started, protocols were set-up for easier-to-handle urine samples. The suitability of NMR for the analysis of urine has been demonstrated previously (Waters et al. 2002). Parts of this chapter have already been published (Gronwald et al. 2008).

### Issues in Quantifying from NMR Spectra

Biofluids may be very complex in composition containing hundreds to thousands of different compounds even in healthy individuals (Holmes et al. 1997). This in turn leads to an even larger number of signals in the corresponding NMR spectra that results in considerable signal overlap especially when only 1D  $^1\text{H}$  spectra are acquired. As a consequence, the high signal number hampers accurate metabolite identification and quantification considerably. A mathematical solution to this problem is to fit overlapped experimental signals to signals modeled from pure compound spectra (Weljie et al. 2006). Experimentally, spreading the signals over two or more dimensions will also reduce overlap. The advantages of multidimensional NMR have been recognized in several metabolomic studies (Holmes et al. 1997; Adosraku et al. 1994; Tang et al. 2004; Zheng et al. 2007). However, in most instances, multidimensional spectra have been acquired solely for metabolite identification and not for quantification. Only recently, the superior resolution of 2D spectra has been utilized for the quantification of metabolites (Hu et al. 2007; Lewis et al. 2007; Shanaiah et al. 2007). The long acquisition times required in the past for 2D spectra had rendered them impractical for high-throughput metabolomic studies. Further, 2D cross-peak intensities depend on a larger number of different factors, such as structure-dependent coupling values and relaxation times, mixing times, evolution times, and uneven excitation profiles, which must be taken into account when they are used for quantification.

2D  $^1\text{H}$ - $^{13}\text{C}$  HSQC spectra offer the advantage of large signal dispersion in the indirect  $^{13}\text{C}$  dimension. Quantification results for standard metabolite mixtures obtained from 2D  $^1\text{H}$ - $^{13}\text{C}$  HSQC spectra were found to be quite accurate, while using 1D spectra underestimated the actual metabolite concentrations (Lewis et al. 2007). The large signal dispersion can be used to reduce signal overlap, as seen in Figure 8.

In a 1D spectrum, a single peak may contain one or more metabolite signals (Figure 8A). In case several signals are present in one peak, reliable quantification is impossible. In a 2D spectrum, these peaks may be separated in the additional frequency axis (Figure 8B). This should allow a more reliable compound identification.

### NMR Measurements

For each sample, the probe was automatically locked, tuned, matched and shimmed using Topspin (Bruker BioSpin, Rheinstetten, Germany). For shimming, the *topshim* command was used. After a three-dimensional shim run on a urine sample and investigation of the observed line shapes, a shim file containing the obtained shim values was saved. This

standard shim file was used as a starting point for the automated shimming procedure of all other samples. To take magnet field variations that occur due to aging effects of the magnet, this shim file was replaced by an up-to-date file periodically. Each sample was allowed to equilibrate for 300 seconds in the magnet before measurement. The temperature unit was calibrated using a deuterated methanol sample. 1D  $^1\text{H}$  and 2D  $^1\text{H}$ - $^{13}\text{C}$  HSQC spectra of each sample were automatically collected using the automated acquisition suite ICON-NMR (Bruker BioSpin, Rheinstetten, Germany). All spectra were acquired without spinning.

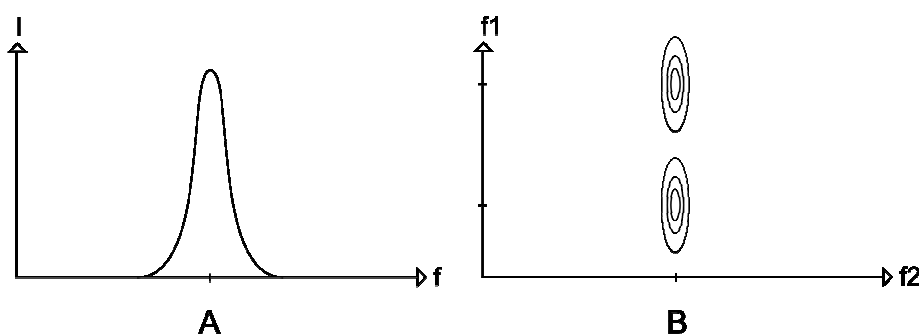


**Figure 8.** Overlap reduction by using multidimensional spectroscopy.

A: A single peak in a 1D spectrum may contain one or more metabolite signals.

B: In a 2D spectrum overlapping peaks can be separated due to their different  $f_1$  frequencies.

Abbreviations:  $f$ : Frequency;  $I$ : Intensity;  $f_1$ ,  $f_2$ : Frequency 1, 2

For each sample, a 1D  $^1\text{H}$  NOESY experiment was recorded. For the 1D spectra, a total of 128 scans was collected into 65536 data points using the pulse program *noesygppr1d* (Bruker BioSpin, Rheinstetten, Germany) with presaturation during relaxation and mixing time for water suppression and additional spoil gradients. A relaxation delay of four seconds, an acquisition time of 2.66 seconds and a mixing time of 0.01 seconds were used. The spectral width was set to 20 parts per million (ppm) for each 1D spectrum and four dummy scans were applied prior to each measurement. These scans were discarded to avoid using data measured before the sample had reached equilibrium conditions. Spectra were automatically Fourier transformed and phase corrected, applying a line broadening of 0.3 Hz and zero filling to 131072 points. A flat baseline was obtained by using the *baseopt* option of Topspin, which performs a correction of the first points of the FID.

It has been shown that metabolite signals are far more separated in the  $^{13}\text{C}$  frequency than in the  $^1\text{H}$  frequency and, thus, using an experiment that employs  $^{13}\text{C}$ -frequencies allows more reliable metabolite identification (Xia et al. 2008). Therefore, a 2D  $^1\text{H}$ - $^{13}\text{C}$  HSQC spectrum was recorded for each sample. For the HSQC spectra, 2048x128 data points were collected with the pulse program *r\_hsqcetgppr* (Bruker BioSpin, Rheinstetten, Germany) using eight scans per increment, a relaxation delay of three seconds, an acquisition time of 0.14 seconds and 16 dummy scans. This resulted in a total acquisition time of 56 minutes per spectrum. The spectral widths were set to 12 and 165 ppm in the proton and carbon dimensions, respectively. Water suppression was achieved using presaturation during the relaxation delay.

For all sample types, additional high-resolution 2D  $^1\text{H}$ - $^{13}\text{C}$  HSQC and HMBC spectra were recorded for representative control samples. The HSQC spectra were collected with 2048x512 data points and 64 scans per increment. For the HMBC spectra, 2048x512 data points and 72 scans were acquired. The total acquisition times for these HSQC and HMBC spectra, which were recorded only once for each sample type, were 15 hours and 25 minutes and 17 hours and 42 minutes, respectively.

### Frequency Adjustment for Water Suppression

For effective water signal suppression it is necessary to adjust the presaturation RF signal, the so-called O1 frequency, to exactly match the resonance frequency of water at around 4.8 ppm. As the change of O1 also causes spectrum baseline distortions, these had to be compensated by adjusting the sixth-order shim coil, the so-called  $z^6$  shim. As the  $z^6$  shim also affects the water resonance signal, these adjustments had to be performed iteratively. For this, first O1 was adjusted to match the maximum position of the water signal of a urine sample. Then, the symmetry of the residual water signal was checked. Depending on the kind of deviation (higher signals left or right of the O1 frequency), the  $z^6$  shim had to be raised or lowered. After this, O1 had to be readjusted. This procedure was repeated until a symmetric residual water signal was observed. While the O1 frequency is part of the acquisition parameters and is stored in the experiment files, the  $z^6$  is stored in the shim file. The O1 frequency had to be readjusted due to magnetic field changes in the magnet on average once a year.

### Spectrum Processing

To transform the time-dependent FID into a frequency-dependent spectrum, Fourier transformation was performed using Topspin. In Fourier transformation, the intensities and phases of the corresponding frequencies are calculated. Due to reasons such as the delay between the RF pulse and the start of the measurement, the phase usually cannot be calculated in the right way and has to be corrected. For 1D spectra, Topspin offers automated phase correction algorithms. These spectra were inspected by eye for correct phase correction. In a few cases with strongly diluted samples, the automatic routine had problems with phase correction, possibly due to the fact that negative artifacts of the suppressed water signal dominated these spectra. Usually, a phase error of  $180^\circ$  was observed in these cases. These samples were phase corrected manually. Software scripts were developed in the programming language *Python* to facilitate additional processing of the raw data. These scripts can be found in Appendix II. All 1D samples were baseline corrected using a third-order polynomial. 2D spectra were semiautomatically processed employing a  $90^\circ$  shifted squared sine-bell window function in both dimensions. For increased resolution in the indirect carbon dimension, the number of data points was doubled prior to Fourier transform using complex forward linear prediction. Due to difficulties in peak picking, caused by residual J-couplings that lead to signal splits, the resolution of the  $^1\text{H}$ -frequency was reduced to 50 %, yielding 1024 data points, in the processing parameters. All 1D and 2D spectra were chemical shift referenced relative to the reference substance signal. As Topspin failed to set the  $^{13}\text{C}$ -frequency of the reference signal to zero in many cases, the  $^{13}\text{C}$ -frequency was corrected using the  $^1\text{H}$ -frequency of the reference signal to calculate the matching  $^{13}\text{C}$ -frequency. All 2D spectra were manually phase corrected in both dimensions and a fifth-order polynomial baseline correction was applied excluding the region around the water artifact.

## 2.5 Measurement of Urine Specimens

### Sample Preparation

100 milliliter (mL) of 0.1 mole per liter (mol/L) potassium phosphate buffer (pH 7.4) was prepared by adding 8.02 mL of 1 mol/L of aqueous potassium hydrogen phosphate solution to 1.98 mL of 1 mol/L of aqueous potassium dihydrogen phosphate solution and filling up to 100 mL with pure water. Finally, 30 milligram (mg) of boric acid was added to prevent bacterial growth.

400 microliter ( $\mu\text{L}$ ) of urine were mixed with 200  $\mu\text{L}$  of potassium phosphate buffer. As urine is more acidic, this yielded final pH values of around 7.0. To allow spectrometer frequency locking, 50  $\mu\text{L}$  of deuterium oxide containing 29.02 millimole per liter (mmol/L) 3-trimethylsilyl-2,2,3,3-tetradeuteriopropionate (TSP) as internal standard were added (Beckonert et al. 2007).

### Identification of Urine Compounds

For initial assignment of the metabolites, the high-resolution 2D  $^1\text{H}$ - $^{13}\text{C}$  HSQC and HMBC spectra of a representative urine specimen were used. First, a manual metabolite assignment was performed on the high-resolution 2D  $^1\text{H}$ - $^{13}\text{C}$  HSQC spectrum aided by the corresponding 1D  $^1\text{H}$  spectra. Amix 3.8.1 (Bruker BioSpin, Rheinstetten, Germany) was used starting with manual picking of peaks in the high-resolution HSQC spectrum. An NMR peak search was performed using the Biological Magnetic Resonance Data Bank (available at <http://www.bmrb.wisc.edu/>) (Seavey et al. 1991), and the Human Metabolome Database (available at <http://www.hmdb.ca/>). To assign the signals, the spectrum was manually overlaid with reference spectra of pure compounds. The reference spectra were taken from the commercially available reference compound database Bbiorefcode 2-0-3 (Bruker BioSpin, Rheinstetten, Germany) that contains reference 1D  $^1\text{H}$ , 2D  $^1\text{H}$ - $^{13}\text{C}$  HSQC and  $^1\text{H}$ - $^{13}\text{C}$  HMBC spectra of metabolite standards measured under a variety of different experimental conditions (e.g. pH values and solvents). As an example, a creatinine reference spectrum was overlaid with a 1D urine spectrum in Figure 9.

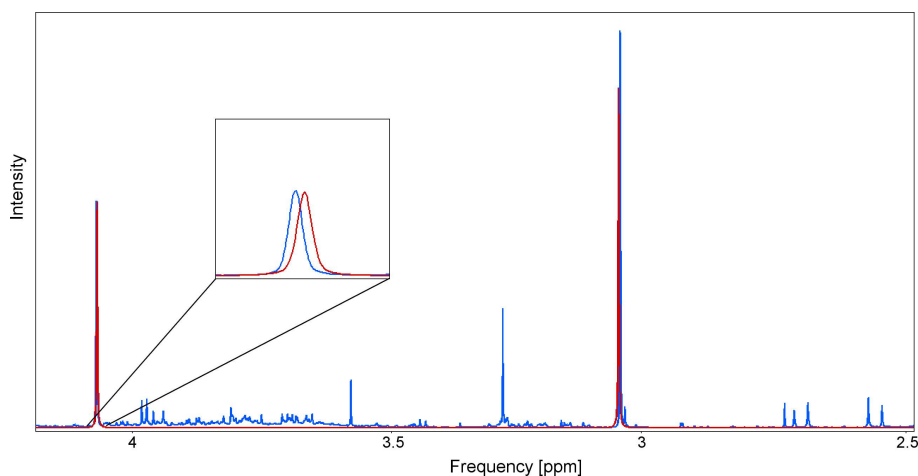


**Figure 9.** Overlay of a urine spectrum (blue) and the reference spectrum of creatinine (red). The two peaks of creatinine fit quite well considering frequency and intensity ratios, but a closer inspection seen in the inset shows frequency shifts.

In the figure, the two creatinine peaks at 3.05 ppm and 4.07 ppm agree quite well with the peaks observed in the urine spectrum considering frequency and intensity ratios. Taking a closer look, frequency differences are visible, though. These might be due to differences in experimental conditions, such as pH value, between the reference spectrum and the urine spectrum. To assure that the peaks in question really stem from the supposed metabolite, the pure metabolite was purchased, solved in pure water and measured under the same conditions as the urine sample to validate the exact peak positions. Additionally, spike-in experiments can be used to assure a peak assignment. In these experiments, a small amount of the pure substance is added to the sample. Comparing the spectra recorded before and after spiking, the peaks belonging to this substance can be identified.

Initial assignments were further validated by long-range proton-carbon couplings obtained from the high-resolution 2D  $^1\text{H}$ - $^{13}\text{C}$  HMBC spectrum. HSQC spectra show a peak at the  $^1\text{H}$  and  $^{13}\text{C}$  frequencies of nuclei connected with one electron bond. HMBC spectra show peaks at the  $^1\text{H}$  and  $^{13}\text{C}$  frequencies of nuclei connected with two electron bonds.

This can be used to validate that several peaks stem from the same molecule. Consider having identified two peaks (peak *a* and peak *b*) in a HSQC spectrum that supposedly arise from the same molecule. In case the two  $^{13}\text{C}$  atoms of peak *a* and peak *b* are directly connected by one electron bond in the molecule, the HMBC spectrum should show a peak *c* at the  $^{13}\text{C}$  frequency of peak *a* and the  $^1\text{H}$  frequency of peak *b*. In case no peak is visible at this position, peak *a* and peak *b* most probably do not stem from the same molecule, or are not directly neighboring in this molecule. This is exemplarily shown for the creatinine signals of a urine sample in Figure 10.

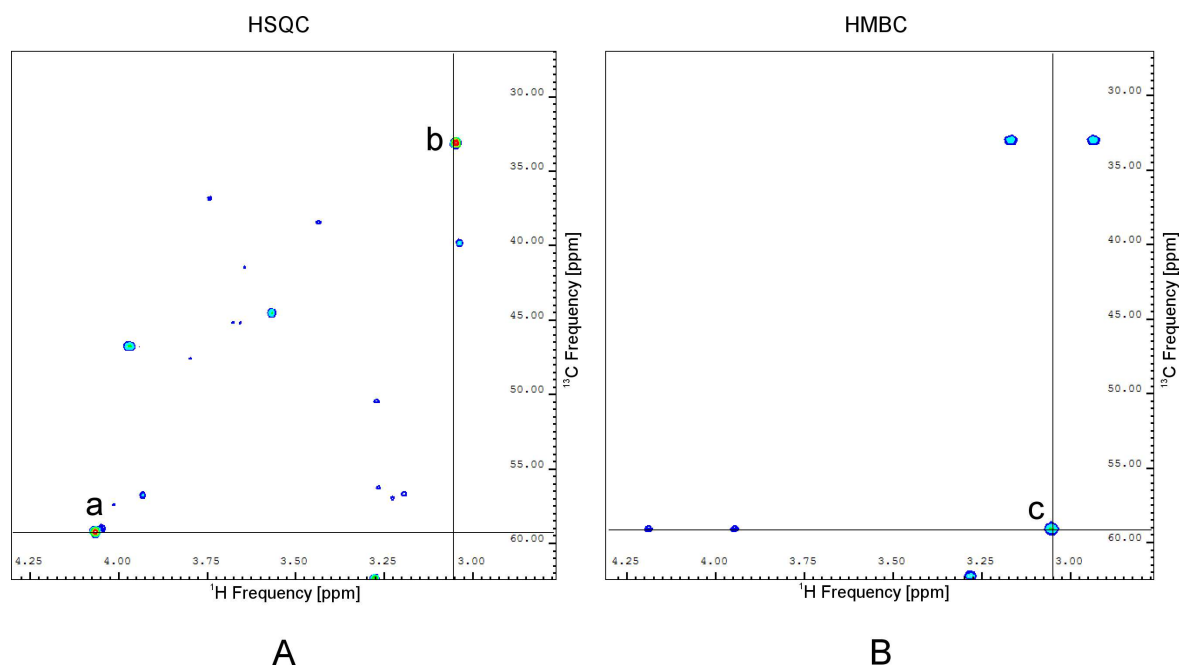


**Figure 10.** Validation of peak assignments using high-resolution HSQC (A) and HMBC (B) spectra. Peaks *a* and *b* in the HSQC spectrum are supposedly from the same molecule. The existence of a peak *c* at the intersection of the corresponding  $^1\text{H}$  and  $^{13}\text{C}$  frequencies in the HMBC spectrum supports this idea. The peaks stem from creatinine in this example.

Additionally, literature research provided hints about highly abundant urinary metabolites that are expected to be visible in the spectra. A summary of the identified urinary compounds including chemical shift data is provided in Tables 1 and 2 in Appendix I. A high-resolution 2D urine spectrum where typical urinary compounds have been marked is shown in Figure 11.

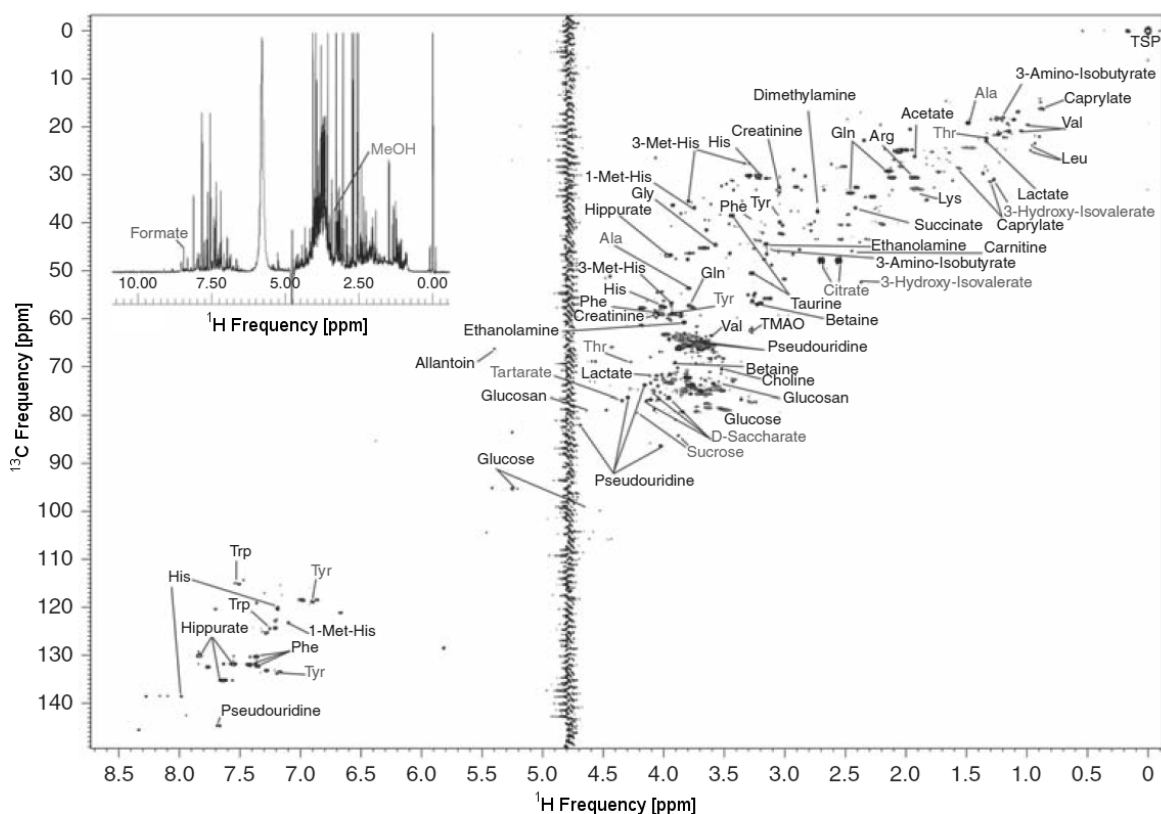


**Figure 11.** 2D  $^1\text{H}$ - $^{13}\text{C}$  HSQC spectrum and 1D  $^1\text{H}$  spectrum (left upper corner inset) of a healthy control urine specimen. Adapted from (Gronwald et al. 2011).

Abbreviations: 1-Met-His: 1-methylhistidine; 3-Met-His: 3-methylhistidine; Ala: Alanine; Arg: Arginine; Gln: Glutamine; Gly: Glycine; His: Histidine; Leu: Leucine; Lys: Lysine; MeOH: Methanol; Phe: Phenylalanine; Thr: Threonine; TMAO: Trimethylamine-N-oxide; TSP: 3-Trimethylsilyl-2,2,3,3-tetra deuterio propionate; Trp: Tryptophan; Tyr: Tyrosine; Val: Valine

### Automated Integration of Metabolite Signals

The obtained chemical shift information of each identified metabolite signal was used for automated integration of the spectral peaks using the Analytical Profiler module of Amix 3.9.3 (Bruker BioSpin, Rheinstetten, Germany).

Amix Analytical Profiler stores the chemical shift information and other data in a text file called knowledge base. To define the regions where the individual metabolite signals in a series of measured spectra are expected, individual chemical shift ranges were specified for each metabolite signal by manually analyzing inter-spectra chemical shift variations in a subset of the measured spectra. Depending on the analyzed type of spectrum, individually optimized chemical shift ranges were determined. In crowded regions of 2D spectra, it is especially important to choose very narrow search ranges to avoid integration of neighboring signals. It is not required that the whole peak is in the search

range - it is sufficient when just the peak maximum is in the search range. In addition to the search range, the knowledge base describes the individual signals of a compound in terms of multiplet patterns, couplings, relative intensities and masses. Coupling values with appropriate error bounds were obtained by analyzing the pure reference compound spectra together with the experimentally measured spectra of real samples. Note that multiplet patterns caused by J-couplings are in most cases only observable in the 1D spectra. In addition, the knowledge base allows the exclusion of overlapping signals located in crowded regions of the real urine spectra from the following quantification process. Overlapping signals were determined by manually analyzing a subset of the measured spectra. In Table 2 (see Appendix I), the metabolite signals used for quantification are listed.

The next step of the analysis was the integration of the signals identified in the previous step. Integration was performed with the Analytical Profiler module of Amix 3.9.3. The 1D  $^1\text{H}$  and 2D  $^1\text{H}$ - $^{13}\text{C}$  HSQC spectra corresponding to the series of measured urine samples were automatically peak-picked using an automated noise level calculation. For this purpose, regions that contained no signals in all spectra were manually defined. Using the information stored in the knowledge base, metabolite signals were identified and integrated. For 1D spectra, multiplet information stored in the knowledge base was used in the integration process to ensure that only the desired signals within the specified chemical shift ranges were integrated. For 2D spectra, multiplet information was not applicable. Here, information from the reference compound spectra database, such as the expected number of signals in a specific region, was used instead.

Next, relative integrals with respect to the reference TSP signal were calculated for the individual metabolite signals. In this process, the number of atoms contributing to a signal was taken into account, i.e. each integral was divided by the number of protons giving rise to it. The use of relative integrals automatically corrects for machine-dependent sensitivity variations between experiments and has the additional advantage that calibration curves have to be determined only once.

### **Dilution Series of Pure Compounds**

For the identified compounds, dilution series of the pure compound were prepared in order to calculate calibration curves and calibration factors for the different metabolites.

For 1D  $^1\text{H}$  spectra, calibration curves for all compounds and their respective signals should be very similar provided that a sufficiently long relaxation delay had been applied. To verify this expectation, calibration curves were generated for all non-overlapping signals of all quantified metabolites at multiple concentration values.

A 10 millimole per liter (mmol/L) standard stock solution of each compound was serially diluted to yield final concentrations of 10000, 5000, 2500, 1250, 625, 312.5, 156.2, 78.1, 39 and 19.5 micromole per liter ( $\mu\text{mol/L}$ ), respectively, and the corresponding spectra were acquired. For creatinine, the concentration range was extended to 15 mmol/L. For lowly abundant metabolites quantified from 1D spectra, serial dilution was continued for the concentration values of 9.8, 4.9, 2.5 and 1.2  $\mu\text{mol/L}$ . Table 2 (see Appendix I) shows the signals that were used for compound quantification. Due to overlap of signals even in the 2D spectra, only a subset of all signals could be used for quantification.

For the lowest concentration values of the dilution series, poor water suppression was observed. When only very low concentrations of solved compounds are present, the water signal shifts slightly. The water presaturation frequency then does no longer match the exact water resonance frequency, resulting in a larger residual water signal. This may cause receiver overflows, leading to decreased spectral quality. One solution for this problem is lowering the receiver gain for these samples, the other solution is adding other compounds to the dilution series in constant amounts. Therefore, 40  $\mu\text{L}$  of 10 mmol/L compound mix were added to 360  $\mu\text{L}$  of the dilution series sample, resulting in concentrations of 1 mmol/L of a standard compound mix present in each sample. This prevented the above described problems.

A typical example for a calibration curve obtained from 1D  $^1\text{H}$  spectra is shown for creatinine in Figure 12A. The peak integrals (relative to the TSP integral) were plotted against the weighed-out concentrations. The curves were measured for the two signals corresponding to the creatinine methylene ( $\text{H}_2\text{A}/\text{H}_2\text{B}$ ) and methyl group ( $\text{H}_6\text{A}/\text{H}_6\text{B}/\text{H}_6\text{C}$ ), respectively. As can be seen, both curves are almost identical and show a linear behavior with  $R^2$  values of 0.999 when fitted to a straight line.

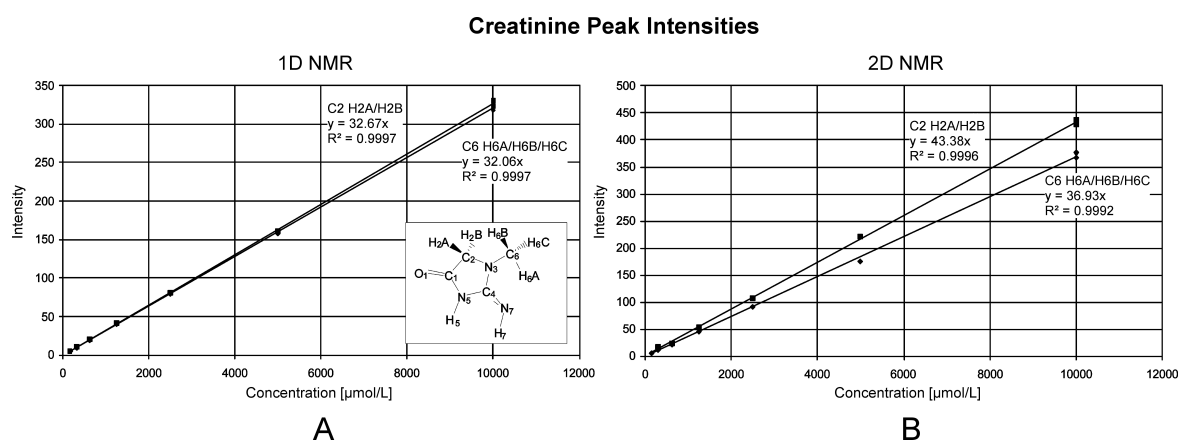


**Figure 12.** 1D (A) and 2D (B) calibration curves for creatinine generated from the signals  $\text{H}_2\text{A}/\text{H}_2\text{B}$  and  $\text{H}_6\text{A}/\text{H}_6\text{B}/\text{H}_6\text{C}$ , respectively. The used atom numbering scheme for creatinine is shown as an inset (A). On the x-axis, the concentration values employed are shown [ $\mu\text{mol/L}$ ] and on the y-axis the corresponding relative integrals are given with respect to the TSP signal.

Adapted from (Gronwald et al. 2008).

In the case of 2D spectra, multidimensional peak intensities are influenced by a number of factors such as non uniform relaxation, different transfer efficiencies of the insensitive nuclei enhanced by polarization transfer (INEPT) steps of the HSQC spectra and uneven excitation profiles. This results in calibration curves of markedly different slopes for the two signals of creatinine (Figure 12B). Linear regression lines were added. The  $R^2$  values near 1 show that signal volumes scale linearly with concentration also for the 2D spectra, but with different slopes for each peak.

Similar results were obtained for most other metabolites. Consequently, if 2D spectra are used for quantification, it is necessary to calibrate each signal individually to obtain a reliable and accurate quantification of a compound. The slope of the regression line can be

used as a calibration factor: Dividing a peak integral by this value will result in the absolute compound concentration.

For calculating the lower limits of detection (LLOQ's), the lowest three points of each calibration curve were measured in triplicate and the corresponding relative standard deviations (RSD's) were determined. Following the recommendation of the Food and Drug Administration (FDA, White Oak, MD, USA) guide for Bioanalytical Method Validation (FDA 2001), the LLOQ was defined as the lowest concentration value that could be determined with an RSD < 20 %. The LLOQ values are shown in Table 2 (see Appendix I). The lowest values of LLOQ were obtained again for compounds with multiple methyl groups, the protons of which give rise in most instances to one sharp singlet signal. The LLOQ's obtained are a function of the NMR acquisition time. Therefore, lower values may be obtained by increasing the acquisition time.

### **Analysis of Citric Acid**

In contrast to NMR spectra of a citric acid standard, two sets of signals for citric acid were present in some urine spectra. It was confirmed that both signal sets belonged to citric acid by addition of exogenous citric acid that resulted in corresponding increases in signal intensities for both sets of signals. The two signal sets of citric acid were separated by 1.61 ppm in the carbon dimension, while only a minor split was observed in the proton dimension. A full description of the measured chemical shift can be found in Table 2 (see Appendix I). For the urine specimens with this "double" citric acid signal, a wide variation of relative intensities was observed between the two forms. There was no clear concentration dependent trend for the intensity ratios obtained. The observed signal splitting agrees with an earlier NMR observation that urinary citric acid is involved in complexation reactions with calcium ions ( $\text{Ca}^{2+}$ ) and magnesium ions ( $\text{Mg}^{2+}$ ) (Neild et al. 1997). As expected, addition of ethylenediaminetetraacetic acid (EDTA) resulted in the presence of a single citric acid state. The possibility of complexation reactions is further supported by the average  $\text{Ca}^{2+}$  and  $\text{Mg}^{2+}$  concentrations of 4.37 and 3.97 mmol/L, respectively, found in the human urine (Ciba-Geigy 1983). Another possible explanation for the observed signal duplication is the use of boric acid as a preservative at the time of urine collection. High concentrations of boric acid lead to citric acid-borate complex formation with distinctive signal duplication (Smith et al. 2009). To elucidate whether addition of EDTA also would render single citrate signals in a citric acid-borate complex, 3 mmol/L boric acid were added to a solution of 1 mmol/L citric acid. This yielded the expected duplication of the citric acid signal. Addition of EDTA in concentrations up to 19 mmol/L yielded no change in the duplication of the citric acid signal. This is another hint that the observed signal duplication is due to  $\text{Ca}^{2+}$  and  $\text{Mg}^{2+}$  ions rather than borate. Consequently, volume integrals for the corresponding citric acid signals were summed for the determination of urinary levels of citric acid in case signal splitting was observed.

### **Mouse and Rat Urine**

Mouse and rat urine are highly concentrated. Their measurement according to the above protocol led to several spectral distortions. Firstly, the high salt concentration led to a high absorption of the RF signal, making very long RF pulses necessary. This may be harmful to the spectrometer due to overstressing of the sensible sending coils and causing extensive heating of the sample. Secondly, the added buffer could no longer achieve a full

pH adjustment, leading to uncontrolled signal shifts. Therefore, mouse and rat urine of 30-100  $\mu\text{L}$  was diluted to 400  $\mu\text{L}$  with pure water, and then prepared as described for urine above. In these diluted samples, the buffer was able to adjust the pH value sufficiently.

It was tested whether an exact pH adjustment gives superior results compared to just adding potassium phosphate buffer. 18 mouse urine samples were pH adjusted by adding small amounts in the low  $\mu\text{L}$  range of hydrochloric acid or sodium hydroxide. Although the group clustering result of a subsequent ICA was somewhat improved, this difference was not large. Taking into account the time and work needed for adjustment of larger sample numbers, the protocol using simple buffer addition was chosen for all analyses.

## 2.6 QUANTIFY: A Tool for Accurate Quantification

In the study on urine, strong signal overlap was observed for many metabolites. As urine may vary strongly in its composition, signals from unexpected molecules may overlap with signals used for quantification of expected metabolites. This may lead to strong over-quantification if not corrected. One possible way to reduce this problem is manual inspection of each peak. An automatic routine would be a more convenient way, as it would not be dependent on the skill and experience of the researcher inspecting the spectra. Additionally, an automated routine would save time especially when quantifying large sample sets. Therefore, an automatic approach using several peaks for each compound was developed.

A software named QUANTIFY was developed using Matlab 2007b (The Mathworks, Natick, MA, USA) to automate these analyses. The manual for QUANTIFY 1.0 is shown in Appendix III. Matlab code and executable files of QUANTIFY 1.0 are attached in Appendix II. The current version can be found in the software section of the Internet page of the Institute of Functional Genomics of the University of Regensburg (Regensburg, Germany): <http://genomics.uni-regensburg.de/>.

A screenshot of the main screen of QUANTIFY is shown in Figure 13.

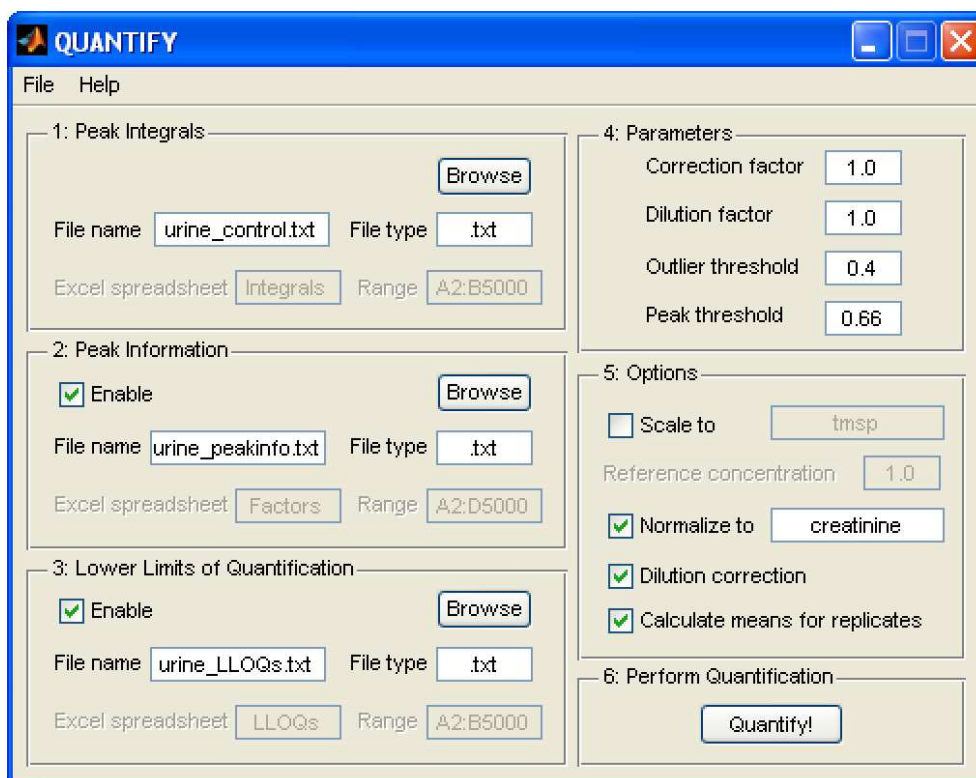


**Figure 13.** Main screen of QUANTIFY. For a detailed description of all items see the manual in Appendix III.

Originally, QUANTIFY was intended only for the analysis of 2D HSQC data, but has proven to provide reliable results also for 1D spectra. It may also easily be used for data from other one- or multidimensional NMR experiments.

To visualize the inputs and outputs of QUANTIFY, a data flow diagram was created. The diagram is shown in Figure 14.

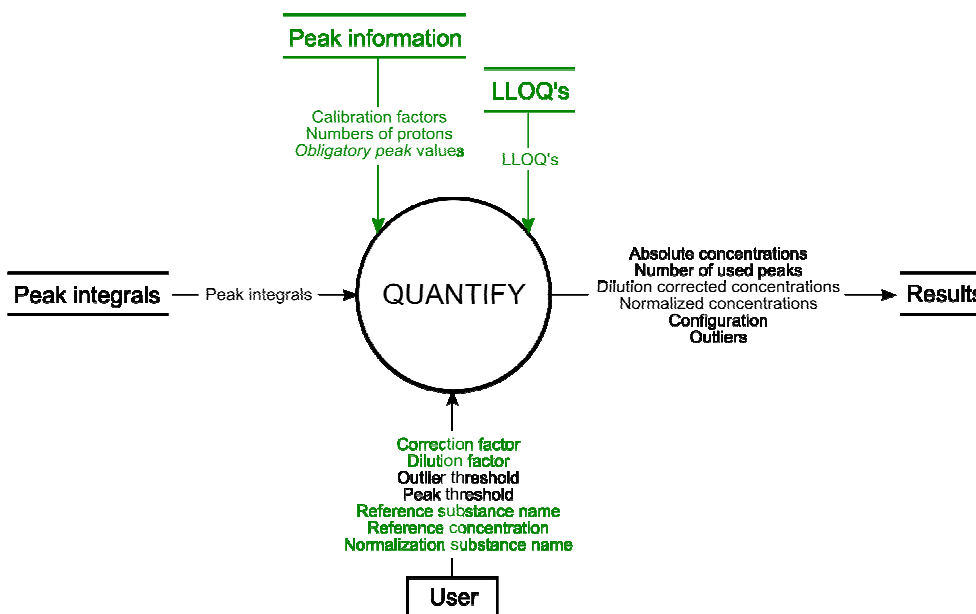


**Figure 14.** Data flow diagram of QUANTIFY. Functions are shown as circles, user inputs as boxes, data storage files as two horizontal lines and data flows as arrows with the transferred data shown on top of the arrows (DeMarco 1979). Optional parameters and files are marked in green.

The program takes as input a file containing the peak integrals of the investigated spectrum. This might either be an Amix Analytic Profiler output file, an Excel file or a text file. The latter two file types were implemented to be able to use QUANTIFY independently of the employed spectrometer software.

In addition to the signal intensities, information about the individual peaks of a metabolite such as calibration factors and number of protons may be provided as an Excel or text file. LLOQ's for each metabolite may be provided in an Excel or text file.

In case individual calibration factors are provided, each peak integral is multiplied by its individual calibration factor, as shown to be necessary for 2D spectra in Section 2.5. As this may not be needed in all cases this function is optional.

## Outlier Detection

The main benefit of QUANTIFY is its ability to identify and to exclude overlapped peaks and outliers. For this, several algorithms were developed. These algorithms raise the reliability of the results of NMR quantification, especially in complex biofluids.

When inspecting several peaks belonging to one compound, single peaks may be overlapped with disturbing signals. Still, it is unlikely that all peaks of one compound are overlapped in the same manner. If single peaks deviate strongly from the other signals, they are therefore assumed to be overlapped. Peaks are excluded as outliers if their integrals differ by more than a chosen *outlier threshold* from the median of all peaks obtained for this compound. In practice, an outlier threshold of 40 % has proven meaningful. If only one peak is left after outlier removal, heavy overlap is assumed, and the median value of all peaks of this compound is chosen. For some metabolites, only two peaks may be available. In case these peaks show a deviation above the outlier threshold, the peak with the smaller concentration value is chosen, as peak overlap usually results in raised concentrations.

For low-abundant compounds with many peaks, many or all of these peaks may not be visible above the noise level. At the same time, each of these peaks may be overlapped, thus giving rise to potentially false quantification results. To make the results for low-abundance metabolites more reliable, only metabolites are quantified where the ratio of peaks left after outlier removal in comparison to all expected peaks is equal or higher than a so-called *peak threshold*. For the peak threshold, a value of 66 % has proven appropriate for the analysis of urine and milk. In case that fewer peaks are found, the quantification results are doubtful. In this case, a reliability check is performed based on the number of protons contributing to these peaks. This reliability check is based on the assumption that in case of low compound concentrations, peaks with more protons should be visible, while peaks with fewer protons will remain below the noise level. For all peaks left after outlier removal, the number of protons contributing to the peak is checked, and the largest number of protons is saved. For all peaks that were not found in this spectrum, the same procedure is applied. If the maximum number of protons of the found peaks is larger than the maximum number of protons of the peaks not found, the peak is considered to be reliable. Otherwise, the compound is marked as not detected. The peak reliability check of QUANTIFY is, to the best of my knowledge, a completely novel feature in NMR quantification.

Single peaks of one compound may be marked as obligatory in QUANTIFY. In case this peak is not observed in the data set, all other peak integrals of this compound are discarded, and the compound is marked as not detected. This is useful for molecules with strong peaks that are often overlapped by other signals. By marking a weaker peak (with fewer protons) of the molecule as obligatory, this compound will only be quantified if the weaker peak is present. This will reduce the number of incorrect results. A similar routine using obligatory peaks has been previously implemented, yet only for compound identification and not for quantification (Xia et al. 2008).

### Additional Features

After these procedures, outliers and doubtful peaks have been removed, and the mean of the remaining peaks is calculated to yield the final concentration value. Optionally, the resulting value may be compared with the individual LLOQ of this compound. Values below the LLOQ will be discarded.

For replicate samples, means and TE's are calculated automatically. The tool optionally performs a concentration correction for diluted samples. Also, a correction for different reference substance concentrations may be performed. Concentrations may be normalized to a chosen compound, e.g. creatinine in urine samples.

All parameters such as peak threshold and outlier threshold may be freely chosen. Finally, the calculated concentrations are saved to an output file. The values of identified outliers are stored in a separate spreadsheet for manual inspection.

### Documentation

A change log listing all changes made between different versions of QUANTIFY can be found in the beginning of the source code file *quantify.m* that can be found in the attachment in Appendix II. Additionally, all previously released versions of QUANTIFY are available in the software section of the Internet page of the Institute of Functional Genomics of the University of Regensburg (Regensburg, Germany): <http://genomics.uni-regensburg.de/>.

For every QUANTIFY run, all parameters, file names, program versions, the user name and the computer name are automatically stored in a configuration spreadsheet in the results file. These data represent an accurate documentation of the quantification procedure. In combination with the change log and the archive of previous versions, the configuration data allow the exact reproduction of quantification procedures in case questions on the results arise at a later time point. Additionally, these configuration spreadsheets may serve as an information archive to facilitate performing similar experiments in the future and shall enable constantly reproducible results.

All NMR quantifications in this thesis were performed using QUANTIFY.

## 2.7 Urine Test Samples

In order to check the precision of the 2D NMR methods developed in the previous chapters, replicates of real biological samples were measured and quantified. To assess the accuracy of the methods, 2D NMR quantification results were compared to quantification results from 1D NMR and other established methods. Fifty human urine samples served as a test set. The values obtained by NMR were validated by measurements of the same samples using other commonly used quantification techniques. Bland-Altman analyses were performed by Wolfram Gronwald. This section has been published in part (Gronwald et al. 2008).

### Collection of Urine Samples

Two sets of human urine samples were analyzed. Control urine was collected from 33 volunteers. A set of 51 samples was prepared out of these 33 specimens, comprising six triplicates (18 samples), five duplicates (10 samples) and 22 single samples. In addition, one blank was included. Urine from patients with inborn errors of metabolism were provided by the Zentrum für Stoffwechselfdiagnostik Reutlingen (Reutlingen, Germany). For the analysis of standard mixtures of known concentration, a certified mixture of amino acids was purchased from the National Institute of Standards and Technology (NIST, Gaithersburg, MD, USA). For the NMR measurements, 400  $\mu\text{L}$  of the undiluted, 1:5 and 1:10 dilutions of the NIST standard with water were prepared as the urine samples. The dilution was necessary as the samples were too acidic to be compensated by the used buffer and thus resulted in NMR signal shifts.

### Comparison of 1D and 2D NMR Urine Measurements

Quantitative results from 1D and 2D NMR urinary spectra were compared to assess the degree of accordance. For a few highly abundant metabolites, such as creatinine, a very good agreement was found between 1D and 2D  $^1\text{H}$ - $^{13}\text{C}$  HSQC spectra with an  $R^2$  value of 0.99 and a slope of 0.95 of the regression line (Figure 15A).

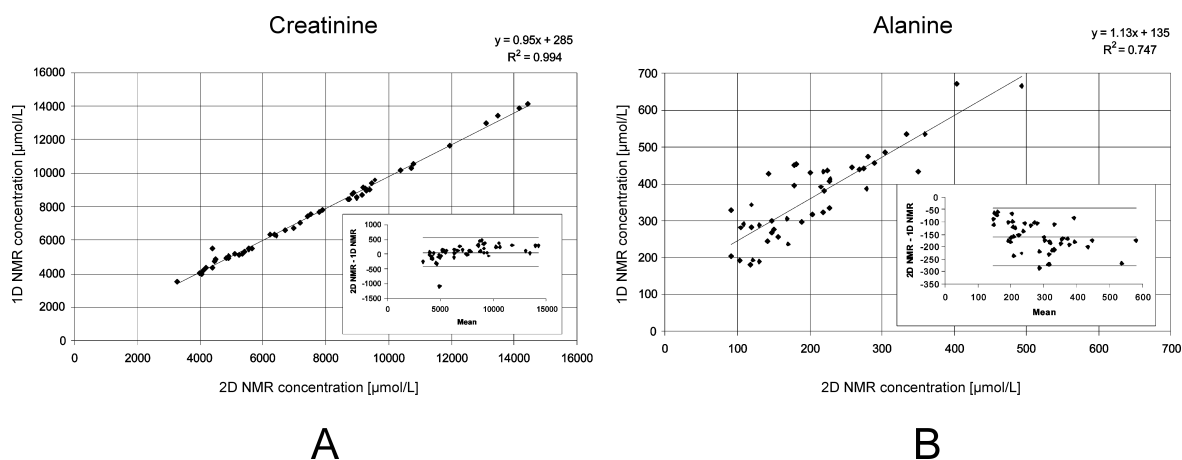


**Figure 15.** Linear regression of the concentration [ $\mu\text{mol/L}$ ] obtained for creatinine (A) and alanine (B) in 50 urine samples by 2D  $^1\text{H}$ - $^{13}\text{C}$  HSQC and 1D  $^1\text{H}$  NMR. The insets show Bland-Altman plots. The centerline in the plots corresponds to the mean difference between 1D and 2D NMR, while the outer lines correspond to 1.96 standard deviations (SD's). Adapted from (Gronwald et al. 2008).

However, for urinary metabolites, such as alanine, which are physiologically present at low  $\mu\text{mol/L}$  concentrations, 1D spectra gave higher concentrations as indicated by the slope of the regression curve of 1.13 and an offset of  $135 \mu\text{mol/L}$  (Figure 15B). This is also demonstrated by the Bland-Altman plots (Bland & Altman 1986) shown as insets in Figure 15.

For alanine, the obtained mean difference between 2D and 1D NMR measurements that is marked by the thick line in the corresponding Bland-Altman plot amounts to  $-161 \mu\text{mol/L}$ . The magnitude of this value is close to the  $135 \mu\text{mol/L}$  offset of the regression analysis. When compared to the measurement range for alanine of  $86 - 465 \mu\text{mol/L}$ , this mean difference amounts to a considerable relative error. A detailed investigation of the analyzed regions in the 1D spectra showed the presence of a high number of overlapping background signals, which stem most likely from urinary peptides and small proteins and cause an overestimation of concentration values. It should be noted that this is true for the alanine signals of the methine as well as the methyl group. It was also verified that the observed over-quantification could not be attributed to poor baseline correction or integral limits set too wide. As mentioned in Section 2.5, expected multiplet information was used in the integration process ensuring that only the desired signals present in the specified chemical shift ranges were integrated. However, this procedure will not correct for completely overlapping signals, as is the case here. In contrast, for the highly abundant creatinine, similar absolute differences in the urinary levels determined by 1D and 2D NMR spectra were observed in the regression analysis ( $285 \mu\text{mol/L}$ ) and Bland-Altman plot ( $71 \mu\text{mol/L}$ ). However, when compared to the corresponding measurement range of  $3069 - 13593 \mu\text{mol/L}$ , the relative error becomes quite small for creatinine. In general, correlation coefficients between results from 1D and 2D spectra also decrease with decreasing abundance of urinary metabolites. These data suggest that when analyzing complex biological matrixes, such as human urine, 1D NMR spectra are only suitable for the quantification of metabolites that are highly abundant or that possess signals in isolated areas of the spectra. Otherwise it is advantageous to use 2D spectra to reduce the amount of overlapping background signals.

### Reproducibility of 2D NMR Urine Measurements

The six different triplicates included in the urine study were used for determining the reproducibility of the 2D NMR results. The observed data, which are summarized in Table 3 (see Appendix I), give the joint reproducibility of the sample preparation, NMR acquisition and data analysis. The calculated RSD's vary between 2 and 21 % with an average of 11 %. RSD's are typically inversely correlated with the abundances of urinary metabolites.

### Accuracy of NMR Urine and Standard Mixture Measurements

For spike-in experiments, 0, 625, 1250 and  $2500 \mu\text{mol/L}$  alanine, creatinine, ethanolamine, glutamine, glycine, hippurate and taurine, respectively, were added to a urine sample. Analysis of the 2D  $^1\text{H}$ - $^{13}\text{C}$  HSQC spectra recorded showed that on average  $106 \pm 2 \%$  of the expected metabolite concentrations were recovered, as exemplified for creatinine, hippurate and glycine in Figure 16. One explanation for the slight over-quantification may be that the internal TSP standard interacts with urinary compounds. This interaction leads to a reduced TSP signal and, consequently, to increased relative integrals and concentration values for the urinary metabolites analyzed. As a consequence, all

concentration values measured in urine were multiplied with a global correction factor calculated as 100/106. Note that for the analysis of a certified standard solution no such correction was necessary, indicating that the observed over-quantification of urinary metabolites is indeed an effect of the biological matrix.

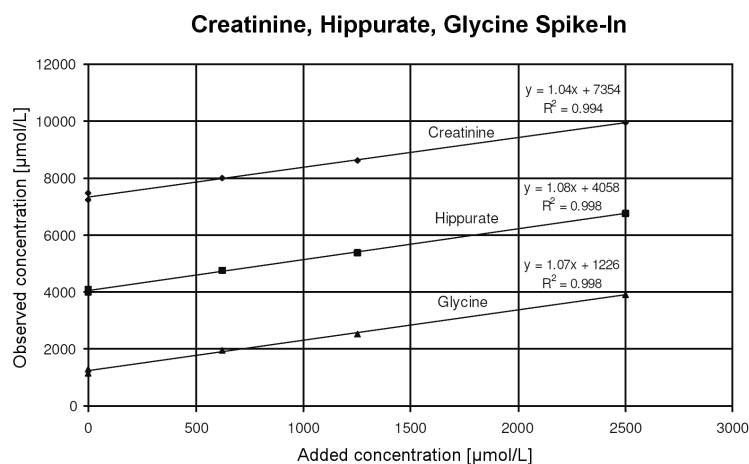


**Figure 16.** Accuracy of quantification. Metabolites of known concentration were spiked into a urine sample. For creatinine, hippuric acid and glycine the correlations between added and observed concentrations [ $\mu\text{mol/L}$ ] are given. The axis intercepts represent the metabolite concentrations present in the native urine sample. Adapted from (Gronwald et al. 2008).

A certified amino acid standard obtained from NIST (Gaithersburg, MD, USA) was investigated by means of 2D NMR, to check the accuracy of the method. This standard reference material (SRM) is an aqueous mixture of 17 amino acids in 0.1 mol/L hydrochloric acid. Samples were prepared and analyzed as the urine samples. Of the 17 amino acids, alanine, glycine, histidine, lysine and arginine were investigated, as they were part of the target set of urinary compounds. Table 4 (see Appendix I) shows the concentration values and standard deviations obtained by 2D NMR.

Due to the low pH of the SRM, major chemical shift changes compared to the previously defined knowledge base values were observed in the undiluted sample for most amino acid signals. Therefore, Table 4 (see Appendix I) shows the 2D NMR values obtained for the 1:5 diluted samples with the exception of histidine, for which even at a dilution of 1:5 significant chemical shift changes were observed. Hence, recovery of histidine was determined for the 1:10 diluted standard. Note that a pH correction of the NIST standard was not performed since this would lead to additional errors caused by the addition of small amounts of extra solvent. For comparison, the means and standard deviations were multiplied with the appropriate dilution factors. The NIST certified concentrations and their estimated uncertainties are based on in-house analysis at NIST and a round robin study that was conducted in cooperation with the Association of Biomolecular Research Facilities (Bethesda, MD, USA). The certified value is the equally weighted mean of the NIST average and the round robin average. Additionally, gravimetric values given by NIST are shown. The gravimetric value is based on the weighed amount of each amino acid used to prepare the solution. The last column of Table 4 (see Appendix I) shows the

recovery of the 2D NMR data in comparison with the NIST certified concentrations. As can be seen, the results obtained by 2D NMR agree well with the NIST certified concentrations. In all cases, the NIST certified concentrations are within the NMR error ranges. The best agreement between NMR data and NIST certified concentrations is observed for glycine with an absolute deviation of zero, while the largest deviation of 0.31 mmol/L is observed for histidine. When analyzing the percentage of recovery given in the last column of Table 4 (see Appendix I), a range between 97 and 111 %, with an average of 102 %, is observed for the different amino acids. These data clearly indicate that 2D NMR allows the accurate determination of metabolite concentrations. It was also analyzed whether concentration-dependent effects can be observed. For that purpose, undiluted, 1:5 and 1:10 diluted SRM was used. As mentioned above, especially for the undiluted standard, major chemical shift changes were observed and a considerable number of the signals had to be reassigned and manually integrated. Additionally, for some amino acids such as arginine, the lowest concentration point was slightly below the LLOQ value of 312  $\mu\text{mol/L}$ . Therefore, these data should be treated with some care. For three metabolites, namely, alanine, arginine and histidine, a linear regression analysis with the corresponding NIST certified concentrations plotted on the y-axis, was performed. Slopes of 1.06, 0.98 and 0.91 were observed for alanine, arginine and histidine, respectively, with corresponding y-axis intercepts in that order of -0.03, 0.02 and -0.06 mmol/L. These data suggest the absence of pronounced concentration-dependent effects for 2D NMR based quantifications. In summary, one can say that 2D NMR allows the accurate quantification of metabolites in standard samples.

### **Comparison of NMR and Colorimetric and Enzymatic Urine Measurements**

The creatinine content of the above set of 50 urine samples was also analyzed enzymatically with the enzymatic PAP method and the Jaffe alkaline picrate colorimetric method by Thomas Bertsch and Christine Aschenneller of the Institute of Clinical Chemistry, Laboratory Medicine and Transfusion Medicine of the Klinikum Nürnberg (Nürnberg, Germany). The comparison to 2D NMR values is shown in Figure 17.

As can be seen in Figure 17, 2D NMR results for creatinine correlated well ( $R^2 > 0.99$ ) with those obtained for both the PAP method (Figure 17A) and the Jaffe method (Figure 17B). Further analysis showed that the colorimetric and enzymatic methods yielded on average somewhat higher concentrations as indicated by the positive axis intercepts of 273 and 245  $\mu\text{mol/L}$ , respectively. This is also demonstrated by the Bland-Altman plots shown as insets in Figure 17, showing a systematic concentration dependence of the obtained deviations between 2D NMR and both the Biomed PAP and the Olympus Jaffe method. Overall, the best agreement was obtained between 2D NMR and the Biomed PAP method. Note that the 2D NMR data were additionally validated by spike-in experiments (Figure 16). For serum samples, it is known from the literature (Peake & Whiting 2006) that interference effects with the biological matrix can lead to an overestimation of creatinine values by both enzymatic and colorimetric methods. It is likely that similar effects in urine account, at least in part, for the observed differences between 2D NMR and the other two methods.

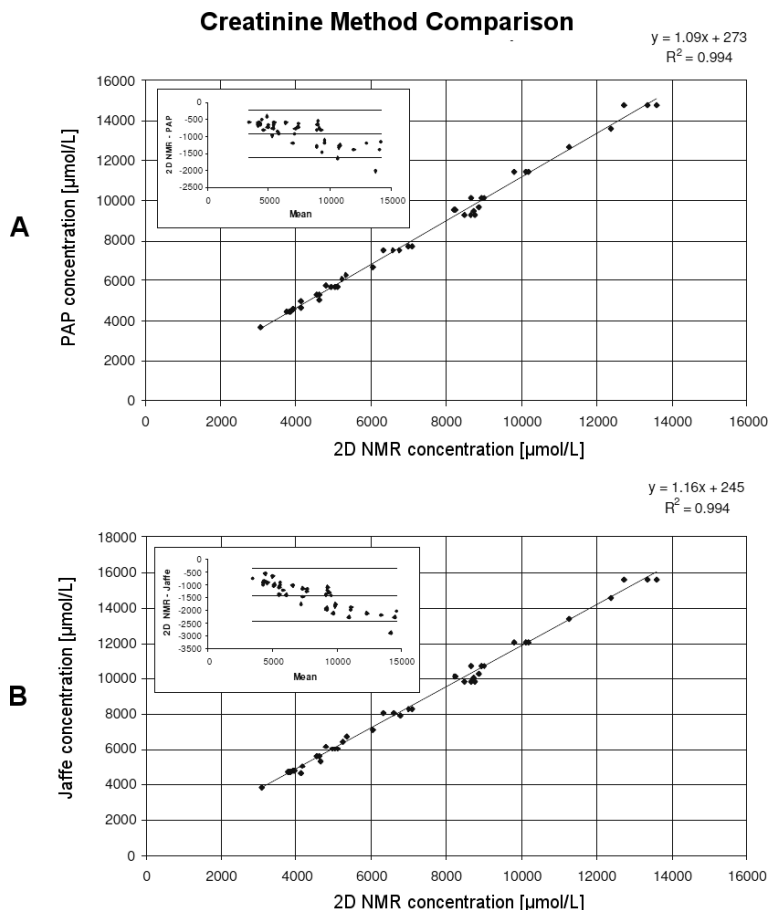


**Figure 17.** Linear regression and Bland-Altman plot of 2D NMR versus enzymatic (A) and colorimetric (B) concentrations [ $\mu\text{mol/L}$ ] for creatinine in 50 urine samples.

Adapted from (Gronwald et al. 2008).

### Comparison of NMR and GC-MS and LC-MS/MS Urine Measurements

The set of 50 urine samples was also analyzed by means of GC-MS by Hannelore Kaspar as described in (Kaspar et al. 2008) and by means of LC-MS/MS by Stephan Fagerer as described in (Gronwald et al. 2008). The results are shown in Table 5 in Appendix I. One important urinary metabolite amenable to both NMR and GC-MS is hippuric acid (Holmes et al. 2008). Figure 18 shows the comparison of the corresponding NMR and GC-MS results. As indicated by the high  $R^2$  value of 0.99, both methods allowed the precise determination of hippuric acid and showed a linear correlation over the entire observed concentration range of 372 - 5392  $\mu\text{mol/L}$ . The slope of the linear regression curve of 0.94 and the positive y-axis intercept of 115  $\mu\text{mol/L}$  confirmed good concordance between NMR and GC-MS data. The Bland-Altman plot in Figure 18A reveals an even smaller mean difference of 22  $\mu\text{mol/L}$  between the 2D NMR and GC-MS measurements. The diagram also demonstrates that in the lower concentration range 2D NMR yielded slightly lower values than GC-MS, while for the higher concentration range somewhat larger values were measured with 2D-NMR. However, this was a minor trend only and in summary both methods agreed well.

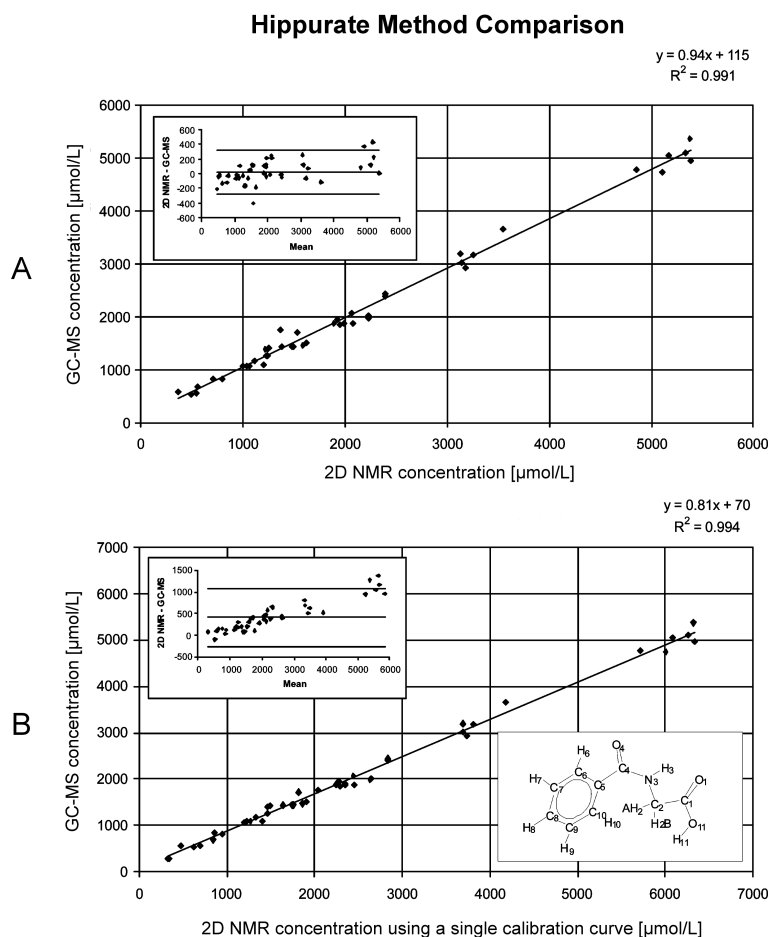


**Figure 18.** Linear regression and Bland-Altman plot of 2D NMR (x-axis) versus GC-MS (y-axis) concentrations [µmol/L] for hippurate in 50 urine samples. 2D NMR values were obtained by averaging the volume integrals of three separate signals for hippurate that had been calculated using either (A) independent calibration curves for each signal or (B) a single calibration for all three signals. The used atom numbering scheme for hippurate is shown as an inset in B.

Adapted from (Gronwald et al. 2008).

Figure 18 also illustrates the importance of generating separate calibration curves for each signal of a compound used for quantification in 2D NMR. As evidenced by the slope of the regression line, a considerable decrease from 0.94 (Figure 18A) to 0.81 (Figure 18B) was observed, when instead of three independent only one calibration curve generated for the CH group in para position of the aromatic ring (C8/H8) was used to calculate the peak volume integrals of the three non-overlapping signals recorded for hippurate. In this case, the use of a single calibration curve led to a significant overestimation of the urinary level of hippuric acid by 2D NMR with the mean difference of measurements between NMR and GC-MS increasing from 22 µmol/L, when using separate calibration curves for the three signals, to 404 µmol/L. The degree of overestimation was the more pronounced the greater the concentration of urinary hippuric acid as indicated in the Bland-Altman plot, which is also reflected by the increase in standard deviation of the mean difference from 156 to 347 µmol/L. Similar observations were made for other metabolites such as lysine, for which multiple signals were available for quantification.

An important group of urinary metabolites are free amino acids, which are well-known markers for inborn errors of metabolism (Constantinou et al. 2005). Figure 19 shows linear regression and Bland-Altman plots for the comparative analysis of urinary glycine values obtained by means of 2D NMR, GC-MS and LC-MS/MS, respectively.

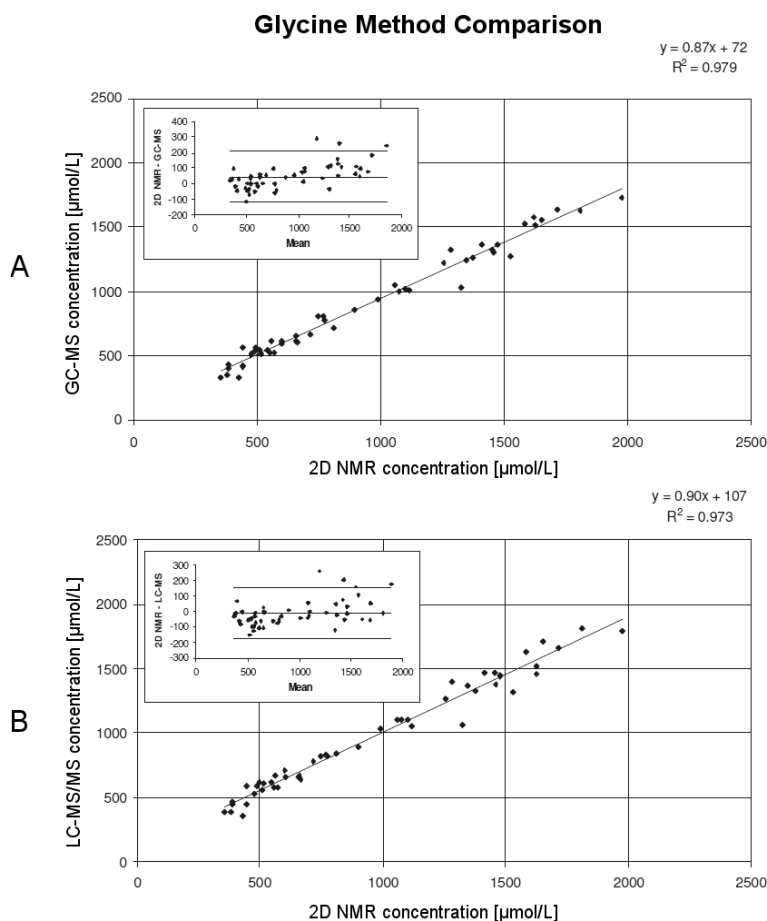


**Figure 19.** Linear regression and Bland-Altman plots of 2D NMR (x-axis) versus GC-MS (A) and LC-MS/MS (B) concentrations [ $\mu\text{mol/L}$ ] for glycine in 50 urine samples. Adapted from (Gronwald et al. 2008).

Over the observed concentration range of 355 - 1976  $\mu\text{mol/L}$ , GC-MS and NMR correlated well with an  $R^2$  value of 0.98 (Figure 19A). As described for hippurate, NMR yielded in general slightly higher concentrations. When comparing NMR and LC-MS/MS data for glycine (Figure 19B), a similar correlation with an  $R^2$  value of 0.97 was obtained. As reflected by the slopes of the regression curves of 0.87 for GC-MS and 0.90 for LC-MS/MS, both methods obtained slightly lower values for glycine in the higher concentration range than 2D NMR. This is further supported by the Bland-Altman plots, which revealed mean differences between 2D NMR and GC-MS and 2D NMR and LC-MS/MS, respectively, of 48 and -13  $\mu\text{mol/L}$ . In general, good agreement was observed between 2D NMR, on the one hand, and GC-MS and LC-MS/MS data, on the other hand, as evidenced in Table 5 (see Appendix I).

However, one can also observe that the degree of correlation decreases when the 2D NMR concentrations of a metabolite are close to its LLOQ in all urine samples (Table 2 in Appendix I). For 3-aminoisobutyrate, in many cases heavy signal overlap of the methyl group was observed in the 2D spectra, and therefore, these measurements were excluded from further analysis. As a consequence, the comparisons with other methods are based on relatively few data points and should be treated with care. Also, the possibility of using the non-overlapped but much weaker signal of the CH group alone for quantification was investigated. However, in this case, an increase of the LLOQ from 312 to 1250  $\mu\text{mol/L}$  was observed, which rendered this approach impractical. Note that for the corresponding GC-MS measurements no isotope labeled internal standard was available, which somewhat compromised the reliability of the GC-MS data.

### Analysis of Urine from Patients with Inborn Errors of Metabolism

2D NMR was applied to the analysis of urine samples collected from patients with inborn errors of metabolism provided by Dr. Herbert Korall from the Zentrum für Stoffwechselfdiagnostik Reutlingen (Reutlingen, Germany). A striking example, namely the 2D  $^1\text{H}$ - $^{13}\text{C}$  HSQC spectrum of a urine sample from a patient suffering from aminoaciduria (Malakauskas et al. 2007), is shown in Figure 20. Aminoaciduria is a condition characterized by high urinary amino acid excretion that might occur in disorders such as Hartnup disease, Dent's disease and Fanconi syndrome. As expected, the spectrum showed considerably increased amino acid levels. This sample and other samples from patients with inborn errors of metabolism were analyzed by Wolfram Gronwald, a discussion of these samples can be found in (Gronwald et al. 2008).

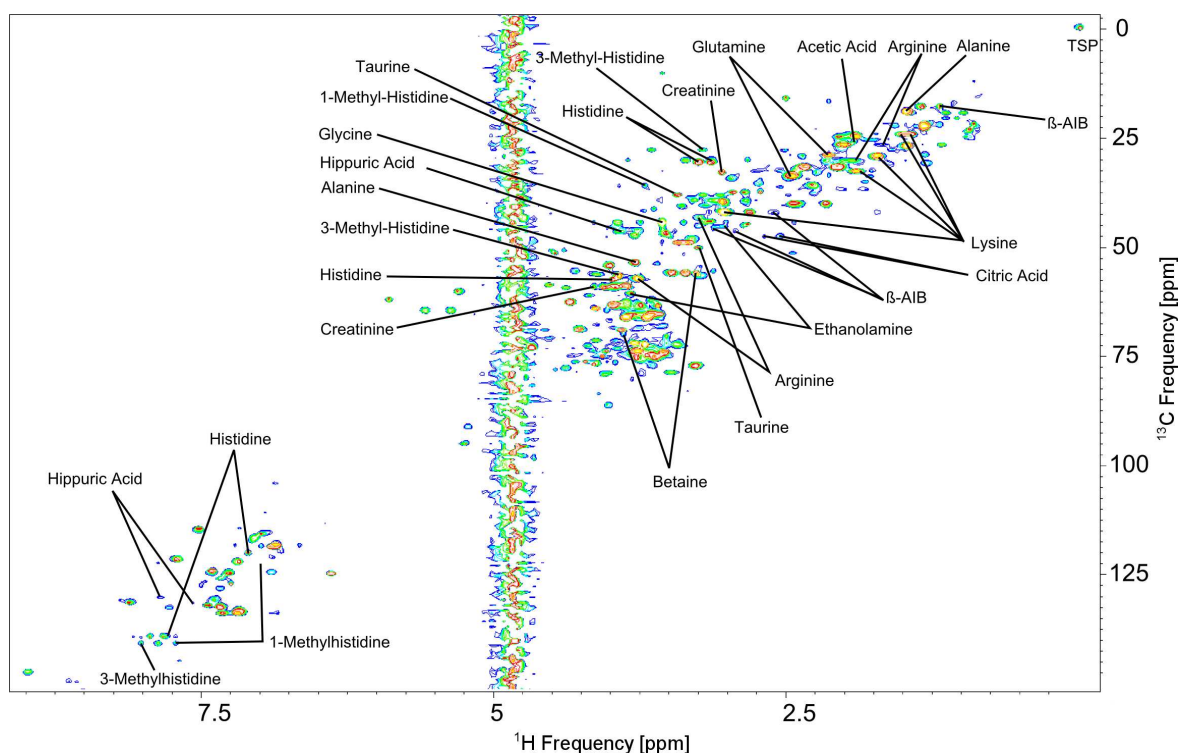


**Figure 20.** 2D  $^1\text{H}$ - $^{13}\text{C}$  HSQC spectrum of a urine sample from an aminoaciduria patient. Adapted from (Gronwald et al. 2008). Abbreviations:  $\beta$ -AIB: Beta-aminoisobutyrate; TSP: 3-Trimethylsilyl-2,2,3,3-tetradeuteropropionate

## 2.8 Measurement of Bovine Milk

After the successful application of NMR to the analysis of urine, a protocol for the analysis of bovine milk was established. Cow's milk has a complex composition, including large amounts of lipids and proteins. These macromolecules give rise to unspecific, broad signals in NMR spectra and thus hamper identification and quantification of small molecules. In addition, complex formation between the used NMR reference compound and proteins was observed, which resulted in a considerably diminished reference signal. To remove the macromolecules, different sample pretreatments were compared. This chapter has in parts already been published (Klein et al. 2010).

A commonly used method for protein removal is ethanol precipitation. A large amount of ethanol is added, leading to reduced solubility and denaturation of the proteins. Here, 3.6 mL of ethanol were added to 400  $\mu$ L of milk and incubated for three hours at  $-20$  °C. After centrifugation for 30 minutes at 4000 gravitational accelerations (g) at  $4$  °C, the liquid phase was removed from the pellet. The pellet was washed with ethanol and the liquid phase removed. The liquid phases were pooled, dried in an evaporator and redissolved in 400  $\mu$ L pure water.

A second method for protein removal is ultrafiltration. The solution is placed in a tube with a membrane consisting of regenerated cellulose. The solution is then forced through the membrane using centrifugation, leaving macromolecules behind. Millipore Amicon Ultra-4 (Millipore, Billerica, MA, USA) filter devices with a molecular weight cutoff of 5 kilodalton (kDa) were used. The filter was rinsed with water to remove filter-preserving substances of the filter such as glycerol and triethylene glycol (TEG). Three mL of water were transferred into the filter device and centrifuged at 4000 g at ambient temperature for 60 minutes. The contaminated filtered water was removed and 1 mL of milk was transferred into the device. The samples were centrifuged at 4000 g at ambient temperature for 60 minutes.

After both protein removal methods, 400  $\mu$ L of sample were prepared and measured as described in Sections 2.4 and 2.5 for urine, with the exception of a reduced receiver gain due to the strong lactose signals. 2D HSQC spectra for untreated milk, precipitated milk and filtered milk are shown in Figure 21. In precipitated milk several prominent signals including citric acid are missing. In the filtered milk sample, these signals are clearly visible, indicating less changing of the sample.

As the filters with 5 kDa cutoff had been discontinued meanwhile, Millipore Amicon ultrafiltration devices with molecular weight cutoffs of 3 and 10 kDa were tested for best metabolite recoveries. The filter with 3 kDa cutoff showed a lower recovery for some metabolites. This indicates that the filter is clotted by the macromolecules. In the 10 kDa filters, this effect was not observed. 10 kDa filters were chosen for all further analyses. The peak areas of the preserving substances contained in the filters, glycerol and TEG, were excluded from further analyses. To ensure that no other pollutants were present in the filters, spectra of the rinsing water were recorded, showing that only glycerol and TEG were present at noteworthy concentrations.

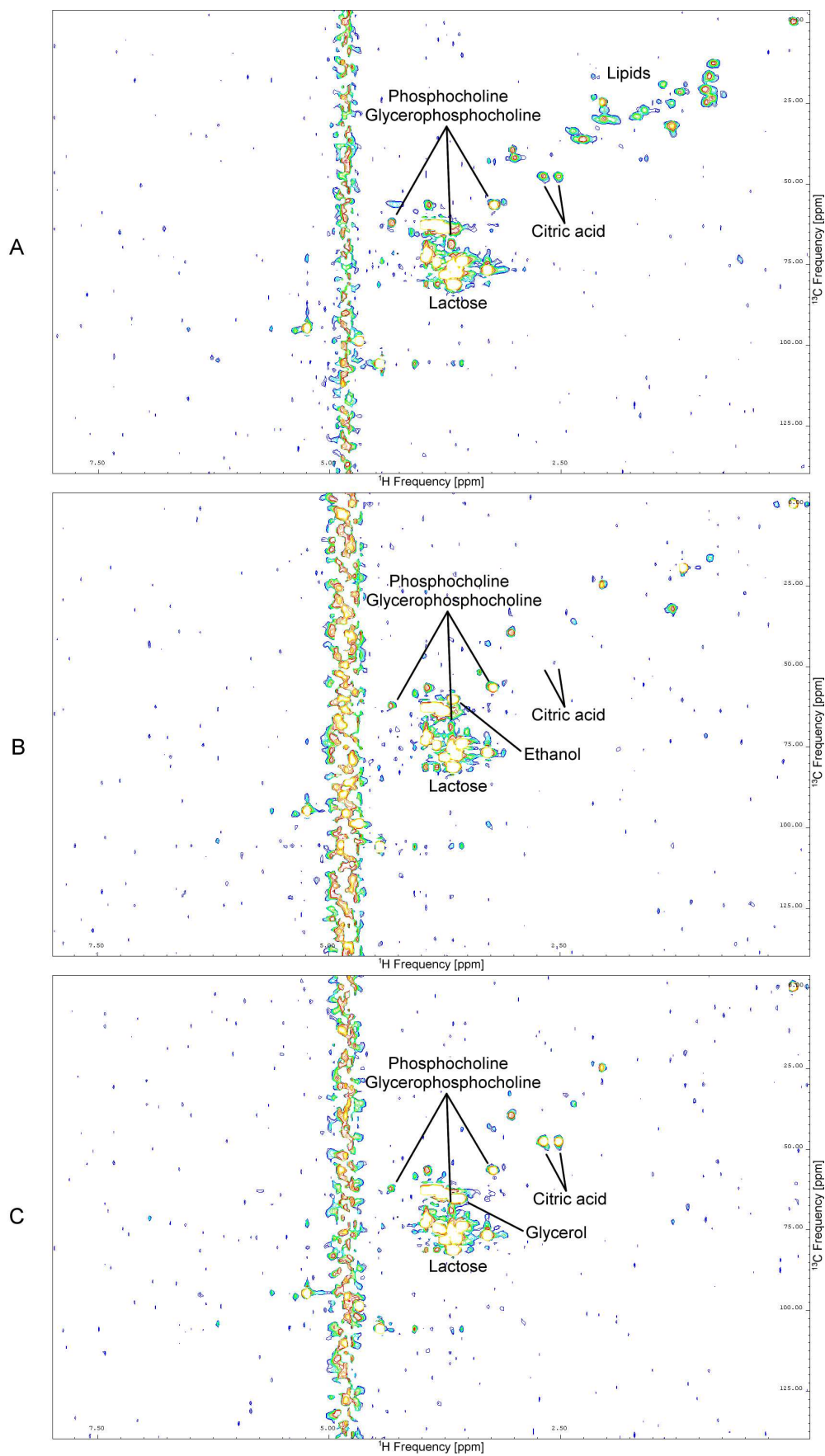


**Figure 21.** 2D  $^1\text{H}$ - $^{13}\text{C}$  HSQC NMR spectra of raw (A), ethanol precipitated (B) and ultrafiltrated cow's milk (C), respectively. Prominent signals are marked.

Milk metabolite identification and quantification was performed as described for urine in Section 2.5. A summary of the obtained chemical shift data is provided in Table 6 (see Appendix I)

Overlapping signals located in crowded regions of the milk spectra were excluded from the quantification process. Especially in the region close to the intensive lactose signals, considerable overlap was present in both 1D and 2D spectra. To gain individual calibration curves, standard stock solutions were serially diluted to yield final concentrations of 9000, 4500, 2250, 1125, 562.5, 281.3, 140.6, 70.3, 35.2, 17.6 and 8.8  $\mu\text{mol/L}$ , and the corresponding spectra were acquired. The concentration range was extended to 166 mmol/L for lactose. Signal volumes scale linearly over the whole range of concentrations, i.e. over five orders of magnitude.

The number of signals that were used for compound identification is presented in Table 6 (see Appendix I) and equals the number of measured calibration curves.

### LLOQ's and TE's

LLOQ's for the 2D  $^1\text{H}$ - $^{13}\text{C}$  HSQC and 1D  $^1\text{H}$  spectra were calculated from calibration standards. The LLOQ values for the individual compounds are given in Table 6 (see Appendix I). The lowest LLOQ values were obtained for compounds with multiple methyl groups such as betaine, where the protons of the methyl group(s) gave rise to a single signal in the corresponding 2D NMR spectra, or for compounds that were identified from 1D spectra. The LLOQ values obtained for 2D spectra of pure compounds were generally higher than those obtained for 1D spectra. 1D spectra were used for quantification of low-abundant compounds such as acetone and beta-hydroxybutyric acid (BHBA); hence, considerably lower LLOQ's were obtained. From the calibration curves, it was obvious that measurements remained linear up to concentrations as high as 166 mmol/L for lactose without readjusting the receiver gain.

Sixty milk specimens were measured as technical replicates to check the precision in terms of TE of measurement. For metabolites with simple peak shapes TE's of around 3 % for alanine were obtained in the 1D spectra, whereas complex multiplet peaks resulted in higher TE's of up to 8 % as seen for glutamic acid. This may be due to imperfections of the used peak fitting methods and increased noise contributions due to the presence of very broad multiplets. In 2D spectra TE's were observed in the range from 0.7 % for lactose up to 14.7 % for galactose-1-phosphate. Obviously, the TE was the lower the higher the observed metabolite concentration was. On average, the TE for 2D measurements was 7.0 %.

### Freezing and Thawing

During the analyses it became clear that freezing and thawing is a crucial point in the preparation of milk samples. Freezing and thawing may unmix the sample (Mai 1912). This leads to drastically increased or decreased concentration values, depending on the pipette tip position in the sample tube. This is especially obvious for lactose concentrations, as these are strongly physiologically regulated and show only little variation. Therefore, it is indispensable not only to vortex the sample after thawing, but to

turn the sample upside down three to four times to achieve a complete mixing of the content.

### Dependence of the Citric Acid Signals on pH Value

The position of citric acid signals is sensitive to changes in pH and salt concentration. It has been reported for mouse and rat urine samples that the citric acid shift is linearly correlated to sample pH (Miyataka et al. 2007). Therefore, it was assessed whether this was true for milk samples as well. An equation describing the correlation of pH and citric acid shift was derived from (Miyataka et al. 2007):

$$pH \approx SC * (-59.48) + 163.42$$

SC is the shift of the citric acid signal in ppm. This equation was derived from data between pH 6.0 and pH 9.0. The shift was calculated as the mean signal position of the four citric acid signals at around 2.61 ppm.

Next, milk samples showing large citric acid shifts were chosen. For these, pH was measured using a thin pH electrode (Mettler Toledo, Greifensee, Switzerland) both for the filtered milk samples and the filtered and buffered milk samples. Assessment of pH values in whole milk was not possible using the pH electrode to avoid membrane contamination with milk fat. A pH test was performed using pH test strips (Macherey-Nagel, Düren, Germany) for the pH range of 6.0 to 7.7, but the narrow range of pH values in milk rendered the test being too rough for this purpose.

Measured pH values for the filtered milk were  $pH 6.80 \pm 0.11$  (mean  $\pm$  SD) and ranged between pH 6.61 and pH 7.00. After buffering, the pH was  $7.10 \pm 0.05$  and ranged between pH 7.02 and pH 7.18, indicating that the buffer effectively reduces pH variations. Only a weak correlation between the measured pH and the pH calculated from the citric acid shift could be observed, though. This could either depend on the more narrow range of pH values detected in milk, or on the fact that other factors such as salt concentration dominated the citric acid signal shifting in milk.

### Long Term Stability

The stability of filtered milk was investigated. Three milk specimens were filtered and split into five aliquots each. Each aliquot was prepared as described above and then either stored for time periods of one, three, seven and 14 days, respectively, or measured directly after preparation. This experiment was performed both at room temperature and at 4 °C, the temperature of the sample changer.

Over the two-week period, only few metabolites, including galactose-1-phosphate, glycerophosphocholine (GPC) and phosphocholine (PC), showed minor changes in concentration when stored at room temperature, while most compounds studied were subject to strong and fast changes in concentration. Lactate, acetone, alanine and glutamic acid stayed constant for one day, but decreased rapidly thereafter. Methanol and acetic acid increased, beginning at three days of storage. Some compounds like creatinine, N-acetyl-carbohydrates and phosphocreatine stayed almost constant for three to seven days and increased slightly thereafter. Acetoacetic acid decreased slowly, starting at day seven. Citric acid concentrations decreased almost exponentially during the observed period with an average decay constant of  $-0.0546 \pm 0.0131$  per day ( $n = 3$ ), representing a half-

value period of  $12.7 \pm 3.06$  days. Additionally, citric acid peaks shifted during the observed period. A closer examination showed that not only a signal shift had occurred during storage, but also the inter-peak distance had changed, indicating changes in pH and in the overall salt concentration in the sample. As seen above, the correlation between citric acid signal shift and pH is not strong in milk. Anyway, the data indicated a slight drop in pH value of about 0.1 during storage.

The lactose signal showed an unexpected behavior during storage: An increase in concentration was observed, showing the shape of a saturation curve, with saturation reached around day 14. Lactose increased by  $9.7 \pm 1.2$  mmol/L during the first seven days. The values for  $\alpha$ - and  $\beta$ -lactose behaved in the same way. This behavior could in part be explained by a solution effect due to the more and more acidic conditions during storage. Taking a closer look at the samples, a small residue of undissolved substances could be found in the NMR tubes. This residue falls out from the filtered milk when the buffer is added. When the conditions of the samples become more acidic during storage, more substances from the residue can be dissolved, thus raising the observed concentrations. To prove this assumption, the residue was carefully separated from the liquid of the sample and redissolved in water. While most concentrations were in the expected range, lactose showed raised levels in the residue on the first day of room temperature storage and dropped to normal values until storage day three.

In the samples stored at 4 °C, only few changes were observed during the first week of storage. Two exceptions were acetic acid, whose levels increased by  $10.7 \pm 7.8$  %, and citric acid, whose levels on average decreased by  $10.3 \pm 1.0$  % during the first three days of storage, respectively. After 14 days, stronger changes in milk composition became visible. These changes were similar to the changes seen in the samples stored at room temperature.

These results show that even filtered milk is relatively unstable at room temperature and that the use of a cooled sample changer is indispensable for measurements of large sample numbers.

### Comparison of NMR and GC-MS Milk Measurements

Alanine, BHBA, glycine, and lactic acid were quantified in a set of 106 milk samples (for details on the milk samples see Section 3.2). These metabolites were additionally analyzed by GC-MS by Martin Almstetter as described in (Klein et al. 2010). A comparison of the corresponding NMR and GC-MS data for glycine is shown in Figure 22.

The high  $R^2$ -value of 0.92 indicates that both methods allowed the precise determination of glycine over the entire concentration range of 0.033 to 1.109 mmol/L. The slope of the linear regression curve of 0.93 and the positive y-axis intercept of 0.018 mmol/L confirmed good concordance between NMR and GC-MS data. The Bland-Altman plot shown as an insert in Figure 22 reveals an even smaller mean difference of 0.04 mmol/L between the 2D NMR and the GC-MS measurements. Similar results were obtained for alanine (slope = 0.84, intercept = 0.22,  $R^2 = 0.65$ ), BHBA (slope = 0.79, intercept = 0.017,  $R^2 = 0.86$ ) and lactic acid (slope = 0.91, intercept = 0.021,  $R^2 = 0.96$ ). In summary, NMR quantification results on milk showed high concordance with GC-MS data on the same metabolites.

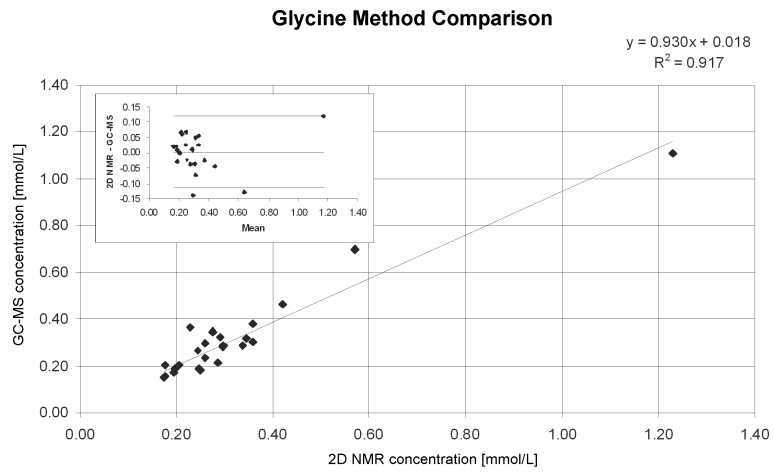


**Figure 22.** Linear regression and Bland-Altman plot of concentrations [mmol/L] of glycine in milk specimens measured by 2D NMR and GC-MS. Adapted from (Klein et al. 2010).

## 2.9 Measurement of Tissue Extracts

Tissues and cell culture samples cannot be easily analyzed as they are, because the complex structure induces strong magnetic field distortions that severely hamper spectrum inspection. Due to the hindered mobility of molecules in intact tissue, dipolar couplings and contributions from chemical shift anisotropy do not average out, leading to very broad lines. Additionally, molecules in the rigid cell parts lead to fast signal relaxation, resulting in very broad background signals. Two often applied means to circumvent these issues are magic angle spinning where the sample is rotated at a high rate to average out anisotropic effects and the other is to use liquid tissue extracts. Here, tissue extraction was chosen for NMR analysis. The suitability of NMR for the analysis of liver extracts has been demonstrated previously (Waters et al. 2002). For analyses of these samples, several approaches are possible.

A methanol/chloroform extraction was chosen as it has the advantage that both hydrophilic and lipophilic compounds are accessible for separate measurements. Samples of about 50 mg were cut into pieces and placed in 600  $\mu\text{L}$  methanol at 0 °C for 15 minutes. After this, the samples were sonicated for 10 seconds using an ultrasound lance (Sonopuls Homogenisator HD2070, Bandelin Electronic, Berlin, Germany), and 600  $\mu\text{L}$  pure water and 600  $\mu\text{L}$  chloroform were added. After four hours at -20 °C, samples were centrifuged at 20000 g for 30 minutes at 4 °C to separate the hydrophilic from the lipophilic phase. Following evaporation, the aqueous phase was dissolved in 400  $\mu\text{L}$  of pure water and treated as described for urine samples in Section 2.5. The chloroform phase was dissolved in 650  $\mu\text{L}$  of deuterated chloroform containing tetramethylsilane (TMS, Merck, Darmstadt, Germany) or octamethylcyclotetrasiloxane (OMS, Sigma-Aldrich, Taufkirchen, Germany) as internal standard (Oostendorp et al. 2006).

### Lipid Analyses

As lipids give rise to broad and quite unspecific signals, area integration of 1D spectra was chosen to assess the lipid concentrations. Signal areas for typical lipid functional groups were determined using measurements of standard samples of saturated fatty acids, unsaturated fatty acids, triacylglycerides, phosphatidylcholine (PtC), cholesterol and cholesterol ester. The identified functional groups and the respective signal frequencies and molecular masses are shown in Table 7 (see Appendix I). The signals were integrated either relative to the signal of the chloroform fraction contained in deuterated chloroform, or relative to the OMS signal.

The molar concentration of unsaturated fatty acid bonds was measured using the signal of methylene groups not adjacent to double bonds. The concentration of polyunsaturated bonds was assessed using the signal of methylene groups adjacent to two double bonds (diallylic group). The molar lipid content was assessed by integrating the glycerol signal present in lipids such as triacylglycerides and phospholipids. The total lipid concentration in terms of weight percentage was estimated by summing up all lipid signals including the glycerol resonance and multiplying each by the molar mass of the associated functional group.

To assess the composition of lipids, several indices were derived from the lipid signals. A saturation index (*SI*), a polyunsaturation index (*PUI*) and a ratio of polyunsaturated fatty acids to monounsaturated fatty acids (*PUFA/MUFA*) were defined as:

$$SI = 1 - \frac{I_{allylic} + I_{diallylic}}{I_{allylic} + I_{diallylic} + I_{methylene} + I_{methyl}}$$

$$PUI = \frac{I_{diallylic}}{I_{allylic} + I_{diallylic} + I_{methylene} + I_{methyl}}$$

$$PUFA / MUFA = \frac{I_{diallylic}}{I_{methene}}$$

where the *I*'s are the integrals of the corresponding lipid signals (Serkova et al. 2006; Johnson et al. 2008; Cobbold et al. 2009). For details on the used signals see Table 7 in Appendix I.

Looking closely at the spectra, it became obvious that the methylene-to-carboxyl signals of free fatty acids differ slightly from those of fatty acids that are part of triacylglycerides and phospholipids. This difference is due to the glycerol that is attached to the carboxyl group in the latter lipid classes.

Some lipophilic metabolites could be quantified exactly using sharp, specific signals, namely PtC, cholesterol and cholesterol ester. These were integrated as described for urine metabolites. The corresponding frequency values can be found in Table 7 (see Appendix I).

It was striking that the signals stemming from the choline group of PtC had much lower calibration factors than those of fatty acids, for details see the peak information file of QUANTIFY attached in Appendix II. This means that at the same concentration, the choline group will show a much lower signal than e.g. the methyl group of a fatty acid. This may be due to the rapid spin relaxation present in long-chain fatty acids, leading to strong signals in the beginning of the FID, with the choline group showing a slower decay. The slower-decaying but weaker choline signals get additionally weakened by the window function used to avoid FID truncations by reducing signals from the later parts of the FID.

### OMS as Internal Standard

TMS is the commonly used frequency reference substance for NMR measurements of organic solvents such as chloroform. When using TMS as a concentration reference in chloroform liver extracts, high variance of replicate samples was observed. This is probably due to the volatility of TMS with a boiling point of 26 °C, causing strong concentration differences due to minimal differences in sample handling times. A common procedure to avoid these variances is to use the signal of residual protonated

chloroform in the deuterated chloroform as a concentration reference. This has two drawbacks: chloroform is volatile, too, and may therefore be present in different concentrations in different samples due to differences in pipetting. Secondly, the residual chloroform concentration is varying between different charges of deuterated chloroform. Therefore, OMS was tested as a substitute. The boiling point of OMS is 175 °C.

To assess the precision of technical replicates, a mouse liver sample was extracted by Caridad Louis and the chloroform extract prepared with OMS as internal standard. The extract was measured 14 times on different days and stored at -20 °C between the measurements. The OMS integral was used as a concentration standard. RSD's were calculated for all lipid signals. On average, the RSD was  $2.3 \pm 2.1$  %. For comparison reasons, integrals were recalculated relative to the signal of residual protonated chloroform. Here, higher RSD's of  $3.5 \pm 1.5$  % were observed (mean over the RSD's of all lipid signals  $\pm$  SD). On average, using OMS reduced the RSD's by 43.6 %.

For analysis of the precision of extraction replicates, mouse liver was extracted repeatedly by Caridad Louis. Lipid signals were quantified as above. With chloroform as concentration reference, relative standard deviations of  $10.0 \pm 4.8$  % were observed. When using OMS, the corresponding values dropped to  $7.4 \pm 0.5$  %. This means that using OMS as concentration standard leads to lower variances in quantification results as compared to using chloroform as concentration standard. Additionally, these variances are of the same range for all signals analyzed, whereas different signals quantified relative to chloroform also have very different variances.

These results show that using OMS as a concentration reference, reproducible quantification results can be achieved. Additionally, OMS can serve as a frequency calibration standard with its resonance frequency at 0.094 ppm for  $^1\text{H}$  and 0.7 ppm in the  $^{13}\text{C}$  dimension.

## 2.10 Measurement of Blood Serum and Blood Plasma

Blood is a very complex matrix, with solid, emulsified and solved contents. In plasma and serum, the solid compounds have been mostly removed. Still, a large amount of protein remains, which induces broad and unspecific NMR signals. There are several approaches to measure such samples.

### Ultrafiltration

This approach is identical to the protocol for milk ultrafiltration described in Section 2.8.

### Pure Samples

A simple approach is to mix 300  $\mu\text{L}$  of plasma or serum with an equal amount of buffer. The buffer was prepared as follows: 0.4 g TSP, 10.05 g disodium phosphoric acid heptahydrate and 5 mL sodium azide (4 %) were dissolved in 380 mL water. The pH was adjusted to 7.4 with small amounts of 1 mol/L sodium hydroxide or hydrochloric acid. Water was added to reach a volume of 400 mL. After this, 100 mL deuterated water were added to yield a final volume of 500 mL of buffer. To remove the signals of macromolecules, a CPMG experiment was employed. The *cpmgpr1d* (Bruker BioSpin, Rheinstetten, Germany) pulse program was used to collect 65536 data points in 128 scans, an acquisition time of 3.07 seconds and a relaxation delay of 4.0 seconds. Four dummy scans were discarded at the beginning of each measurement. This resulted in a total acquisition time per spectrum of 15 minutes and 47 seconds. The number of loops was set to 128, resulting in a filtering delay of 76.8 milliseconds before the start of the FID acquisition.

As the macromolecules bind to TSP, the reference signal is observed with a large line width and shifted from its original position. Additionally, its intensity is lowered dramatically, leading to a large concentration overestimation of the other metabolites. As a result, neither frequency calibration nor absolute quantification is possible in this way. Instead, frequencies were calibrated using the alanine doublet at 1.48 ppm.

2D HSQC spectra were recorded in the same way as described in Section 2.4 for urine, showing only little disturbance caused by protein content, apart from reduced intensity and shifting of the TSP signal.

As a first step, a relative quantification was performed, where the integrals were divided by the TSP integral. The calibration factors for pure compounds were divided by a factor of 1.56 to correct for the lowered intensity values caused by the filtering of the CPMG pulse program. This value was determined as the ratio of the alanine signal of a standard sample measured with the CPMG program divided by the alanine integral obtained using a 1D NOESY spectrum of the same sample. For absolute quantification, a solution of standard metabolites was prepared in the same way as the blood samples. This standard sample was measured before and after each batch of blood samples. For each sample, absolute TSP integrals were calculated. The previously obtained relative quantification results were corrected for each sample as follows:

$$C_{corrected} = C_{original} \cdot \frac{I_{TSP, sample}}{I_{TSP, standard, mean}}$$

where the  $c$ 's are the metabolite concentrations and the  $I$ 's represent the TSP integral of the sample or the mean of the TSP integrals of the standard samples, respectively.

To develop a suitable protocol for measuring plasma and serum samples, different pulse programs and sample preparations were tested. The analyzed samples included mouse serum and cow plasma.

### Validation of Quantification Results

To test the quantification results, a spike-in experiment was performed on three cow plasma samples. Different amounts of a solution containing common metabolites were added to the samples, resulting in concentration levels raised by 0.91, 0.45 or 0.23 mmol/L, respectively. These spiked plasma samples were then prepared both as pure samples with buffer addition as well as with ultrafiltration in order to compare the different preparation methods. When the quantification results were plotted against the expected concentrations, for all used preparation protocols and pulse programs linear responses were obtained with  $R^2$  values near one. Except for the CPMG spectra of unfiltered plasma, the slope of the observed dose-response-curves was close to one, indicating correct quantification results. The only exception was citric acid, where lower mean slopes of 0.79 (unfiltered samples) and 0.69 (filtered samples) were obtained, indicating consistently too low quantification values.

In the CPMG spectra of unfiltered plasma, too low slope values were observed for all metabolites, usually in the range of 0.45. As the slope for HSQC spectra of unfiltered plasma were close to one, the effect observed in the CPMG spectra cannot be explained by binding of metabolites to proteins.

Fourteen serum samples from dairy cows were provided by Stefanie Klinger of the Tierärztliche Hochschule Hannover (Hannover, Germany). Samples were prepared by ultrafiltration by Caridad Louis, and measured and quantified using 2D spectra. Glucose and BHBA were quantified photometrically by the staff of the Tierärztliche Hochschule Hannover (Hannover, Germany) using the Glucose Hexokinase Fluid 5+1 kit (mti diagnostics, Idstein, Germany) and the Ranbut kit (Randox Laboratories, Crumlin, Co. Antrim, UK), respectively. The comparison to 2D NMR quantification results is shown in Figure 23.

As can be seen, the methods agree well with each other, with  $R^2$  values of 0.86 and 0.85 for glucose and BHBA, respectively. NMR showed slightly higher values, resulting in slopes of 1.10 for glucose and 1.04 for BHBA. This was possibly due to TSP binding to remaining low-molecular weight proteins.

### Long Term Stability

Ten mouse serum specimens were provided by Claus Hellerbrand at the University Clinic of Regensburg (Regensburg, Germany). The samples were prepared and measured without filtering as described above. When the samples were measured again two weeks later after storage at  $-20\text{ }^{\circ}\text{C}$ , strong differences were visible. Signals appeared or grew

strongly, for example at 3.6382, 3.6281, 3.6086, 3.2319, 3.2057 and 0.1664 ppm. On the other hand, signals at 2.2370, 1.9233, 1.3390 and 1.3279 ppm decreased in intensity. After storing these samples for two days in the cooled sample changer at 4 °C, these changes had increased again, thus meaning that the changes were not only due to freezing and thawing, but also occur at cooled storage. This means that untreated serum samples are subject to strong concentration changes, possibly due to residual enzyme activity.

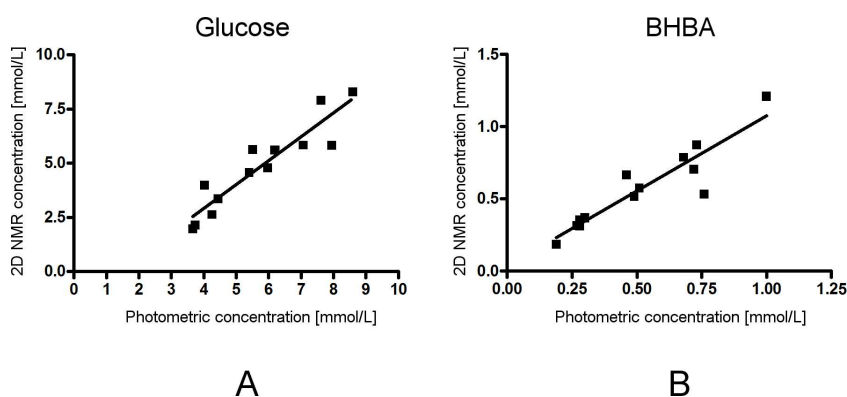


**Figure 23.** Comparison of serum quantification results by 2D NMR and photometric methods for glucose (A) and BHBA (B).

Stability was assessed for unfiltered lithium heparin cow plasma. Two samples were stored for one week at -20 °C and 4 °C, respectively. As for serum, strong changes were visible, although to a smaller extent. Signals at 3.2043 ppm and 0.1634 ppm had increased both at -20 °C and 4 °C. Citric acid had decreased and shifted in position for both temperatures. A signal at 7.7969 ppm had shifted to 7.8005 ppm during sample storage at 4 °C. During storage at -20 °C, no shifting was observed for this signal.

A second experiment was performed on cow plasma samples that were ultrafiltrated by Caridad Louis. The samples were stored at 4 °C for one week. Interestingly, these samples showed much less time-dependent changes than the unfiltered samples mentioned above. No shifting was observed for the citric acid signal. Intensities stayed within a 20 %-margin after one week, indicating only slow changes, the most prominent increase was observed for signals a 3.2043 ppm and 0.1634 ppm. A slight frequency shift was observed for the signal at 7.8586 ppm that shifted to 7.8563 ppm after four days.

These observations show that plasma is overall more stable than serum and that ultrafiltration seems to be a more convenient preparation method than measuring untreated samples. It has been shown recently that ultrafiltration also enables measuring low-intensity signals that are not visible in pure samples at all (Stolzenburg et al. 2011).

### Methanol/Chloroform Extraction

For lipid measurements, plasma was extracted using the following protocol: 100 µL of plasma were added to 500 µL 2:1 chloroform/methanol mixture and vortexed. 100 µL of 0.2 mol/L potassium chloride solution was added, and after vortexing the sample was centrifuged at ambient temperature at 5700 g for 10 minutes. The lower phase was

removed. Two washing steps were performed by adding chloroform/methanol mixture and repeating the above procedure. After each washing step, the lower phase was collected. The collected phases were pooled and dried under a stream of nitrogen. The residue was dissolved in 650  $\mu\text{L}$  of deuterated chloroform with OMS as internal standard. Quantification was performed as described in Section 2.9. For PtC, results were validated by spike-in experiments. Known amounts of an aqueous PtC emulsion were added to the plasma sample prior to extraction. In comparison to the unspiked sample, the PtC concentration increased in the expected manner.

## 2.11 Data Preprocessing for Machine Learning Algorithms

Due to the complex nature of NMR spectra, they are not easily interpreted by machine learning algorithms such as PCA, ICA and SVM. This renders preprocessing steps necessary.

### Spectral Binning

One of the most common methods is spectral binning. Here, the spectrum is split into small areas called bins or buckets. For each bin, the contained signals are integrated. The bin is then assigned the integral value. Thereby, a less complex spectrum is created. This method compensates for small signal shifts caused by differences in pH and salt concentration. The signal that exhibits the highest inter-sample shifts is citric acid. The bin size should be at least the average peak width. Larger bins can correct larger signal shifts, but will result in loss of information as signals of different metabolites are summed up. Figure 24 shows an example for a binned spectrum.

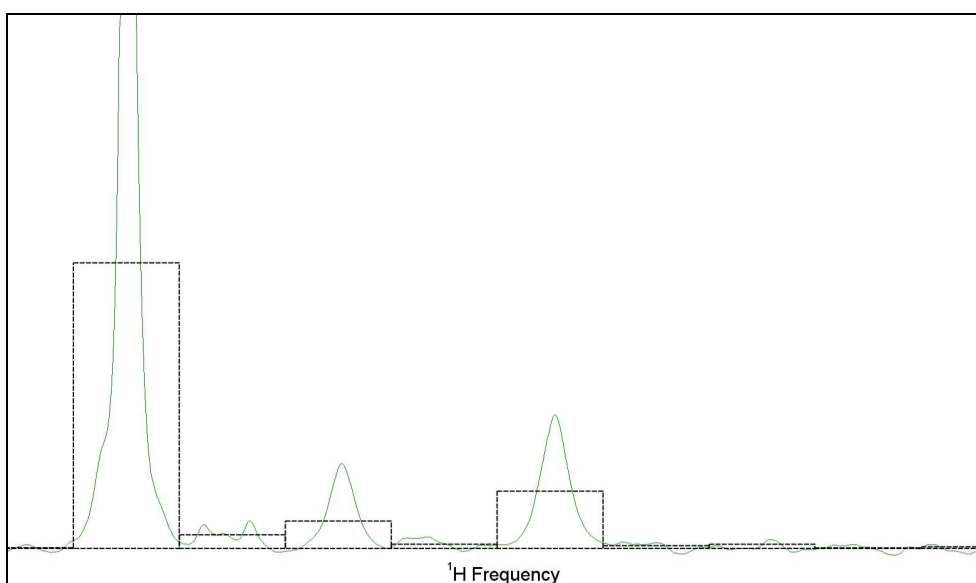


**Figure 24.** Exemplary binning shown for a section of a urinary 1D NMR spectrum. The spectrum (green line) is split into evenly spaced bins (black dotted line). For each bin the spectrum within the bin is integrated.

Binning replaces a complex spectrum with a vector of integral values that can be more easily handled by computer algorithms. 1D spectra were evenly split into bins of 0.01 ppm width using Amix 3.92 (Bruker BioSpin, Rheinstetten, Germany). For 2D HSQC spectra, a bin size of 1.50 ppm and 0.05 ppm was used in the  $^{13}\text{C}$  and the  $^1\text{H}$  direction, respectively. Bins were created in the regions between 150.00 - 5.00 ppm ( $^{13}\text{C}$  direction) and 9.00 - 0.50 ppm ( $^1\text{H}$  direction). The solvent area was excluded from the binning, for details see Table 8 in Appendix I. Urea caused a very broad peak due to proton exchange with the presaturated water protons. Therefore, the urea peak was excluded from binning as well. As methanol impurities were inconsistently present in different buffer batches,

the methanol signal was excluded from binning in case more than one buffer batch was used for the preparation of the analyzed sample set.

In a PCA analysis on 2D spectra of milk samples, signals in the lactose region caused a group separation that seemed to have no biological background. This clustering is due to the fact that the lactose signal is higher by a factor of  $10^4$  compared to the smallest observed concentrations, and even small technical variances will lead to enormous differences. A typical technically caused SD of 3 % would yield a concentration difference of more than 4 mmol/L, this is still by a factor of 20 more than the smallest observed concentrations. Additionally, the large lactose signals cause large baseline fluctuations in their surroundings due to wiggles caused by technical imperfections in the FID's. This is especially true for 2D spectra. The lactose region was therefore excluded from further analyses. In the filter used for milk ultrafiltration glycerol and TEG were present even after rinsing the filters with water. Therefore, the corresponding spectral regions were excluded from binning. All excluded areas can be found in Table 8 (see Appendix I).

### Scaling and Normalizing

After binning, different scaling and normalization methods may be used (Kohl et al. 2011). These methods aim at removing disturbing technical or biological variances.

One of the most basic methods is normalization to the sum of all bins of one spectrum. This shall correct for dilution effects such as in urine and for differences in signal intensities due to technical reasons. Each bin value is divided through the sum of all bin values.

Another method commonly used for urine samples is normalization to creatinine content. As urine may be diluted in different specimens depending on the amount of water consumption of the individual, a compound is needed that is excreted in constant amounts throughout the day. Creatinine is usually chosen for this aim. In creatinine normalization, all bin intensities are divided by the intensity of one of the bin of the creatinine signals.

Beside these very basic transformations, a plethora of other scaling and normalization methods is available. The most common transformations have been tested and compared recently by Stefanie Kohl (Kohl et al. 2011). For this publication, a Latin Square design was set up. A Latin Square design is a sample set that shall allow the assessment of the quality of data analysis methods. In this design, several compounds are spiked into aliquots of a reference sample in different concentrations. The difference to a dilution series is that all compounds added to one aliquot have different concentrations. In total, the sum of concentrations of added compounds is identical for each aliquot. This is done to avoid confusing effects that might occur when the aliquots have very differing overall concentrations in the end. Eight metabolites present in urine were chosen as spike-in compounds in a manner that their signals showed no overlapping regions. Aliquots of a reference urine sample were spiked with the chosen eight compounds by Nadine Nürnberger. Two Latin Square sets with different concentration ranges were prepared in this way. For the two sets, 1D  $^1\text{H}$  and 2D  $^1\text{H}$ - $^{13}\text{C}$  HSQC spectra were recorded.

---

## 3 Biomedical Application

### 3.1 Autosomal Dominant Polycystic Kidney Disease

In Chapter 2 it was shown that quantification results from 1D and 2D NMR spectra have a high accuracy and precision and that the spectra are well suited for disease analysis. Therefore, other meaningful applications of the technique were looked for. Autosomal dominant polycystic kidney disease (ADPKD) is an inherited kidney disease that leads to the formation of cysts in the kidney. These cysts are growing slowly, yet continuously, resulting in reduced kidney function and, eventually, kidney failure (Gabow 1993). As ADPKD is manifested in the kidney, changes in the urinary profile are to be expected. Therefore, ADPKD was chosen as an aim for an NMR-aided disease diagnosis approach.

Urine specimens from 64 ADPKD patients, 46 healthy volunteers and 68 patients with other kidney diseases were provided by the University of Erlangen-Nürnberg (Nürnberg, Germany) and the University Clinic of Regensburg (Regensburg, Germany). Samples were prepared and measured as described in Sections 2.4 and 2.5. The spectra were evaluated using a support vector machine (SVM) by Wolfram Gronwald (Gronwald et al. 2011). The SVM could distinguish between ADPKD patients and healthy controls as well as other kidney diseases with an accuracy of more than 85 %. Unknown discriminating compounds were identified jointly together with Wolfram Gronwald. Among the significantly different metabolites, methanol was the most unexpected one. To ensure that the observed signal really stems from methanol, several spike-in experiments were performed. Additionally, methanol was quantified by Liane Paul and Thomas Gilg at the Institute of Forensic Medicine, Ludwigs-Maximilians-University (Munich, Germany) using headspace-gas chromatography. These measurements confirmed the assumption

that raised methanol levels were observed for ADPKD patients. Other discriminating bins contained signals at typical protein signal positions. To confirm the identification as protein signals, CPMG spectra were recorded to remove the protein signals. In addition, an acid hydrolysis of the urine was performed by Caridad Louis to remove proteins. After hydrolysis, the samples were evaporated and redissolved in pure water. After pH adjustment, the samples were measured again. The concerning signals had disappeared, while amino acid signals had risen. By this result, the discriminating signals could be positively identified as protein signals.

## 3.2 Metabolic Differences Between Dairy Cow Breeds

In the previous sections, NMR was successfully employed for metabolite quantification in urine samples and for discrimination of samples from human disease patients from healthy control samples. Besides projects considering human diseases, one of the main topics of this thesis is related to animal health issues, especially those of dairy cows. In the following sections, analyses performed on biofluid specimens collected from dairy cows are presented. The chemical analyses in this section were performed jointly with Martin Almstetter. They have in parts already been published (Klein et al. 2010) and are also part of the Ph.D. thesis of Martin Almstetter.

Over the last few decades milk production in dairy cows has dramatically increased. However, this has been accompanied by a substantially raised rate of health and fertility problems (Pryce et al. 1997). The enhanced energy requirements during early lactation due to selection of high-yielding cows result in an increased allocation of available energy resources to milk synthesis and less to functions relevant to fertility and fitness (Hüttmann et al. 2009). If energy requirements exceed energy availability from daily food intake, body fat is mobilized (Banos et al. 2005), which is a physiological mammalian process. However, excessive mobilization is thought to play a major role in the increased occurrence of so-called production diseases. In addition, the presence of health problems has been related to the extent and duration of the energy deficit in early lactation (Collard et al. 2000).

Production diseases are the main health issues in dairy cows, including ketosis, mastitis and ruminal acidosis, which lead to animal suffering, reduced longevity and economic loss (Ingvarsen et al. 2003). Ketosis is a condition where large amounts of ketone bodies (acetone, beta-hydroxybutyric acid (BHBA) and acetoacetic acid) are released into the blood stream (Geishauser et al. 2000). These ketones are formed in the liver from acetyl-CoA from fatty acid breakdown and serve as energy sources in the body. Ruminal acidosis is the lowering of the pH value in the rumen below physiological levels caused by an imbalance between production and use of lactic acid. Ruminal acidosis is often caused by digestion of non-fiber carbohydrates from high grain diets (Huber 1976). Mastitis is an inflammation of the udder. The economic costs of production diseases amount for hundreds of millions of euro per year for France and the UK alone (Bishop et al. 2009).

Measurement of selected milk constituents to monitor the udder health or the metabolic status of cows has attracted much attention in dairy research and is widely used on dairy farms. Milk somatic cell count (SCC) and *N*-acetyl- $\beta$ -D-glucosaminidase activity are well-known indicators of intramammary infections (Pyörälä 2003). Furthermore, the biochemical milk profile has been related to the health status of the cow and, in particular, to imbalances during early lactation (Duffield et al. 2009). Acetone, acetoacetic acid and BHBA in milk are biomarkers for subclinical ketosis. BHBA milk concentrations  $\geq 0.10$  millimole per liter (mmol/L) indicate subclinical ketosis yielding a sensitivity, specificity and a positive and negative predictive value of 69, 95, 75 and 93 %, respectively. In another study, thresholds of 0.16 mmol/L for milk acetone and 0.07 mmol/L for milk BHBA have been proposed (Enjalbert et al. 2001). On the basis of the

close interaction between blood circulation and milk secretion, changes in additional milk metabolites that have yet to be defined can be assumed to reflect the metabolic and health conditions of the cow and the mammary gland. Previously, both NMR (Belloque & Ramos 2002; Hu et al. 2007) and gas chromatography-mass spectrometry (GC-MS) (Toso et al. 2002; Boudonck et al. 2009) have been applied successfully to the analysis of compounds in commercially available milk samples. Here, NMR and GC-MS were applied to the determination of a total of 44 milk compounds in milk specimens obtained from individual dairy cows of two different breeds during early and late lactation, with an emphasis on metabolites related to energy metabolism. The ultimate aim of the study was to identify compounds that are highly correlated to the metabolic status of the individual animals.

### Collection of Milk Samples

Morning milk specimens were collected by Steffi Wiedemann and Gregor Schlamberger from the Department of Physiology of the Technical University Munich (Freising, Germany) at two research farms from cow breeds representing different milk production levels. At the research farm Veitshof (Freising, Germany; farm #1), milk samples were collected from highly productive Brown Swiss cows with an average 305-day milk yield of 9200 kilogram (kg). Samples were collected for three groups of animals: 27 samples in early lactation ( $42.8 \pm 25.3$  days in milk (DIM)), seven samples in mid lactation ( $143.4 \pm 21.5$  DIM) and 24 samples in late lactation ( $345.7 \pm 159.2$  DIM). At the Bavarian State Research Center for Agriculture (Grub, Germany; farm #2), milk samples of Simmental Fleckvieh cows with an average 305-day milk yield of 8300 kg were collected. Twenty-eight samples were collected in early lactation ( $25.0 \pm 12.3$  DIM) and 20 samples were collected in late lactation ( $261.8 \pm 41.3$  DIM). All cows were offered ad libitum a partial total mixed ration (TMR) based on corn and grass silage. Concentrates were offered according to milk yield.

One aliquot of the collected milk samples was analyzed by MPR Bayern (Wolnzach, Germany) for milk protein, fat, lactose, urea and pH by MilkoScan FT 6000 and for SCC by Fossomatic-FC. The second aliquot was defatted by centrifugation for 15 minutes at 3000 gravitational accelerations (g) at a temperature of four degrees Celsius ( $^{\circ}\text{C}$ ), and skim milk was immediately stored at  $-20^{\circ}\text{C}$  until analysis.

Twenty-three metabolites were quantified in the milk samples using one-dimensional (1D) and two-dimensional (2D) NMR. These metabolites were amenable to NMR analysis due to their high abundance respectively a high number of chemically equivalent protons giving rise to a single signal. Concentrations of amino acids, BHBA, glucose and citric acid were determined by means of GC-MS by Martin Almstetter (Klein et al. 2010). Analysis of the results was performed jointly with Martin Almstetter. Bland-Altman analyses were performed by Wolfram Gronwald.

### Analysis of Milk Metabolites

The observed concentration range for each of the milk metabolites analyzed exclusively by NMR is given in Table 9 (see Appendix I). The ranges were calculated over all milk samples from both farms, and, because for some metabolites concentration values above their lower limit of quantification (LLOQ) were not available for all samples, no average

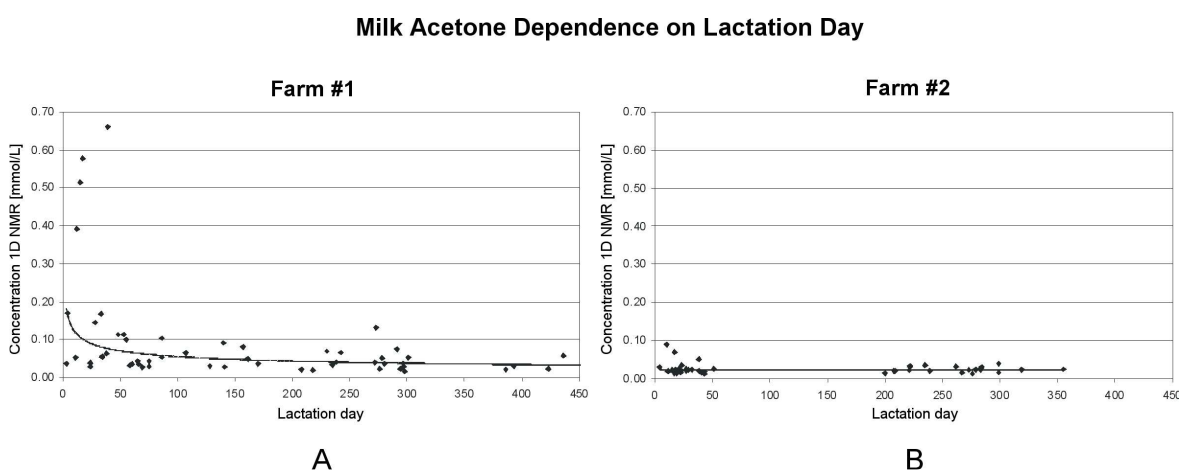
values and standard deviations are given. As expected from the literature, concentrations of lactose in milk fell within a relatively narrow concentration range of 118 to 160 mmol/L (Roginski & Fuquay 2004). In contrast, metabolites such as phosphocholine (PC) showed an almost 10-fold difference between the lowest (0.143 mmol/L) and the highest (1.355 mmol/L) concentration measured.

Pearson correlation coefficients between the quantified metabolites were calculated and are shown in Table 10 (Appendix I). Significant correlations were marked, using conservative global limits for the correlation coefficient  $R$  above 0.5 and below -0.5. At the 5 % level, statistical significance is generally reached with these  $R$  values for a sample size less than 20. For some metabolites up to 106 measurements above the individual LLOQ were available, while the number was considerably smaller for others. Therefore, these global limits for  $R$  ensured that only significant correlations were marked as such.

### Investigation of Metabolic Status During Early Lactation

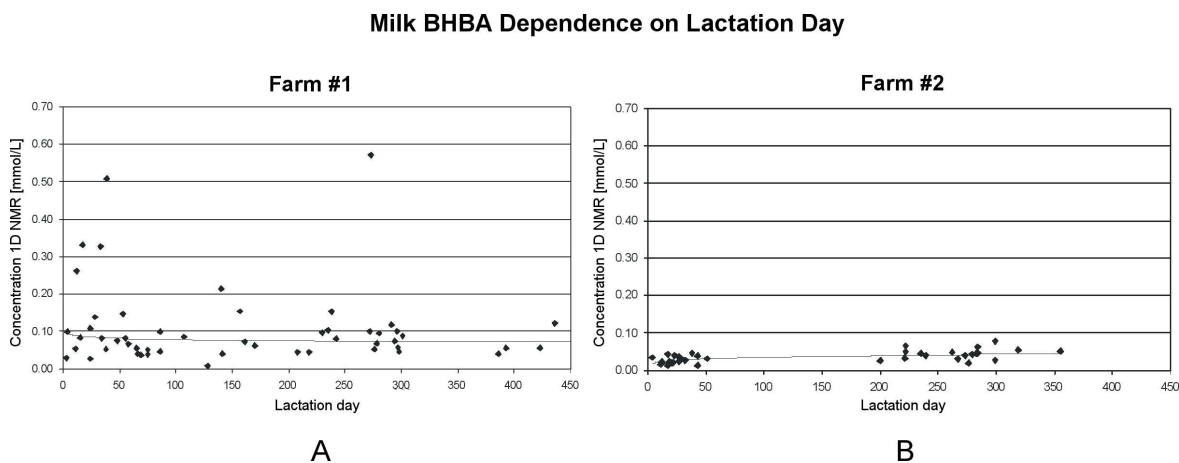
An important objective of this thesis was the measurement of metabolites that might serve as indicators of a metabolic imbalance during early lactation. In the following, metabolites quantified by NMR are reported and discussed. For analytes measured by GC-MS see (Klein et al. 2010) and the Ph.D. thesis of Martin Almstetter.

Figure 25A shows the correlation between lactation day and observed acetone concentration for farm #1. Some cows yielded significantly increased acetone values above the threshold concentration for detection of subclinical ketosis of 0.16 mmol/L during the first days of lactation (Enjalbert et al. 2001). Drastically lower acetone values of about 0.04 mmol/L were found for other cows at a similar lactation stage. Generally, acetone values decreased during the first 70 days of lactation and remained fairly constant thereafter. Figure 25B shows the correlation between acetone concentration and lactation day for farm #2. Here, only slightly increased acetone concentrations of up to 0.088 mmol/L were observed for a few cows during the first 70 days of lactation.



**Figure 25.** Correlation between lactation day and acetone concentration [mmol/L] for milk specimens from farm #1 (A) and farm #2 (B). To clarify the general trend of the data, potential regression lines were added. Adapted from (Klein et al. 2010).

Generally, the observed acetone concentrations were lower for cows from farm #2. During late lactation, average values of 0.024 mmol/L were observed for cows from farm #2, while the corresponding values for farm #1 were about 0.030 mmol/L. Similar but less pronounced effects were observed for BHBA (Figure 26).



**Figure 26.** Correlation between lactation day and BHBA concentration [mmol/L] for milk specimens from farm #1 (A) and farm #2 (B). To clarify the general trend of the data, a potential regression line was added. Adapted from (Klein et al. 2010).

In the early lactation period, increased values above the threshold concentration of 70  $\mu\text{mol/L}$  for the detection of subclinical ketosis (Enjalbert et al. 2001) were found in 29 cows from farm #1. Note that for one cow increased BHBA values were obtained during late lactation, indicating a possible health problem. In contrast to farm #1, cows from farm #2 showed constant BHBA concentrations over the entire lactation period. Acetone and BHBA showed a good correlation over all cows, with a Pearson correlation coefficient of  $R = 0.69$  (Table 10, Appendix I).

This is in agreement with a published correlation of milk acetone to BHBA of  $R = 0.68$  (Enjalbert et al. 2001). Citric acid has been suggested as a marker of energy status in the dairy cow, being correlated with ketones in milk and de novo fatty acid synthesis (Baticz et al. 2002). This suggestion is supported by the data with an observed Pearson correlation coefficient of  $R = 0.45$  between citric acid and acetone in milk and a corresponding correlation coefficient of  $R = 0.39$  between citric acid and BHBA. Milk citric acid concentration has been found to vary widely throughout lactation (Garnsworthy et al. 2006) depending on nutrition and season (Holt & Muir 1979). Generally, it is higher in early lactation and decreases gradually as lactation progresses (Konar et al. 1971). In the study reported here, citric acid remained fairly constant throughout lactation ( $6.270 \pm 1.311$  mmol/L), but concentrations that were determined by GC-MS were higher than those obtained by NMR in commercial milk in a previous study (Hu et al. 2007). In this context, it should be noted that citric acid was also determined by 2D NMR. However, spike-in experiments where known amounts of citric acid were added to milk showed that, for this metabolite, the GC-MS measurements were more accurate. One likely explanation for the observed discrepancies to the NMR measurements is that milk

citric acid is located in part in the colloidal phase of milk and, therefore, could not be determined by NMR. The analysis of specific metabolites throughout lactation showed increased PC concentrations for all cows in early lactation (Figure 27), with a maximum of 1.355 and 0.991 mmol/L for cows from farm #1 and farm #2, respectively.

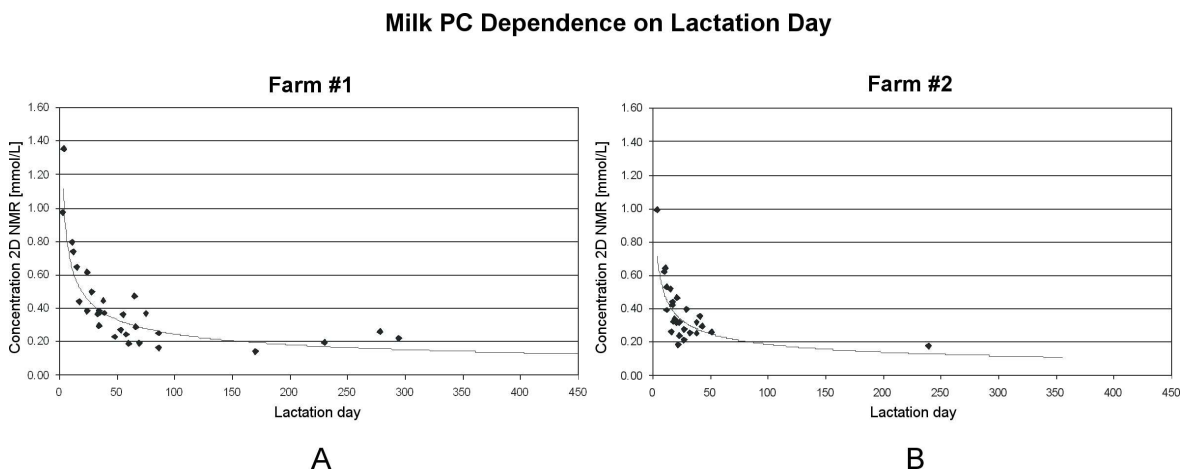


**Figure 27.** Correlation between lactation day and PC concentration [mmol/L] for milk specimens from farm #1 (A) and farm #2 (B) as measured by 2D NMR. To clarify the general trend of the data, a potential regression line was added. Adapted from (Klein et al. 2010).

Around day 70 of lactation, PC concentrations had decreased to approximately 0.25 mmol/L at both farms and remained relatively constant thereafter. Note that in the last lactation third, PC concentrations had decreased below the LLOQ in some cows. PC is a precursor of choline and serves as its storage form within the cytosol. It showed a slightly negative correlation with DIM ( $R = -0.42$ ). Choline values in early lactation were found to be somewhat lower than values from the last lactation third ( $R = 0.38$ ). These findings agree only partly with those in human milk, where a distinct decrease during lactation in the concentrations of PC and free choline was found, but only for the first 90 days and three weeks, respectively, after delivery (Holmes et al. 2000). Choline in milk can be derived by active uptake from maternal circulation (Chao et al. 1988) and from de novo synthesis within the mammary gland. Higher needs of dairy cows for the limiting amino acid methionine for transmethylation reactions and milk protein synthesis lead to altered methyl group metabolism (Pinotti et al. 2002). Choline plays an important role in the metabolic pathways of methyl groups via the tetrahydrofolate system, which might explain the correlation between milk protein content and free choline in milk ( $R = 0.50$ ). Furthermore, it has been demonstrated previously that abomasal infusion of choline and administration or feeding of rumen-protected choline increases milk protein content (Sharma & Erdman 1989; Erdman & Sharma 1991). The quantification of *N*-acetylcarbohydrates (*N*-acetyl-lactosamine and *N*-acetyl-glucosamine) by NMR was described previously and values were in a similar range as those presented here (Hu et al. 2007). Acetyllactosamine is found in many glycoproteins and glycolipids. That might explain the correlation between *N*-acetylcarbohydrates and protein content in milk ( $R = 0.57$ ) and between other membrane-associated analytes such as PC ( $R = 0.57$ ) and betaine ( $R = 0.74$ ). As seen in Figures 25, 26 and 27, metabolite concentrations differ between the two

analyzed breeds both in metabolites connected to energy metabolism such as acetone and in metabolites connected to other areas of the metabolism. To analyze these differences, metabolites were selected for which a sufficient number of measurements were available for the last lactation third. The median concentrations of most metabolites were higher in milk samples from Brown Swiss cows than from Simmental Fleckvieh cows. A metabolite that should remain almost constant is lactose and, as expected, almost no difference was observed between the two breeds. The metabolic differences observed between the herds are most likely associated with differences in breed and feed management.

### **Correlations Between Milk and Plasma Metabolites**

Plasma samples from the animals analyzed above were provided from the Department of Physiology of the Technical University Munich (Freising, Germany). Plasma metabolites were quantified by means of GC-MS by Martin Almstetter. Martin Almstetter compared the plasma metabolite levels to the milk metabolite levels quantified by NMR and GC-MS. This work is currently being prepared for submission by Martin Almstetter. To assess the correlation between milk and plasma metabolites, an algorithm for correction of correlation coefficients according to partial correlations was developed as described in Section 2.3. The algorithm uses partial correlation coefficients to find significant “real” correlations, in the meaning that these correlations do not depend on correlations to a third metabolite that both metabolite in question share. The R code can be found in Appendix II. Results showed that metabolites connected to energy metabolism such as acetone and BHBA were highly correlated between plasma and milk, whereas most other metabolites do not show strong correlations.

### 3.3 Metabolic Predictors for Dairy Cow Health Status

In the previous chapter, milk samples from two different herds were analyzed. However, for each animal, only one sample was available. As the results revealed partly pronounced changes in milk composition throughout lactation, a second study was performed on a large herd of highly productive Holstein-Friesian (HF) cows. For each animal, a time course of milk samples was measured to specifically search for metabolites that show prognostic potential with regard to animal health. This section has been published in part (Klein et al. 2011a).

Of the production diseases, ketosis is one of the most common ailments. In milk, elevated levels of the ketone bodies BHBA, acetoacetate and acetone are accepted biomarkers for ketotic conditions (Geishauser et al. 2000; Enjalbert et al. 2001). However, currently no biomarkers are available that show long-term prognostic potential, i.e. which predict a cow's susceptibility to ketosis during lactation prior to a rise in the milk levels of the ketone bodies. Such biomarkers are of great interest for an early treatment of susceptible animals and for the selection of metabolically stable animals for breeding purposes. Therefore, the detection of prognostic metabolic biomarkers was the aim of this study.

Since milk can be collected on a routine and non-invasive basis, it is well suited for metabolic analyses in dairy cows (Klein et al. 2010). In this study, individual time series analyses of milk constituents were performed for animals from a herd of HF cows, reflecting levels and changes of milk metabolites during early and mid lactation. For all animals a complete description of health issues that had occurred during the study period was available.

#### Collection of Milk and Plasma Samples

Milk samples from HF cows were collected by the staff of the Karkendamm research farm (Bimöhlen, Germany) and provided by Nina Buttchereit from the Christian-Albrechts-University (Kiel, Germany). Preselected high yielding cows with an average energy corrected milk yield of  $32.8 \pm 4.7$  kg per day were investigated. The animals were offered a TMR ad libitum. To all cows in the first lactation fixed amounts of concentrates were offered until DIM 180 (average  $2.3 \pm 0.5$  kg). Composition of TMR varied over the observation period. Crude protein, bypass protein and the net energy content for lactation (NEL) of TMR were kept relatively constant. NEL of TMR ranged between 6.9 and 7.2 megajoule per kilogram (MJ/kg) of dry matter. A detailed overview of the feeding practice is given in a previous publication (Buttchereit et al. 2010a).

From each cow weekly evening milk samples were collected during the first five weeks of lactation and an additional milk sample in month six postpartum (mid lactation). At this time point, performance data collected so far was evaluated by the research farm staff according to a bull dam test for a subset of cows in their first lactation. Under-performing cows were sent off the farm. For the remaining (heavily selected) animals, another milk sample was collected around day 305, prior to the cows being dried off. In total, 1587 milk samples were collected from 308 animals between October 2008 and June 2010. At the research farm in Karkendamm mostly cows in the first lactation are kept, resulting in a smaller number of animals from higher lactations. Note that due to various reasons (e.g.

serious health issues), a complete time series could not be obtained for all cows. Milk yield was recorded on a daily basis and milk composition was analyzed weekly based on samples from two consecutive milkings by the staff of the research farm. Animals were held with permission of the Christian-Albrechts-University (Kiel, Germany), and were treated in conformance with commonly practiced ethical standards. Breeding values for energy balance (EB) and fat-to-protein ratio (FPR) were estimated by Nina Buttchereit from the Christian-Albrechts-University (Kiel, Germany).

Blood was drawn from the *vena caudalis mediana* into lithium heparin coated tubes at varying time points during the first five weeks of lactation. Plasma was prepared by immediately centrifuging the collection tube at 2800 g and 15 °C for 20 minutes. Plasma was stored at -80 °C until analysis. Milk samples were prepared and measured jointly with Sebastian Miemczyk, Ann-Kathrin Immervoll, Caridad Louis and Nadine Nürnberger.

### Choice of Milk Samples

The selection step described above, the so-called bull dam test, changes the group composition drastically after lactation month six. Therefore, the milk samples from day 305 were excluded from further analyses to avoid misleading correlation patterns resulting from group inhomogeneities (Köhler et al. 2002). 1267 milk specimens from 264 animals in the first lactation and 232 milk specimens from 57 animals in lactation two to seven were chosen for further analysis. For the analysis of blood plasma metabolites, 88 plasma specimens from different cows were analyzed. Of these, 66 samples were obtained for the investigation of hydrophilic metabolites. Lipophilic plasma metabolites were analyzed from the remaining 22 plasma samples collected in the second week of lactation.

### Observed Diseases

Metadata for the cows were collected based on the data received from Nina Buttchereit. Considering only the animals from the first lactation, 51 out of 264 animals suffered from ruminal acidosis during the lactation. Fourteen out of 264 animals suffered from ketosis. Apart from these metabolic diseases, 90 of the 264 animals enrolled in the study suffered from mastitis at least once during the lactation. 57 of the total 308 animals had stayed healthy throughout the whole observed period. Animals diagnosed with mastitis were treated as acutely ill for five days, as the milk of diseased cows had to be discarded for five days on average. For the other diseases analyzed in this study, a time of eight days was used before an animal was classed as healthy again (Buttchereit 2011). All metabolic health issues diagnosed for animals in their first lactation are shown in Table 11 (see Appendix I).

As animals were treated as soon as a diagnosis had been made, the samples marked as acutely ill may contain drug traces or may show other alterations due to treatment-related metabolic changes. Therefore, these samples were not a good base for searching biomarkers and were not used for discriminatory analyses. Instead, all samples from animals that suffered from a certain disease at least once during lactation were assigned to a *diseased during lactation* group.

### **Pre-Investigations**

An initial principal component analysis (PCA) analyses performed on samples from lactation month six showed a slight group separation mainly driven by the citric acid signal. The signal intensities showed no significant differences between the groups, but the citric acid signal showed shifts in position. pH values of 16 samples with extreme shifts of the citric acid signal were measured, but no significant differences between the groups observed in PCA were found. Possibly, the group separation depended more on other factors such as salt concentration. The groups observed showed no correlation to disease status.

### **Main Investigations**

Milk metabolites were quantified as described in Section 2.8. In Table 12 (Appendix I), milk metabolite concentrations of cows in the first lactation are shown. Metabolites that could only be quantified with concentration values above the individual LLOQ in less than 20 % of the samples were excluded from further analyses. As can be seen, many compounds are subject to strong concentration changes during the first weeks of lactation.

### **Time Series**

For ketone bodies, time series were analyzed. The animals that were not diagnosed as diseased at any time were used as a healthy control group. Most milk samples taken within one month before an acute ketosis showed raised levels of acetone and BHBA. For acetoacetic acid no clear trend was visible in this direction. At the time of an acute disease, acetone and BHBA levels had dropped strongly in all cases and were mostly in the normal range. As animals diagnosed with ketosis received either glucose infusions or orally administered glucoplastic substances, the drop in ketone bodies is most probably treatment-related. After acute disease, the ketone levels were in the range of the healthy control group. Two striking findings became obvious: Not all animals diagnosed with ketosis showed raised levels of acetone or BHBA before or during the disease. Ketosis had been diagnosed mostly based on the experience of the farm staff, not on laboratory tests. This raised the possibility of false positive diagnoses. The second finding was that even in the healthy control group more than 10 animals showed ketone levels above the threshold for subclinical ketosis. All of these animals had normal levels at mid-lactation. This might be due to undiagnosed ketosis, or due to the fact that this group of animals can cope better with negative energy balance and raised ketone levels. Ketone levels were generally higher in milk from HF cows than in milk from the Brown Swiss and Simmental Fleckvieh cows analyzed in Section 3.2. This fits with the finding that HF cows have the highest milk yield of these three breeds (Zobel et al. 2011). A high milk yield leads to high energy requirements and, thus, may lead to stronger negative energy balance, causing more body fat mobilization and ketosis.

### **Searching for Genetic Subgroups**

The main aim of this study was the identification of metabolic factors indicating an inheritable long-time metabolic stability. In Section 3.2 it was shown that different animals of the same breed kept under identical conditions on the same farm coped quite differently with the metabolic stress of early lactation. Therefore, the presence of genetically different subgroups in the population analyzed here was suspected. It can be expected that within these subgroups metabolites connected directly or indirectly to the

respective genes are affected and that for some metabolites in each subgroup a distinct distribution of concentrations is observed. In turn, this will lead to non-normally distributed data when considering the whole population, with a distinct two-peak distribution in case of two subgroups. To test for this, milk samples from lactation month six were chosen, as the strong concentration fluctuations of milk constituents in the first lactation third had diminished which led to almost stable levels by then.

All quantified milk compounds were tested for agreement with a normal distribution. For most compounds, normal distributions were found. In contrast, for GPC, fumarate and oxaloacetate, two-peak distributions were found with significant deviations from normal distributions with p-values of 0.014, 0.0025 and  $5.8 \cdot 10^{-6}$ , respectively.

In Figure 28, N-acetyl-carbohydrate (NAC) and GPC concentrations are shown as examples for normally and non-normally distributed compounds. A Gaussian distribution and a sum of two Gaussian distributions were used to approximate the observed data, respectively.

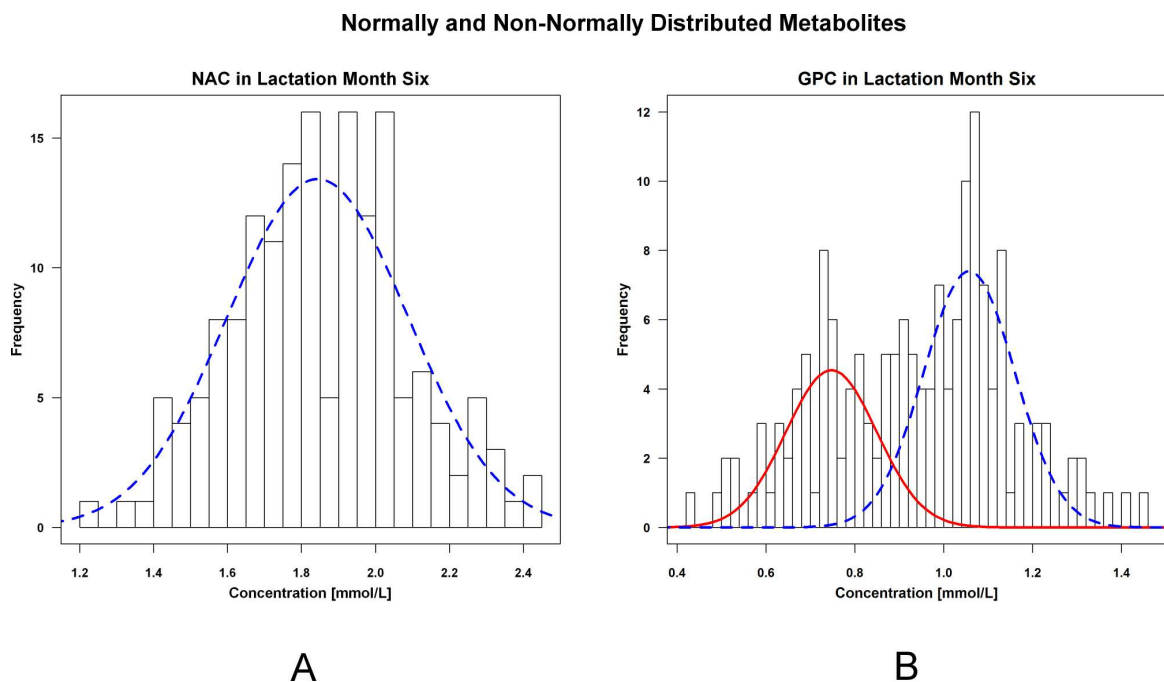


**Figure 28.** Histograms of normally and non-normally distributed metabolite concentrations [mmol/L], exemplarily shown in (A) for NAC and in (B) for GPC in lactation month six of the first lactation. One respectively two Gaussian functions were fitted to illustrate the different distributions. The frequency values indicate the number of animals contributing to one bar of the shown histograms. Adapted from (Klein et al. 2011a).

For each of the three non-normally distributed compounds, the population was divided into two subgroups with high respective low values. The threshold was calculated as the inter-peak minimum of the fitted sum of Gaussians.

To assess the validity of the mentioned group classification, milk samples from other time points were analyzed. Only for GPC the difference in concentration levels was conserved

throughout the whole lactation, i.e. animals with high (respectively low) GPC values in mid lactation also had high (respectively low) GPC values in early and late lactation. This indicates that GPC is a robust measure for the underlying, metabolically differing, subgroups.

Therefore, the subsequent analyses concentrated on the differences in GPC. For GPC, the calculated threshold was 0.87 mmol/L.

Next, it was analyzed whether correlations between the GPC value and disease status were present. Animals were grouped for each disease into one of two groups: Group #1 contained all animals that were diagnosed at least once considering the whole lactation period with a certain disease, e.g. ketosis, while group #2 contained all other animals. The subgroup with ketosis had significantly lower GPC values compared to the non-ketotic subgroup, with a p-value of 0.036. For the other metabolic diseases shown in Table 11 (see Appendix I), no significant correlations to GPC were found. The distributions of GPC for ketotic and non-ketotic animals are shown as a density plot in Figure 29.

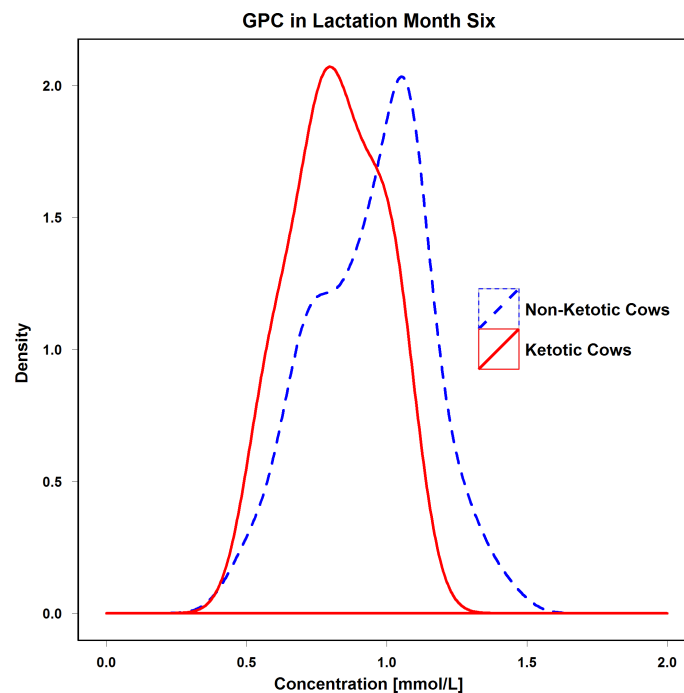


**Figure 29.** Distribution of GPC concentrations [mmol/L] for ketotic and non-ketotic cows in month six of the first lactation. The group of ketotic animals contained all animals that were diagnosed at least once with ketosis during the entire lactation period, while the non-ketotic animals stayed healthy throughout lactation. Both curves were normalized to a total area of one and were smoothed using a Gaussian kernel density estimator. Adapted from (Klein et al. 2011a).

The figure shows that the concentration distributions differ both in range and maximum position between ketotic and non-ketotic animals. The shoulders left of the maximum of the non-ketotic group and right of the maximum of the ketotic group are striking. The first shoulder might be caused by animals with an undiagnosed, subclinical ketosis. The second shoulder might then be due to healthy animals that were erroneously diagnosed

with ketosis. It is obvious that the maxima of the ketotic and the non-ketotic population correspond to the two peaks of the overall distribution seen in Figure 28.

In the group of animals with above-threshold GPC levels, significantly lower PC concentrations were observed during the first four lactation weeks, with p-values of 0.013,  $2.5 \cdot 10^{-5}$ ,  $9.8 \cdot 10^{-3}$  and  $2.6 \cdot 10^{-4}$ , for week one, two, three and four, respectively.

Due to the observed interdependence of GPC and PC, the ratio GPC/PC was calculated from the respective molar concentrations. For the GPC/PC ratio, density plots were calculated for ketotic and non-ketotic animals according to the definitions given above. As an example, the density plots for lactation week three are shown in Figure 30.

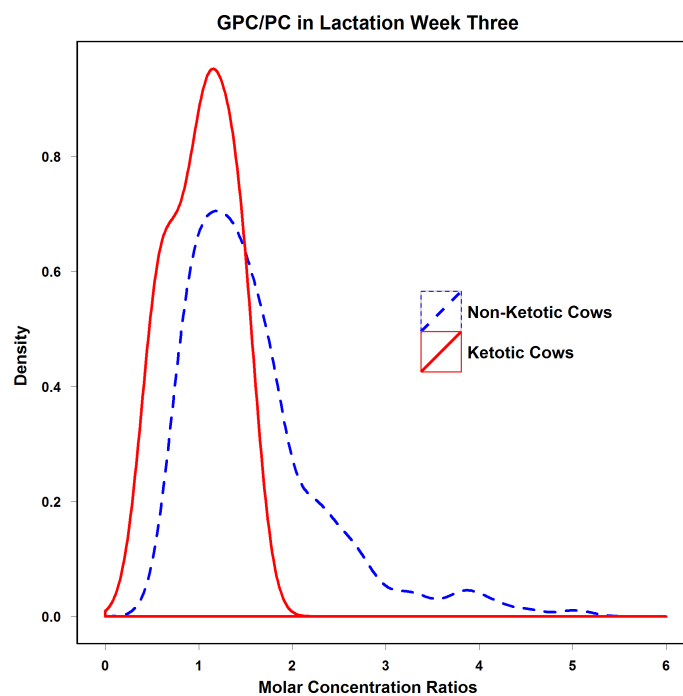


**Figure 30.** GPC/PC ratios for ketotic and non-ketotic cows at week three of the first lactation. The group of ketotic animals contained all animals that were diagnosed at least once with ketosis during the entire lactation period, while the non-ketotic animals stayed healthy throughout lactation. Both curves were normalized to a total area of one and were smoothed using a Gaussian kernel density estimator. Adapted from (Klein et al. 2011a).

The distributions of GPC/PC ratios for ketotic and non-ketotic animals are very similar concerning maximum and width, but differ in the right-hand tail for healthy animals. Obviously, animals with high GPC/PC ratios are less prone to ketosis. This effect can be seen in the first four weeks of lactation but vanishes later on. This is due to the fact that GPC and PC levels decrease almost exponentially during the first weeks of lactation, but as PC continues to drop, GPC levels start rising again around week five, approaching the starting concentration by mid lactation (Table 12 in Appendix I).

The observations made so far clearly show that it is possible to define a threshold for the GPC/PC ratio above which healthy animals are safely detected. A ratio of 2.5 for GPC/PC was manually selected to identify healthy animals within the population. Using this threshold, the samples from the first four lactation weeks were classified. Most of the

animals that were above threshold dropped below threshold at least once during the first four lactation weeks. To take this into account, the GPC/PC ratio was determined several times during the first four weeks of lactation, and all animals showing ratios above threshold at least once were selected. This resulted in 41 out of 260 animals (16 %) with at least one milk sample above the threshold.

No animal in this subgroup suffered from ketosis at any time during the entire lactation period, compared to an incidence of 6.4 % in the subgroup below threshold. This means that during the first few weeks of lactation a safe prognosis for animals that will not develop ketosis later on is possible based on the GPC/PC ratio. Correspondingly, acetone and BHBA values were lower in the high GPC/PC group during the first four lactation weeks, indicating lower incidence of acute subclinical ketosis in this group. The difference in acetone was significant in weeks one, three and four, with p-values of  $4.6 \cdot 10^{-2}$ ,  $2.1 \cdot 10^{-2}$  and  $4.1 \cdot 10^{-3}$ , respectively. The difference in BHBA was significant in weeks three and four, with p-values of  $4.3 \cdot 10^{-2}$  and  $1.0 \cdot 10^{-3}$ , respectively.

A low ketosis risk in the first lactation is expected to be predictive for the health during the next lactations, as high correlations have been observed between ketosis incidences in different lactations (Erb & Grohn 1988). In the analyzed data set, disease data from the second lactation was only available for four of the 41 animals above GPC/PC threshold in the first lactation period. None of these four had developed ketosis during the next lactation. Although this number is very low, it supports the idea that the GPC/PC ratio has predictive abilities for following lactations.

Milk parameters were compared between the groups above and below GPC/PC threshold. Milk yield, fat and protein content of each animal were averaged over all measurements for week one to five and for month six. For milk yield and protein content no significant differences were observed between the groups at any time point. For fat content, the group above threshold showed lower values at all six time points. This difference was significant at all six time points with p-values of  $1.4 \cdot 10^{-3}$ ,  $3.2 \cdot 10^{-3}$ ,  $1.0 \cdot 10^{-2}$ ,  $7.4 \cdot 10^{-4}$ ,  $4.2 \cdot 10^{-5}$  and  $7.1 \cdot 10^{-5}$ , respectively. On average, the milk of animals above the threshold contained 0.4 % less fat than milk from animals below threshold. The concentration values are shown in Table 13 (see Appendix I).

As an alternative for using the GPC/PC ratio, in cases where no values from the first weeks of lactation are available, GPC concentrations from mid lactation were evaluated for their ketosis predictive power. From Figure 29 it is obvious that at high GPC values only healthy individuals are present. As a threshold, a value of equal or greater than 1.2 mmol/L was chosen: 9.3 % of the samples lay above this threshold and no animal in this group had developed ketosis, compared to 7.5 % incidence in the group below threshold. Only one animal above the GPC/PC threshold was available from the second lactation. This animal had not developed ketosis during the second lactation, neither, again hinting at the predictive power of the measurement. Further comparison of Figures 29 and 30 shows that by using the GPC/PC ratio substantially more animals can be detected than by GPC values alone.

### **Correlations Between Milk Metabolites and EB and FPR Breeding Values**

EB and FPR are genetically determined (with low and moderate heritability, respectively) and have been shown to be associated with liability to metabolic disorders, with high EB and low FPR values being favorable (Buttchereit et al. 2010b; Buttchereit 2011). Breeding

values provide estimates whether the progeny of an animal will have desired or undesired values considering a certain feature, for example disease liability or milk yield. Breeding values for EB and FPR were estimated for the animals in this study by Nina Buttchereit from the Christian-Albrechts-University (Kiel, Germany) as described in (Klein et al. 2011a). Breeding values for FPR were multiplied by (-1) as a low FPR is considered to be preferable. Milk GPC, PC and GPC/PC values determined in this study were analyzed for correlations with EB and FPR breeding values.

For EB breeding values, only GPC showed a significant positive correlation ( $p = 4.1 \cdot 10^{-3}$ ). For FPR breeding values, all correlations were significant, with p-values of  $1.8 \cdot 10^{-3}$ ,  $1.0 \cdot 10^{-8}$  and  $5.5 \cdot 10^{-8}$  for PC, GPC and GPC/PC, respectively. High GPC values and low PC values were connected to high FPR values. Please note that high FPR breeding values indicate low fat-to-protein ratios due to the definition of FPR breeding values. FPR can serve as an indicator whether cows can or cannot adapt to the challenge of early lactation (Buttchereit et al. 2010b). This fits with the finding of GPC and PC values being indicators for susceptibility to ketosis.

### Plasma Analyses

Next, hydrophilic metabolites in 66 plasma specimens collected within the first five weeks of lactation were analyzed. No PC values could be obtained above the LLOQ. For GPC, values of  $5.3 \pm 1.9 \mu\text{mol/L}$  (mean  $\pm$  standard deviation (SD),  $n = 23$ ) were observed. However, no significant correlation between blood and milk GPC was observed. As GPC is formed in the breakdown of phosphatidylcholine (PtC), PtC concentrations were estimated for 22 plasma samples obtained in the second week of lactation. For this, the choline content of lipophilic plasma extracts was quantified (Cheung & Olson 1990). The observed concentrations ranged between 59.4 and 970  $\mu\text{mol/L}$ . Obtained values were validated by spike-in experiments and extraction of aqueous PtC emulsions. Blood PtC was positively correlated to milk PC and negatively correlated to milk GPC and milk GPC/PC ratios with Spearman correlation coefficients of  $R = 0.35$ ,  $-0.37$  and  $-0.38$ , respectively. However, these correlations were not significant at the 5 % level with p-values of 0.12, 0.10 and 0.092, respectively. Free fatty acids were quantified in plasma, but no significant differences could be observed. The corresponding signals were close to the noise level and thus not very reliable, though.

### Validation of the Results

In the following, the results obtained so far were validated on additional groups of animals. As the threshold of 2.5 for the GPC/PC ratio was based only on samples from the HF herd that were collected during the first lactation, milk samples from higher lactations (lactation two to seven) of the same herd were analyzed as well. Although this group contained only samples from 57 animals, a similar distribution with a tail of healthy animals at high GPC/PC ratios was observed. However, one of the samples with a GPC/PC ratio above threshold came from a diseased animal, leading to 5.0 % ketotic animals in the group above threshold, compared to 11 % ketosis incidence in the group below threshold. Odds ratios were calculated as described in Section 2.3. An odds ratio of 2.38 was found, indicating a more than double ketosis risk in the group below the threshold. The acetone and BHBA values were generally lower in the high GPC/PC group, indicating a lower incidence of acute ketosis, although this difference was not

significant. When looking at GPC concentrations at mid lactation, 5.3 % of the animals were above the threshold of 1.2 mmol/L. None of these animals developed ketosis during the lactation, compared to 11 % incidence in the group below threshold. These findings indicate that the suggested thresholds generally hold true even for higher lactations of the observed breed.

In a second step, the animal collective presented in Section 3.2 was re-evaluated. For the herd of 31 Brown Swiss cows, 22 % of the animals were above the GPC/PC threshold during the first four weeks of lactation. For this herd only severe diseases had been recorded. One of the observed animals was downed (unable to stand) due to ketosis. This animal was in the group below threshold, consistent with the assumption of low ketosis risk in the group above threshold. The subgroup above threshold had significantly lower acetone and BHBA levels with p-values of 0.030 and 0.012, respectively. This indicates a lower incidence of acute subclinical ketosis in the subgroup above the threshold.

In the 39 Simmental Fleckvieh cows from the same study, 73 % of the animals were above the GPC/PC threshold in the first weeks of lactation. This high number of animals above threshold fits with the finding that this breed has drastically lower acetone and BHBA values in early lactation compared to Brown Swiss and HF cows, implying considerably lower ketosis susceptibility in this breed. Ketosis values were not available for this herd, but animals downed due to metabolic diseases were recorded. The number of animals downed at least once during this lactation was 20 % for the subgroup below threshold and 14 % in the group above threshold, corresponding to an odds ratio of 1.5. This means that high GPC/PC values are favorable even concerning overall metabolic health.

In the Brown Swiss herd, the GPC values at mid and late lactation were above the threshold for 86 % of the samples, and in the Simmental Fleckvieh herd 90 % were above the GPC threshold in late lactation. These numbers are much higher than those obtained for the corresponding GPC/PC ratios. It seems that the absolute GPC value is varying greatly between different breeds, depending on different milk yields and breed-specific differences in milk composition, and that using the GPC/PC ratio corrects for the differences in absolute concentration levels.

### Cortisol Values

Cortisol values were measured in a subset of the milk samples by Heike Kliem from the Department of Physiology of the Technical University Munich (Freising, Germany). Cortisol values from the first half of the first lactation were analyzed for correlations using Spearman rank correlation coefficients and a Benjamini-Hochberg false discovery rate (FDR) of 5 % as a significance threshold. Significant correlations were found for the energy markers acetone (Spearman  $R = 0.19$ ,  $p = 5.5 \cdot 10^{-4}$ ), BHBA (Spearman  $R = 0.23$ ,  $p = 7.7 \cdot 10^{-5}$ ) and acetoacetic acid (Spearman  $R = 0.20$ ,  $p = 1.1 \cdot 10^{-3}$ ). This means that cortisol values may be markers for energy disbalance, with raised values in acute ketosis. Other significant correlations were observed for lactose content (Spearman  $R = -0.16$ ,  $p = 4.9 \cdot 10^{-3}$ ), glycine (Spearman  $R = 0.27$ ,  $p = 8.2 \cdot 10^{-5}$ ) and galactose-1-phosphate (Spearman  $R = 0.15$ ,  $p = 1.5 \cdot 10^{-2}$ ). Cortisol has been described to prevent lactose leakage from the mammary epithelium into the blood plasma (Stelwagen et al. 1998). This might explain the positive correlation between cortisol and milk lactose content. An increase in plasma glycine of lactating cows has been shown upon administration of adrenocorticotrophic hormone to increase plasma cortisol values (Ndibualonji et al. 1995).

## Discussion

GPC is an osmolyte that is accumulated in renal medulla cells to protect the cells against high interstitial salt and urea concentrations present in the kidney (Gallazzini & Burg 2009). GPC is formed in the breakdown of PtC, the connected synthesis and catabolism pathway is shown in Figure 31 (Gallazzini & Burg 2009; Iorio et al. 2005). This pathway is active in many body tissues, including mammary tissue (Holmes-McNary et al. 1996). The mammary gland has been shown to break down blood PtC to GPC and free fatty acids to gain fatty acids for the synthesis of milk triacylglycerides and phospholipids (Easter et al. 1970). Therefore, the measured milk GPC probably stems from mammary gland breakdown of blood PtC. This assumption is supported by the negative correlation of blood PtC to milk GPC values. As no correlation was found between milk GPC and plasma GPC, the GPC found in milk is probably not GPC absorbed from the blood stream. In comparison to blood GPC values reported for humans (Ilcol et al. 2005), considerably lower values were observed in the bovine plasma. The same is true for PtC, where the bovine plasma values of this study are distinctively lower than those previously published on other animals (Easter et al. 1970; Kuksis et al. 1983). As expected from literature values reported for human specimens (Ilcol et al. 2005) no bovine plasma PC values were observed above the LLOQ.

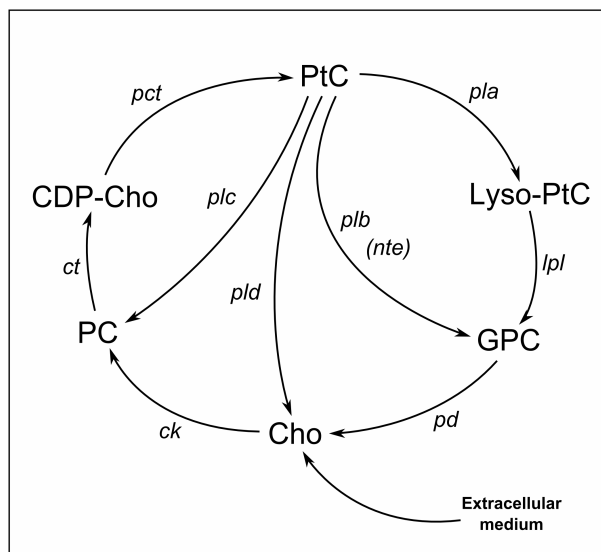


**Figure 31.** The main parts of the GPC pathway. Adapted from (Klein et al. 2011a).

Abbreviations: CDP: Cytidine diphosphate; Cho: Choline; ck: Choline kinase; ct: Cytidylyltransferase;

lpl: Lysophospholipase; nte: Neuropathy target esterase; pct: Phosphocholine transferase;

pla: Phospholipase A2 and A1; plb/c/d: Phospholipase B/C/D; pd: Glycerophosphocholine phosphodiesterase

Changes concerning GPC and PC levels have been reported in a wide range of research. Hypoxia, which is present in many cancers, is known to cause raised PC levels, whereas GPC levels are not affected (Glunde et al. 2008). A change of the GPC/PC ratio has been noticed for cancer and immortalized cell lines of humans. There, in comparison to healthy cells, a decrease in the GPC/PC ratio has been observed (Iorio et al. 2005; Podo 1999; Aboagye & Bhujwala 1999). In tumors, PtC degradation via phospholipase C (plc), respectively phospholipase D (pld) and subsequent choline kinase (ck) are the main

causes of changed PC levels (Iorio et al. 2010). An increase of GPC and a decrease in PC was observed in mouse cell lines under a *slow acidosis*, i.e. lowering the pH from 7.3 to 6.5 for around 12 hours (Galons et al. 1995). They suggested as an explanation for this so-called *GPC to PC switch* the activation of phospholipid breakdown as an alternative energy source for the cells, as glycolysis was hampered due to the low pH. The breakdown of PtC via phospholipase A2 and A1 (pla) and lysophospholipase (lpl) respectively phospholipase B (plb) subsequently leads to GPC accumulation. Recently it has been shown that plb is identical to neuropathy target esterase (nte) (Gallazzini et al. 2008). In renal medulla, the pathway via plb/nte has been shown to be the dominant way of PtC breakdown for GPC production (Gallazzini & Burg 2009). Regarding the differences observed in milk between ketotic and non-ketotic animals, these most closely resemble the changes observed in the *slow acidosis* experiment by (Galons et al. 1995). However, no hints for acidic conditions were observed in the investigated bovine plasma samples.

The differences observed in this study between healthy animals and animals suffering from ketosis can be summarized as follows: Healthy animals have higher levels of milk GPC and lower levels of milk PC. The animals were divided into two groups according to their GPC/PC ratio. The subgroup with high GPC/PC ratios showed lower plasma PtC levels and lower milk fat levels.

Based on these observations, a possible explanation for the positive effect of high GPC values might be as follows. High GPC/PC ratios and GPC concentrations, respectively, are caused by a high rate of blood PtC breakdown, possibly due to higher enzyme concentrations or activities of pla and lpl, respectively plb/nte. These animals can, therefore, use more blood PtC as a fatty acid source for milk lipids. It has been previously shown that fatty acids derived from blood PtC may be utilized by the mammary gland for milk triacylglyceride synthesis (Easter et al. 1970).

An alternative source for fatty acids for milk lipid synthesis are free blood fatty acids. Free blood fatty acids are produced by the mobilization of body fat, with excessive body fat mobilization being suspected to decrease the food intake of cows (Ingvartsen & Andersen 2000). In addition, body fat mobilization leads to the formation of ketone bodies such as acetone and BHBA in the liver. Using more PtC for milk lipid synthesis, and thus saving free blood fatty acids, may, therefore, lower the body fat mobilization. Animals with lower fat mobilization will suffer less from the negative side effects such as the decrease in food intake. This, in turn, has positive effects on the energy balance and thus prevents metabolic diseases. Additionally, in animals with high GPC/PC ratios a decreased milk fat content was observed. These two effects together, namely high blood PtC breakdown as evidenced by high GPC/PC ratios together with lower milk fat content, will lead to a decreased mobilization of body fat. Animals with lower PtC breakdown rates will develop a more negative energy balance and a higher body fat mobilization during the first weeks of lactation, leading to a higher risk of metabolic disorders. The assumption of a constantly higher PtC breakdown in the high GPC/PC group is backed by the fact that GPC shows high levels not only during the negative energy balance of the first lactation weeks, but throughout the whole lactation period.

Selecting animals with high GPC/PC or GPC values should yield animals that can cope better with the negative energy balance of the first lactation weeks and, therefore, are less prone to ketosis. The significant correlations between FPR based breeding values and PC, GPC and GPC/PC levels indicate that the observed metabolic differences are directly

connected to genetic discrepancies and, therefore, a heritability of these effects can be expected.

### **Conclusions**

Taking all results obtained so far into account, the ratio of GPC to PC during the first four weeks of lactation and the concentration of GPC at mid lactation may serve as markers to identify cows that cope well with metabolic stress. These data suggest that the GPC/PC threshold for determining ketosis risk could be universally applicable, being independent of lactation number, breed or feeding conditions. The chosen GPC threshold seems to be applicable only for HF cows, and will need to be individually recalculated for other breeds. To the best of my knowledge, this is the first report of GPC and PC values indicating the ketosis risk in dairy cows. The measurement of GPC and PC is superior to using just thresholds for acetone and BHBA, as these values can only identify acute ketosis (Enjalbert et al. 2001). In contrast, the method proposed here allows the early identification of metabolically stable animals that are not prone to ketosis for breeding purposes.

Reconsidering the milk samples analyzed in this thesis, it could be shown that NMR is a versatile tool for the investigation of the health status of dairy cows. In three different breeds metabolites representative for the health status of the cows were analyzed. Based on the analysis of metabolites of energy metabolism it could be shown that animals of the same breed cope quite differently with the metabolic stress of early lactation. Most interestingly it was possible to predict the risk for developing ketosis based on GPC/PC values, with odds ratios between 1.5 and 2.38, although these ratios are based on a very low number of animals and may therefore be imprecise. Taken together these findings should help in selecting metabolically stable animals for breeding purposes.

### 3.4 Nonalcoholic Fatty Liver Disease and Steatohepatitis

In the previous chapters it was discussed that during the first lactation days dairy cows needed more energy than food intake could deliver (Collins & Reid 1980). To compensate for this negative balance, first glycogen and then lipids are mobilized as energy source. This puts great pressure on the organism, especially on the liver metabolism. Mobilized lipids are transported to the liver for subsequent metabolization. When the amount of mobilized lipids is too high or insufficient energy supplies for the metabolization are available, the lipids accumulate in the liver and lead to steatosis (Kalaitzakis et al. 2010). Steatosis has a quite benign prognosis but may develop into a steatohepatitis, where inflammation and accumulation of fibers are observed in the liver. To distinguish this ailment from steatohepatitis caused by alcohol abuse, it is usually referred to as non-alcoholic steatohepatitis (NASH). NASH has a malign prognosis and may develop further to liver cirrhosis. The causes of NASH are still mostly unknown. To gain more insight into the pathophysiology of NASH, samples from a murine NASH model were analyzed and compared to a mouse model for steatosis and a healthy mouse control group. This chapter has in part already been published (Klein et al. 2011b).

Nonalcoholic fatty liver disease (NAFLD) is the most common cause of hepatic dysfunction affecting about one third of the population in western countries. The spectrum of NAFLD ranges from simple fatty liver to NASH, in which fibrosis may progress to cirrhosis, resulting in significant morbidity and mortality (Brunt 2010).

Sonography is commonly used to assess hepatic steatosis (Saverymuttu et al. 1986). However, it does not allow a distinction between simple steatosis and NASH. Therefore, assessment of the degree of inflammation and hepatic fibrosis, which are hallmarks of NASH, still requires the histopathological examination of liver biopsies (Adams & Lindor 2007).

The aim of this study was the detection of metabolic changes associated with NAFLD and NASH in mouse livers and urine by NMR measurements. Urine measurements are a noninvasive tool and liver analyses may also be performed noninvasively using *in vivo* NMR spectroscopy. In this study, however, liver extracts were used for liver analysis. The NMR measurements were combined with subsequent independent component analysis (ICA). To that end, three groups of BALB/c mice were studied: A healthy control group, a group suffering from NAFLD without significant inflammation and a group diseased with NASH.

#### Collection of Mouse Urine and Liver Samples

Christoph Dorn at the University Clinic Regensburg (Regensburg, Germany) provided liver and urine specimens from male BALB/c mice. Three equal groups of six animals each were fed for 12 weeks either a control diet, a high-fat diet (HFD) containing 30 weight percent (wt%) lard or a so-called Paigen diet containing in addition to 30 wt% lard 1.25 wt% cholesterol and 0.5 wt% sodium cholate (ssniff Spezialdiäten GmbH, Soest, Germany). As shown recently (Dorn et al. 2010a; Dorn et al. 2010b), both HFD's induce significant steatosis, while hepatic inflammation is only observed in the Paigen group. Liver tissue and urine specimens were stored at -80 °C. All animals received human care

and the study protocols complied with guidelines of the central animal facility at the University of Regensburg (Regensburg, Germany).

Urine specimens of 30 microliter ( $\mu\text{L}$ ) to 100  $\mu\text{L}$  were prepared jointly with Ann-Kathrin Immervoll as described in Section 2.5. Liver specimens of approximately 30 milligram were extracted by Ann-Kathrin Immervoll as described in Section 2.9. Urine, lipophilic and hydrophilic liver extracts were measured by 1D and 2D NMR. Spectra were binned and normalized to a total sum of one. No further scaling was performed on the data.

### NMR Analysis of Lipophilic Liver Extracts

To gain deeper insight in the data, ICA was performed for each sample type. Figure 32 shows the ICA of 1D NMR fingerprints of the chloroform liver extracts of six mice each fed a standard chow or diets inducing simple steatosis and NASH, respectively.

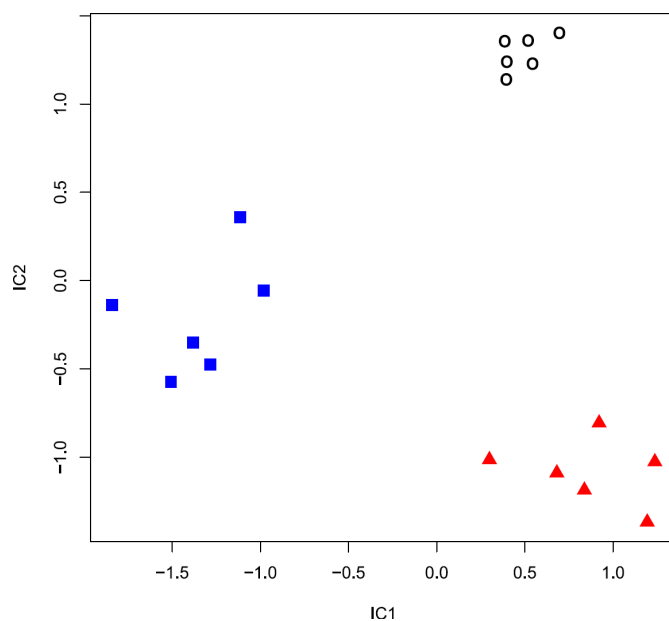


**Figure 32.** ICA of 1D NMR spectra of lipophilic liver extracts

Circles: Standard chow; Squares: Steatosis-inducing diet; Triangles: NASH-inducing diet.

Abbreviations: IC 1: First independent component; IC 2: Second independent component.

Adapted from (Klein et al. 2011b).

A complete group separation was achieved. In Figure 33, a typical 1D spectrum of a lipophilic liver extract from a NASH mouse (Figure 33A) is compared to a spectrum-like visualization of the loading factors obtained for the first two independent components (IC's). Positive areas in Figures 33B and 33C indicate correlated signals, while negative areas are anti-correlated.

An ICA of the 2D spectra of the chloroform extracts also yielded a complete group separation (Figure 34). The IC's of the 2D spectra were used to identify the compounds distinguishing the groups. To that end, the 25 highest rated bins of each of the two shown IC's were further analyzed (for loadings see Tables 14 and 15 in Appendix I).

To verify that these bins contained indeed the group separating information, all but the 25 highest ranked bins of each IC were set to 0 and multiplied by the so-called *un-mixing matrix* of the original ICA. The resulting group separation was almost identical to that obtained with the original data (Figure 35).

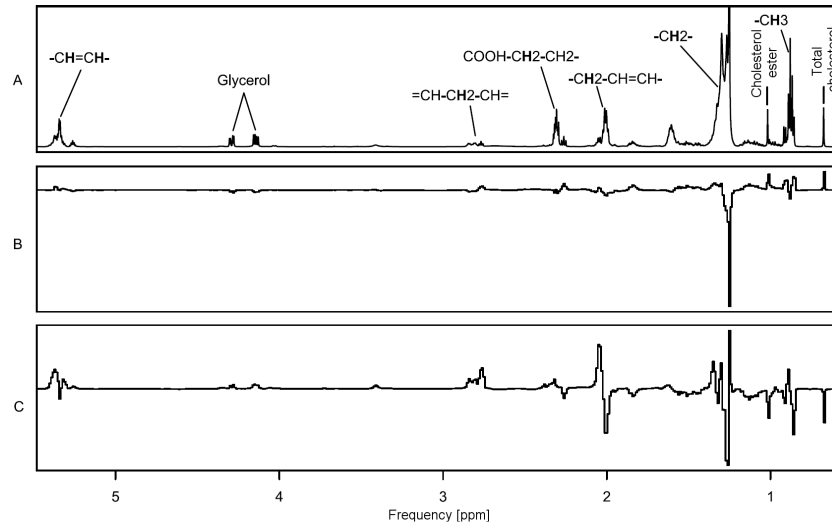


**Figure 33.** 1D NMR spectrum of a lipophilic liver extract and derived IC loadings.

A: Exemplary NMR spectrum of a lipophilic liver extract of a mouse NASH model in the 0.75 - 5.3 ppm region; Loadings of IC 1 (B) and IC 2 (C). Adapted from (Klein et al. 2011b).

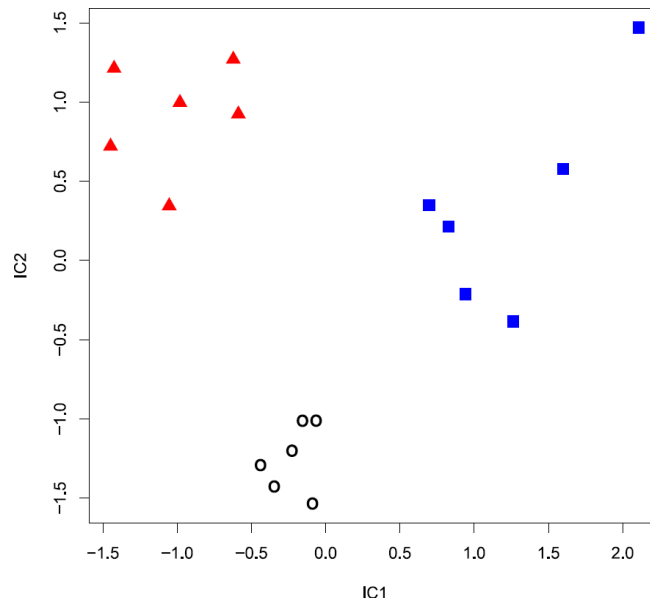


**Figure 34.** ICA of 2D NMR spectra of lipophilic liver extracts.

Circles: Standard chow; Squares: Steatosis-inducing diet; Triangles: NASH-inducing diet. Abbreviations: IC 1: First independent component; IC 2: Second independent component.

Adapted from (Klein et al. 2011b).

The separation of the steatosis model from the other two groups in IC 1 depended mostly on an elevated signal at 1.26 ppm, which was attributed to the fatty acyl protons of the methylene groups of both free and esterified fatty acids. Several signals, belonging to free cholesterol, cholesterol ester and lipids, accounted for the group separation in the second dimension. The lipid signals resulted again mostly from the lipid methylene resonance, but some of the signals also originated from monounsaturated and polyunsaturated fatty acids. Of the highest rated bins, these compounds explained all but one unknown peak at 1.135 ppm.

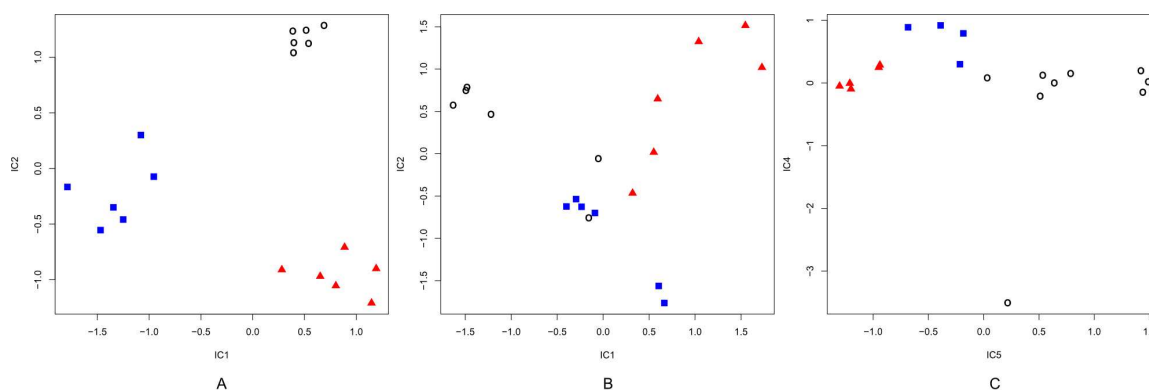


**Figure 35.** ICA reconstructions based only on the 25 best 1D bins of the two used IC's.

A: Lipophilic liver extracts; B: Hydrophilic liver extracts; C: Urine.

Circles: Standard chow; Squares: Steatosis-inducing diet; Triangles: NASH-inducing diet.

Abbreviations: IC 1: First independent component; IC 2: Second independent component; IC 4: Fourth independent component; IC 5: Fifth independent component.

Adapted from (Klein et al. 2011b).

The concentrations of the substances identified as discriminatory by the ICA were measured and are shown in Table 16 (see Appendix I). Due to technical reasons, three spectra were excluded from quantification. Cholesterol ester showed a more than 20-fold increase in NASH mice compared to the control group. Free cholesterol was also significantly increased in the NASH group. No significant differences for free cholesterol and cholesterol ester were found between controls and the steatosis group.

For the lipid signals, the trend is not clear. While some signals are positively correlated to the cholesterol signal, others show a negative correlation. This indicates not only a change in the overall concentration, but also in the composition of lipids. The estimated total lipid content (Table 16, Appendix I) was increased in both HFD groups, albeit not significantly, with the highest values in the NASH group. The molar concentration of the glycerol group contained in lipids such as triacylglycerides and phospholipids was also increased, albeit not significantly, with the highest values observed in the steatosis model.

Next, the saturation index (*SI*), the polyunsaturation index (*PUI*) and the ratio of polyunsaturated fatty acids to monounsaturated fatty acids (*PUFA/MUFA*) were estimated from the lipid signals (Table 16 in Appendix I). The *SI* was significantly elevated in both the steatosis and the NASH group. The *PUI* was significantly decreased in the steatosis

group and lowest in the NASH group. A significant decrease of the PUFA/MUFA score was observed in both NAFLD groups, as the composition of lipids shifted from polyunsaturated to monounsaturated fatty acids. Significant reductions of 38 % ( $p = 3.0 \cdot 10^{-3}$ ) and 51 % ( $p = 5.3 \cdot 10^{-4}$ ), respectively, were observed for the concentrations of polyunsaturated bonds in the steatosis and NASH groups. The value determined for unsaturated bonds includes both lipids with mono- and polyunsaturated bonds. Since the amount of polyunsaturated bonds can be determined from the diallylic signal, the amount of lipids with monounsaturated bonds can be estimated indirectly. As the total amount of unsaturated bindings showed no significant difference it can be assumed that the decrease in polyunsaturated bonds in the NAFLD groups was connected with a simultaneous increase in MUFA concentrations.

For the highest ranked bins, a heatmap was generated (Figure 36). The values of the bins were represented by a color code, where high, median and low values were depicted as yellow, black and blue, respectively. A hierarchical clustering seen at the top of the figure sorted the samples into their correct groups, once again showing a clear group separation.

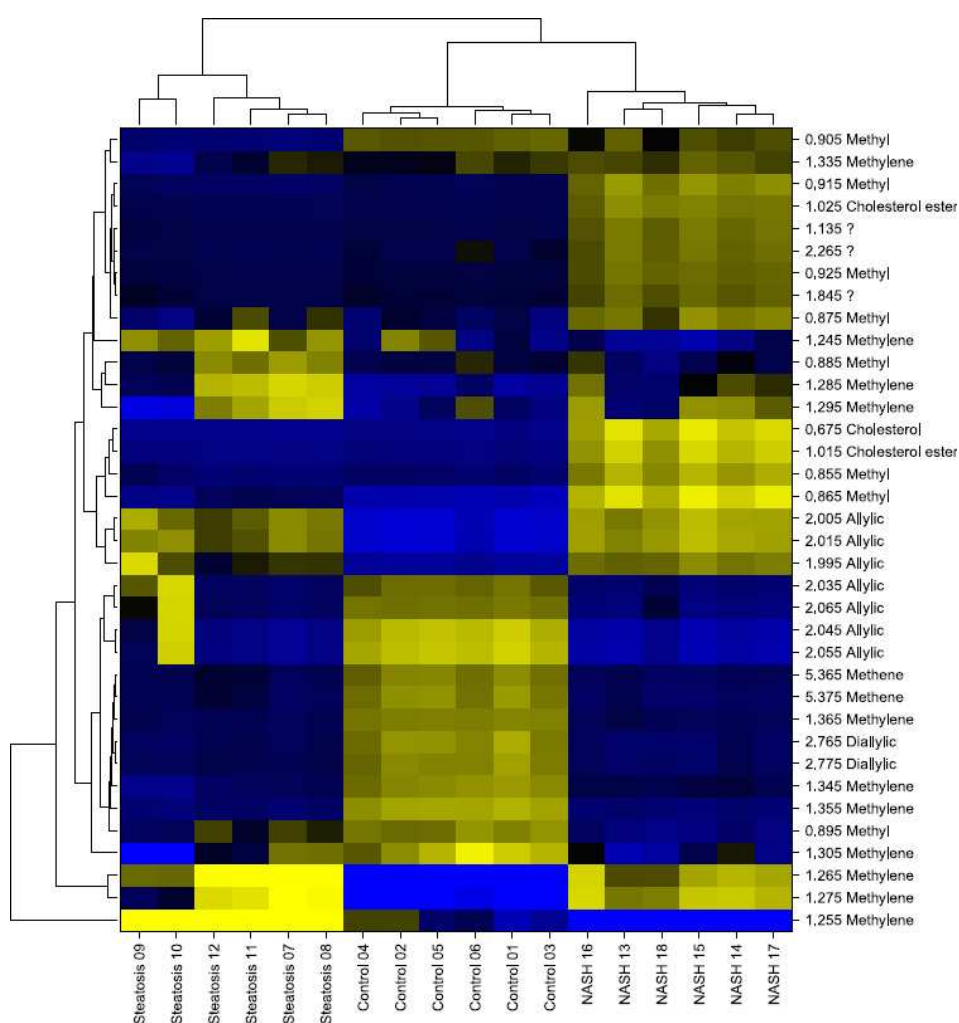


**Figure 36.** Heatmap of the highest ranked 1D bins of the lipophilic liver extracts. Blue: Low values; Black: Medium values; Yellow: High values. Adapted from (Klein et al. 2011b).

### Hydrophilic Liver Extracts

Next, the 1D NMR spectra of the aqueous liver extracts were analyzed by ICA (Figure 37). A clear clustering of the three groups, albeit not as complete as for the chloroform extracts, was observed. In IC 1, a partial separation is apparent between all three groups. IC 2 further discriminated the steatosis group from the other two groups. The use of 2D spectra did not improve the group separation.

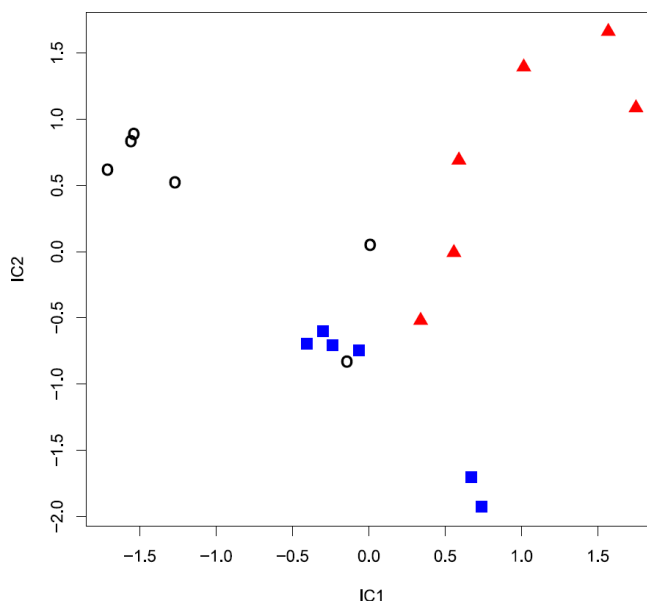


**Figure 37.** ICA of 1D NMR spectra of hydrophilic liver extracts.

Circles: Standard chow; Squares: Steatosis-inducing diet; Triangles: NASH-inducing diet.  
Abbreviations: IC 1: First independent component; IC 2: Second independent component.  
Adapted from (Klein et al. 2011b).

In Figure 38A, a spectrum of an aqueous NASH liver extract is shown together with the separating IC's (Figures 38B and 38C). The 25 highest loadings for each of these IC's are shown in the Tables 17 and 18 in Appendix I. Betaine, glucose and taurine could be identified as discriminatory metabolites. Other peaks contributing to group separation were tentatively identified as isoleucine, lactate, leucine and valine. Amongst the highest rated bins of both IC's, 19 bins could be assigned to specific compounds.

Betaine, lactate and taurine showed high loadings in both dimensions. Isoleucine, leucine and valine were found in IC 1, thus separating all three groups. Glucose showed high values only in IC 2 and separated the steatosis group from the other two groups. Quantitative data for the metabolites identified, except for betaine that could not be measured above the LLOQ, and the p-values for the analysis of variance (ANOVA) tests and all t-statistics are given in Table 19 (see Appendix I). For taurine significantly increased values were found in the steatosis group compared to both the control and the NASH group.

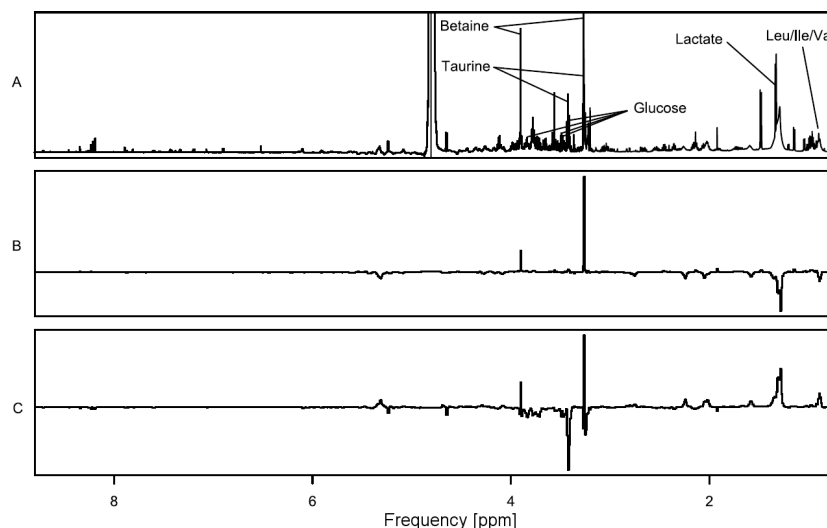


**Figure 38.** 1D NMR spectrum of a hydrophilic liver extract and derived IC loadings.

A: Exemplary NMR spectrum of a hydrophilic liver extract of a NASH model mouse in the 1.0 - 8.5 ppm region; Loadings of IC 1 (B) and IC 2 (C). Abbreviations: Leu: Leucine; Ile: Isoleucine; Val: Valine. Adapted from (Klein et al. 2011b).

## Urine Samples

Next, nine urine specimens from the control group, four from the steatosis model and five from the NASH model were analyzed. The difference in the number of samples analyzed per group was due to the inability to obtain sufficient amounts of urine from all animals studied and the inclusion of additional controls held under identical conditions, respectively. An ICA of the urinary NMR spectra is shown in Figure 39.

Samples from the second cohort were marked as empty circles in Figure 39 as it has been shown previously that different cohorts of the same strain of animals can differ in differential analyses (Schnackenberg et al. 2007; Jahns et al. 2009). A complete separation of the three groups was achieved by a single IC (IC 5), with IC 4 adding to the separation of the steatosis group. Note, IC's 1 to 3 reflect inter-sample variance not related to steatosis and NASH.

An exemplary NASH urine spectrum is shown in Figure 40A, together with the loadings of IC 4 and IC 5 (Figures 40B and 40C). In Tables 20 and 21 (see Appendix I), the highest loading factors are shown. Ascorbic acid, citric acid, creatinine, leucine, phenylalanine, phosphocreatine, taurine, trimethylamine (TMA) and trimethylamine-N-oxide (TMAO) showed up in both ICA's performed on 1D and 2D NMR data and, therefore, were considered as unambiguously identified. Signals with high loadings only in the ICA performed on 1D NMR data were tentatively identified as ethanolamine and isoleucine. These metabolites represented 40 of the highest ranked bins.

While most metabolites showed high loadings in both dimensions, ethanolamine, phenylalanine and phosphocreatine were found only in IC 5; they facilitated the separation of all three groups seen in Figure 39. Leucine showed high loadings only in IC 4 and separated the steatosis group from the other two groups. In Table 22 in Appendix I,

quantitative results and p-values of the ANOVA tests and all t-statistics for these compounds are shown.

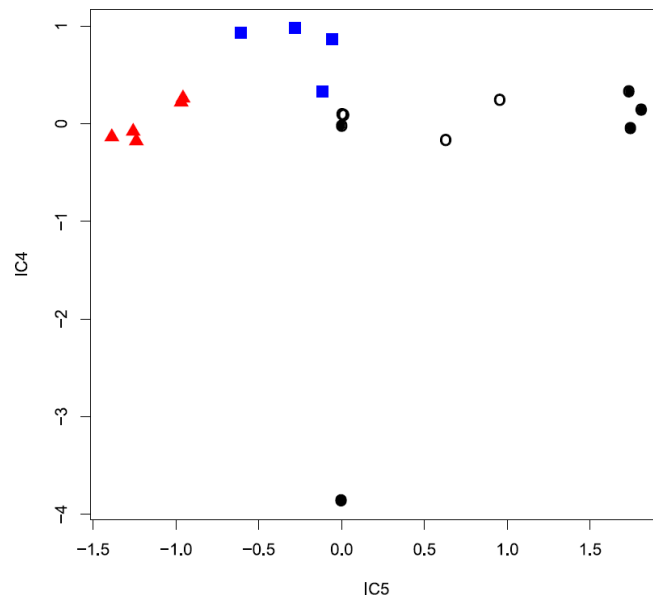


**Figure 39.** ICA of urinary 1D NMR spectra.

Circles: Standard chow; Squares: Steatosis-inducing diet; Triangles: NASH-inducing diet.

Abbreviations: IC 4: Fourth independent component; IC 5: Fifth independent component.

The filled and empty circles represent the first and second cohort of the control group, respectively.

Adapted from (Klein et al. 2011b).

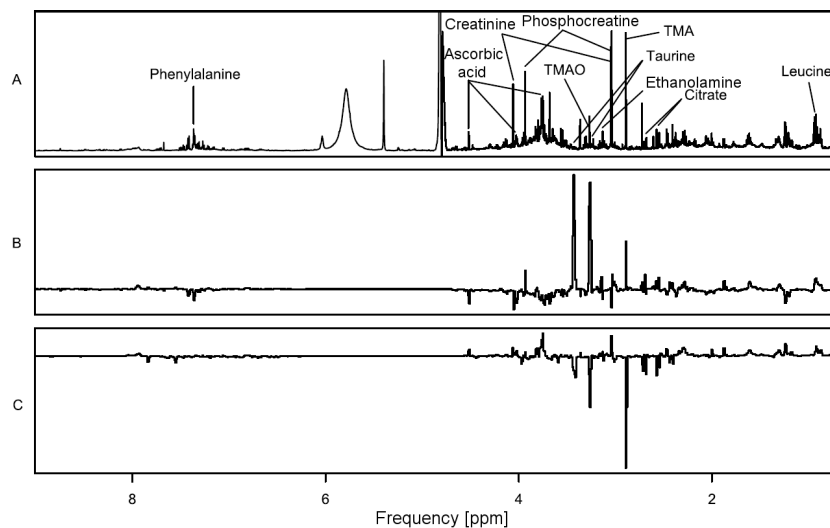


**Figure 40.** 1D NMR spectrum of urine and derived IC loadings.

A: Exemplary NMR spectrum of urine recorded for a NASH model mouse in the 1.0 - 8.7 ppm region; Loadings of IC 4 (B) and IC 5 (C). Adapted from (Klein et al. 2011b).

## Discussion of the NASH Analyses

### Analysis of Liver Tissue

Free cholesterol and cholesterol ester were significantly increased in the lipophilic liver extracts of NASH mice over controls and mice with simple steatosis. A similar increase in free cholesterol has been reported for chloroform/methanol extracts of human NASH liver biopsies (Puri et al. 2007). The latter study, however, failed to detect the significant increase in cholesterol ester observed in the present study. Another striking difference between human NAFLD and the BALB/c mouse model studied here concerns the absence of a significant increase in di- and triacylglycerol, which is generally considered a hallmark of human NAFLD (Puri et al. 2007). Both studies observed a decreased ratio of PUFA to MUFA in NAFLD. But in contrast to the human situation, there was a systematic decrease in the concentration of PUFA, both in this and a previously reported mouse model (Cobbold et al. 2009). A reduced PUFA/MUFA ratio is considered a marker of lipid peroxidation in association with oxidative stress (Serkova et al. 2006).

The behavior of the saturation and polyunsaturation indices (Table 16 in Appendix I) agrees with the finding that SI and PUI are correlated and anti-correlated, respectively, with the fibrosis grade in hepatitis C patients (Cobbold et al. 2010). It is noteworthy that a similar trend was observed in both humans and mice. The significant increase in the lipid methylene resonance observed in animals fed a HFD (Table 14 in Appendix I) is in concordance with the previously reported increased expression levels of fatty acid synthase in an identical mouse model of simple steatosis (Dorn et al. 2010b).

ICA of the aqueous liver extracts showed increased levels of betaine, an intermediate of the methionine cycle, in the NASH model, probably reflecting an impaired conversion of homocysteine to methionine (Abdelmalek et al. 2009). In contrast, lactic acid concentrations were significantly ( $p = 2.05 \times 10^{-2}$ ) decreased in the NASH model compared to the mice with simple steatosis, indicating that adaptive glycolysis was upregulated in the latter model. In a study of obese Zucker rats, increased lactic acid levels were observed in both blood and liver tissues compared to lean controls (Serkova et al. 2006), while an *in vitro* study on hepatocytes isolated from obese and lean Zucker rats showed the opposite effect (Seoane et al. 1999). These findings together with the data of this study indicate that regulation of glycolysis depends on a variety of factors and might change as the disease progresses.

Taurine is of interest, because its administration in rats and children has proven effective in treating fatty liver (Chen et al. 2006; Obinata et al. 1996). In the present study, taurine was significantly elevated in the hydrophilic liver extracts of the steatosis group as compared to the other two groups (Table 19, Appendix I), probably in response to the oxidative stress associated with HFD intake. The comparatively lower levels of taurine in the NASH model, on the other hand, may be either a consequence of increased tauroconjugation in response to an increased dietary intake of sodium cholate (Hardison & Proffitt 1977), or a sign of increased microbial degradation of taurine due to obesity-associated changes in gut flora composition (Turnbaugh et al. 2006; Backus et al. 1994).

### Analysis of Urine

Literature search indicates that this may be the first report on the successful discrimination of simple steatosis from NASH based on changes in the composition of urine. Previous studies had reported only the successful discrimination of NAFLD from

healthy controls in mice using NMR metabolite fingerprinting (Dumas et al. 2006), respectively of human NASH patients from controls on the basis of elevated urinary levels of neopterin (Yaman et al. 2005), an indicator of activated immune cells, and 8-isoprostane (Kojima et al. 2007), a marker of oxidative stress due to increased lipid peroxidation.

Among the discriminating urinary metabolites found here was ascorbic acid. In contrast to humans, mice can synthesize ascorbic acid. Urinary levels of ascorbic acid were increased slightly, albeit significantly with a p-value of  $3.33 \times 10^{-2}$  in the NAFLD group (Table 22 in Appendix I). This agrees with the finding of increased ascorbic acid synthesis in mice suffering from health problems (Mårtensson & Meister 1992). In humans, liver disease is typically associated with decreased urinary levels of ascorbic acid (Dubey et al. 1987).

Urinary levels of citric acid were significantly decreased in both steatosis and NASH, with respective p-values of  $2.53 \times 10^{-3}$  and  $3.33 \times 10^{-3}$ . In a recent study on mice, an elevated expression of hepatic ATP-citrate lyase was linked to a derangement of the lipid metabolism (Wang et al. 2009). Urinary levels of leucine were also significantly decreased, as a result of either a reduced dietary intake of leucine, as 30 % of the standard chow had been replaced with lard, or an increased demand of leucine for processes such as the synthesis of alanine and glutamine and the maintenance of glucose homeostasis. For phenylalanine, a somewhat different picture was observed; its urinary concentration was decreased significantly only in the steatosis model, but did not differ between the control and the NASH group.

For phosphocreatine, reduced urinary values were seen in both steatosis and NASH mice. Phosphocreatine acts as a store and transporter of high-energy phosphate. The reduced urinary levels seen here may be due to dietary reasons: About half of the daily requirement of creatine comes from dietary intake, while the remainder is synthesized from glycine, arginine and methionine, the content of all being reduced in the HFD.

Urinary levels of taurine were significantly reduced in both steatosis and NASH mice, with respective p-values of  $5.48 \times 10^{-4}$  and  $2.39 \times 10^{-4}$ . Taurine forms conjugates with cholic acid and chenodeoxycholic acid, thereby ensuring that they are negatively charged at the pH found in the intestinal tract and, thus, improving their surfactant properties. As the amount of tauroconjugated bile acids will rise with increasing dietary fat intake, levels of free taurine will decrease (Hardison & Proffitt 1977). The reduced renal excretion of taurine may also be caused by its increased microbial degradation in the intestine as a result of obesity-associated changes in gut microflora composition (Turnbaugh et al. 2006; Backus et al. 1994).

For TMA decreased levels were observed for both HFD groups. TMA is a product of the metabolism of dietary choline by intestinal bacteria (Zeisel et al. 1989). Both HFD's contained reduced amounts of choline. As a consequence, the observed differences in TMA levels were most probably due to dietary effects. However, urinary levels of microbiota-derived methylamines may vary significantly depending on the mouse strain used to study the pathophysiological effects of fat feeding (Dumas et al. 2006).

### 3.5 Analysis of Early Liver Disease Progression

A second mouse model of NASH was analyzed. Here, female C57/BL6 mice were fed either a NASH-inducing Paigen diet or a control diet. The aim of this study was the assessment of early disease progression. Animals were sacrificed at day two, four, six, 10, 14, 20, 30 and 40, and liver samples were collected. Samples were provided by Anja Thomas, sample extraction was performed jointly with Anja Thomas, Ann-Kathrin Immervoll and Caridad Louis as described in Section 2.9. For lipophilic liver extracts, 1D spectra were recorded, while for hydrophilic extracts both 1D and 2D spectra were acquired. The differences observed between the NASH group and the control group were similar to those observed for BALB/c mice described in Section 3.4. One interesting observation was that already after two days of feeding, a significantly higher hepatic triacylglyceride content was observed for the NASH group, as evidenced by the glycerol content of lipophilic extracts. In the BALB/c mice, no significant difference in glycerol was observed even after 12 weeks of Paigen diet. This fits with the finding that C57/BL6 mice show much stronger HFD-induced metabolic changes than BALB/c mice (Olson et al. 2010). Additionally, a stronger difference in liver taurine levels was observed in the C57/BL6 mice as compared to BALB/c mice, with taurine being significantly decreased in the NASH group. The importance of taurine in liver diseases has been pointed out in Section 3.4. Other findings of the studies performed by Anja Thomas showed that while signs of hepatic steatosis are visible very fast, inflammatory and fibrotic conditions were not seen before day 40 (data to be published). This fits with the finding from the study on BALB/c mice, where taurine was significantly decreased in the steatosis group, but not in the NASH group.

---

## 4 Summary

Three specific aims were pursued in this thesis. The first aim was to elucidate whether reliable quantification can be performed using nuclear magnetic resonance (NMR) spectra of complex biofluids. Novel quantification methods were developed using two-dimensional (2D) proton-carbon-13 ( $^1\text{H}$ - $^{13}\text{C}$ ) heteronuclear single quantum coherence (HSQC) spectra acquired at natural  $^{13}\text{C}$ -abundance by means of a cryo-probe. It was shown that these 2D spectra allow the reliable quantification of metabolites present in native urine samples at micromole per liter ( $\mu\text{mol/L}$ ) levels over a concentration range spanning three orders of magnitude. As shown by the results presented for the analysis of urinary metabolites, one-dimensional (1D) NMR is often not as quantitatively accurate as 2D NMR. However, the price for this gain in accuracy is a longer NMR acquisition time. Precision and accuracy of 2D NMR measurements increase with the number of well-resolved signals integrated per analyte provided that separate calibration curves are generated for the different signals. A software tool named QUANTIFY was developed to overcome some of the pitfalls of NMR quantification from biofluids, such as unforeseen signal overlap due to metabolites inconsistently present in the samples. Lower limits of quantification (LLOQ's) were found to be the lowest for metabolites containing multiple methyl groups such as trimethylamine-N-oxide. Including quantification results from 1D spectra, the range of reliably measured concentrations spanned five orders of magnitude. Limits of detection may be further lowered by moving to higher field strengths or by using considerably longer measurement times. NMR quantification results were found to agree well with those obtained by mass spectrometry (MS) and other methods commonly used in clinical chemistry. NMR measurements are less prone to errors due to interfering compounds or matrix effects including ion suppression, which are common occurrences in the mass spectrometric analysis of complex biological matrixes. Further, while

hyphenated MS methods are more sensitive than NMR, their application is typically limited to compounds sharing similar physicochemical properties. In contrast, NMR is a more universal detector as exemplified by the different metabolites that could be detected in this thesis. The comparison of NMR results obtained for urine and milk spectra with both gas chromatography-mass spectrometry (GC-MS) and liquid chromatography-tandem mass spectrometry (LC-MS/MS) measurements showed a good agreement between the methods.

The second specific aim was to identify whether the health status of an individual gives rise to a distinct change in its body fluid composition, and if this change is within the scope of the used measurement techniques. One main topic of this thesis was related to the health status of dairy cows. In this context two extensive sets of milk samples derived from three different breeds of dairy cows were investigated. With regard to human diseases, non-alcoholic steatohepatitis (NASH) was investigated in samples derived from a mouse model. In addition, human urinary samples were measured for the analysis of autosomal dominant polycystic kidney disease. However, data analysis of the latter samples was beyond the scope of this thesis.

With regard to the project on NASH, male BALB/c mice were fed for 12 weeks either a control or two different high-fat diets leading to hepatic steatosis and NASH, respectively. Metabolic differences were determined by independent component analysis (ICA) of NMR spectra of lipophilic and hydrophilic liver extracts and urine specimens. The results from ICA clearly discriminated the three investigated groups. Discriminatory biomarkers in the lipophilic liver extracts were free cholesterol, cholesterol ester and lipid methylene. Discrimination of the hydrophilic liver extracts was mainly mediated by betaine, glucose and lactate, whereas in urine taurine, trimethylamine-N-oxide and trimethylamine were the most discriminatory biomarkers. In summary, a clear discrimination between the three investigated groups of mice was obtained. Especially, NMR metabolite fingerprinting of spot urine samples allowed the noninvasive distinction of NASH and steatosis. This is of special interest, as this might pave the way for a non-invasive diagnosis of NASH. At the moment, a definitive diagnosis of NASH still requires a liver biopsy. Whether these results from mouse strains will hold true for humans will require further studies.

In the set of milk samples from Brown Swiss and Simmental Fleckvieh cows, the abundance of numerous milk metabolites in early and late lactation was systematically investigated, with an emphasis on metabolites related to energy metabolism. The aim of the study was the identification and correlation of milk constituents to the metabolic status of the cows. To investigate the influence of lactation stage on physiological and metabolic variables, two breeds of different productivity were selected. Forty-four different milk metabolites could be reliably quantified. Large differences in concentrations of known biomarkers of energy metabolism such as acetone and beta-hydroxybutyric acid were observed during early lactation, indicating that individual animals cope very differently with the metabolic stress in this period. This was particularly true for high-producing animals that yielded highly discrepant values for these markers. These two sample sets demonstrate the ability of NMR to identify profiles of different metabolic states of an organism, and that the distinguishing molecules may be deduced from these profiles.

The third specific aim concerned the prediction of so-called production diseases in lactating dairy cows on the basis of metabolic fingerprints of milk and other physiological fluids.. Results from a herd of Holstein-Friesian cows showed a high predictive potential for two milk compounds, namely glycerophosphocholine (GPC) and phosphocholine (PC) that are well-known milk constituents. GPC and PC are part of the phosphatidylcholine (PtC) breakdown pathway (Holmes-McNary et al. 1996). High PtC breakdown seems to be beneficial concerning the ketosis risk, possibly due to a reduced need for fatty acids from body fat mobilization. Although GPC and PC levels have been previously assessed using a variety of methods, including high pressure liquid chromatography and GC-MS (Pomfret et al. 1989), NMR (Govindaraju et al. 2000) and enzymatic assays (Chap et al. 1988; Murray et al. 1990) their relation to production diseases such as ketosis was not known so far. Results were validated on samples obtained from two other breeds, namely Brown Swiss and Simmental Fleckvieh, indicating the general applicability of the findings. This shows that NMR analyses are not only able to identify metabolites with prognostic value, but that new hypotheses for (patho-)physiological mechanisms may be deduced using NMR results.

---

## 5 References

- Abdelmalek, M. F., Sanderson, S. O., Angulo, P., Soldevila-Pico, C., Liu, C., Peter, J., Keach, J., Cave, M., Chen, T., McClain, C. J., & Lindor, K. D. (2009). Betaine for nonalcoholic fatty liver disease: results of a randomized placebo-controlled trial. *Hepatology*, 50, 1818–1826.
- Abdi, H. & Williams, L. J. (2010). Principal component analysis. *Wiley Interdisciplinary Reviews: Computational Statistics*, 2, 433–459.
- Aboagye, E. O. & Bhujwala, Z. M. (1999). Malignant transformation alters membrane choline phospholipid metabolism of human mammary epithelial cells. *Cancer Res*, 59, 80–84.
- Adams, L. A. & Lindor, K. D. (2007). Nonalcoholic fatty liver disease. *Ann Epidemiol*, 17, 863–869.
- Adosraku, R. K., Choi, G. T., Constantinou-Kokotos, V., Anderson, M. M., & Gibbons, W. A. (1994). NMR lipid profiles of cells, tissues, and body fluids: proton NMR analysis of human erythrocyte lipids. *J Lipid Res*, 35, 1925–1931.
- Alberts, B., Bray, D., Johnson, A., Lewis, J., Raff, M., Roberts, M., & Walter, P. (2001). *Lehrbuch der Molekularen Zellbiologie*. Wiley-Vch, Weinheim, Germany.
- Almstetter, M. F., Appel, I. J., Gruber, M. A., Lottaz, C., Timischl, B., Spang, R., Dettmer, K., & Oefner, P. J. (2009). Integrative Normalization and Comparative Analysis for Metabolic Fingerprinting by Comprehensive Two-Dimensional Gas Chromatography-Time-of-Flight Mass Spectrometry. *Anal Chem*, 81, 5731–5739. PMID: 19522528.
- Backus, R. C., Rogers, Q. R., & Morris, J. G. (1994). Microbial degradation of taurine in fecal cultures from cats given commercial and purified diets. *J Nutr*, 124, 2540S–2545S.
- Banos, G., Coffey, M., & Brotherstone, S. (2005). Modeling Daily Energy Balance of Dairy Cows in the First Three Lactations. *J Dairy Sci*, 88, 2226 – 2237.
- Baticz, O., Tömösközi, S., Vida, L., & Gaál, T. (2002). Relationship between concentration of citrate and ketone bodies in cow's milk. *Acta Vet Hung*, 50, 253–261.
- Beckonert, O., Keun, H. C., Ebbels, T. M. D., Bundy, J., Holmes, E., Lindon, J. C., & Nicholson, J. K. (2007). Metabolic profiling, metabolomic and metabonomic procedures for NMR spectroscopy of urine, plasma, serum and tissue extracts. *Nat Protoc*, 2, 2692–2703.
- Belloque, J. & Ramos, M. (2002). Determination of the casein content in bovine milk by 31P-NMR. *J Dairy Res*, 69, 411–418.
- Benjamini, Y. & Hochberg, Y. (1995). Controlling the False Discovery Rate: A Practical and Powerful Approach to Multiple Testing. *Journal of the Royal Statistical Society Series B (Methodological)*, 57, pp. 289–300.

- Berger, S. & Braun, S. (1998). *200 and More NMR Experiments*. Wiley-Vch, Weinheim, Germany.
- Bishop, S. C., Axford, R. F. E., Nicholas, F. W., & Owen, J. B., editors (2009). *Breeding for Disease Resistance in Farm Animals*. CABI, Wallingford, UK.
- Bland, J. M. & Altman, D. G. (1986). Statistical methods for assessing agreement between two methods of clinical measurement. *Lancet*, 1, 307–310.
- Bloch, F. (1946). Nuclear Induction. *Phys Rev*, 70, 460–474.
- Blow, N. (2008). Metabolomics: Biochemistry's new look. *Nature*, 455, 697–700.
- Boudonck, K., Mitchell, M., Wulff, J., & Ryals, J. (2009). Characterization of the biochemical variability of bovine milk using metabolomics. *Metabolomics*, 5, 375–386. 10.1007/s11306-009-0160-8.
- Brunt, E. M. (2010). Pathology of nonalcoholic fatty liver disease. *Nat Rev Gastroenterol Hepatol*, 7, 195–203.
- Buttchereit, N. (2011). *Model evaluation and estimation of genetic parameters for energy balance and related traits in dairy cows*. Ph.D. thesis, Christian-Albrechts-University, Kiel, Germany.
- Buttchereit, N., Stamer, E., Junge, W., & Thaller, G. (2010). Evaluation of five lactation curve models fitted for fat:protein ratio of milk and daily energy balance. *J Dairy Sci*, 93, 1702–1712.
- Buttchereit, N., Stamer, E., Junge, W., & Thaller, G. (2010). Relationship of energy balance and fat protein ratio of milk to disease liability in dairy cattle. *Proc WCGALP*, 9, 315.
- Buttchereit, N., Stamer, E., Junge, W., & Thaller, G. (2011). Short communication: Genetic relationships among daily energy balance, feed intake, body condition score, and fat to protein ratio of milk in dairy cows. *J Dairy Sci*, 94, 1586 – 1591.
- Cammann, K., editor (2000). *Instrumentelle Analytische Chemie*. Spektrum Akademischer Verlag, Heidelberg, Germany.
- Cardoso, J.-F. & Souloumiac, A. (1993). Blind Beamforming for Non Gaussian Signals. *IEE Proceedings-F*, 140, 362–370.
- Chao, C. K., Pomfret, E. A., & Zeisel, S. H. (1988). Uptake of choline by rat mammary-gland epithelial cells. *Biochem J*, 254, 33–38.
- Chap, H. J., Moatti, J. P., Mieusset, R., Nieto, M., Laneelle, G., Bennet, P. J., Mansat, A., Pontonnier, F., & Douste-Blazy, L. (1988). Simple, rapid enzymatic determination of glycerophosphocholine in human seminal plasma. *Clin Chem*, 34, 106–109.
- Chen, S.-W., Chen, Y.-X., Shi, J., Lin, Y., & Xie, W.-F. (2006). The restorative effect of taurine on experimental nonalcoholic steatohepatitis. *Dig Dis Sci*, 51, 2225–2234.

Cheung, A. P. & Olson, L. L. (1990).  $^1\text{H-NMR}$  assay of phosphatidylcholine and phosphatidylethanolamine in AL721. *J Pharmaceut Biomed*, 8, 729 – 734. Papers from the Second International Symposium on Pharmaceutical and Biomedical Analysis, April 1990.

Ciba-Geigy (1983). *Wissenschaftliche Tabellen Geigy*. CIBA-GEIGY, Basel, Switzerland.

Cobbold, J. F. L., Anstee, Q. M., Goldin, R. D., Williams, H. R. T., Matthews, H. C., North, B. V., Absalom, N., Thomas, H. C., Thursz, M. R., Cox, R. D., Taylor-Robinson, S. D., & Cox, I. J. (2009). Phenotyping murine models of non-alcoholic fatty liver disease through metabolic profiling of intact liver tissue. *Clin Sci (Lond)*, 116, 403–413.

Cobbold, J. F. L., Patel, J. H., Goldin, R. D., North, B. V., Crossey, M. M. E., Fitzpatrick, J., Wylezinska, M., Thomas, H. C., Cox, I. J., & Taylor-Robinson, S. D. (2010). Hepatic lipid profiling in chronic hepatitis C: an in vitro and in vivo proton magnetic resonance spectroscopy study. *J Hepatol*, 52, 16–24.

Collard, B., Boettcher, P., Dekkers, J., Petitclerc, D., & Schaeffer, L. (2000). Relationships Between Energy Balance and Health Traits of Dairy Cattle in Early Lactation. *J Dairy Sci*, 83, 2683 – 2690.

Collins, R. A. & Reid, I. M. (1980). A correlated biochemical and stereological study of periparturient fatty liver in the dairy cow. *Res Vet Sci*, 28, 373–376.

Constantinou, M. A., Papakonstantinou, E., Spraul, M., Sevastiadou, S., Costalos, C., Koupparis, M. A., Shulpis, K., Tsantili-Kakoulidou, A., & Mikros, E. (2005).  $^1\text{H NMR}$ -based metabonomics for the diagnosis of inborn errors of metabolism in urine. *Anal Chim Acta*, 542, 169 – 177.

Cornfield, J. (1951). A method of estimating comparative rates from clinical data; applications to cancer of the lung, breast, and cervix. *J Natl Cancer Inst*, 11, 1269–1275.

de la Fuente, A., Bing, N., Hoeschele, I., & Mendes, P. (2004). Discovery of meaningful associations in genomic data using partial correlation coefficients. *Bioinformatics*, 20, 3565–3574.

DeMarco, T. (1979). *Structured Analysis and System Specification*. Prentice Hall, Upper Saddle River, NJ, USA.

Dorn, C., Kraus, B., Motyl, M., Weiss, T. S., Gehrig, M., Schölmerich, J., Heilmann, J., & Hellerbrand, C. (2010). Xanthohumol, a chalcon derived from hops, inhibits hepatic inflammation and fibrosis. *Mol Nutr Food Res*, Epub ahead of print.

Dorn, C., Riener, M.-O., Kirovski, G., Saugspier, M., Steib, K., Weiss, T., Gäbele, E., Kristiansen, G., Hartmann, A., & Hellerbrand, C. (2010). Expression of fatty acid synthase in nonalcoholic fatty liver disease. *Int J Clin Exp Pathol*, 3, 505–514.

Dubey, S. S., Palodhi, G. R., & Jain, A. K. (1987). Ascorbic acid, dehydroascorbic acid and glutathione in liver disease. *Indian J Physiol Pharmacol*, 31, 279–283.

Duffield, T. F., Lissemore, K. D., McBride, B. W., & Leslie, K. E. (2009). Impact of hyperketonemia in early lactation dairy cows on health and production. *J Dairy Sci*, 92, 571–580.

Dumas, M.-E., Barton, R. H., Toye, A., Cloarec, O., Blancher, C., Rothwell, A., Fearnside, J., Tatoud, R., Blanc, V., Lindon, J. C., Mitchell, S. C., Holmes, E., McCarthy, M. I., Scott, J., Gauguier, D., & Nicholson, J. K. (2006). Metabolic profiling reveals a contribution of gut microbiota to fatty liver phenotype in insulin-resistant mice. *Proc Natl Acad Sci U S A*, 103, 12511–12516.

Easter, D. J., Patton, S., & McCarthy, R. D. (1970). Metabolism of Phospholipid in Mammary Gland: I. The Supply of Phospholipid for Milk Synthesis in the Rat and Goat. *Lipids*, 6, 844–849.

Enjalbert, F., Nicot, M. C., Bayourthe, C., & Moncoulon, R. (2001). Ketone bodies in milk and blood of dairy cows: relationship between concentrations and utilization for detection of subclinical ketosis. *J Dairy Sci*, 84, 583–589.

Erb, H. & Grohn, Y. (1988). Epidemiology of Metabolic Disorders in the Periparturient Dairy Cow. *J Dairy Sci*, 71, 2557 – 2571.

Erdman, R. A. & Sharma, B. K. (1991). Effect of dietary rumen-protected choline in lactating dairy cows. *J Dairy Sci*, 74, 1641–1647.

Fan, T. W. M., Lane, A. N., Higashi, R. M., Farag, M. A., Gao, H., Bousamra, M., & Miller, D. M. (2009). Altered regulation of metabolic pathways in human lung cancer discerned by (13)C stable isotope-resolved metabolomics (SIRM). *Mol Cancer*, 8, 41.

FDA (2001). Guidance for Industry: Bioanalytical Method Validation.

Gabow, P. A. (1993). Autosomal dominant polycystic kidney disease. *Am J Kidney Dis*, 22, 511–512.

Gallazzini, M. & Burg, M. B. (2009). What's New About Osmotic Regulation of Glycerophosphocholine. *Physiology*, 24, 245–249.

Gallazzini, M., Ferraris, J. D., Kunin, M., Morris, R. G., & Burg, M. B. (2008). Neuropathy target esterase catalyzes osmoprotective renal synthesis of glycerophosphocholine in response to high NaCl. *Proc Natl Acad Sci USA*, 105, 11026–11031.

Galons, J. P., Job, C., & Gillies, R. J. (1995). Increase of GPC levels in cultured mammalian cells during acidosis. A 31P MR spectroscopy study using a continuous bioreactor system. *Magn Reson Med*, 33, 422–426.

Garnsworthy, P., Masson, L., Lock, A., & Mottram, T. (2006). Variation of Milk Citrate with Stage of Lactation and De Novo Fatty Acid Synthesis in Dairy Cows. *J Dairy Sci*, 89, 1604 – 1612.

- Geishauser, T., Leslie, K., Tenhag, J., & Bashiri, A. (2000). Evaluation of eight cow-side ketone tests in milk for detection of subclinical ketosis in dairy cows. *J Dairy Sci*, 83, 296–299.
- Glunde, K., Shah, T., Winnard, P. T., Raman, V., Takagi, T., Vesuna, F., Artemov, D., & Bhujwala, Z. M. (2008). Hypoxia regulates choline kinase expression through hypoxia-inducible factor-1 alpha signaling in a human prostate cancer model. *Cancer Res*, 68, 172–180.
- Govindaraju, V., Young, K., & Maudsley, A. A. (2000). Proton NMR chemical shifts and coupling constants for brain metabolites. *NMR Biomed*, 13, 129–153.
- Grob, R. L. & Barry, E. F., editors (2004). *Modern Practice of Gas Chromatography*. John Wiley & Sons, Hoboken, NJ, USA.
- Gronwald, W., Klein, M. S., Kaspar, H., Fagerer, S. R., Nürnberger, N., Dettmer, K., Bertsch, T., & Oefner, P. J. (2008). Urinary metabolite quantification employing 2D NMR spectroscopy. *Anal Chem*, 80, 9288–9297.
- Gronwald, W., Klein, M. S., Zeltner, R., Schulze, B.-D., Reinhold, S. W., Deutschmann, M., Immervoll, A.-K., Böger, C. A., Banas, B., Eckardt, K.-U., & Oefner, P. J. (2011). Detection of autosomal dominant polycystic kidney disease by NMR spectroscopic fingerprinting of urine. *Kidney Int*, 79, 1244–1253.
- Hardison, W. G. & Proffitt, J. H. (1977). Influence of hepatic taurine concentration on bile acid conjugation with taurine. *Am J Physiol*, 232, E75–E79.
- Holmes, E., Foxall, P. J., Spraul, M., Farrant, R. D., Nicholson, J. K., & Lindon, J. C. (1997). 750 MHz <sup>1</sup>H NMR spectroscopy characterisation of the complex metabolic pattern of urine from patients with inborn errors of metabolism: 2-hydroxyglutaric aciduria and maple syrup urine disease. *J Pharm Biomed Anal*, 15, 1647–1659.
- Holmes, E., Loo, R. L., Stampler, J., Bictash, M., Yap, I. K. S., Chan, Q., Ebbels, T., Iorio, M. D., Brown, I. J., Veselkov, K. A., Davignus, M. L., Kesteloot, H., Ueshima, H., Zhao, L., Nicholson, J. K., & Elliott, P. (2008). Human metabolic phenotype diversity and its association with diet and blood pressure. *Nature*, 453, 396–400.
- Holmes, H. C., Snodgrass, G. J., & Iles, R. A. (2000). Changes in the choline content of human breast milk in the first 3 weeks after birth. *Eur J Pediatr*, 159, 198–204.
- Holmes-McNary, M. Q., Cheng, W. L., Mar, M. H., Fussell, S., & Zeisel, S. H. (1996). Choline and choline esters in human and rat milk and in infant formulas. *Am J Clin Nutr*, 64, 572–576.
- Holt, C. & Muir, D. D. (1979). Inorganic constituents of milk: I. Correlation of soluble calcium with citrate in bovine milk. *J Dairy Res*, 46, 433–439.
- Hoult, D. I. & Ginsberg, N. S. (2001). The Quantum Origins of the Free Induction Decay Signal and Spin Noise. *J Magn Reson*, 148, 182 – 199.

Hüttmann, H., Stamer, E., Junge, W., Thaller, G., & Kalm, E. (2009). Analysis of feed intake and energy balance of high-yielding first lactating Holstein cows with fixed and random regression models. *Anim*, 3, 181–188.

Hu, F., Furihata, K., Kato, Y., & Tanokura, M. (2007). Nondestructive quantification of organic compounds in whole milk without pretreatment by two-dimensional NMR spectroscopy. *J Agric Food Chem*, 55, 4307–4311.

Huber, T. L. (1976). Physiological effects of acidosis on feed lot cattle. *J Anim Sci*, 43, 902–909.

Hyvärinen, A. & Oja, E. (2000). Independent component analysis: algorithms and applications. *Neural Netw*, 13, 411–430.

Ilcol, Y. O., Ozbek, R., Hamurtekin, E., & Ulus, I. H. (2005). Choline status in newborns, infants, children, breast-feeding women, breast-fed infants and human breast milk. *J Nutr Biochem*, 16, 489–499.

Ingvartsen, K. & Andersen, J. (2000). Integration of Metabolism and Intake Regulation: A Review Focusing on Periparturient Animals. *J Dairy Sci*, 83, 1573 – 1597.

Ingvartsen, K., Dewhurst, R., & Friggens, N. (2003). On the relationship between lactational performance and health: is it yield or metabolic imbalance that cause production diseases in dairy cattle? A position paper. *Livest Prod Sci*, 83, 277 – 308.

Iorio, E., Mezzanzanica, D., Alberti, P., Spadaro, F., Ramoni, C., D'Ascenzo, S., Millimaggi, D., Pavan, A., Dolo, V., Canevari, S., & Podo, F. (2005). Alterations of choline phospholipid metabolism in ovarian tumor progression. *Cancer Res*, 65, 9369–9376.

Iorio, E., Ricci, A., Bagnoli, M., Pisanu, M. E., Castellano, G., Vito, M. D., Venturini, E., Glunde, K., Bhujwalla, Z. M., Mezzanzanica, D., Canevari, S., & Podo, F. (2010). Activation of phosphatidylcholine cycle enzymes in human epithelial ovarian cancer cells. *Cancer Res*, 70, 2126–2135.

Jahns, G. L., Kent, M. N., Burgoon, L. D., DelRaso, N., Zacharewski, T. R., & Reo, N. V. (2009). Development of analytical methods for NMR spectra and application to a 13C toxicology study. *Metabolomics*, 5, 253–262.

Johnson, N. A., Walton, D. W., Sachinwalla, T., Thompson, C. H., Smith, K., Ruell, P. A., Stannard, S. R., & George, J. (2008). Noninvasive assessment of hepatic lipid composition: Advancing understanding and management of fatty liver disorders. *Hepatology*, 47, 1513–1523.

Kalaitzakis, E., Panousis, N., Roubies, N., Giadinis, N., Kaldrymidou, E., Georgiadis, M., & Karatzias, H. (2010). Clinicopathological evaluation of downer dairy cows with fatty liver. *Can Vet J*, 51, 615–622.

Kaspar, H., Dettmer, K., Gronwald, W., & Oefner, P. J. (2008). Automated GC-MS analysis of free amino acids in biological fluids. *J Chromatogr B Analyt Technol Biomed Life Sci*, 870, 222–232.

- Köhler, W., Schachtel, G., & Voleske, P. (2002). *Biostatistik*. Springer, Berlin, Germany.
- Klein, M. S. (2007). *ESR-Untersuchungen zu strahleninduzierten Radikalen in Fingernägeln*. Diploma thesis, University of Regensburg, Germany.
- Klein, M. S., Almstetter, M. F., Schlamberger, G., Nürnberger, N., Dettmer, K., Oefner, P. J., Meyer, H. H. D., Wiedemann, S., & Gronwald, W. (2010). Nuclear magnetic resonance and mass spectrometry-based milk metabolomics in dairy cows during early and late lactation. *J Dairy Sci*, 93, 1539–1550.
- Klein, M. S., Buttchereit, N., Miemczyk, S., Immervoll, A.-K., Louis, C., Wiedemann, S., Junge, W., Thaller, G., Oefner, P. J., & Gronwald, W. (2011). NMR Metabolomic Analysis of Dairy Cows Reveals Milk Glycerophosphocholine to Phosphocholine Ratio as Prognostic Biomarker for Risk of Ketosis. *J Prot Res*.
- Klein, M. S., Dorn, C., Saugspier, M., Hellerbrand, C., Oefner, P. J., & Gronwald, W. (2011). Discrimination of steatosis and NASH in mice using nuclear magnetic resonance spectroscopy. *Metabolomics*, 7, 237–246. 10.1007/s11306-010-0243-6.
- Kohl, S., Klein, M. S., Hochrein, J., Oefner, P. J., Spang, R., & Gronwald, W. (2011). State-of-the art data normalization methods improve NMR-based metabolomic analysis. *Metabolomics*, 1–15. 10.1007/s11306-011-0350-z.
- Kojima, H., Sakurai, S., Uemura, M., Fukui, H., Morimoto, H., & Tamagawa, Y. (2007). Mitochondrial abnormality and oxidative stress in nonalcoholic steatohepatitis. *Alcohol Clin Exp Res*, 31, S61–S66.
- Konar, A., Thomas, P. C., & Rook, J. A. F. (1971). The concentrations of some water-soluble constituents in the milks of cows, sows, ewes and goats. *J Dairy Res*, 38, 333–341.
- Kuksis, A., Roberts, A., Thompson, J., Myher, J., & Geher, K. (1983). Plasma phosphatidylcholine/free cholesterol ratio as an indicator for atherosclerosis. *Arteriosclerosis*, 4, 389–397.
- Lewis, I. A., Schommer, S. C., Hodis, B., Robb, K. A., Tonelli, M., Westler, W. M., Sussman, M. R., & Markley, J. L. (2007). Method for determining molar concentrations of metabolites in complex solutions from two-dimensional <sup>1</sup>H-<sup>13</sup>C NMR spectra. *Anal Chem*, 79, 9385–9390.
- Lilliefors, H. W. (1967). On the Kolmogorov-Smirnov Test for Normality with Mean and Variance Unknown. *J A S A*, 62, 399–402.
- Lindon, J. C., Holmes, E., & Nicholson, J. K. (2006). Metabonomics techniques and applications to pharmaceutical research & development. *Pharm Res*, 23, 1075–1088.
- Lindon, J. C. & Nicholson, J. K. (2008). Spectroscopic and Statistical Techniques for Information Recovery in Metabonomics and Metabolomics. *Annu Rev Anal Chem*, 1, 45–69.
- Mai, C. (1912). Der Einfluss des Gefrierens auf die Zusammensetzung der Milch. *Zeitschrift für Lebensmitteluntersuchung und -Forschung A*, 23, 250–254.

- Malakauskas, S. M., Quan, H., Fields, T. A., McCall, S. J., Yu, M.-J., Kourany, W. M., Frey, C. W., & Le, T. H. (2007). Aminoaciduria and altered renal expression of luminal amino acid transporters in mice lacking novel gene collectrin. *Am J Physiol Renal Physiol*, 292, F533–F544.
- Miyataka, H., Ozaki, T., & Himeno, S. (2007). Effect of pH on <sup>1</sup>H-NMR spectroscopy of mouse urine. *Biol Pharm Bull*, 30, 667–670.
- Mårtensson, J. & Meister, A. (1992). Glutathione deficiency increases hepatic ascorbic acid synthesis in adult mice. *Proc Natl Acad Sci U S A*, 89, 11566–11568.
- Murray, J. J., Dinh, T. T., Truett, A. P., & Kennerly, D. A. (1990). Isolation and enzymic assay of choline and phosphocholine present in cell extracts with picomole sensitivity. *Biochem J*, 270, 63–68.
- Ndibualonji, B. B., Dehareng, D., Eenaeme, C. V., & Godeau, J. M. (1995). Response of milk yield, plasma cortisol, amino acids, urea and glucose to a single low-dose administration of adrenocorticotrophic hormone in lactating cows. *Vet Res*, 26, 32–42.
- Neild, G. H., Foxall, P. J., Lindon, J. C., Holmes, E. C., & Nicholson, J. K. (1997). Uroscopy in the 21st century: high-field NMR spectroscopy. *Nephrol Dial Transplant*, 12, 404–417.
- Nicholson, J. K., Foxall, P. J. D., Spraul, M., Farrant, R. D., & Lindon, J. C. (1995). 750 MHz <sup>1</sup>H and <sup>1</sup>H-<sup>13</sup>C NMR Spectroscopy of Human Blood Plasma. *Anal Chem*, 67, 793–811.
- Nicholson, J. K. & Lindon, J. C. (2008). Systems biology: Metabonomics. *Nature*, 455, 1054–1056.
- Nielsen, J. & Jewett, M. C., editors (2007). *Metabolomics*. Springer, Berlin, Germany.
- Obinata, K., Maruyama, T., Hayashi, M., Watanabe, T., & Nittono, H. (1996). Effect of taurine on the fatty liver of children with simple obesity. *Adv Exp Med Biol*, 403, 607–613.
- Olson, L. K., Tan, Y., Zhao, Y., Aupperlee, M. D., & Haslam, S. Z. (2010). Pubertal exposure to high fat diet causes mouse strain-dependent alterations in mammary gland development and estrogen responsiveness. *Int J Obes (Lond)*, 34, 1415–1426.
- Oostendorp, M., Engelke, U. F., Willemsen, M. A., & Wevers, R. A. (2006). Diagnosing Inborn Errors of Lipid Metabolism with Proton Nuclear Magnetic Resonance Spectroscopy. *Clin Chem*, 52, 1395–1405.
- Overhauser, A. W. (1953). Polarization of Nuclei in Metals. *Phys Rev*, 92, 411–415.
- Peake, M. & Whiting, M. (2006). Measurement of serum creatinine—current status and future goals. *Clin Biochem Rev*, 27, 173–184.
- Pearson, H. (2007). Meet the human metabolome. *Nature*, 446, 8.
- Pearson, K. (1901). On Lines and Planes of Closest Fit to Systems of Points in Space. *Philosophical Magazine*, 2, 559–572.

Pinotti, L., Baldi, A., & Dell'Orto, V. (2002). Comparative mammalian choline metabolism with emphasis on the high-yielding dairy cow. *Nutr Res Rev*, 15, 315–332.

Podo, F. (1999). Tumour phospholipid metabolism. *NMR Biomed*, 12, 413–439.

Pomfret, E. A., daCosta, K. A., Schurman, L. L., & Zeisel, S. H. (1989). Measurement of choline and choline metabolite concentrations using high-pressure liquid chromatography and gas chromatography-mass spectrometry. *Anal Biochem*, 180, 85–90.

Pryce, J. E., Veerkamp, R. F., Thompson, R., Hill, W. G., & Simm, G. (1997). Genetic aspects of common health disorders and measures of fertility in Holstein Friesian dairy cattle. *Anim Sci*, 65, 353–360.

Purcell, E. M., Torrey, H. C., & Pound, R. V. (1946). Resonance absorption by nuclear magnetic moments in a solid. *Phys Rev*, 69, 37:38.

Puri, P., Baillie, R. A., Wiest, M. M., Mirshahi, F., Choudhury, J., Cheung, O., Sargeant, C., Contos, M. J., & Sanyal, A. J. (2007). A lipidomic analysis of nonalcoholic fatty liver disease. *Hepatology*, 46, 1081–1090.

Pyörälä, S. (2003). Indicators of inflammation in the diagnosis of mastitis. *Vet Res*, 34, 565–578.

Roginski, H. & Fuquay, J. W. (2004). *Encyclopedia of Dairy Sciences*. Academic Press, London, UK.

Saverymuttu, S. H., Joseph, A. E., & Maxwell, J. D. (1986). Ultrasound scanning in the detection of hepatic fibrosis and steatosis. *Br Med J (Clin Res Ed)*, 292, 13–15.

Schnackenberg, L. K., Dragan, Y. P., Reily, M. D., Robertson, D. G., & Beger, R. D. (2007). Evaluation of NMR spectral data of urine in conjunction with measured clinical chemistry and histopathology parameters to assess the effects of liver and kidney toxicants. *Metabolomics*, 3, 87–100.

Scholz, M., Gatzek, S., Sterling, A., Fiehn, O., & Selbig, J. (2004). Metabolite fingerprinting: detecting biological features by independent component analysis. *Bioinformatics*, 20, 2447–2454.

Seavey, B. R., Farr, E. A., Westler, W. M., & Markley, J. L. (1991). A relational database for sequence-specific protein NMR data. *J Biomol NMR*, 1, 217–236.

Seoane, J., Barberà, A., Télémaque-Potts, S., Newgard, C. B., & Guinovart, J. J. (1999). Glucokinase overexpression restores glucose utilization and storage in cultured hepatocytes from male Zucker diabetic fatty rats. *J Biol Chem*, 274, 31833–31838.

Serkova, N. J., Jackman, M., Brown, J. L., Liu, T., Hirose, R., Roberts, J. P., Maher, J. J., & Niemann, C. U. (2006). Metabolic profiling of livers and blood from obese Zucker rats. *J Hepatol*, 44, 956–962.

Shanaiah, N., Desilva, M. A., Gowda, G. A. N., Raftery, M. A., Hainline, B. E., & Raftery, D. (2007). Class selection of amino acid metabolites in body fluids using chemical derivatization and their enhanced  $^{13}\text{C}$  NMR. *Proc Natl Acad Sci U S A*, 104, 11540–11544.

Sharma, B. K. & Erdman, R. A. (1989). Effects of dietary and abomasally infused choline on milk production responses of lactating dairy cows. *J Nutr*, 119, 248–254.

Smith, L. M., Maher, A. D., Want, E. J., Elliott, P., Stamler, J., Hawkes, G. E., Holmes, E., Lindon, J. C., & Nicholson, J. K. (2009). Large-Scale Human Metabolic Phenotyping and Molecular Epidemiological Studies via  $^1\text{H}$  NMR Spectroscopy of Urine: Investigation of Borate Preservation. *Anal Chem*, 81, 4847–4856.

Spearman, C. (1904). The proof and measurement of association between two things. *Am J Psychol*, 15, 72–101.

Stelwagen, K., van Espen, D. C., Verkerk, G. A., McFadden, H. A., & Farr, V. C. (1998). Elevated plasma cortisol reduces permeability of mammary tight junctions in the lactating bovine mammary epithelium. *J Endocrinol*, 159, 173–178.

Stolzenburg, S., Lauridsen, M., Toft, H., Zalloua, P., & Baunsgaard, D. (2011). Improved quality of  $^1\text{H}$  NMR spectroscopic data for enhanced metabolic profiling of low molecular weight metabolites in human serum. *Metabolomics*, 7, 270–277.

Tang, H., Wang, Y., Nicholson, J. K., & Lindon, J. C. (2004). Use of relaxation-edited one-dimensional and two dimensional nuclear magnetic resonance spectroscopy to improve detection of small metabolites in blood plasma. *Anal Biochem*, 325, 260–272.

Toso, B., Procida, G., & Stefanon, B. (2002). Determination of volatile compounds in cows' milk using headspace GC-MS. *J Dairy Res*, 69, 569–577.

Töpel, A. (2004). *Chemie und Physik der Milch*. Behr's Verlag, Hamburg, Germany.

Turnbaugh, P. J., Ley, R. E., Mahowald, M. A., Magrini, V., Mardis, E. R., & Gordon, J. I. (2006). An obesity-associated gut microbiome with increased capacity for energy harvest. *Nature*, 444, 1027–1031.

Waldhier, M. C., Almstetter, M. F., Nürnberger, N., Gruber, M. A., Dettmer, K., & Oefner, P. J. (2011). Improved enantiomer resolution and quantification of free d-amino acids in serum and urine by comprehensive two-dimensional gas chromatography-time-of-flight mass spectrometry. *J Chromatogr A*, 1218, 4537 – 4544.

Wang, Q., Jiang, L., Wang, J., Li, S., Yu, Y., You, J., Zeng, R., Gao, X., Rui, L., Li, W., & Liu, Y. (2009). Abrogation of hepatic ATP-citrate lyase protects against fatty liver and ameliorates hyperglycemia in leptin receptor-deficient mice. *Hepatology*, 49, 1166–1175.

Waters, N. J., Holmes, E., Waterfield, C. J., Farrant, R. D., & Nicholson, J. K. (2002). NMR and pattern recognition studies on liver extracts and intact livers from rats treated with alpha-naphthylisothiocyanate. *Biochem Pharmacol*, 64, 67–77.

Weljie, A. M., Newton, J., Mercier, P., Carlson, E., & Slupsky, C. M. (2006). Targeted profiling: quantitative analysis of <sup>1</sup>H NMR metabolomics data. *Anal Chem*, 78, 4430–4442.

Wishart, D. S. (2008). Quantitative metabolomics using NMR. *TrAC Trends in Analytical Chemistry*, 27, 228 – 237. Metabolomics.

Wishart, D. S., Lewis, M. J., Morrissey, J. A., Flegel, M. D., Jeroncic, K., Xiong, Y., Cheng, D., Eisner, R., Gautam, B., Tzur, D., Sawhney, S., Bamforth, F., Greiner, R., & Li, L. (2008). The human cerebrospinal fluid metabolome. *J Chromatogr B Analyt Technol Biomed Life Sci*, 871, 164–173.

Xia, J., Bjorndahl, T., Tang, P., & Wishart, D. (2008). MetaboMiner - semi-automated identification of metabolites from 2D NMR spectra of complex biofluids. *BMC Bioinformatics*, 9, 507.

Yaman, H., CakIr, E., Ozcan, O., Yesilova, Z., Ozcan, A., Akgul, E. O., Erbil, M. K., Bagci, S., Bilgi, C., & Dagalp, K. (2005). Elevated urine neopterin levels in nonalcoholic steatohepatitis. *Clin Biochem*, 38, 187 – 190.

Zeisel, S. H., daCosta, K. A., Youssef, M., & Hensey, S. (1989). Conversion of dietary choline to trimethylamine and dimethylamine in rats: dose-response relationship. *J Nutr*, 119, 800–804.

Zheng, M., Lu, P., Liu, Y., Pease, J., Usuka, J., Liao, G., & Peltz, G. (2007). 2D NMR metabonomic analysis: a novel method for automated peak alignment. *Bioinformatics*, 23, 2926–2933.

Zobel, R., Tkalcic, S., Buic, V., Pipal, I., Geres, D., & Samardzija, M. (2011). Repeat breeder syndrome in dairy cows: influence of breed and age on its prevalence and the success of a hormone therapy. *Turk J Vet Anim Sci*, 35.

---

## **6 About the Author**

## 6.1 Curriculum Vitae

Name	Matthias Stefan Klein
Date of birth	July 14, 1980
Place of birth	Bad Reichenhall, Germany
Nationalities	German, Swedish

### Education

Mar 2008 - present	Ph.D. thesis at the University of Regensburg, Regensburg, Germany
Oct 2006 - Nov 2007	Diploma thesis in Biophysics (Advisor: Prof. Dr. Elmar Lang) Topic: <i>ESR Analyses on Radiation-Induced Radicals in Fingernails</i>
Apr 2002 - Nov 2007	Physics studies at the University of Regensburg, Regensburg, Germany
Sep 1991 - June 2000	High school (Karls gymnasium, Bad Reichenhall, Germany)

## 6.2 Publications

Klein, M. S. (2007). *ESR-Untersuchungen zu strahleninduzierten Radikalen in Fingernägeln*. Diploma thesis, University of Regensburg, Germany.

Gronwald, W., Klein, M. S., Kaspar, H., Fagerer, S. R., Nürnberger, N., Dettmer, K., Bertsch, T., & Oefner, P. J. (2008). Urinary metabolite quantification employing 2D NMR spectroscopy. *Anal Chem*, 80, 9288–9297.

Klein, M. S., Almstetter, M. F., Schlamberger, G., Nürnberger, N., Dettmer, K., Oefner, P. J., Meyer, H. H. D., Wiedemann, S., & Gronwald, W. (2010). Nuclear magnetic resonance and mass spectrometry-based milk metabolomics in dairy cows during early and late lactation. *J Dairy Sci*, 93, 1539–1550.

Klein, M. S., Dorn, C., Saugspier, M., Hellerbrand, C., Oefner, P. J., & Gronwald, W. (2011). Discrimination of steatosis and NASH in mice using nuclear magnetic resonance spectroscopy. *Metabolomics*, 7, 237–246.

Gronwald, W., Klein, M. S., Zeltner, R., Schulze, B.-D., Reinhold, S. W., Deutschmann, M., Immervoll, A.-K., Böger, C. A., Banas, B., Eckardt, K.-U., & Oefner, P. J. (2011). Detection of autosomal dominant polycystic kidney disease by NMR spectroscopic fingerprinting of urine. *Kidney International*, 79, 1244–1253.

Kohl, S., Klein, M. S., Hochrein, J., Oefner, P. J., Spang, R., & Gronwald, W. (2011). State-of-the art data normalization methods improve NMR-based metabolomic analysis. *Metabolomics*.

Klein, M. S., Buttchereit, N., Miemczyk, S., Immervoll, A.-K., Louis, C., Wiedemann, S., Junge, W., Thaller, G., Oefner, P. J., & Gronwald, W. (2011). NMR Metabolomic Analysis of Dairy Cows Reveals Milk Glycerophosphocholine to Phosphocholine Ratio as Prognostic Biomarker for Risk of Ketosis. *J Prot Res*. DOI: 10.1021/pr201017n

## In Preparation

Almstetter, M. F., Nürnberger, N., Schlamberger, G., Gronwald, W., Klein, M. S., Wiedemann, S., Meyer, H. H., Oefner, P. J., & Dettmer, K. (2011). Mass Spectrometry Based Plasma Metabolomics in Dairy Cows during Early and Late Lactation. *In preparation*.

Hochrein, J., Klein, M. S., Spang, R., Oefner, P. J., & Gronwald, W. (2011). Optimized Classification of Metabolomic Data. *In preparation*.

Klein, M. S., Oefner, P. J., & Gronwald, W. (2011). OMS as NMR Quantification Standard in Lipophilic Samples. *In preparation*.

Klein, M. S., Oefner, P. J., & Gronwald, W. (2011). QUANTIFY - A Tool for Quantification from 1D and 2D NMR Spectra. *In preparation*.

Thomas, A., Reinders, J., Stevens, A. P., Klein, M. S., Hellerbrand, C., Dettmer-Wilde, K., Gronwald, W., & Oefner, P. J. (2011). Analysis of early changes in the liver soluble proteome from mice fed a non-alcoholic steatohepatitis inducing diet. *In preparation*.

### 6.3 Poster Presentations

September 22 - 25, 2008: *Urinary Metabolite Quantification Employing 2D NMR Spectroscopy* at the annual discussion meeting of the Magnetic Resonance Spectroscopy Division of the German Chemical Society (GDCh) in Regensburg, Germany

September 21 - 24, 2009: *NMR and Mass Spectrometry Based Milk Metabolomics in Dairy Cows During Early and Late Lactation* at the annual discussion meeting of the Magnetic Resonance Spectroscopy Division of the German Chemical Society (GDCh) in Dresden, Germany

January 28 - 29, 2011: *Discrimination of Steatosis and NASH in Mice Using Nuclear Magnetic Resonance Spectroscopy* at the annual meeting of the German Association for the Study of the Liver (GASL) in Regensburg, Germany

August 21 - 25, 2011: *NMR Analyses of Milk Metabolites Allow Disease Prediction for Dairy Cows* at the annual meeting of the European Magnetic Resonance Community (EUROMAR) in Frankfurt/Main, Germany

### 6.4 Conference Talks

September 21, 2010: *Discrimination of Steatosis and NASH in Mice Using NMR* at the annual discussion meeting of the Magnetic Resonance Spectroscopy Division of the German Chemical Society (GDCh) in Münster, Germany

April 14, 2011: *Urinary NMR Fingerprinting in the Differential Diagnosis of Autosomal Dominant Polycystic Kidney Disease* at the associate seminar of the Bavarian Genome Research Network (BayGene) in Grosshadern/Martinsried, Germany

---

## **Appendix**

### **Appendix I: Tables**

**Table 1.** Analysis of Human Urinary Metabolites: Chemical Shift Values of Urinary Metabolites for the High-Resolution 2D  $^1\text{H}$ - $^{13}\text{C}$  HSQC Spectrum of a Healthy Control Urine Specimen (Figure 11). Adapted from (Gronwald et al. 2011).

$^{13}\text{C}$ Frequency [ppm]	$^1\text{H}$ Frequency [ppm]	Compound
36.74	3.74	1-methylhistidine
30.62	3.23	
30.62	3.20	
30.62	3.15	
30.62	3.12	
123.12	7.10	1-methylhistidine/anserine
51.43	4.48	1-methylnicotinamide
118.28	7.01	2,5-furandicarboxylic acid
24.14	1.63	2-aminoadipic acid
32.94	1.86	
57.68	3.74	
36.27	2.28	
36.33	2.25	2-hydroxyglutaric acid
29.65	1.36	2-hydroxyisobutyric acid
46.25	3.78	2-methylbutyrylglycine
14.02	0.89	
46.25	3.81	2-methylbutyrylglycine/ tiglylglycine
24.32	0.93	2-oxo-isocaproic acid
32.15	3.38	3,7-dimethyluric acid
31.10	3.43	
45.45	3.11	3-aminoisobutyric acid
45.28	3.04	
18.05	1.19	3-aminoisobutyric acid/ methylmalonic acid
29.01	1.32	3-hydroxy-3-methylglutaric acid
51.40	2.46	
51.41	2.43	
52.37	2.37	3-hydroxyisovaleric acid
30.94	1.27	3-hydroxyisovaleric acid/ caprylic acid
42.86	2.44	3-hydroxypropionic acid
61.89	3.80	
27.56	3.33	3-methylhistidine
27.56	3.28	
35.45	3.79	3-methylhistidine/anserine
56.73	3.93	3-methylhistidine/ phosphocreatine/ creatine
32.23	3.52	3-methylxanthine
27.71	1.82	4-guanidinobutyric acid
37.08	2.25	
43.68	3.20	
46.73	3.94	4-hydroxyhippuric acid
118.44	6.97	
132.31	7.75	4-hydroxyphenylacetic acid
46.27	3.45	
118.28	6.87	4-hydroxyphenylacetic acid/N-acetyltyrosine
133.43	7.16	5-aminopentanonic acid
29.33	1.68	
25.30	1.64	
39.64	2.24	5-aminopentanonic acid/2-aminoadipic acid
26.11	1.92	acetic acid
33.06	2.23	acetone
23.43	2.15	acetyl-L-carnitine
43.35	2.55	
56.73	3.20	acetyl-L-carnitine/choline/isobutyrylcarnitine
43.35	2.72	acetyl-L-carnitine/ guanidinosuccinic acid
69.60	5.60	acetyl-L-carnitine/ isobutyrylcarnitine
70.91	3.88	
71.07	3.61	
53.50	3.79	
19.02	1.48	alanine
66.24	5.40	allantoin
138.48	8.27	anserine
73.47	3.59	arabitol
73.32	3.94	

65.75	3.84	
43.51	3.24	
26.75	1.65	arginine
26.62	1.72	arginine/ethylmalonic acid
30.46	1.92	arginine/ornithine/N-acetyl-L-glutamine
37.55	2.88	
37.54	2.94	asparagine
54.32	4.01	
36.59	2.58	
39.68	3.19	$\beta$ -alanine
68.97	3.90	
56.24	3.26	betaine
36.27	3.92	
146.76	7.89	caffeine
33.08	3.42	
30.54	3.29	caffeine/1,3-dimethyluric acid
72.84	3.43	
45.77	2.44	
56.91	3.23	carnitine
66.98	4.57	
70.42	3.52	
58.34	4.06	choline
46.41	3.14	
128.43	5.81	cis-aconitic acid
49.47	2.65	
28.04	1.34	citramalic acid
47.86	2.71	
47.86	2.68	
47.86	2.56	citric acid
47.86	2.54	
39.81	3.04	creatine/phosphocreatine/N-acetyltyrosine
59.14	4.06	
33.04	3.04	creatinine
56.24	4.13	
40.29	3.16	
40.63	3.41	cystine
40.67	3.38	
40.64	3.20	
74.29	3.97	
74.48	4.28	D-galactonic acid
72.68	3.66	
32.24	2.68	dihydrouracil
37.58	2.73	dimethylamine
72.20	3.80	
66.23	3.88	D-mannitol
73.83	3.77	D-mannitol/arabitol
66.07	3.68	D-mannitol/galactitol/threonic acid/arabitol/D-galactonic acid
76.39	3.95	
77.03	4.14	
76.55	4.10	D-saccharic acid
74.77	4.08	
99.59	4.58	
95.25	5.20	
68.01	3.32	
77.03	3.23	D-xylose
72.35	3.62	
75.74	3.65	
78.75	3.42	
65.59	3.77	
65.59	3.79	erythritol
19.18	1.15	ethanol/2-methylbutyryl-glycine
60.59	3.83	
44.32	3.16	ethanolamine
14.80	0.88	ethylmalonic acid
72.36	3.69	galactitol
73.00	3.98	galactitol/D-galactonic acid
104.31	5.46	
67.90	4.10	glucosan
68.02	3.76	
73.01	3.54	

73.75	3.68	
79.11	4.63	
74.94	3.69	glucosan/erythritol
75.58	3.73	
74.45	3.84	
72.52	3.41	
63.66	3.91	
63.66	3.89	
63.66	3.72	glucose
63.49	3.85	
63.33	3.79	
95.10	5.25	
98.95	4.64	
77.05	3.25	
78.73	3.48	
74.42	3.54	glucose/D-xylose
33.68	2.45	
29.17	2.14	glutamine
57.21	3.78	glutamine/lysine/arginine/glutamic acid/ornithine
44.48	3.57	glycine
64.14	3.95	glycolic acid
27.24	1.64	
25.14	0.93	glycyl-L-leucine
23.54	0.89	
47.52	3.80	guanidinoacetate
43.35	2.74	
57.70	4.24	guanidinosuccinic acid
43.35	2.53	guanidinosuccinic acid/ isobutyrylcarnitine
135.04	7.64	
131.66	7.55	hippuric acid
130.05	7.82	
46.73	3.97	
120.22	7.19	
57.37	4.01	
29.98	3.22	
30.13	3.31	histidine
29.98	3.28	
29.98	3.23	
70.39	4.38	
27.89	2.15	hydroxyacetone
119.08	7.35	
115.08	7.50	indoxyl sulfate
120.27	7.69	
59.78	3.96	isethionic acid
20.79	1.14	
43.04	2.62	isobutyrylcarnitine
21.43	1.12	isobutyrylglucine
51.64	3.00	
40.35	2.53	isocitric acid
40.33	2.48	
22.96	1.33	
71.83	4.11	lactic acid
24.82	0.97	
23.69	0.96	
26.98	1.73	leucine
26.97	1.70	
61.24	4.18	
32.55	2.40	
28.20	2.51	L-pyroglutamic acid
28.20	2.04	
32.88	1.92	
32.71	1.91	
29.33	1.73	
29.17	1.75	
24.33	1.47	
24.33	1.41	lysine
24.17	1.53	
24.17	1.51	
24.17	1.44	
24.17	1.49	

42.22	3.03	lysine/4-hydroxyphenylacetic acid/5-aminopentanoic acid
131.66	7.36	mandelic acid
130.21	7.41	
52.00	3.37	methanol
27.72	2.61	methylamine
30.17	2.83	methylguanidine
18.18	1.24	methylmalonic acid
55.76	3.16	methylmalonic acid/ isethionic acid
75.10	4.07	myo-inositol
74.77	3.61	
73.85	3.54	
77.04	3.29	
62.85	3.72	
46.41	2.93	N,N-dimethylglycine
41.74	3.20	N8-acetylspermidine
24.82	1.99	
26.75	2.09	N8-acetylspermidine/2-oxoisocaproic acid
24.82	2.03	N-acetyl-L-glutamine
57.69	4.18	
34.48	2.27	
30.47	2.12	
59.30	4.43	
24.66	1.94	N-acetyltyrosine
28.85	2.92	N-methylnicotinamide
138.29	8.16	N-methylnicotinamide/ histidine
71.39	3.52	pantothenic acid
23.37	0.93	
21.92	0.89	
71.39	3.41	
78.65	3.99	
45.12	3.67	
46.25	3.75	phenylacetylglutamine
131.82	7.42	phenylacetylglutamine/2-methylbutyrylglutamine/1-isobutyrylglutamine
132.14	7.36	phenylacetylglutamine/ phenylalanine/ mandelic acid/tropic acid/ phenylethylamine
130.21	7.36	phenylacetylglutamine/ phenylalanine/ phenylethylamine
39.16	3.27	phenylalanine
58.85	4.04	
43.09	3.29	
35.92	3.04	phenylethylamine
24.32	1.67	piperidine
25.16	1.78	
47.54	3.17	
73.81	4.15	
76.22	4.29	
144.55	7.66	
86.22	4.02	pseudouridine
81.87	4.69	
64.46	3.86	
64.46	3.84	
64.46	3.73	
18.37	2.48	pyridoxine
29.33	2.38	pyruvic acid
76.55	3.35	scyllo-inositol
63.17	4.01	serine
63.17	3.98	
63.17	3.96	
63.17	3.94	
59.30	3.85	
31.26	1.30	suberic acid/sebacic acid/azelaic acid/caprylic acid
40.29	2.19	suberic acid/sebacic acid/valeric acid/azelaic acid
28.52	1.55	suberic acid/sebaic acid/azelaic acid
36.78	2.41	succinic acid
32.39	2.80	succinimide
75.58	3.77	sucrose
72.20	3.48	
65.43	3.82	
64.30	3.68	
63.01	3.82	
95.00	5.42	
84.11	3.87	

79.37	4.22	
76.86	4.06	
75.26	3.84	
73.97	3.56	
76.86	4.34	tartaric acid
50.44	3.27	taurine
38.35	3.43	taurine/dihydrouracil
146.82	7.91	
36.27	3.93	theobromine
31.86	3.48	
45.78	3.49	thiodiacetic acid/thioglycolic acid
75.74	3.98	threonic acid
75.26	4.02	threonic acid/2-hydroxyglutaric acid/
65.59	3.64	threonic acid/erythritol
68.97	4.27	
22.24	1.33	threonine
63.49	3.60	threonine/valine
14.33	1.85	
136.17	6.49	tiglyglycine
40.15	3.46	trans-aconitic acid
51.12	4.44	
130.54	8.08	trigonelline
62.37	3.27	trimethylamine-N-oxide
66.23	3.87	
131.02	7.36	tropic acid
114.91	7.54	
121.37	7.72	tryptophan
128.13	7.32	
29.34	3.47	
125.21	7.27	tryptophan/indoxyl sulfate
122.80	7.20	
118.77	6.89	
38.19	3.05	tyrosine
58.79	3.93	
133.43	7.16	tyrosine/4-hydroxyphenyl-acetic acid/N-acetyltyrosine
24.66	1.31	valeric acid
16.12	0.87	
24.73	1.29	valeric acid/caprylic acid
20.79	1.04	
19.50	0.98	valine
31.99	2.28	

In case that more than one compound contributed to a signal all corresponding names are given.

**Table 2.** Analysis of Human Urinary Metabolites: Chemical Shift Values and LLOQ's of Urinary Metabolites Quantified in this Thesis. Adapted from (Gronwald et al. 2008).

Compound	Number of Protons	<sup>1</sup> H Frequency [ppm]	<sup>13</sup> C Frequency [ppm]	LLOQ [μmol/L]	Quantified From 1D or 2D Spectra
Acetic acid	3	1.92	25.8	78	2D
Ascorbic acid	1	4.02	72.4	312	2D
	1	4.52	81.2		
	2	3.74	65.2		
Alanine	3	1.48	18.9	78	2D
3-Aminoisobutyrate	1	2.62	42.0	312	2D
Arginine	2	1.74/1.66	26.6	312	2D
	2	3.20	43.4		
Betaine	2	3.90	68.7	78	2D
	3	3.26	56.0		
Citric acid	1	2.67	49.2	312	2D
	1	2.55	49.2		
Citric acid_2	1	2.70	47.6	312	2D
	1	2.54	47.6		
Creatinine	2	4.06	59.0	78	2D
	3	3.05	32.8		
Ethanolamine	2	3.83	60.3	312	2D
	2	3.15	44.0		
Glucose	1	3.4	72.2	563	2D
	1	3.46	78.2		
	1	3.82	63.5		
	1	3.55	74.4		
	1	3.25	76.9		
	1	4.65	98.7		
	1	3.84	74.3		
Glutamine	2	2.14	28.9	312	2D
	2	2.45	33.6		
Glycine	2	3.57	44.2	156	2D
Hippurate	1	7.55	131.2	312	2D
	1	7.64	134.8		
	1	7.84	129.6		
Histidine	1	7.12	119.6	156	2D
Lactate	3	1.332	-	3.25	1D
Leucine	6	0.96	23.9	156	2D
	1	1.73	26.8		
	2	1.73	42.6		
	1	3.74	56.2		
Lysine	2	1.908	32.6	312	2D
	2	1.45/1.48	24.1		
	2	1.73	29.2		
	2	3.03	42.0		
1-Methylhistidine	3	3.71	36.1	312	2D
	1	7.03	122.4		
	1	7.75	140.7		
3-Methylhistidine	2	3.30/2.25	27.5	78	2D
	3	3.74	34.7		
	1	7.14	125.7		
Phenylalanine	1	3.28	39.0	141	2D
	1	3.98	58.5		
	1	3.12	39.0		
	2	7.42	131.7		
	2	7.33	131.7		
	1	7.38	130.3		
Phosphocreatine	3	3.03	39.1	141	2D
	2	3.93	56.1		
Taurine	2	3.43	38.2	312	2D
	2	3.27	50.2		
TMA	9	5.16	47.4	39	2D
TMAO	9	3.27	62.1	39	2D

**Table 3.** Reproducibility of 2D NMR-Based Quantification: Average Concentrations and Ranges for Selected Urinary Metabolites. Adapted from (Gronwald et al. 2008).

Compound	Concentration Mean $\pm$ SD [ $\mu\text{mol/L}$ ]	RSD [%] (n = 6)	Range [ $\mu\text{mol/L}$ ]
Acetic acid	367 $\pm$ 284	9.6	88 - 931
Alanine	194 $\pm$ 84	20.6	86 - 465
3-Aminoisobutyrate	1505 $\pm$ 437	6.9	898 - 2037
Arginine	ND	ND	ND
Betaine	176 $\pm$ 105	19.6	37 - 637
Citrate	1421 $\pm$ 593	14.8	152 - 2673
Creatinine	7069 $\pm$ 2748	2.0	3069 - 13593
Ethanolamine	363 $\pm$ 47	14.8	176 - 496
Glutamine	431 $\pm$ 121	19.4	314 - 666
Glycine	953 $\pm$ 472	4.8	355 - 1976
Hippurate	2140 $\pm$ 1434	4.6	372 - 5392
Histidine	626 $\pm$ 264	10.4	165 - 1297
Lysine	544 $\pm$ 159	13.4	90 - 832
1-Methylhistidine	215 $\pm$ 109	14.0	78 - 569
3-Methylhistidine	450 $\pm$ 393	13.1	80 - 1640
Taurine	868 $\pm$ 502	3.7	224 - 2571
Trimethylamine-N-oxide	650 $\pm$ 745	3.4	61 - 2419

**Table 4.** Accuracy of 2D NMR Quantification: Concentrations of Amino Acids in a Certified Standard in Comparison to Reference Values. Adapted from (Gronwald et al. 2008).

Compound	2D NMR Concentration [mmol/L] (n = 3)	NIST Certified Concentration [mmol/L]	NIST Gravimetric Value [mmol/L]	Analyte Recovery [%]
Alanine	2.44 $\pm$ 0.08	2.51 $\pm$ 0.09	2.50	97
Arginine	3.09 $\pm$ 0.40	2.94 $\pm$ 0.14	2.83	105
Glycine	2.45 $\pm$ 0.13	2.45 $\pm$ 0.08	2.51	100
Histidine	3.14 $\pm$ 0.55	2.83 $\pm$ 0.11	2.49	111
Lysine	2.45 $\pm$ 0.25	2.47 $\pm$ 0.10	2.51	99

Recovery of amino acids for 2D NMR is based on the NIST certified concentrations.

**Table 5.** Quantitative Comparison of NMR and Alternative Methods: Analysis of Human Urine. Adapted from (Gronwald et al. 2008).

Method	Compound	Linear Regression			Bland-Altman	
		Y-Intercept [ $\mu\text{mol/L}$ ]	Slope	R <sup>2</sup>	Difference [ $\mu\text{mol/L}$ ]	1.96 SD
PAP	Creatinine	273	1.09	0.99	-924	719
Jaffe	Creatinine	245	1.16	0.99	-1401	1082
GC-MS	Alanine	28	0.96	0.83	-19	73
	3-Aminoisobutyrate	314	1.06	0.80	-407	461
	Glutamine	28	0.86	0.86	32	91
	Glycine	72	0.87	0.98	48	169
	Hippurate	115	0.94	0.99	22	313
	Histidine	47	0.84	0.88	53	183
	Lysine	-93	0.91	0.87	141	116
LC-MS/MS	Alanine	49	0.93	0.79	-36	81
	3-Aminoisobutyrate	370	0.82	0.91	-101	279
	Glutamine	25	0.99	0.82	-22	110
	Glycine	107	0.90	0.97	-13	170
	Histidine	91	0.84	0.85	8	202
	Lysine	-174	1.11	0.81	115	176
	3-Methylhistidine	2	1.10	0.97	46	179
	Taurine	73	1.05	0.97	-117	174

For each comparison the y-intercept, slope and R<sup>2</sup> value of the linear regression are given. Additionally, Bland-Altman analyses were conducted. Given are the mean difference and 1.96 times the standard deviation ( $\pm 1.96$  SD) of the differences. For normally distributed differences, it can be expected that 95 % of all differences lie within the limits of agreement defined as  $\pm 1.96$  SD.

**Table 6.** Chemical Shift Values for Bovine Milk Metabolites. Adapted from (Klein et al. 2010).

Compound	Number of Protons	<sup>1</sup> H Frequency [ppm]	<sup>13</sup> C Frequency [ppm]	LLOQ [μmol/L]	Quantified From 1D or 2D Spectra
2-oxoglutaric acid	2	3.009	-	3.25	1D
Acetate	3	1.923	-	3.25	1D
Acetoacetate	3	3.447	-	2.5	1D
Acetone	6	2.236	-	1.76	1D
Alanine	3	1.482	-	3.25	1D
Betaine	2	3.90	67.7	450	2D
BHBA	3	1.203	-	1.62	1D
Carnitine	2	2.44	44.8	281	2D
Choline	2	3.51	69.9	141	2D
Cis-aconitate	1	5.725	-	3.25	1D
Citrate	1	2.70	46.7	312	2D
	1	2.54	46.7		
Creatinine	3	3.05	31.3	78	2D
Ethanolamine	2	3.83	60.3	312	2D
	2	3.15	44.0		
Fumarate	2	6.522	-	3.25	1D
Galactose α	1	4.07	72.8	1125	2D
Galactose β	1	4.57	98.8	1125	2D
	1	3.49	74.4		
Galactose-1-Phosphate	1	4.18	73.3	281	2D
	1	4.00	71.6		
	1	3.91	71.7		
	1	5.46	95.9		
Glutamate	2	2.358	-	3.25	1D
	2	4.32	62.1		
GPC	2	3.87	69.4	141	2D
	2	3.57	42.9		
Glycine	2	3.57	42.9	156	2D
Lactate	3	1.332	-	3.25	1D
Lactose (total)	1	4.45	105.0	453	2D
	1	3.73	77.6		
	1	3.94	71.0		
Lactose α	1	5.23	94.2	1813	2D
	2	3.88	62.3		
Lactose β	1	4.67	98.2	1813	2D
	1	3.29	76.2		
	1	3.96	62.4		
	1	3.60	77.3		
3-Methylhistidine	2	3.30/2.25	27.5	78	2D
	3	3.74	34.7		
	1	7.14	125.7		
N-acetyl-carbohydrates	3	2.05	23.8	141	2D
Orotate	1	6.19	104.0	156	2D
Oxaloacetate	2	2.376	-	3.25	1D
Phosphocholine	2	4.16	60.6	141	2D
	2	3.58	69.0		
Phosphocreatine + Creatine	3	3.03	39.1	141	2D
	2	3.93	56.1		
Taurine	2	3.43	38.2	312	2D
	2	3.27	50.2		
Trimethylamine-N-oxide	3	3.27	62.1	39	2D

**Table 7.** Investigation of Lipophilic Tissue Extracts: Chemical Shifts of Quantified Compounds. Adapted from (Klein et al. 2011b).

Extract Type	Compound	Explanation	<sup>1</sup> H Frequency [ppm]	Number of Protons	Molecular Mass
Lipophilic	Lipid methene*	-CH=CH-	5.45 - 5.20	2	26.0 (2H + 2C)
	Lipid diallylic*	=CH-CH <sub>2</sub> -CH=	2.90 - 2.74	2	14.0 (2H + C)
	Lipid allylic*	-CH <sub>2</sub> -CH=CH-	2.14 - 1.93	2	14.0 (2H + C)
	Lipid methylene*	-CH <sub>2</sub> -	1.41 - 1.20	2	14.0 (2H + C)
	Lipid methyl*	-CH <sub>3</sub>	0.94 - 0.80	3	15.0 (3H + C)
	Lipid α-methylene to carboxyl*	COO-CH <sub>2</sub> -CH <sub>2</sub> -	2.3326 - 2.250	2	58.0 (2H + 2C + 2O)
	Free fatty acid α-methylene to carboxyl*	COO-CH <sub>2</sub> -CH <sub>2</sub> -	2.3773 - 2.3326	2	58.0 (2H + 2C + 2O)
	Lipid glycerol*		4.325 - 4.260	2	41.0 (5H + 3C)
			4.175 - 4.110	2	
	Cholesterol		1.009	3	not used
	Cholesterol ester		1.019	3	not used
Phosphatidylcholine		3.233	9	not used	
Hydrophilic	GPC		3.231	9	not used
	PC		3.222	9	not used

\*Signals used for the estimation of the total lipid content.

**Table 8.** Preprocessing for Statistical Data Analysis: Areas Excluded from Spectral Binning. Adapted from (Klein et al. 2011b).

Sample Type	Spectrum Type	<sup>1</sup> H Area [ppm]	<sup>13</sup> C Area [ppm]	Compound
Urine	1D	6.2 - 4.7	-	Water, urea
	2D	6.2 - 4.0	150 - 5	Water, urea
Milk	1D	4.9 - 4.7	-	Water
		3.371 - 3.359	-	Methanol
		3.815 - 3.755	-	Glycerol
		3.681 - 3.626	-	Glycerol, TEG
		3.592 - 3.3	-	Glycerol
		3.77 - 3.705	-	TEG
		4.7 - 4.655	-	Lactose
		4.484 - 4.429	-	Lactose
		4.0 - 3.52	-	Lactose
		3.33 - 3.258	-	Lactose
		3.24 - 3.208	-	GPC, PC
		3.714 - 3.57	-	GPC, PC
		3.986 - 3.854	-	GPC, PC
		4.212 - 4.12	-	GPC, PC
	4.37 - 4.29	-	GPC, PC	
	2D	5.6 - 4.0	150 - -5	Water, Lactose
		3.85 - 3.7	76.3 - 73.0	Glycerol
		3.7 - 3.5	66.33 - 64.12	Glycerol
		3.41 - 3.29	52.74 - 50.56	Methanol
		3.85 - 3.6	78.4 - 59.0	TEG
4.1 - 3.61		65.4 - 60.8	Lactose	
4.08 - 3.8		75.4 - 69.0	Lactose	
3.86 - 3.39		82.8 - 71.6	Lactose	
3.45 - 3.12	78.3 - 74.6	Lactose		
Other aqueous samples	1D	4.9 - 4.7	-	Water
	2D	5.6 - 4.0	150 - 5	Water
Lipophilic extracts	1D	7.6 - 6.9	-	Chloroform
	2D	7.6 - 6.9	85 - 75	Chloroform

**Table 9.** Brown Swiss and Simmental Fleckvieh Cows: Milk Metabolites Quantified by NMR. Adapted from (Klein et al. 2010).

Metabolite	TE (n = 2) [mmol/L]	Number of Values Above LLOQ <sup>1</sup>	Milk Concentration Range [mmol/L]
Acetic acid	0.090	25	0.108 - 0.701 <sup>3</sup>
Acetone	0.002	106	0.012 - 0.661 <sup>4</sup>
Betaine	0.564	24	0.459 - 1.410 <sup>3</sup>
Carnitine	0.084	1	0.346 <sup>2,3</sup>
Choline	0.112	56	0.150 - 0.997 <sup>3</sup>
Creatinine	0.034	73	0.080 - 0.167 <sup>3</sup>
Ethanolamine	0.026	1	0.323 <sup>2,3</sup>
$\alpha$ -Galactose	0.468	5	1.200 - 1.760 <sup>3</sup>
Glycerophosphocholine	0.095	106	0.284 - 1.460 <sup>3</sup>
Lactose (total)	2.131	106	118.186 - 160.121 <sup>3</sup>
$\alpha$ -Lactose	1.768	106	45.792 - 61.243 <sup>3</sup>
$\beta$ -Lactose	2.179	106	75.067 - 99.360 <sup>3</sup>
3-Methylhistidine	0.168	2	0.103 - 0.151 <sup>3</sup>
N-Acetyl-carbohydrates	0.086	106	1.135 - 4.240 <sup>3</sup>
Phosphocholine	0.082	56	0.143 - 1.355 <sup>3</sup>
Phosphocreatine	0.179	106	0.585 - 2.567 <sup>3</sup>
Taurine	0.076	3	0.327 - 0.621 <sup>3</sup>
Trimethylamine-N-oxide	ND	2	0.043 - 0.046 <sup>3</sup>

<sup>1</sup> The number of values above LLOQ varies from metabolite to metabolite because individual LLOQ were determined for each metabolite; also the abundance of the various metabolites greatly varies. In total, 106 milk samples were analyzed, which results in a maximum number of 106 values that could be obtained for a single metabolite.

<sup>2</sup> Only one value detected.

<sup>3</sup> Concentrations obtained from <sup>1</sup>H-<sup>13</sup>C 2D HSQC spectra.

<sup>4</sup> Concentrations obtained from <sup>1</sup>H 1D NMR spectra.

Table 10. Brown Swiss and Simmental Fleckvieh Cows: Pearson Correlation Matrix of Milk Features. Adapted from (Klein et al. 2010).

	Days in Milk	Milk (kg)	Fat (%)	Protein (%)	Somatic Cell Count	$\alpha$ -Aminobutyric acid	Acetate	Acetone	Alanine	Aspartate	Betaine	$\beta$ -Hydroxybutyrate (NMR)	Choline	Choline compounds	Citrate	Creatinine	Fumarate	Glutamate	Glucose	Glycine	Glycerophosphocholine	Isoleucine	Lactate	Lactose	Leucine	Lysine	Malate	N-Acetylcarbohydrates	Ornithine	Phenylalanine	Phosphocholine	Phosphocreatine	Proline	Pyruvate	Succinate	Threonine	Tryptophane	Tyrosine	Valine		
Days in Milk	1.00	-0.29	0.34	0.53	0.08	-0.48	0.59	-0.20	0.09	-0.37	-0.37	-0.03	0.38	-0.04	-0.15	0.01	-0.03	-0.29	0.27	-0.38	0.31	0.11	0.07	-0.20	0.14	0.51	0.15	0.13	-0.19	0.06	-0.42	-0.17	-0.11	0.06	-0.32	0.03	0.48	-0.07	0.09		
Milk (kg)	-0.29	1.00	-0.29	-0.37	0.44	0.04	n.d.	-0.10	0.14	0.04	n.d.	-0.32	-0.28	-0.04	0.06	-0.03	0.02	0.15	0.05	0.13	-0.24	0.20	-0.12	0.08	-0.05	-0.09	-0.06	-0.09	-0.03	-0.02	0.02	0.14	0.40	-0.11	-0.01	0.20	-0.23	n.d.	0.18		
Fat (%)	0.34	-0.29	1.00	0.36	0.10	0.13	0.38	0.44	0.00	-0.43	0.50	-0.58	0.44	0.49	0.05	-0.22	0.50	-0.34	0.12	0.10	0.34	0.25	-0.21	0.06	0.13	0.10	0.51	0.30	-0.44	0.17	0.30	0.27	0.18	-0.22	-0.24	-0.35	0.08	0.39	-0.04		
Protein (%)	0.53	-0.37	0.36	1.00	0.02	-0.37	0.71	0.02	-0.38	-0.15	0.16	0.55	0.22	-0.49	-0.12	-0.10	-0.27	0.12	-0.35	0.51	0.23	0.03	-0.11	0.37	-0.57	-0.01	0.57	-0.17	0.18	0.08	-0.07	-0.10	-0.20	-0.27	0.16	0.38	0.54	0.13			
Somatic Cell Count	0.08	0.44	0.19	0.02	1.00	0.08	-0.14	0.08	-0.03	-0.26	0.19	0.37	0.07	0.05	0.21	0.20	0.18	-0.26	-0.12	0.05	-0.15	0.27	-0.08	-0.13	0.11	0.11	0.40	0.06	-0.27	0.08	0.29	0.05	0.16	-0.10	-0.24	0.21	0.21	-0.35	0.03		
$\alpha$ -Aminobutyric acid	-0.48	0.04	0.13	-0.37	0.08	1.00	-0.33	0.13	0.45	0.31	0.29	0.00	-0.08	0.42	0.21	0.14	0.17	0.40	-0.21	0.66	0.06	0.16	-0.22	0.17	0.07	0.14	0.44	0.47	0.29	-0.25	0.12	0.15	-0.12	0.37	0.24	0.03	0.24				
Acetate	0.65	n.d.	0.38	0.71	-0.14	-0.33	1.00	0.30	-0.32	-0.14	n.d.	0.26	0.39	-0.13	0.15	-0.05	-0.09	-0.19	-0.12	-0.25	-0.07	0.08	0.52	-0.01	-0.03	0.38	-0.01	-0.15	0.49	-0.04	0.18	-0.10	-0.14	0.43	0.25	-0.22	0.25	n.d.	-0.16		
Acetone	-0.20	-0.10	0.44	-0.06	0.08	0.13	0.30	1.00	-0.35	-0.11	0.13	0.69	-0.15	0.03	0.45	-0.12	0.22	0.01	-0.17	0.22	-0.30	0.28	-0.30	0.25	-0.13	0.02	0.08	-0.07	0.24	0.02	-0.20	0.11	0.22	0.16	0.03	-0.11	0.03	-0.09	-0.15	0.46	-0.04
Alanine	0.09	0.14	0.00	-0.06	-0.03	0.45	-0.32	-0.35	1.00	0.29	0.41	-0.34	0.22	0.35	-0.23	0.42	0.03	0.41	0.17	0.22	0.39	0.29	-0.10	0.05	0.27	-0.03	-0.14	0.36	0.03	0.32	0.10	0.30	0.44	-0.18	0.05	0.24	0.33	0.36	0.51		
Aspartate	-0.37	0.04	-0.43	-0.38	-0.26	0.31	-0.14	-0.11	0.29	1.00	-0.23	-0.17	-0.02	0.04	0.37	-0.26	0.61	-0.03	0.16	-0.02	-0.08	0.43	0.03	-0.13	-0.32	-0.45	-0.07	0.49	-0.06	-0.02	0.05	0.42	0.44	-0.24	-0.08	-0.14	0.04				
Betaine	-0.37	n.d.	0.50	-0.15	0.19	0.29	n.d.	0.13	0.41	-0.01	1.00	0.06	-0.04	0.77	-0.34	0.39	0.32	-0.14	0.58	0.39	0.71	0.43	-0.09	0.46	0.39	-0.21	-0.13	0.74	-0.18	0.45	0.32	0.55	0.60	-0.27	0.05	0.33	0.25	n.d.	0.67		
$\beta$ -Hydroxybutyrate (NMR)	-0.03	-0.32	0.55	0.16	0.37	0.00	0.26	0.69	-0.34	-0.23	0.06	1.00	0.08	-0.15	0.39	-0.11	0.33	0.01	-0.26	0.13	-0.31	0.47	-0.11	-0.04	0.37	0.15	0.46	-0.08	-0.28	0.30	0.07	-0.11	0.07	-0.07	-0.13	-0.06	0.04	0.60	0.08		
Choline	0.38	-0.28	0.44	0.50	0.07	-0.08	0.39	-0.15	0.22	-0.17	-0.04	0.08	1.00	0.26	-0.28	0.22	0.18	-0.25	-0.15	-0.17	0.00	0.45	0.02	-0.02	0.37	0.44	0.22	0.29	-0.16	0.44	-0.42	-0.08	0.37	-0.08	-0.25	0.13	0.47	0.47	0.44		
Choline compounds	-0.04	-0.04	0.49	0.22	0.05	0.42	-0.13	0.03	0.35	-0.02	0.77	-0.15	0.26	0.99	-0.16	0.21	0.13	-0.13	-0.30	0.89	0.93	0.27	-0.07	0.12	0.26	-0.05	-0.18	0.88	-0.13	0.35	0.70	0.66	0.57	-0.13	0.03	0.15	0.13	0.32	0.59		
Citrate	-0.15	0.06	0.05	-0.46	0.21	0.21	0.15	0.45	-0.23	0.04	-0.34	0.39	-0.28	-0.16	0.06	-0.12	0.31	0.12	0.00	0.28	-0.36	0.13	0.03	0.14	-0.04	-0.29	0.47	-0.21	-0.16	-0.05	0.09	0.05	-0.15	0.14	0.03	-0.12	-0.03	-0.15	-0.19		
Creatinine	0.01	-0.03	-0.22	-0.12	0.20	0.14	-0.05	-0.12	0.42	0.37	0.39	-0.11	0.22	0.21	-0.12	0.00	0.01	0.12	-0.16	0.12	0.29	0.21	0.29	-0.04	0.27	0.08	-0.21	0.24	0.23	0.35	0.04	0.14	0.38	0.14	0.11	0.13	0.22	0.17	0.42		
Fumarate	-0.03	0.02	0.50	-0.10	0.18	0.17	-0.09	0.22	0.03	-0.26	0.32	0.33	0.18	0.13	0.31	-0.01	1.00	-0.11	-0.11	0.06	0.04	0.30	-0.26	0.08	0.23	-0.09	0.72	0.21	-0.42	0.36	-0.08	0.18	0.35	-0.22	-0.20	0.18	-0.04	0.36	0.10		
Glutamate	-0.29	0.15	-0.34	-0.27	-0.26	0.40	-0.19	-0.01	0.41	0.61	-0.14	0.01	-0.25	-0.13	0.12	0.12	-0.11	1.00	0.44	0.12	-0.05	0.13	-0.17	0.24	0.04	-0.37	-0.07	-0.10	0.12	-0.07	-0.11	-0.09	0.02	-0.18	0.19	-0.10	-0.06	0.17	0.12		
Glucose	0.27	0.05	-0.12	0.12	-0.12	-0.21	-0.12	-0.27	0.17	-0.03	0.68	-0.26	-0.15	-0.30	0.00	-0.16	-0.11	0.44	1.00	-0.32	0.08	-0.16	-0.29	0.00	-0.07	-0.05	0.04	-0.13	0.01	-0.23	-0.37	-0.26	-0.27	-0.14	0.01	0.04	-0.30	-0.05			
Glycine	-0.38	0.13	0.10	-0.35	0.05	0.66	-0.25	0.28	0.22	0.16	0.39	0.13	-0.17	0.58	0.26	0.12	0.06	0.12	-0.32	1.00	0.04	0.23	-0.10	0.15	0.08	-0.27	-0.07	0.46	-0.08	0.18	0.81	0.67	0.30	-0.13	0.29	0.11	-0.03	0.44	0.35		
Glycerophosphocholine	0.31	-0.24	0.34	0.51	-0.15	0.06	-0.07	-0.30	0.39	-0.02	0.71	-0.31	0.00	0.67	-0.36	0.29	0.04	-0.05	0.08	0.04	1.00	0.14	0.05	0.00	0.27	0.08	-0.21	0.67	-0.05	0.29	0.17	0.34	0.48	-0.02	-0.16	0.21	0.23	0.16	0.49		
Isoleucine	0.11	0.20	0.25	0.23	0.07	0.16	0.08	0.25	0.29	-0.08	0.43	0.47	0.45	0.27	0.13	0.21	0.30	0.13	-0.16	0.23	0.14	1.00	-0.16	-0.17	0.85	0.29	0.26	0.40	-0.18	0.80	0.19	0.18	0.59	-0.20	0.00	-0.01	0.42	0.76	0.72		
Lactate	0.07	-0.12	-0.21	0.03	-0.08	-0.22	0.52	-0.13	-0.10	0.43	-0.09	-0.11	0.02	-0.07	0.03	0.29	-0.36	-0.17	-0.29	-0.10	0.05	-0.16	1.00	-0.05	-0.10	0.06	-0.43	-0.11	0.67	0.02	-0.15	-0.04	-0.13	0.01	0.87	0.36	-0.23	0.13	-0.04	-0.09	
Lactose	-0.20	0.08	0.06	-0.11	-0.13	0.17	-0.01	0.02	0.05	0.03	0.46	-0.04	-0.02	0.12	0.14	-0.04	0.08	0.24	0.00	0.15	0.00	-0.17	-0.05	1.00	-0.26	-0.40	0.14	-0.01	0.02	-0.22	0.11	0.05	-0.13	-0.05	-0.05	0.07	-0.19	-0.07	-0.18		
Leucine	0.14	-0.05	0.13	0.37	0.11	0.07	-0.03	0.08	0.27	-0.13	0.39	0.37	0.37	0.26	-0.04	0.27	0.23	0.04	-0.07	0.08	0.27	0.85	-0.10	-0.26	1.00	0.44	0.12	0.40	-0.12	0.90	0.05	0.09	0.67	-0.14	-0.06	-0.05	0.54	0.69	0.80		
Lysine	0.51	-0.09	0.10	0.57	0.11	-0.39	0.38	-0.07	-0.03	-0.32	-0.21	0.15	0.44	-0.05	-0.28	0.08	-0.09	-0.37	-0.05	-0.27	0.08	0.29	0.06	-0.40	0.44	0.98	0.02	0.08	-0.09	0.35	-0.27	-0.20	0.10	0.06	-0.08	-0.02	0.39	0.08	0.29		
Malate	0.13	-0.09	0.51	0.01	0.40	0.04	-0.01	0.24	-0.14	-0.45	-0.13	0.45	0.22	-0.18	0.47	-0.21	0.72	-0.07	0.04	-0.07	-0.21	0.26	-0.43	0.14	0.12	0.02	1.00	-0.09	0.58	0.09	-0.16	-0.06	0.06	-0.37	-0.36	0.16	-0.02	0.05	-0.16		
N-Acetylcarbohydrates	-0.19	-0.03	-0.44	-0.17	-0.27	-0.07	0.49	-0.20	0.03	0.49	-0.18	-0.28	-0.16	-0.13	-0.16	0.23	-0.42	0.12	0.01	-0.08	-0.05	-0.18	0.57	0.02	-0.12	-0.09	-0.33	-0.22	1.00	-0.02	-0.16	-0.12	-0.03	0.62	0.42	-0.23	-0.04	0.13	-0.05		
Phenylalanine	0.06	-0.02	0.17	0.18	0.08	0.14	-0.04	0.11	0.32	-0.06	0.45	0.30	0.44	0.35	-0.05	0.35	0.36	-0.07	-0.23	0.18	0.29	0.50	0.02	-0.22	0.30	0.35	0.09	0.46	-0.02	1.00	0.06	0.26	0.75	-0.04	0.10	-0.08	0.48	0.66	0.78		
Phosphocholine	-0.42	0.02	0.30	0.08	0.29	0.44	0.18																																		

**Table 11.** Analysis of Holstein-Friesian Cows: Diagnosed Metabolic Disorders. Adapted from (Klein et al. 2011a).

	Week 1 <sup>1</sup>	Week 2 <sup>1</sup>	Week 3 <sup>1</sup>	Week 4 <sup>1</sup>	Week 5 <sup>1</sup>	Month 6 <sup>1</sup>	Whole Lactation <sup>2</sup>
<b>Ruminal acidosis</b>	8.3 %	3.9 %	3.0 %	2.2 %	0.9 %	1.8 %	19.3 %
<b>Ketosis</b>	0.9 %	2.2 %	1.3 %	0.4 %	0.9 %	0.0 %	5.3 %
<b>Milk fever</b>	0.0 %	0.0 %	0.0 %	0.0 %	0.0 %	0.0 %	0.0 %
<b>Fever</b>	0.0 %	0.4 %	0.0 %	0.4 %	0.4 %	0.0 %	1.1 %
<b>Healthy</b>	90.8 %	93.5 %	95.7 %	97.0 %	97.8 %	98.2 %	74.3 %
<b>Number of animals</b>	109	230	232	223	223	164	264



<sup>1</sup> Listed is the health status diagnosed within the same week in which the corresponding milk sample was collected. This is also true for the penultimate column corresponding to lactation month six.

<sup>2</sup> Listed is the health status diagnosed at any time point over the whole lactation period irrespectively of time points of milk collection.

**Table 12.** Analysis of Holstein-Friesian Cows: Milk Metabolite Concentration Ranges Throughout Lactation. Adapted from (Klein et al. 2011a).

		Week 1	Week 2	Week 3	Week 4	Week 5	Month 6
2-oxoglutarate <sup>1</sup>	max	75	81	88	96	101	156
	min	38	37	41	45	50	70
Acetate <sup>1</sup>	max	35	36	36	37	37	29
	min	15	13	14	13	13	14
Acetoacetate <sup>1</sup>	max	13	14	11	14	10	7
	min	4	4	4	4	4	4
Acetone <sup>1</sup>	max	497	211	111	106	64	40
	min	29	22	20	20	19	17
Alanine <sup>2</sup>	max	74	78	64	55	54	57
	min	33	35	33	29	30	30
Betaine <sup>2</sup>	max	1263	947	837	864	794	761
	min	626	575	508	509	489	497
BHBA <sup>1</sup>	max	121	97	69	82	63	40
	min	17	12	13	14	13	15
Choline <sup>2</sup>	max	446	432	476	380	320	479
	min	152	154	159	154	158	180
Cis-aconitate <sup>1</sup>	max	140	140	141	142	142	157
	min	76	73	79	82	84	102
Citrate <sup>2</sup>	max	7435	6921	6368	6395	6428	5776
	min	4156	3768	3692	4021	3832	3719
Creatinine <sup>2</sup>	max	114	125	111	115	113	114
	min	83	81	81	81	81	82
Fumarate <sup>1</sup>	max	16	18	17	19	18	23
	min	8	7	8	9	9	10
Glutamate <sup>2</sup>	max	592	734	740	703	629	597
	min	270	316	331	316	311	306
Glycine <sup>2</sup>	max	855	578	414	346	312	244
	min	274	193	171	163	164	163
GP <sup>2</sup>	max	2070	1878	1503	1422	1227	856
	min	1188	1078	932	835	700	561
GPC <sup>2</sup>	max	1217	1001	949	872	895	1162
	min	572	482	439	413	395	663
Lactate <sup>1</sup>	max	136	87	87	68	70	95
	min	40	35	33	32	32	45
Lactose <sup>2</sup>	max	144329	148278	150414	151672	153216	150268
	min	124736	130102	133692	135328	135972	135185
NAC <sup>2</sup>	max	3138	2560	2147	2021	1950	2155
	min	2204	1794	1567	1467	1361	1537
Orotate <sup>2</sup>	max	439	498	533	552	577	1002
	min	208	251	253	286	309	475
Oxaloacetate <sup>1</sup>	max	24	24	22	19	19	25
	min	7	8	7	7	7	8
Phosphocholine <sup>2</sup>	max	941	825	640	566	495	278
	min	483	419	322	287	234	183
Phosphocreatine+Creatine <sup>2</sup>	max	2311	1929	1632	1528	1423	1186
	min	1392	1170	983	962	868	800


  
 Low concentrations High concentrations

Concentrations in  $\mu\text{mol/L}$ . Min and max refer to the 10 and 90 % concentration quantiles, respectively. The color code was individually determined for each metabolite with the highest and lowest observed concentrations of a given metabolite corresponding to dark red and dark blue, respectively.

<sup>1</sup> Concentrations determined by 1D NMR.

<sup>2</sup> Concentrations determined by 2D NMR

**Table 13.** Analysis of Holstein-Friesian Cows: Milk Fat Content of Animals Above and Below GPC/PC Threshold<sup>1</sup>. Adapted from (Klein et al. 2011a).

Time Point	Mean Concentration		Number of Animals		P-Value
	Animals Below Threshold	Animals Above Threshold	Below Threshold	Above Threshold	
Week 1	5.93 %	5.21 %	97	24	1.4*10 <sup>-3</sup>
Week 2	5.02 %	4.60 %	198	33	3.2*10 <sup>-3</sup>
Week 3	4.38 %	4.06 %	204	42	1.0*10 <sup>-2</sup>
Week 4	4.16 %	3.86 %	203	38	7.4*10 <sup>-4</sup>
Week 5	3.98 %	3.62 %	205	41	4.2*10 <sup>-5</sup>
Month 6	3.58 %	3.26 %	202	36	7.1*10 <sup>-5</sup>

<sup>1</sup> A GPC/PC ratio equal or larger than 2.5 was chosen to select animals not prone to ketosis.

**Table 14.** Investigation of Non-Alcoholic Steatohepatitis: Loadings of IC 1 of Lipophilic Liver Extracts. Adapted from (Klein et al. 2011b).

Factor	<sup>1</sup> H Frequency [ppm]	Compound	P-Value Control / NAFLD	P-Value Control / NASH	P-Value NAFLD / NASH
-1.51*10 <sup>-2</sup>	1.255	(CH <sub>2</sub> ) <sub>n</sub>	4.25*10 <sup>-5</sup>	2.73*10 <sup>-4</sup>	1.80*10 <sup>-7</sup>
-4.12*10 <sup>-3</sup>	1.265	(CH <sub>2</sub> ) <sub>n</sub>	8.86*10 <sup>-5</sup>	2.51*10 <sup>-7</sup>	9.28*10 <sup>-2</sup>
-2.66*10 <sup>-3</sup>	1.275	(CH <sub>2</sub> ) <sub>n</sub>	4.86*10 <sup>-4</sup>	9.46*10 <sup>-8</sup>	7.68*10 <sup>-1</sup>
2.38*10 <sup>-3</sup>	0.675	Cholesterol (total)	1.18*10 <sup>-2</sup>	4.18*10 <sup>-5</sup>	4.15*10 <sup>-5</sup>
-2.20*10 <sup>-3</sup>	1.245	(CH <sub>2</sub> ) <sub>n</sub>	9.76*10 <sup>-3</sup>	1.11*10 <sup>-1</sup>	3.69*10 <sup>-4</sup>
-2.06*10 <sup>-3</sup>	1.285	(CH <sub>2</sub> ) <sub>n</sub>	5.60*10 <sup>-3</sup>	2.21*10 <sup>-3</sup>	7.62*10 <sup>-2</sup>
2.03*10 <sup>-3</sup>	1.015	Cholesterol ester	2.21*10 <sup>-2</sup>	7.65*10 <sup>-5</sup>	6.57*10 <sup>-5</sup>
1.70*10 <sup>-3</sup>	0.865	CH <sub>3</sub>	1.34*10 <sup>-4</sup>	6.60*10 <sup>-6</sup>	5.53*10 <sup>-6</sup>
1.54*10 <sup>-3</sup>	0.855	CH <sub>3</sub>	4.11*10 <sup>-1</sup>	4.16*10 <sup>-5</sup>	1.21*10 <sup>-5</sup>
1.25*10 <sup>-3</sup>	0.905	CH <sub>3</sub>	9.26*10 <sup>-11</sup>	5.14*10 <sup>-2</sup>	4.53*10 <sup>-5</sup>
1.18*10 <sup>-3</sup>	0.915	CH <sub>3</sub>	7.20*10 <sup>-5</sup>	5.59*10 <sup>-5</sup>	3.06*10 <sup>-5</sup>
-1.13*10 <sup>-3</sup>	0.885	CH <sub>3</sub>	3.95*10 <sup>-2</sup>	5.10*10 <sup>-1</sup>	2.46*10 <sup>-2</sup>
9.18*10 <sup>-4</sup>	1.025	Cholesterol ester	1.86*10 <sup>-1</sup>	1.96*10 <sup>-5</sup>	1.23*10 <sup>-5</sup>
8.90*10 <sup>-4</sup>	1.345	(CH <sub>2</sub> ) <sub>n</sub>	1.09*10 <sup>-6</sup>	3.34*10 <sup>-6</sup>	3.18*10 <sup>-2</sup>
8.24*10 <sup>-4</sup>	1.305	(CH <sub>2</sub> ) <sub>n</sub>	1.85*10 <sup>-2</sup>	4.29*10 <sup>-4</sup>	7.95*10 <sup>-1</sup>
8.07*10 <sup>-4</sup>	2.265	(CH <sub>2</sub> COO)	8.04*10 <sup>-2</sup>	5.53*10 <sup>-6</sup>	1.54*10 <sup>-5</sup>
7.85*10 <sup>-4</sup>	1.355	(CH <sub>2</sub> ) <sub>n</sub>	8.00*10 <sup>-9</sup>	9.61*10 <sup>-8</sup>	3.13*10 <sup>-1</sup>
7.48*10 <sup>-4</sup>	1.135	?	2.88*10 <sup>-1</sup>	3.19*10 <sup>-5</sup>	2.18*10 <sup>-5</sup>
-7.46*10 <sup>-4</sup>	2.005	CH <sub>2</sub> C=C	1.84*10 <sup>-6</sup>	9.87*10 <sup>-9</sup>	5.04*10 <sup>-2</sup>
6.90*10 <sup>-4</sup>	0.925	CH <sub>3</sub>	1.52*10 <sup>-2</sup>	1.83*10 <sup>-5</sup>	5.45*10 <sup>-6</sup>
6.82*10 <sup>-4</sup>	1.335	(CH <sub>2</sub> ) <sub>n</sub>	7.66*10 <sup>-2</sup>	1.31*10 <sup>-2</sup>	1.65*10 <sup>-2</sup>
-6.72*10 <sup>-4</sup>	2.015	CH <sub>2</sub> C=C	7.28*10 <sup>-8</sup>	2.87*10 <sup>-9</sup>	1.02*10 <sup>-2</sup>
-6.51*10 <sup>-4</sup>	1.295	(CH <sub>2</sub> ) <sub>n</sub>	3.69*10 <sup>-1</sup>	3.46*10 <sup>-2</sup>	8.55*10 <sup>-1</sup>
6.23*10 <sup>-4</sup>	1.845	(CH <sub>2</sub> CH=CH)	1.24*10 <sup>-1</sup>	3.14*10 <sup>-5</sup>	2.48*10 <sup>-6</sup>
6.10*10 <sup>-4</sup>	0.875	CH <sub>3</sub>	3.58*10 <sup>-1</sup>	3.83*10 <sup>-5</sup>	2.21*10 <sup>-3</sup>

**Table 15.** Investigation of Non-Alcoholic Steatohepatitis: Loadings of IC 2 of Lipophilic Liver Extracts. Adapted from (Klein et al. 2011b).

Factor	<sup>1</sup> H Frequency [ppm]	Compound	P-Value Control / NAFLD	P-Value Control / NASH	P-Value NAFLD / NASH
-6.19*10 <sup>-3</sup>	1.265	(CH <sub>2</sub> ) <sub>n</sub>	8.86*10 <sup>-5</sup>	2.51*10 <sup>-7</sup>	9.28*10 <sup>-2</sup>
-5.81*10 <sup>-3</sup>	1.275	(CH <sub>2</sub> ) <sub>n</sub>	4.86*10 <sup>-4</sup>	9.46*10 <sup>-8</sup>	7.68*10 <sup>-1</sup>
4.74*10 <sup>-3</sup>	1.255	(CH <sub>2</sub> ) <sub>n</sub>	4.25*10 <sup>-5</sup>	2.73*10 <sup>-4</sup>	1.80*10 <sup>-7</sup>
-3.70*10 <sup>-3</sup>	0.865	CH <sub>3</sub>	1.34*10 <sup>-4</sup>	6.60*10 <sup>-6</sup>	5.53*10 <sup>-6</sup>
3.58*10 <sup>-3</sup>	2.055	CH <sub>2</sub> C=C	7.16*10 <sup>-3</sup>	6.93*10 <sup>-10</sup>	1.02*10 <sup>-1</sup>
-3.55*10 <sup>-3</sup>	2.015	CH <sub>2</sub> C=C	7.28*10 <sup>-8</sup>	2.87*10 <sup>-9</sup>	1.02*10 <sup>-2</sup>
-3.55*10 <sup>-3</sup>	2.005	CH <sub>2</sub> C=C	1.84*10 <sup>-6</sup>	9.87*10 <sup>-9</sup>	5.04*10 <sup>-2</sup>
3.44*10 <sup>-3</sup>	2.045	CH <sub>2</sub> C=C	1.08*10 <sup>-2</sup>	2.72*10 <sup>-9</sup>	1.00*10 <sup>-1</sup>
-2.72*10 <sup>-3</sup>	0.675	Cholesterol (total)	1.18*10 <sup>-2</sup>	4.18*10 <sup>-5</sup>	4.15*10 <sup>-5</sup>
-2.36*10 <sup>-3</sup>	1.015	Cholesterol ester	2.21*10 <sup>-2</sup>	7.65*10 <sup>-5</sup>	6.57*10 <sup>-5</sup>
2.21*10 <sup>-3</sup>	1.355	(CH <sub>2</sub> ) <sub>n</sub>	8.00*10 <sup>-9</sup>	9.61*10 <sup>-8</sup>	3.13*10 <sup>-1</sup>
2.10*10 <sup>-3</sup>	1.305	(CH <sub>2</sub> ) <sub>n</sub>	1.85*10 <sup>-2</sup>	4.29*10 <sup>-4</sup>	7.95*10 <sup>-1</sup>
-2.02*10 <sup>-3</sup>	1.995	CH <sub>2</sub> C=C	6.10*10 <sup>-3</sup>	1.09*10 <sup>-7</sup>	5.59*10 <sup>-1</sup>
-1.73*10 <sup>-3</sup>	0.855	CH <sub>3</sub>	4.11*10 <sup>-1</sup>	4.16*10 <sup>-5</sup>	1.21*10 <sup>-5</sup>
-1.70*10 <sup>-3</sup>	1.285	(CH <sub>2</sub> ) <sub>n</sub>	5.60*10 <sup>-3</sup>	2.21*10 <sup>-3</sup>	7.62*10 <sup>-2</sup>
1.69*10 <sup>-3</sup>	2.065	CH <sub>2</sub> C=C	1.86*10 <sup>-1</sup>	2.76*10 <sup>-5</sup>	1.60*10 <sup>-1</sup>
1.69*10 <sup>-3</sup>	2.765	=CH-CH <sub>2</sub> -CH=	2.86*10 <sup>-5</sup>	1.07*10 <sup>-5</sup>	6.00*10 <sup>-2</sup>
-1.67*10 <sup>-3</sup>	1.295	(CH <sub>2</sub> ) <sub>n</sub>	3.69*10 <sup>-1</sup>	3.46*10 <sup>-2</sup>	8.55*10 <sup>-1</sup>
1.58*10 <sup>-3</sup>	0.895	CH <sub>3</sub>	3.83*10 <sup>-4</sup>	1.37*10 <sup>-7</sup>	2.67*10 <sup>-3</sup>
1.57*10 <sup>-3</sup>	5.375	CH=CH	3.41*10 <sup>-6</sup>	7.49*10 <sup>-6</sup>	6.03*10 <sup>-2</sup>
1.54*10 <sup>-3</sup>	2.775	=CH-CH <sub>2</sub> -CH=	2.77*10 <sup>-5</sup>	5.62*10 <sup>-6</sup>	1.98*10 <sup>-2</sup>
1.46*10 <sup>-3</sup>	2.035	CH <sub>2</sub> C=C	3.53*10 <sup>-1</sup>	1.44*10 <sup>-8</sup>	1.73*10 <sup>-1</sup>
1.41*10 <sup>-3</sup>	1.345	(CH <sub>2</sub> ) <sub>n</sub>	1.09*10 <sup>-6</sup>	3.34*10 <sup>-6</sup>	3.18*10 <sup>-2</sup>
1.38*10 <sup>-3</sup>	1.365	(CH <sub>2</sub> ) <sub>n</sub>	1.50*10 <sup>-11</sup>	1.21*10 <sup>-11</sup>	4.54*10 <sup>-1</sup>
1.36*10 <sup>-3</sup>	5.365	CH=CH	1.87*10 <sup>-6</sup>	5.73*10 <sup>-6</sup>	7.16*10 <sup>-2</sup>

**Table 16.** Investigation of Non-Alcoholic Steatohepatitis: Compounds and Indices in Lipophilic Liver Extracts. Adapted from (Klein et al. 2011b).

Compound	Control (n = 6)	Steatosis (n = 4)	NASH (n = 5)	ANOVA P-Value	P-Value Control / Steatosis	P-Value Control / NASH	P-Value Steatosis / NASH
Free cholesterol <sup>1</sup>	0.57 ± 0.15	0.60 ± 0.13	1.03 ± 0.12	2.8*10 <sup>-4</sup> **	7.6*10 <sup>-1</sup>	3.8*10 <sup>-4</sup> **	2.1*10 <sup>-3</sup> *
Cholesterol ester <sup>1</sup>	0.46 ± 0.16	0.34 ± 0.12	13.0 ± 2.8	3.2*10 <sup>-8</sup> **	2.3*10 <sup>-1</sup>	5.5*10 <sup>-4</sup> **	5.3*10 <sup>-4</sup> **
Glycerol containing lipids <sup>1</sup>	110 ± 25	129 ± 14	115 ± 19	3.9*10 <sup>-1</sup>	1.6*10 <sup>-1</sup>	6.7*10 <sup>-1</sup>	2.7*10 <sup>-1</sup>
Total Lipids <sup>2</sup>	0.092 ± 0.019	0.105 ± 0.010	0.113 ± 0.015	1.1*10 <sup>-1</sup>	1.6*10 <sup>-1</sup>	6.2*10 <sup>-2</sup>	3.7*10 <sup>-1</sup>
Unsaturated bonds <sup>1</sup>	610 ± 120	624 ± 56	694 ± 96	3.8*10 <sup>-1</sup>	8.0*10 <sup>-1</sup>	2.3*10 <sup>-1</sup>	2.2*10 <sup>-1</sup>
Polyunsaturated bonds <sup>1</sup>	317 ± 57	197 ± 10	156 ± 18	4.2*10 <sup>-5</sup> **	3.0*10 <sup>-3</sup> *	5.3*10 <sup>-4</sup> **	4.5*10 <sup>-3</sup> *
SI <sup>3</sup>	0.7986 ± 0.0065	0.8365 ± 0.0017	0.8213 ± 0.0030	7.1*10 <sup>-8</sup> **	9.3*10 <sup>-6</sup> **	9.6*10 <sup>-5</sup> **	4.5*10 <sup>-5</sup> **
PUI <sup>3</sup>	0.0698 ± 0.0045	0.0361 ± 0.0028	0.0271 ± 0.0020	2.3*10 <sup>-10</sup> **	4.9*10 <sup>-7</sup> **	1.1*10 <sup>-7</sup> **	2.6*10 <sup>-3</sup> *
PUFA/MUFA <sup>3</sup>	0.599 ± 0.029	0.363 ± 0.031	0.259 ± 0.022	3.6*10 <sup>-10</sup> **	1.6*10 <sup>-5</sup> **	4.3*10 <sup>-9</sup> **	2.2*10 <sup>-3</sup> *

Given are mean values and standard deviations in nanomole per milligram<sup>1</sup>, weight percent<sup>2</sup> or molar ratios<sup>3</sup>.

The number of values n is given in parentheses. For the t-statistics only p-values are marked as significant where the corresponding ANOVA p-values are significant.

\* p<0.05, \*\* p<0.001

**Table 17.** Investigation of Non-Alcoholic Steatohepatitis: Loadings of IC 1 of Hydrophilic Liver Extracts. Adapted from (Klein et al. 2011b).

Factor	<sup>1</sup> H Frequency [ppm]	Compound	P-Value Control / NAFLD	P-Value Control / NASH	P-Value NAFLD / NASH
2.29*10 <sup>-2</sup>	3.265	Betaine*	2.04*10 <sup>-3</sup>	7.25*10 <sup>-4</sup>	4.32*10 <sup>-3</sup>
-9.27*10 <sup>-3</sup>	1.285	?	3.45*10 <sup>-2</sup>	5.07*10 <sup>-2</sup>	5.58*10 <sup>-1</sup>
5.17*10 <sup>-3</sup>	3.905	Betaine*	2.11*10 <sup>-2</sup>	2.58*10 <sup>-3</sup>	4.44*10 <sup>-3</sup>
-5.11*10 <sup>-3</sup>	1.305	?	7.86*10 <sup>-2</sup>	2.06*10 <sup>-1</sup>	2.69*10 <sup>-1</sup>
-4.82*10 <sup>-3</sup>	1.315	?	5.85*10 <sup>-2</sup>	1.93*10 <sup>-1</sup>	2.09*10 <sup>-1</sup>
-4.36*10 <sup>-3</sup>	1.295	?	3.53*10 <sup>-1</sup>	5.89*10 <sup>-1</sup>	5.05*10 <sup>-1</sup>
-3.68*10 <sup>-3</sup>	1.275	?	4.81*10 <sup>-2</sup>	4.21*10 <sup>-2</sup>	9.91*10 <sup>-1</sup>
-2.18*10 <sup>-3</sup>	0.895	?	3.42*10 <sup>-2</sup>	1.66*10 <sup>-1</sup>	1.18*10 <sup>-1</sup>
-2.03*10 <sup>-3</sup>	1.325	Lactate	3.34*10 <sup>-1</sup>	4.68*10 <sup>-1</sup>	6.40*10 <sup>-1</sup>
-1.52*10 <sup>-3</sup>	1.345	Lactate	5.94*10 <sup>-2</sup>	2.26*10 <sup>-1</sup>	1.72*10 <sup>-1</sup>
-1.51*10 <sup>-3</sup>	0.885	?	2.79*10 <sup>-2</sup>	1.69*10 <sup>-1</sup>	3.79*10 <sup>-2</sup>
-1.46*10 <sup>-3</sup>	1.355	?	3.66*10 <sup>-2</sup>	1.50*10 <sup>-1</sup>	1.37*10 <sup>-1</sup>
-1.44*10 <sup>-3</sup>	2.245	?	2.79*10 <sup>-2</sup>	7.14*10 <sup>-2</sup>	1.96*10 <sup>-1</sup>
-1.41*10 <sup>-3</sup>	5.315	?	2.53*10 <sup>-2</sup>	7.08*10 <sup>-2</sup>	1.44*10 <sup>-1</sup>
-1.40*10 <sup>-3</sup>	2.055	?	2.96*10 <sup>-3</sup>	5.13*10 <sup>-3</sup>	5.37*10 <sup>-2</sup>
1.40*10 <sup>-3</sup>	3.275	Taurine*	1.31*10 <sup>-2</sup>	3.52*10 <sup>-1</sup>	1.93*10 <sup>-2</sup>
-1.26*10 <sup>-3</sup>	5.325	?	3.64*10 <sup>-2</sup>	1.25*10 <sup>-1</sup>	2.44*10 <sup>-1</sup>
-1.19*10 <sup>-3</sup>	2.045	?	4.48*10 <sup>-3</sup>	1.47*10 <sup>-2</sup>	1.69*10 <sup>-2</sup>
-1.17*10 <sup>-3</sup>	1.365	?	2.54*10 <sup>-2</sup>	8.91*10 <sup>-2</sup>	1.63*10 <sup>-1</sup>
-1.11*10 <sup>-3</sup>	1.335	Lactate	5.46*10 <sup>-1</sup>	6.83*10 <sup>-1</sup>	7.83*10 <sup>-1</sup>
-1.09*10 <sup>-3</sup>	2.255	?	4.02*10 <sup>-2</sup>	7.98*10 <sup>-2</sup>	3.73*10 <sup>-1</sup>
-1.09*10 <sup>-3</sup>	5.335	?	3.03*10 <sup>-2</sup>	4.47*10 <sup>-2</sup>	7.22*10 <sup>-1</sup>
-1.08*10 <sup>-3</sup>	0.905	Isoleucine, leucine, valine	7.34*10 <sup>-2</sup>	3.70*10 <sup>-1</sup>	1.51*10 <sup>-1</sup>
-1.03*10 <sup>-3</sup>	1.585	?	3.09*10 <sup>-2</sup>	1.10*10 <sup>-1</sup>	1.46*10 <sup>-1</sup>
-9.51*10 <sup>-4</sup>	5.305	?	3.04*10 <sup>-2</sup>	4.15*10 <sup>-2</sup>	5.90*10 <sup>-1</sup>

\* Confirmed by 2D ICA

**Table 18.** Investigation of Non-Alcoholic Steatohepatitis: Loadings of IC 2 of Hydrophilic Liver Extracts. Adapted from (Klein et al. 2011b).

Factor	<sup>1</sup> H Frequency [ppm]	Compound	P-Value Control / NAFLD	P-Value Control / NASH	P-Value NAFLD / NASH
1.04*10 <sup>-2</sup>	3.265	Betaine*	2.04*10 <sup>-3</sup>	7.25*10 <sup>-4</sup>	4.32*10 <sup>-3</sup>
-9.09*10 <sup>-3</sup>	3.425	Taurine*	2.71*10 <sup>-3</sup>	7.04*10 <sup>-1</sup>	2.92*10 <sup>-3</sup>
5.54*10 <sup>-3</sup>	1.285	?	3.45*10 <sup>-2</sup>	5.07*10 <sup>-2</sup>	5.58*10 <sup>-1</sup>
-5.49*10 <sup>-3</sup>	3.415	Taurine*	2.47*10 <sup>-3</sup>	7.08*10 <sup>-1</sup>	2.82*10 <sup>-3</sup>
4.34*10 <sup>-3</sup>	1.305	?	7.86*10 <sup>-2</sup>	2.06*10 <sup>-1</sup>	2.69*10 <sup>-1</sup>
4.20*10 <sup>-3</sup>	1.315	?	5.85*10 <sup>-2</sup>	1.93*10 <sup>-1</sup>	2.09*10 <sup>-1</sup>
-4.10*10 <sup>-3</sup>	3.435	Taurine*	2.83*10 <sup>-3</sup>	7.85*10 <sup>-1</sup>	3.67*10 <sup>-3</sup>
-3.98*10 <sup>-3</sup>	3.255	Betaine*	1.70*10 <sup>-3</sup>	9.98*10 <sup>-1</sup>	5.45*10 <sup>-3</sup>
3.98*10 <sup>-3</sup>	1.295	?	3.53*10 <sup>-1</sup>	5.89*10 <sup>-1</sup>	5.05*10 <sup>-1</sup>
3.59*10 <sup>-3</sup>	3.905	Betaine*	2.11*10 <sup>-2</sup>	2.58*10 <sup>-3</sup>	4.44*10 <sup>-3</sup>
-3.28*10 <sup>-3</sup>	3.245	Betaine*	5.42*10 <sup>-3</sup>	3.39*10 <sup>-1</sup>	2.05*10 <sup>-3</sup>
-3.10*10 <sup>-3</sup>	3.275	Taurine*	1.31*10 <sup>-2</sup>	3.52*10 <sup>-1</sup>	1.93*10 <sup>-2</sup>
2.16*10 <sup>-3</sup>	1.325	Lactate	3.34*10 <sup>-1</sup>	4.68*10 <sup>-1</sup>	6.40*10 <sup>-1</sup>
2.00*10 <sup>-3</sup>	0.895	?	3.42*10 <sup>-2</sup>	1.66*10 <sup>-1</sup>	1.18*10 <sup>-1</sup>
1.88*10 <sup>-3</sup>	1.275	?	4.81*10 <sup>-2</sup>	4.21*10 <sup>-2</sup>	9.91*10 <sup>-1</sup>
-1.66*10 <sup>-3</sup>	3.405	Glucose*	2.98*10 <sup>-2</sup>	8.82*10 <sup>-2</sup>	5.49*10 <sup>-3</sup>
1.54*10 <sup>-3</sup>	1.345	Lactate	5.94*10 <sup>-2</sup>	2.26*10 <sup>-1</sup>	1.72*10 <sup>-1</sup>
1.45*10 <sup>-3</sup>	0.885	?	2.79*10 <sup>-2</sup>	1.69*10 <sup>-1</sup>	3.79*10 <sup>-2</sup>
-1.45*10 <sup>-3</sup>	3.835	Glucose*	1.87*10 <sup>-2</sup>	4.04*10 <sup>-1</sup>	7.02*10 <sup>-3</sup>
1.42*10 <sup>-3</sup>	1.335	Lactate	5.46*10 <sup>-1</sup>	6.83*10 <sup>-1</sup>	7.83*10 <sup>-1</sup>
-1.40*10 <sup>-3</sup>	3.475	Glucose*	2.92*10 <sup>-2</sup>	7.29*10 <sup>-2</sup>	5.64*10 <sup>-3</sup>
-1.37*10 <sup>-3</sup>	3.495	Glucose*	3.46*10 <sup>-2</sup>	5.48*10 <sup>-2</sup>	5.92*10 <sup>-3</sup>
-1.36*10 <sup>-3</sup>	3.845	Glucose*	1.65*10 <sup>-2</sup>	6.25*10 <sup>-1</sup>	9.10*10 <sup>-3</sup>
-1.36*10 <sup>-3</sup>	3.715	?	2.12*10 <sup>-2</sup>	1.66*10 <sup>-1</sup>	6.14*10 <sup>-3</sup>
1.34*10 <sup>-3</sup>	1.355	?	3.66*10 <sup>-2</sup>	1.50*10 <sup>-1</sup>	1.37*10 <sup>-1</sup>

\* Confirmed by 2D ICA

**Table 19.** Investigation of Non-Alcoholic Steatohepatitis: Compounds in Hydrophilic Liver Extracts. Adapted from (Klein et al. 2011b).

Compound	Control	Steatosis	NASH	ANOVA P-Value	P-Value Control / Steatosis	P-Value Control / NASH	P-Value Steatosis / NASH
Betaine	ND	ND	8.5 ± 2.9 (4)	ND	ND	ND	ND
Glucose	13.7 ± 3.8 (5)	14.4 ± 3.7 (6)	10.3 ± 2.7 (3)	2.9*10 <sup>-1</sup>	7.7*10 <sup>-1</sup>	1.9*10 <sup>-1</sup>	1.1*10 <sup>-1</sup>
Lactate	5.8 ± 2.2 (6)	6.12 ± 0.86 (6)	4.86 ± 0.71 (6)	3.0*10 <sup>-1</sup>	7.5*10 <sup>-1</sup>	3.5*10 <sup>-1</sup>	2.1*10 <sup>-2</sup>
Taurine	11.8 ± 2.5 (6)	21.7 ± 2.5 (6)	10.3 ± 5.2 (5)	1.4*10 <sup>-4</sup> **	4.5*10 <sup>-5</sup> **	6.0*10 <sup>-1</sup>	5.2*10 <sup>-3</sup> *

Given are mean concentrations and standard deviations in nanomole per milligram. The number of values n is given in parentheses. For the t-statistics only p-values are marked as significant where the corresponding ANOVA p-values are significant.

\* p&lt;0.05, \*\* p&lt;0.001.

**Table 20.** Investigation of Non-Alcoholic Steatohepatitis: Loadings of IC 5 for Urine. Adapted from (Klein et al. 2011b).

Factor	<sup>1</sup> H Frequency [ppm]	Compound	P-Value Control / NAFLD	P-Value Control / NASH	P-Value NAFLD / NASH
5.60*10 <sup>-3</sup>	3.435	Taurine*	1.25*10 <sup>-2</sup>	3.39*10 <sup>-4</sup>	9.94*10 <sup>-3</sup>
5.25*10 <sup>-3</sup>	3.265	TMAO*	6.43*10 <sup>-3</sup>	2.59*10 <sup>-3</sup>	3.11*10 <sup>-2</sup>
4.05*10 <sup>-3</sup>	3.275	TMAO*	8.76*10 <sup>-3</sup>	2.87*10 <sup>-3</sup>	3.14*10 <sup>-2</sup>
3.34*10 <sup>-3</sup>	3.425	Taurine*	9.51*10 <sup>-4</sup>	4.03*10 <sup>-5</sup>	1.16*10 <sup>-2</sup>
2.61*10 <sup>-3</sup>	3.445	Taurine*	1.77*10 <sup>-2</sup>	8.25*10 <sup>-4</sup>	1.24*10 <sup>-2</sup>
2.41*10 <sup>-3</sup>	3.255	Taurine*	2.90*10 <sup>-3</sup>	4.84*10 <sup>-5</sup>	1.90*10 <sup>-2</sup>
2.35*10 <sup>-3</sup>	2.895	TMA*	9.02*10 <sup>-3</sup>	2.29*10 <sup>-2</sup>	1.10*10 <sup>-1</sup>
-1.01*10 <sup>-3</sup>	4.055	Creatinine*	6.62*10 <sup>-2</sup>	3.32*10 <sup>-2</sup>	4.15*10 <sup>-1</sup>
9.08*10 <sup>-4</sup>	3.935	Phosphocreatine*	1.29*10 <sup>-1</sup>	2.20*10 <sup>-1</sup>	3.11*10 <sup>-2</sup>
-9.07*10 <sup>-4</sup>	3.045	Creatinine*	1.81*10 <sup>-1</sup>	1.65*10 <sup>-3</sup>	3.21*10 <sup>-2</sup>
-7.78*10 <sup>-4</sup>	3.735	Ascorbic acid*	1.36*10 <sup>-2</sup>	9.33*10 <sup>-8</sup>	7.20*10 <sup>-1</sup>
-7.31*10 <sup>-4</sup>	3.685	?	8.73*10 <sup>-1</sup>	5.25*10 <sup>-4</sup>	3.26*10 <sup>-3</sup>
-7.19*10 <sup>-4</sup>	4.515	Ascorbic acid*	4.32*10 <sup>-3</sup>	6.16*10 <sup>-6</sup>	7.38*10 <sup>-1</sup>
-7.07*10 <sup>-4</sup>	3.745	Ascorbic acid*	9.03*10 <sup>-3</sup>	2.67*10 <sup>-5</sup>	4.79*10 <sup>-1</sup>
7.03*10 <sup>-4</sup>	3.035	Phosphocreatine*	2.03*10 <sup>-1</sup>	1.91*10 <sup>-1</sup>	5.91*10 <sup>-2</sup>
7.03*10 <sup>-4</sup>	2.695	Citrate*	3.92*10 <sup>-2</sup>	1.33*10 <sup>-2</sup>	4.12*10 <sup>-1</sup>
-6.98*10 <sup>-4</sup>	4.025	Ascorbic acid*	1.06*10 <sup>-2</sup>	5.84*10 <sup>-6</sup>	9.35*10 <sup>-1</sup>
-6.96*10 <sup>-4</sup>	1.245	?	3.56*10 <sup>-5</sup>	7.38*10 <sup>-5</sup>	4.06*10 <sup>-2</sup>
5.95*10 <sup>-4</sup>	3.145	Ethanolamine	2.66*10 <sup>-1</sup>	3.49*10 <sup>-1</sup>	4.88*10 <sup>-1</sup>
-5.89*10 <sup>-4</sup>	3.675	?	6.74*10 <sup>-1</sup>	6.89*10 <sup>-4</sup>	2.07*10 <sup>-2</sup>
-5.85*10 <sup>-4</sup>	1.235	?	3.96*10 <sup>-5</sup>	1.68*10 <sup>-4</sup>	2.51*10 <sup>-2</sup>
5.62*10 <sup>-4</sup>	2.555	Citrate*	2.67*10 <sup>-2</sup>	5.23*10 <sup>-2</sup>	3.01*10 <sup>-1</sup>
-5.60*10 <sup>-4</sup>	3.775	Ascorbic acid*	1.61*10 <sup>-4</sup>	1.61*10 <sup>-4</sup>	4.70*10 <sup>-2</sup>
-5.56*10 <sup>-4</sup>	7.365	Phenylalanine*	6.78*10 <sup>-1</sup>	4.71*10 <sup>-3</sup>	1.79*10 <sup>-2</sup>
-5.25*10 <sup>-4</sup>	3.755	Ascorbic acid*	7.02*10 <sup>-3</sup>	1.76*10 <sup>-2</sup>	2.31*10 <sup>-1</sup>

\* Confirmed by 2D ICA

**Table 21.** Investigation of Non-Alcoholic Steatohepatitis: Loadings of IC 4 for Urine. Adapted from (Klein et al. 2011b).

Factor	<sup>1</sup> H Frequency [ppm]	Compound	P-Value Control / NAFLD	P-Value Control / NASH	P-Value NAFLD / NASH
-8.88*10 <sup>-3</sup>	2.895	TMA*	9.02*10 <sup>-3</sup>	2.29*10 <sup>-2</sup>	1.10*10 <sup>-1</sup>
-4.04*10 <sup>-3</sup>	2.885	TMA*	1.95*10 <sup>-1</sup>	2.13*10 <sup>-1</sup>	1.57*10 <sup>-2</sup>
-4.04*10 <sup>-3</sup>	3.265	TMAO*	6.43*10 <sup>-3</sup>	2.59*10 <sup>-3</sup>	3.11*10 <sup>-2</sup>
1.81*10 <sup>-3</sup>	3.755	Ascorbic acid*	7.02*10 <sup>-3</sup>	1.76*10 <sup>-2</sup>	2.31*10 <sup>-1</sup>
-1.67*10 <sup>-3</sup>	3.415	Taurine*	3.01*10 <sup>-2</sup>	3.12*10 <sup>-2</sup>	9.53*10 <sup>-1</sup>
1.61*10 <sup>-3</sup>	3.045	Creatinine*	1.81*10 <sup>-1</sup>	1.65*10 <sup>-3</sup>	3.21*10 <sup>-2</sup>
-1.52*10 <sup>-3</sup>	2.575	Citrate*	1.49*10 <sup>-2</sup>	2.65*10 <sup>-2</sup>	6.09*10 <sup>-2</sup>
-1.44*10 <sup>-3</sup>	3.425	Taurine*	9.51*10 <sup>-4</sup>	4.03*10 <sup>-5</sup>	1.16*10 <sup>-2</sup>
-1.44*10 <sup>-3</sup>	2.685	Citrate*	4.39*10 <sup>-2</sup>	1.09*10 <sup>-1</sup>	1.46*10 <sup>-2</sup>
-1.43*10 <sup>-3</sup>	3.275	Taurine*	8.76*10 <sup>-3</sup>	2.87*10 <sup>-3</sup>	3.14*10 <sup>-2</sup>
1.29*10 <sup>-3</sup>	3.765	Ascorbic acid*	5.72*10 <sup>-3</sup>	2.21*10 <sup>-2</sup>	8.07*10 <sup>-2</sup>
-1.19*10 <sup>-3</sup>	2.715	Citrate*	1.21*10 <sup>-1</sup>	1.40*10 <sup>-1</sup>	8.09*10 <sup>-1</sup>
-1.13*10 <sup>-3</sup>	3.435	Taurine*	1.25*10 <sup>-2</sup>	3.39*10 <sup>-4</sup>	9.94*10 <sup>-3</sup>
-9.99*10 <sup>-4</sup>	3.255	Taurine*	2.90*10 <sup>-3</sup>	4.84*10 <sup>-5</sup>	1.90*10 <sup>-2</sup>
9.69*10 <sup>-4</sup>	1.245	?	3.56*10 <sup>-5</sup>	7.38*10 <sup>-5</sup>	4.06*10 <sup>-2</sup>
-8.89*10 <sup>-4</sup>	2.545	Citrate*	5.08*10 <sup>-2</sup>	6.81*10 <sup>-2</sup>	1.02*10 <sup>-1</sup>
-8.59*10 <sup>-4</sup>	3.445	Taurine*	1.77*10 <sup>-2</sup>	8.25*10 <sup>-4</sup>	1.24*10 <sup>-2</sup>
8.51*10 <sup>-4</sup>	1.235	?	3.96*10 <sup>-5</sup>	1.68*10 <sup>-4</sup>	2.51*10 <sup>-2</sup>
7.70*10 <sup>-4</sup>	0.925	Leucine*	4.33*10 <sup>-2</sup>	8.07*10 <sup>-1</sup>	3.23*10 <sup>-3</sup>
7.42*10 <sup>-4</sup>	3.775	Ascorbic acid*	1.61*10 <sup>-4</sup>	1.61*10 <sup>-4</sup>	4.70*10 <sup>-2</sup>
6.85*10 <sup>-4</sup>	2.295	?	6.32*10 <sup>-2</sup>	5.85*10 <sup>-1</sup>	2.07*10 <sup>-4</sup>
6.67*10 <sup>-4</sup>	4.065	Creatinine*	2.84*10 <sup>-1</sup>	1.82*10 <sup>-2</sup>	2.26*10 <sup>-1</sup>
6.51*10 <sup>-4</sup>	1.875	?	2.53*10 <sup>-2</sup>	9.66*10 <sup>-1</sup>	1.91*10 <sup>-3</sup>
6.50*10 <sup>-4</sup>	2.305	?	2.98*10 <sup>-2</sup>	1.59*10 <sup>-1</sup>	4.50*10 <sup>-3</sup>
-6.41*10 <sup>-4</sup>	2.725	?	7.66*10 <sup>-3</sup>	1.69*10 <sup>-1</sup>	2.52*10 <sup>-2</sup>

\* Confirmed by 2D ICA

**Table 22.** Investigation of Non-Alcoholic Steatohepatitis: Compounds in Urine. Adapted from (Klein et al. 2011b).

Compound	Control	Steatosis	NASH	ANOVA P-Value	P-Value Control / Steatosis	P-Value Control / NASH	P-Value Steatosis / NASH
Ascorbic acid	0.93 ± 0.33 (9)	1.38 ± 0.26 (4)	1.09 ± 0.22 (5)	6.6*10 <sup>-2</sup>	3.3*10 <sup>-2</sup>	3.1*10 <sup>-1</sup>	1.3*10 <sup>-1</sup>
Citrate	2.5 ± 1.6 (9)	0.173 ± 0.082 (4)	0.278 ± 0.066 (5)	1.4*10 <sup>-3</sup> *	2.5*10 <sup>-3</sup> *	3.3*10 <sup>-3</sup> *	8.5*10 <sup>-2</sup>
Creatinine <sup>1</sup>	5.5 ± 2.0 (9)	10.9 ± 1.5 (4)	11.2 ± 0.51 (5)	1.4*10 <sup>-5</sup> **	6.0*10 <sup>-4</sup> **	1.6*10 <sup>-5</sup> **	7.9*10 <sup>-1</sup>
Leucine	0.46 ± 0.11 (9)	0.271 ± 0.062 (4)	0.235 ± 0.041 (5)	4.7*10 <sup>-4</sup> **	1.6*10 <sup>-3</sup> *	1.8*10 <sup>-4</sup> **	3.1*10 <sup>-1</sup>
Phenylalanine	0.725 ± 0.095 (9)	0.51 ± 0.12 (4)	0.75 ± 0.22 (5)	4.4*10 <sup>-2</sup> *	2.7*10 <sup>-2</sup> *	8.5*10 <sup>-1</sup>	8.0*10 <sup>-2</sup>
Phosphocreatine	2.98 ± 0.82 (8)	0.97 ± 0.67 (4)	1.91 ± 0.37 (5)	2.6*10 <sup>-3</sup> *	2.3*10 <sup>-3</sup> *	8.9*10 <sup>-3</sup> *	5.9*10 <sup>-2</sup>
Taurine	6.8 ± 2.9 (9)	1.52 ± 0.48 (4)	0.684 ± 0.070 (2)	4.4*10 <sup>-4</sup> **	5.5*10 <sup>-4</sup> **	2.4*10 <sup>-4</sup> **	3.7*10 <sup>-2</sup> *
TMA	1.3 ± 1.5 (9)	0.114 ± 0.060 (4)	0.166 ± 0.039 (5)	1.0*10 <sup>-1</sup>	4.1*10 <sup>-2</sup>	4.9*10 <sup>-2</sup>	2.0*10 <sup>-1</sup>
TMAO	1.2 ± 1.7 (9)	0.051 ± 0.021 (4)	0.070 ± 0.013 (5)	3.1*10 <sup>-1</sup>	7.5*10 <sup>-2</sup>	8.0*10 <sup>-2</sup>	1.7*10 <sup>-1</sup>

Given are mean concentrations and standard deviations of molar ratios relative to the creatinine content.

<sup>1</sup>Creatinine concentrations are given in mmol/L. The number of values n is given in parentheses. For the t-statistics only p-values are marked as significant where the corresponding ANOVA p-values are significant.

\* p<0.05, \*\* p<0.001

---

## Appendix II: Attached Files

In the printed version of this thesis, you will find a CD containing the attached files on the last page of the thesis.

In the electronic *.pdf* version of this thesis, you will find the attached files on this page. Depending on your *.pdf* viewer, the files should show up as pin icons in the left upper corner of this page. To save the files to your computer, right-click on the pin icon and select the corresponding menu entry. The files come as zipped folders, in order to unzip the folders, the file extension *.removethis* has to be removed. For example, the file *QUANTIFY.zip.removethis* has to be renamed to *QUANTIFY.zip*. After this, the files may be unzipped. This procedure is necessary due to safety settings of the Adobe Reader.

List of attached files:

- R code
- Python code
- QUANTIFY 1.0

---

## **Appendix III: Manual for QUANTIFY 1.0**

# QUANTIFY 1.0

## Manual

Matthias S. Klein  
Institute of Functional Genomics  
University of Regensburg  
Josef-Engert-Str. 9  
D-93053 Regensburg, Germany

[matthias.klein@klinik.uni-regensburg.de](mailto:matthias.klein@klinik.uni-regensburg.de)

## Table of Contents

1 License Agreement .....	1
2 Introduction.....	2
3 Installation .....	3
3.1 System Requirements.....	3
3.2 Installation .....	3
4 Manual.....	4
4.1 User Files .....	4
4.2 Step-by-Step Guide.....	7
4.3 Quick Start .....	14
5 Troubleshooting.....	16
6 Creating Peak Integrals Using AMIX .....	17
6.1 AMIX Peak Integrals from 1D Spectra .....	17
6.2 AMIX Peak Integrals from 2D HSQC Spectra .....	19

# 1 License Agreement

This program comes with no warranty, you use it at your own risk. You may use and distribute this program freely, as long as credit is given to the original author.

All product, brand and company names in this document may be trademarks of their respective owners.

## 2 Introduction

QUANTIFY is an aid for quantifying small molecules like amino acids in 1D and 2D NMR spectra of biologic fluid samples. Biofluids such as urine, blood plasma or milk and other biologic fluid samples such as liver extracts are very complex in their composition, and compounds may be present at high concentrations in some samples, while they may not be visible in other samples. This makes exact quantification of selected compounds a hard task, as each peak of the compound may or may not be overlapped with other compounds. This is not only true for 1D spectra, but also for 2D spectra such as  $^1\text{H}$ - $^{13}\text{C}$  HSQC spectra.

QUANTIFY employs several algorithms to successfully detect and exclude such outliers. This leads to reliably accurate and precise quantification results.

QUANTIFY takes peak integrals derived from NMR spectra as input and returns absolute concentration values of the observed compounds as output.

### **The features of QUANTIFY include:**

- Multiplication of each integral with an individual calibration factor
- Checking for obligatory peaks before quantification
- Automatic outlier removal
- Reliability checking for compounds where only few peaks are visible in the spectrum
- Checking lower limits of quantification
- Automatic normalization to single compounds, e.g. creatinine
- Automatic correction for different dilutions
- Calculation of means and technical errors for replicate measurements
- Logging of the used parameters and configuration to allow reproducible results

## 3 Installation

### 3.1 System Requirements

*Quantify.exe* may be run using the following operating systems:

- Windows XP (Service Pack 1 or 2)
- Windows 2000 (Service Pack 3 or 4)
- Windows Server 2003 (Service Pack 1 or 2)
- Windows Vista

On other operating systems such as Linux or Mac OS X, you may run the source code file *quantify.m* directly. For this, it is required to have installed the mathematical software Matlab (The Mathworks, Natick, MA, USA). Copy the files *quantify.m* and *quantify.fig* from the folder *QUANTIFY* to your Matlab working directory, start Matlab and type *quantify* to start QUANTIFY. QUANTIFY is backward compatible at least until Matlab version 7.1.0.246 (R14) Service Pack 3.

### 3.2 Installation

Open the file *quantify.zip* with unzipping software (e.g. Winzip) and extract the files.

Run the file *MCRInstallerR2007b.exe*. This installs the required Matlab run-time routines and should be available from the same source as the file *quantify.zip*, for example from the software section on <http://genomics.uni-regensburg.de/>.

To start QUANTIFY, run the unzipped file *quantify.exe*.

## 4 Manual

### 4.1 User Files

#### 4.1.1 Required Files

##### Peak Integral File

A file containing the peak integral values from one spectrum or from several spectra is required to use QUANTIFY. This file may be a Microsoft Excel *.xls* file, a tab stop separated *.txt* file or an AMIX Analytic Profiler (Bruker BioSpin, Rheinstetten, Germany) *.txt* file.

The data have to be present as follows in the file:

title: <i>Spectrum 1</i>	
<i>Compound A</i>	
<i>Peak 1</i>	<i>Integral value*</i>
<i>Peak 2</i>	<i>Integral value*</i>
<i>Peak 3</i>	<i>Integral value*</i>
<i>Compound B</i>	
<i>Peak 1</i>	<i>Integral value*</i>
<i>Peak 2</i>	<i>Integral value*</i>
title: <i>Spectrum 2</i>	
<i>Compound A</i>	
<i>Peak 1</i>	<i>Integral value*</i>
<i>Peak 2</i>	<i>Integral value*</i>
...	...

\* The integral values should have been divided by the number of nuclei contributing to the peak.

Each spectrum title has to start with 'title: '. Please make sure to include a blank line after each spectrum title and after the last peak of each compound. For each spectrum, the number and order of compounds has to be the same. Peaks that shall not be used for quantification may be included in the list, in these cases the integral values has to be replaced by a string, for example not used. For example files see the folder *QUANTIFY\Examples*.

The *.txt* files have to contain exactly two columns that are separated by a tabulator.

For using AMIX *.txt* files please see Chapter 6 for further information.

In case you want to use individual *dilution factors* (see Section 4.2 for details), the individual dilution factor has to be written at the end of the spectrum title and has to start with *df*. All concentrations of this spectrum will then be multiplied by this factor. The individual dilution factor has to consist of exactly four digits, including the decimal point (.).

Example: You have diluted sample 1 by factor 4, sample 2 by factor 13.7 and sample 3 by factor 200. The peak integral file then has to look as follows:

title: Spectrum 1 <b>df4.00</b>	
...	...
title: Spectrum 2 <b>df13.7</b>	
...	...
title: Spectrum 3 <b>df200.</b>	
...	...

The dot (.) after 200 in sample 3 has to be inserted to achieve a length of four digits.

In case you measure single samples repeatedly, QUANTIFY can calculate means and technical errors (see Section 4.2). Replicate spectra have to be titled \*a, \*b, \*c and so on, where \* may be any string in the peak integral file, e.g. sample1\_a, sample1\_b, sample1\_c.

### 4.1.2 Optional Files

Optionally, a file containing peak information and a file containing lower limits of quantification may be used.

#### Peak Information File

This file contains additional information about the peaks of a compound to enable accurate quantification results. This file may be either a Microsoft Excel *.xls* file or a tab stop separated *.txt* file. The data have to be present in the file as in the following example:

	Obligatory peak	Number of nuclei	Calibration factor
Compound A			
Peak 1	0	3	1.39
Peak 2	1	1	1.12
Peak 3	0	1	-1
Compound B			
Peak 1	0	1	1.23
Peak 2	0	2	1.07
...	...	...	...

The column *Obligatory peak* can be used to mark single peaks as obligatory. This may be useful for molecules with both high-intensity and low-intensity peaks, where one strong peak that are often overlapped by other signals. By marking a weaker peak of the molecule as obligatory, this compound will only be quantified if the weaker peak is present. This is only meaningful if one of the weaker peaks is seldom overlapped. This will reduce the number of incorrect quantification results. Possible values are 0 and 1. 0 means that the peak is not required to be present and 1 means that the peak must be present to quantify the compound. Usually, 0 should be chosen for all peaks.

In the column *Number of nuclei*, the number of nuclei contributing to the peak has to be entered. This number is used for a reliability check in case less peaks than the *peak threshold* are available for one compound.

In the column *Calibration factor*, calibration factors for each peak have to be entered. Negative values mean that the peak is not used for quantification. The calibration factors can be determined experimentally using a dilution series of the pure compound. The measured peak integrals and concentration values have to be fitted with a regression line going through the point of origin. The slope of the regression line is the calibration factor.

The *.txt* file has to contain exactly four columns that are separated by a tab stop.

### Lower Limits of Quantification File

In this file, the lower limits of quantification (LLOQ's) are stored for automated checking of the quantification results. This file may be either a Microsoft Excel *.xls* file or a tab stop separated *.txt* file. The LLOQ's may be any value and have to be present as follows in the file:

Compound	LLOQ [mmol/L]
<i>Compound A</i>	<i>0.15</i>
<i>Compound B</i>	<i>0.30</i>
...	...

The tab stop separated *.txt* file has to contain exactly two columns that are separated by one tab stop.

## 4.2 Step-by-Step Guide

In this section, the usage of QUANTIFY will be described step by step. For each step an example is given (painted in blue). The main window of QUANTIFY (Figure 4.1) is divided into six panels that are intended to be filled out in their numerical order.

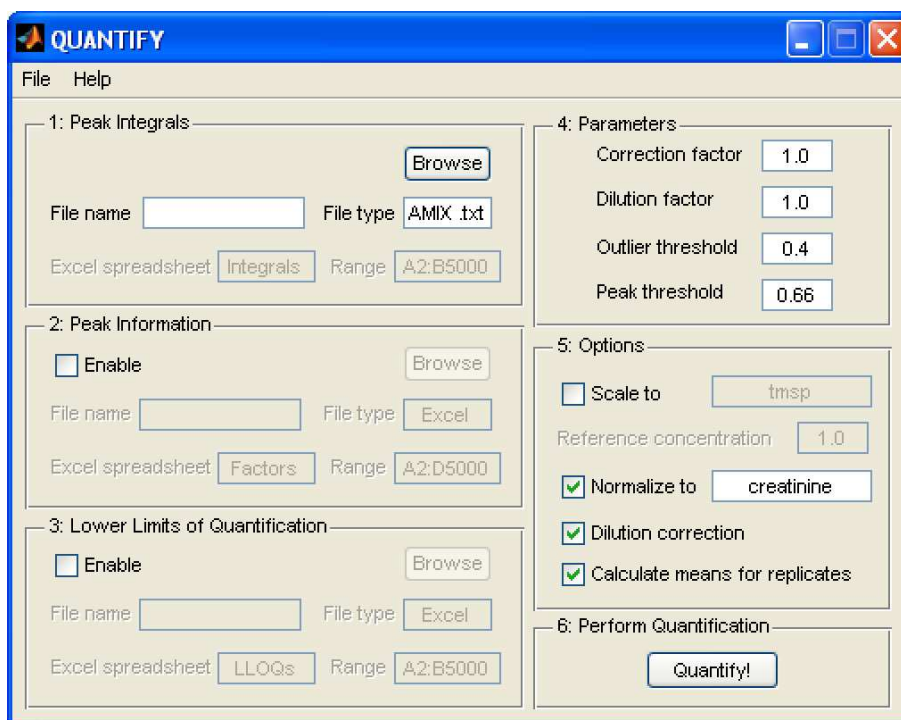


Figure 4.1. The main window with default parameters

For all fields of the main window, a help text is available that will pop up when you hold the mouse cursor over the field. When starting QUANTIFY, default parameters will be filled out in most fields. In the following paragraphs, all items of QUANTIFY are described.

## Menu Bar

### File

- *Load default parameters* will load the default parameters.
- *Load custom parameters* will load previously saved parameters.
- *Save custom parameters* will save the current parameters except for the peak integral file.
- *Exit* will close QUANTIFY.

### Help

- *Manual* will open the manual (this document).
- *About QUANTIFY* will show the program version.

## Panel 1: Peak Integrals

As a first step, you have to choose a file where the integral values are stored. For information on the data format of the used files please see Section 4.1.1. Select *Browse* and choose the peak integral file. The file may be either an Excel *.xls* file, a tab stop separated *.txt* file or an AMIX Analytic Profiler *.txt* file. The file name including the path of the chosen file is shown in the field *File name*. The file type of the chosen file is shown in the field *File type*.

Please note that Microsoft Excel is required to read Excel files. If Excel is not installed on your computer, please use *.txt* files instead.

For Microsoft Excel files, you will have to enter the name of the spreadsheet containing the data (default is *Integrals*) in the field *Sheet* and the range where the values are stored (default is *A2:B5000*) in the field *Range*. Make sure not to include headlines in the given range.

QUANTIFY can also read data from Bruker AMIX Analytic Profiler *mprofile.txt* output files. For details on the parameters to use in AMIX Analytic Profiler see Chapter 6.

**Example:** Click *Browse*. A file selection window will pop up. Change the file type to *Tab stop separated .txt* and choose the file *urine\_control.txt* in the folder *QUANTIFY\Examples\Peak integral files*.

## Panel 2: Peak Information

In this panel you have to choose if you want to use additional peak information. This information is necessary for individual peak calibration and additional peak reliability checks. To use this additional information, check the *Enable* check mark.

In this case, you will have to specify a file where the information is stored by selecting *Browse*. For the data format of the used file please see Section 4.1.2. The file may be either an Excel *.xls* file or a tab stop separated *.txt* file. The file name including the path of the chosen file is shown in the field *File name*. The file type of the chosen file is shown in the field *File type*.

Please note that Microsoft Excel is required to read Excel files. If Excel is not installed on your computer, please use *.txt* files instead.

When using Excel files, you will have to specify the spreadsheet name and the range where the values are stored in the fields *Sheet* and *Range*. Please make sure not to include any headlines in the area defined in the *Range* field.

**Example:** Click on the check box *Enable*. Click *Browse*. A file selection window will pop up. Change the file type to *Tab stop separated .txt* and choose the file *urine\_peakinfo.txt* in the folder *QUANTIFY\Examples\Peak information and LLOQ files*.

### Panel 3: Lower Limits of Quantification

Here you have to choose if you want to check if the calculated concentrations are above individually defined LLOQ's. Check the *Enable* check box to activate this function.

You will have to specify a file where the LLOQ's are stored by selecting *Browse*. For the data format of the used files please see Section 4.1.2. The file may be either an Excel *.xls* file or a tab stop separated *.txt* file. The file name including the path of the chosen file is shown in the field *File name*. The file type of the chosen file is shown in the field *File type*.

Please note that Microsoft Excel is required to read Excel files. If Excel is not installed on your computer, please use *.txt* files instead.

When using Excel files, you will have to specify the spreadsheet name and the range where the values are stored in the fields *Sheet* and *Range*. Please make sure not to include any headlines in the area defined in the *Range* field.

**Example:** Click on the check box *Enable*. Click *Browse*. A file selection window will pop up. Change the file type to *Tab stop separated .txt* and choose the file *urine\_LLOQs.txt* in the folder *QUANTIFY\Examples\Peak information and LLOQ files*.

### Panel 4: Parameters

These parameters control the outlier detection and reliability checking of the results, among others. The parameters are pre-filled with defaults that should yield good results. Anyway, you may change these parameters in order to optimize your results.

#### Correction Factor

Each concentration is multiplied by this factor before checking if the concentration is above the LLOQ. The value has to be positive ( $>0$ ), default value is 1 (no correction).

This factor is useful for example if your reference substance concentration is different in some of your spectrum sets, for example due to a change of supplier. The difference to the dilution factor described below is that the correction factor is applied before checking for the LLOQ's, as a change in the reference substance concentration will result in false absolute concentrations in the first hand.

#### Dilution Factor

Each concentration is multiplied by this factor after checking if the concentration is above the LLOQ. The factor has to be positive ( $>0$ ), default value is 1 (no correction).

This may be used if all samples are diluted in the same way. The difference to the correction factor named above is that diluting the sample will not result in false absolute concentrations. Therefore, the dilution factor is applied after checking the

LLOQ's. If each sample is diluted in a different way, you may use the individual *Dilution Correction* in Panel 5.

### Outlier Threshold

This is a threshold for outlier detection. For compounds having more than one peak, the median of all peaks is calculated. Values that differ more than the *outlier threshold* from the median relatively are excluded as outliers. The outlier threshold has to be positive ( $>0$ ), default value is 0.4.

### Peak Threshold

This is a threshold for controlling the reliability of a result by checking how many of the peaks available for a molecule are present in a spectrum. The ratio of found peaks to total peaks has to exceed the *peak threshold*. The peak threshold has to be in the range of 0 to 1, default is 0.66.

**Example:** Leave all parameters on their default settings.

## Panel 5: Options

This panel controls additional functions of QUANTIFY.

### Scale To

If this check box is enabled, all integral values of one spectrum will be divided by the value of the first valid peak of the reference substance specified in the corresponding text field. In case your peak integrals are already scaled to the reference substance signal, as in AMIX files, this check box does not need to be enabled.

### Reference Concentration

Here you may enter the concentration of the reference substance specified in the *Scale to* field. The *Reference Concentration* has to be positive ( $>0$ ). It is important to use the concentration corrected to your sample amount. For example, if you add 400  $\mu\text{L}$  of sample to 50  $\mu\text{L}$  of  $\text{D}_2\text{O}$  containing 10 mmol/L tmsp, you have to enter 1.25 as reference concentration, as  $10 \text{ mmol/L} * (50 \mu\text{L} / 400 \mu\text{L}) = 1.25 \text{ mmol/L}$ .

### Normalize To

If this check box is enabled, all concentrations will be divided by the concentration of the compound entered in the corresponding text field. For urine, this is usually done with the creatinine concentration, but you may choose any compound here.

### Dilution Correction

If this check box is activated, individual *Dilution Correction* will be performed on all spectra. This may be used in case different sample amounts were used for the different spectra, or in case of tissue extracts, where different tissue amounts were employed. The *individual dilution factor* for each spectrum has to be provided in the *peak integral file* as part of the spectrum title. For details see Section 4.1.1.

## Calculate Means for Replicates

If this check box is activated, QUANTIFY will search for replicate spectra of the same sample, indicated by the spectrum title. For details see Section 4.1.1.

Means and technical errors (TE's) will be calculated in case replicates are found. For TE calculation only the first two replicate spectra are used.

**Example:** Enable the check box *Normalize to* and enter *creatinine* in the corresponding text field. Disable the check boxes *Scale to*, *Dilution correction* and *Calculate means for replicates*.

## Panel 6: Perform Quantification

After filling in all fields, the main window of QUANTIFY will look like Figure 4.2.

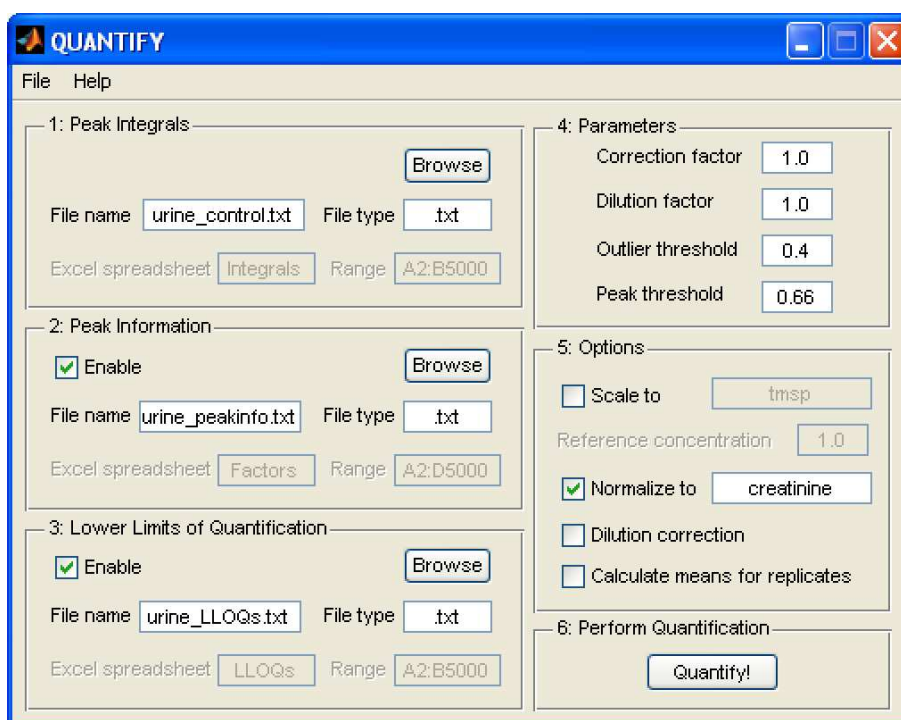


Figure 4.2. The main window of QUANTIFY after filling in all fields according to the example files.

When the button *Quantify!* is selected, you are requested to choose an output file. This may either be a tab stop separated *.txt* file or a Microsoft Excel file. Please note that Microsoft Excel is required to write Excel files. If Excel is not installed on your computer, please use *.txt* output files instead. For Excel files, it will automatically be determined which Excel version is installed on the computer and the matching file format and file extension (*.xls* or *.xlsx*) will be chosen.

**Example:** Click *Quantify!* A *save as* window will pop up. Select *Save*.

The status of the calculations is shown as a progress bar during the quantification. After successful quantification, the result file will be automatically opened.

An example for an Excel result file is shown in Figure 4.3. Additional example result files can be found in the folder *QUANTIFY\Examples*.

The compound concentration values will be stored in the spreadsheet *Results*. For each compound the mean, the standard deviation and the minimal and maximal values over all spectra will be shown at the lower end of the table. Additionally, the number of spectra containing this compound is added.

All used parameters, file and folder names, additional information such as date and version numbers, user data, warnings and error messages will be stored in the spreadsheet *Configuration*. All factors will be extended with an underscore ( \_ ) to circumvent Excel to convert the variable type in an unwanted way.

	A	B	C	D	E	F	G	
1	mmol/L	tmsp	alanine	creatinine	hippuricacid	taurine	citricacid	
2	M02a	6,01106035		5,11151127		0,5425398	0,6672607	
3	M03a	6,01106035	0,31333764	11,3110268	4,52818979		1,37600122	
4	M05a	6,01106035	0,38812946	11,9302793	0,88494328	0,56647469	1,07826411	
5	M06a	6,01106035		4,83247691	5,6322102			
6	M07a	6,01106035	0,64464121	8,96948977	0,53190112	0,32959717	1,18644781	
7	W01a	6,01106035	0,53265229	4,75414713	1,23225415		2,1372904	
8	W02a	6,01106035	0,10385545	4,42004131	0,91935238		1,60446228	
9	W03a	6,01106035	0,26222326	17,0044899	4,10001793		2,16415063	
10	W05a	6,01106035	0,32378463	13,0993454	17,0690314	0,61037674	4,56921526	
11	W06a	6,01106035		6,10641444	1,70205886	0,79236957	0,87220087	
12	z1 Mean	6,01106035	0,36694628	8,75392222	4,06666212	0,56827159	1,73947703	
13	z2 SD	9,3622E-16	0,17792423	4,39777696	5,21866019	0,16554726	1,18010724	
14	z3 Min	6,01106035	0,10385545	4,42004131	0,53190112	0,32959717	0,6672607	
15	z4 Max	6,01106035	0,64464121	17,0044899	17,0690314	0,79236957	4,56921526	
16	z5 N		10	7	10	9	5	9
17								

Original values / Outliers / Normalized to creatinine / Used peaks / Configuration / Results

Figure 4.3. An Excel result file. The different spreadsheets of the file can be seen on the lower margin of the figure.

Information about the number of used peaks for each compound of each spectrum will get stored in the spreadsheet *Used peaks*. For each metabolite, two entries are given, the left one containing the concentration from the *Results* spreadsheet, the right one indicating the ratio of used peaks to available peaks for this compound. For example, (6/6) would mean that all six peaks were used for the calculation of the mean value, indicating a low variance in peak intensities, as indicated by the lack of excluded outliers. This implies a high reliability of the result. In contrast, a value of (1/6) would mean that only one out of six values was used, indicating either a low number of visible peaks or a high variance that led to outlier exclusions. In such cases, a manual checking of the other peaks, for example in the *Outliers* spreadsheet, might be necessary.

In case *Dilution Correction* was chosen in Panel 5, the dilution corrected concentrations are stored in the spreadsheet *Dilution corrected* in the output file.

In case *Calculate Means for Replicates* was chosen in Panel 5, means and TE's will be written to the spreadsheet *Mean* in the output file.

In case *Normalize to* was chosen in Panel 5, a spreadsheet named *Normalized to compound name* is created, e.g. *Normalized to creatinine*. This spreadsheet contains the normalized values.

All original values (before checking for LLOQ's and multiplying by correction and dilution factors) will be stored in the spreadsheet *Original values*.

If you choose *.txt* files as output, up to eight *.txt* files will be generated containing these data. The files will have a fixed number of columns that are separated by a tabulator. The file names are derived from the entered file name by adding extensions, for example *filename\_results.txt*.

## 4.3 Quick Start

QUANTIFY is pre-configured to allow a quick start. In this mode, most implemented features are disabled. Still, this mode may allow a quick view on your data. Please note that quantification results from this mode are only semi-quantitative. For accurate quantification, please refer to the step-by-step guide in Section 4.2. The main feature active in this mode is automatic outlier removal based on deviations from the median.

For quantification, you need a file that contains the NMR peak integral values obtained for the different compounds you are interested in. For details on the format of the file see Section 4.1.1.

Run the file *quantify.exe*. The main window will show up (Figure 4.4).

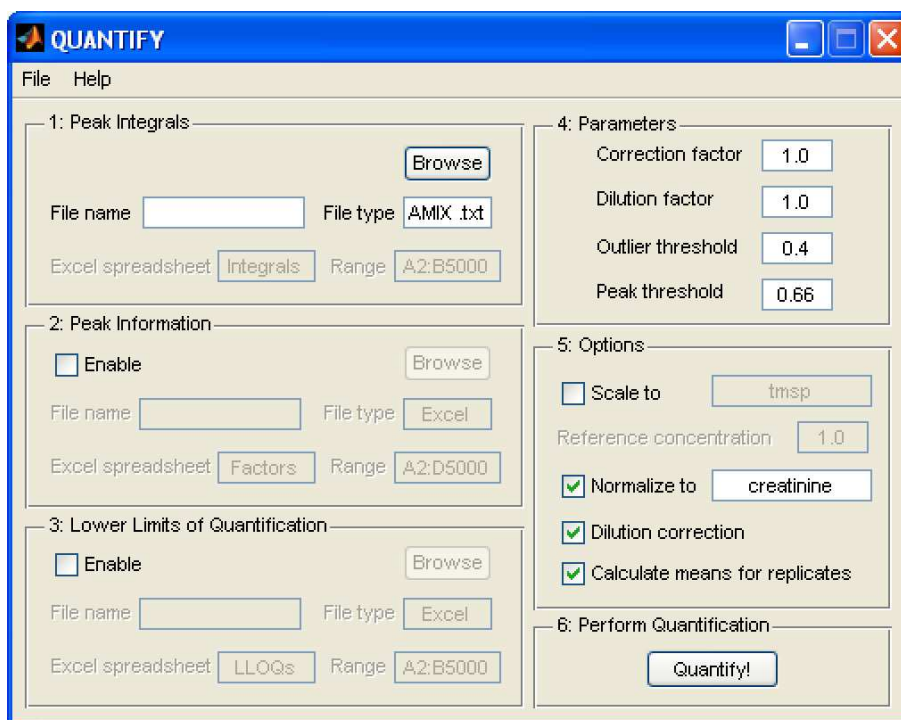


Figure 4.4. The main window of QUANTIFY in quick start mode with default parameters

### Panel 1: Peak Integrals

Select *Browse* and choose the file containing the peak integral values.

### Panels 2 - 4

You do not need to change the pre-filled default values in these panels.

**Panel 5: Options**

Activate the *Scale to* check box and enter the name of your reference substance. Enter the concentration of your reference substance in the field *Reference concentration*.

**Panel 6: Perform Quantification**

Select the button *Quantify!*. This will open a dialog where you can choose the output file name. Afterward, quantification is performed and the result file opened.

## 5 Troubleshooting

- **Starting QUANTIFY Fails**

If QUANTIFY fails to open, please install the file *MCRInstallerR2007b.exe*. This file is available from the same source as *quantify.zip*, for example from the software section on <http://genomics.uni-regensburg.de/site/institute>.

- **Error: *Subscripted assignment dimension mismatch***

- **Error: *Attempted to access ...; index out of bounds***

These error messages indicate problems while reading a peak integral value file. Make sure that for each spectrum in the peak integral file the number of compounds and corresponding peaks, and the order of compounds is identical.

- **Error: *Data format not supported. No AMIX file?***

If you encounter this error message when reading peak integral values from a *.txt* file, most probably QUANTIFY tried to open a tab stop separated *.txt* file as an AMIX *.txt* file. In case you use AMIX *.txt* files, something seems to be wrong with the file format. Make sure you follow the steps in Chapter 6 when creating AMIX *.txt* files.

In case you use a tab stop separated *.txt* file, make sure you choose the matching entry from the file type menu when selecting the file using *Browse* in Panel 1 (see Figure 5.1).

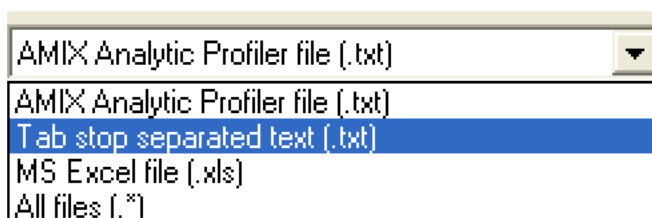


Figure 5.1. Choosing the integral value file type

## 6 Creating Peak Integrals Using AMIX

In order to create peak integral files using AMIX Analytic Profiler (Bruker BioSpin, Rheinstetten, Germany), you should follow the steps described below to ensure that the files are readable for QUANTIFY. The procedure is described for AMIX version 3.9.3 and may differ for other versions. Parameters not explicitly named in this section should not affect the readability of the files and may therefore be chosen according to your preferences.

You have to activate both *identification* and *quantification* in AMIX in order to get usable files.

### 6.1 AMIX Peak Integrals from 1D Spectra

To quantify compounds from 1D spectra, the *.txt* file may not contain any 2D HSQC data. To achieve this, you have to deactivate the buttons for 2D/HSQC identification and quantification.

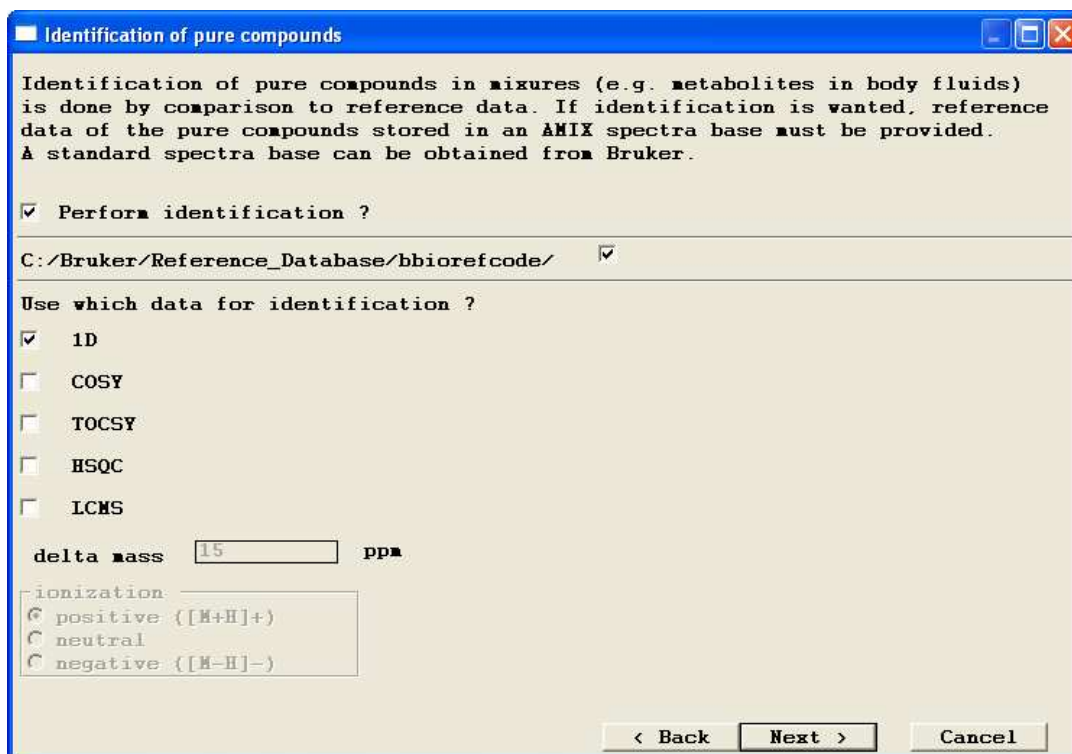


Figure 6.1. *Perform identification* and *1D* have to be enabled

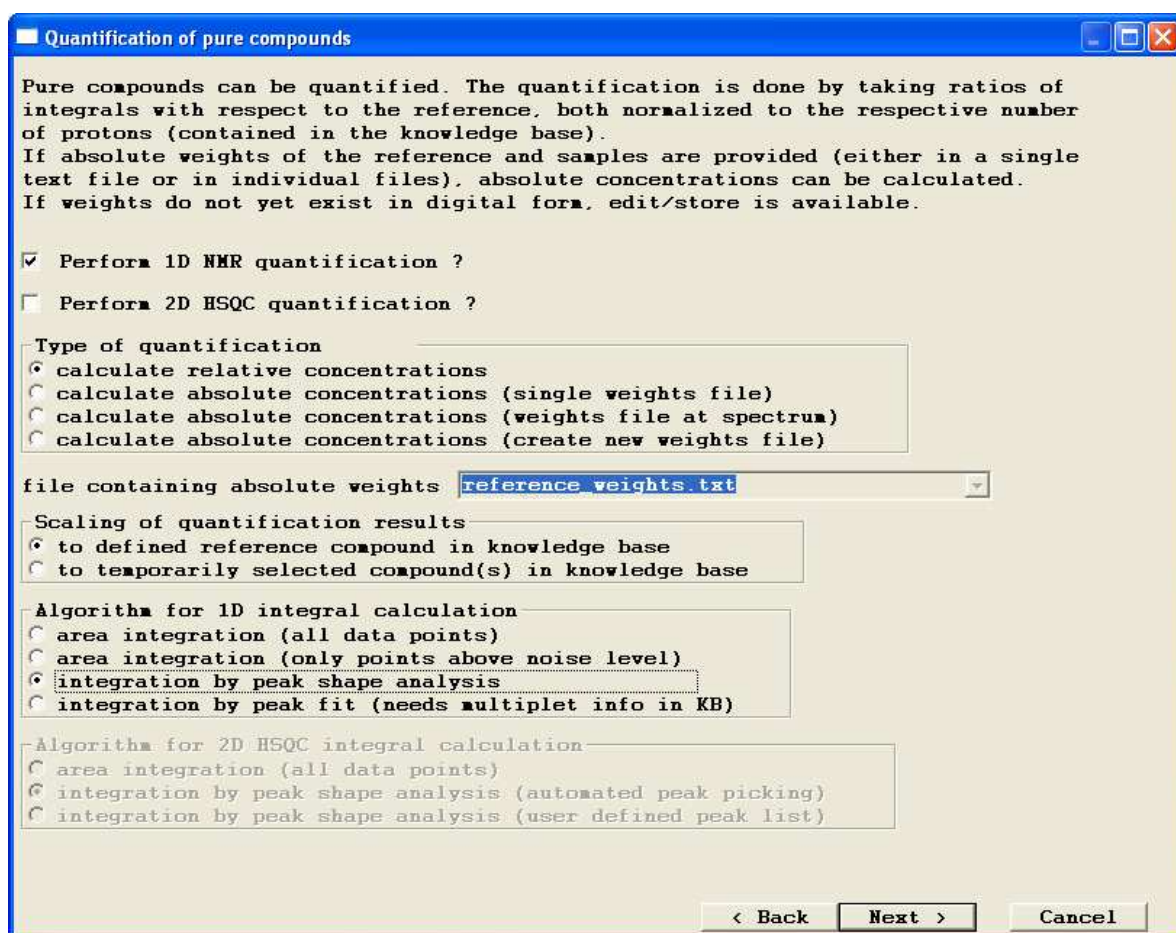


Figure 6.2. Perform 1D quantification has to be enabled

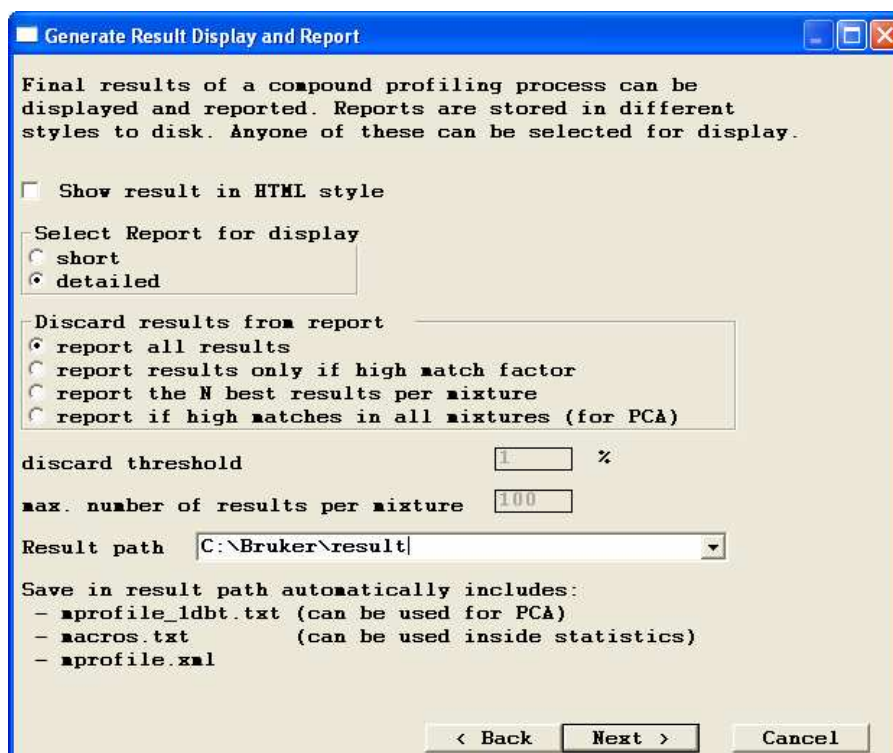


Figure 6.3. Detailed and Report all results have to be enabled

## 6.2 AMIX Peak Integrals from 2D HSQC Spectra

When quantifying from 2D HSQC spectra, 1D spectra have to be quantified as well, although this data will not be used later on. QUANTIFY will look for 2D HSQC data in the file and use these for quantification.

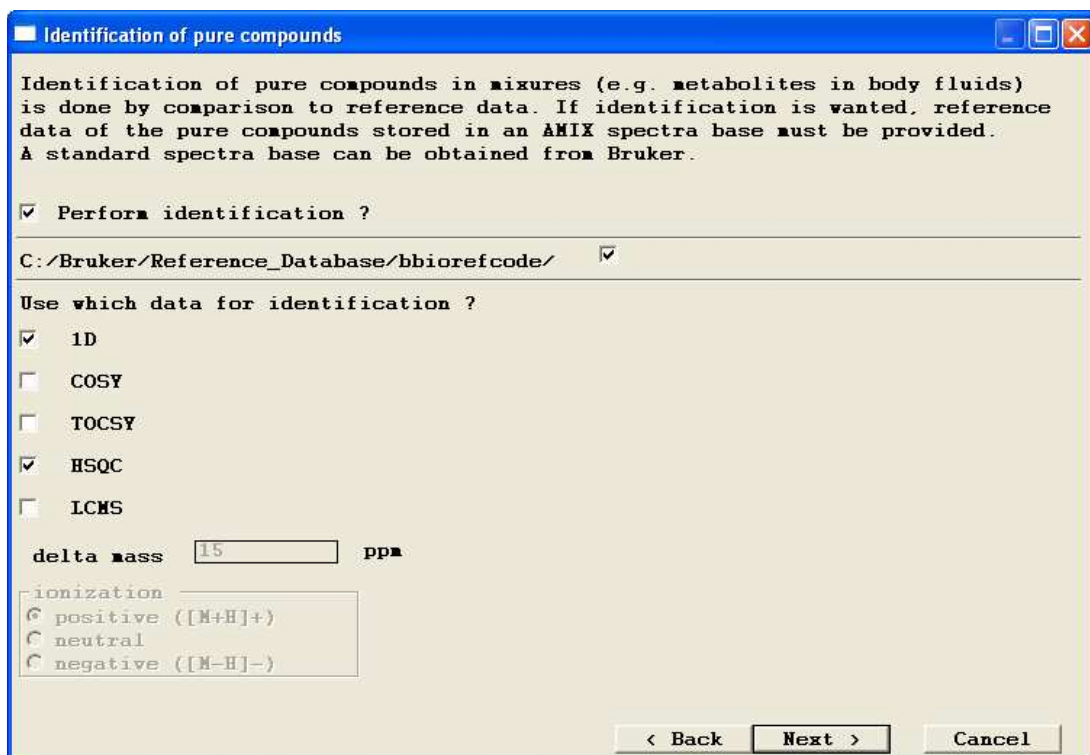


Figure 6.4. *Perform identification* has to be enabled both for *1D* and *HSQC*

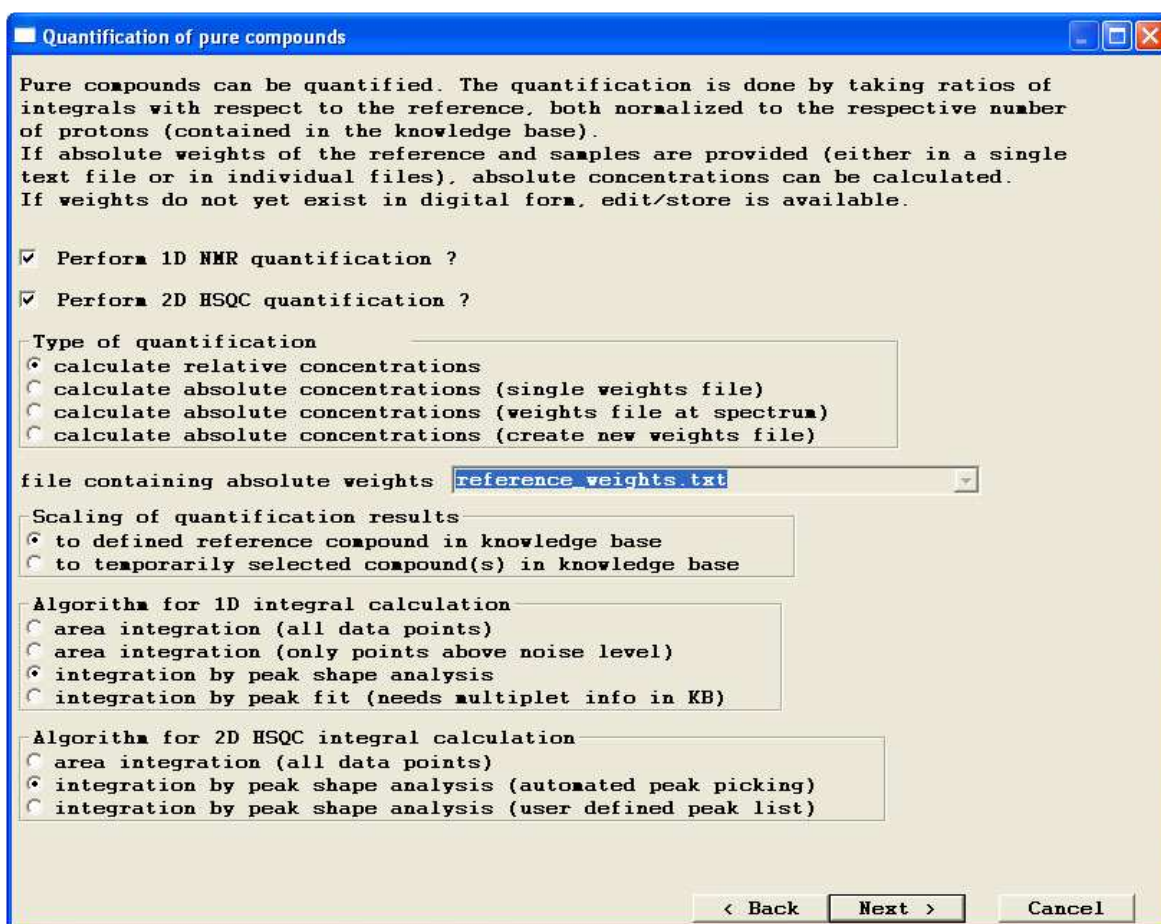


Figure 6.5. Both *Perform 1D quantification* and *Perform 2D quantification* have to be enabled

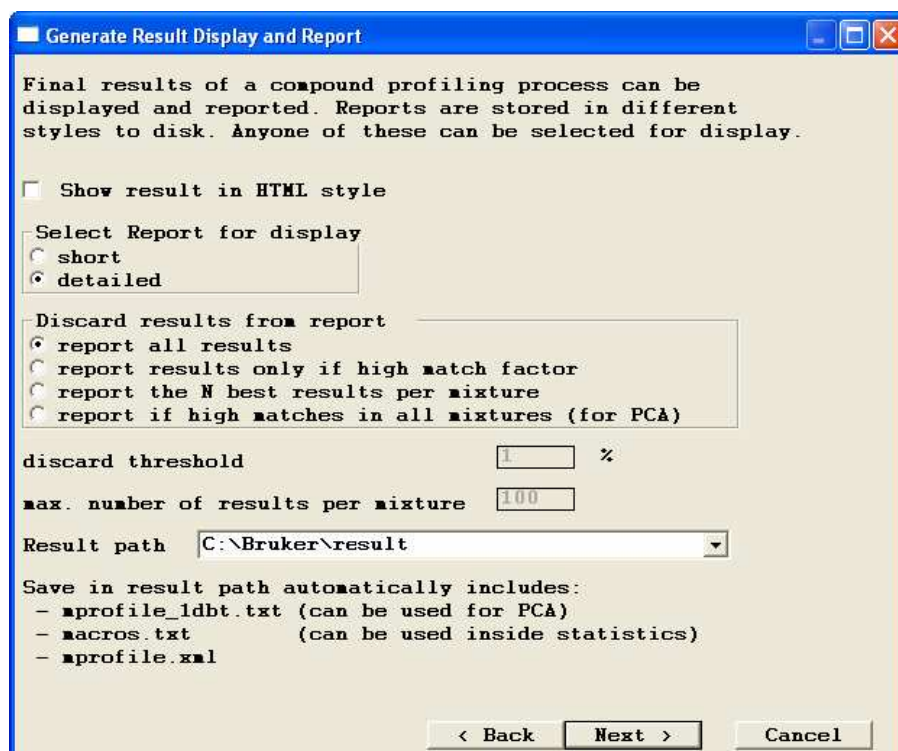


Figure 6.6. *Detailed* and *Report all results* have to be enabled